GUIDING GREEN STORMWATER INFRASTRUCTURE PLANNING THROUGH SOCIO-ECOLOGICAL VULNERABILITY: AN INTEGRATED AND SPATIALLY SCALABLE PRIORITIZATION FRAMEWORK

BY

SAMUEL J. RIVERA

DISSERTATION

Submitted in partial fulfillment of the requirements
for the degree of Doctor of Philosophy in Civil Engineering
in the Graduate College of the
University of Illinois at Urbana-Champaign, 2018

Urbana, Illinois

Doctoral Committee:

Professor Barbara Minsker, Chair
Research Professor Arthur Schmidt, Co-Chair
Professor Julie Cidell
Dr. Morgan Grove, US Forest Service

ABSTRACT

Green stormwater infrastructure (GSI; e.g., rain gardens, bioswales, green roofs) is widely used as a climate change mitigation strategy for its potential to reduce stormwater management problems (e.g., poor water quality, increased streamflow velocities, and flood risk due to impervious surfaces), while providing other human and ecosystem benefits, such as urban heat island reduction. Despite the increased popularity of GSI, its implementation has significant challenges associated with stakeholder resistance, budget constraints, and lack of methods for integrated catchment-scale assessment of socio-ecological multifunctionality.

Current approaches used for the spatial planning of GSI are often limited to a specific spatial scale (e.g., household, neighborhood) and are only intended for the evaluation of a specific objective (e.g., heat mitigation, flooding) by a particular stakeholder (e.g., homeowners, government agencies). As such, planning decisions are often based on limited information about where different types of GSI will be most effective and have failed to consider their potential benefits to the entire suite of socio-ecological systems and the risks associated with multiple hazards. These limitations have prevented the integration of regional/city assessments and neighborhood/site planning, which can lead to unsustainable solutions and stakeholder resistance to GSI installation. *The central premise of this dissertation is to explore the use of vulnerability of socio-ecological systems as the driver for prioritizing locations and types of GSI installations in urban settings.*

Using commonly available data in cities, the concepts of "service-benefiting areas" and "service-needing areas" are used to first propose a new spatial analytical framework needed to better define and understand spatial relationships between GSI projects and the vulnerability of socio-economic, socio-ecological, and engineered systems to multiple hazards (i.e., flooding and urban heat island). The method allows rapid identification of the most vulnerable communities to potential hazard risks at the site scale (i.e., 10-30 meter raster cells) and quantification of risk mitigation potential of GSI at the appropriate spatial scale (site and catchment scale). Using screening rules associated with different design criteria and planning regulations, the method then identifies areas with the greatest suitability for GSI implementation. Lastly, a spatially scalable optimization approach is used to maximize the multifunctionality of GSI locations and types under multiple objectives (e.g., reducing flash flooding risk while increasing ecologic connectivity). The

proposed framework uses a graph-based approach with a simplified distributed hydrologic model and mixed-integer linear programming to maximize the potential delivery of GSI benefits to the most vulnerable areas. This enables a better understanding of the impact that multiple stakeholder opinions could have on the prioritization of potential locations and types of GSI.

Results from applying the proposed framework in multiple cities show that current methods used for quantifying socio-ecological vulnerability have failed to consider the appropriate scales at which GSI projects need to be planned and have often misestimated the spatial correlation of vulnerability. In particular, a new approach used to quantify social susceptibility is shown to be more robust to factors associated with data uncertainty and methodological decisions compared to previous methods. Furthermore, the use of a smaller spatial unit (i.e., Census Blocks) significantly reduces the impact of these factors on the spatial patterns of vulnerability.

Comparing the results with actual GSI projects implemented in the City of Philadelphia, PA, shows that the lack of integrated methods for spatial planning of GSI projects has led to their siting in areas that do not maximize benefits for the most vulnerable communities (i.e., those most susceptible to suffer loss/damage during a hazard event and least likely to recover from the event). Using the presented framework to explore spatial synergies and tradeoffs among the socio-ecologic vulnerabilities, the most vulnerable areas were found to be significantly less likely to receive the potential GSI benefits. Additionally, "high priority" areas for GSI installations that are within one mile of current or planned GSI installations were identified. This suggests that a more integrated approach to the spatial planning of GSI could have avoided this problem.

Lastly, results from applying the optimization framework to spatial prioritization of infiltration structures (e.g., rain gardens and ponds) and trees show the spatial synergies and tradeoffs that exist between these two types of GSI when different hazard mitigation goals are considered. Moreover, the results show that the consideration of vulnerability in the spatial planning of GSI has significant impacts to its spatial allocation, which could result in aggravating disparities in social justice if ignored. These results suggest that by using the proposed approach, city and regional organizations can reduce the cost and time associated with identifying suitable areas for GSI implementation, allow more informed design work, and improve social justice and community buy-in. However, the results of this study also suggest the need for more effective tools that enable better participatory and integrated assessment of GSI projects to promote social justice. Moreover, they suggest the need for more detailed distributed hydrologic and micro-climate

models that enable a more accurate estimation of the impacts of implementing GSI to reduce vulnerability at multiple spatial scales.

To Sahid and my family,
to those that I lost in the process and to the ones I have yet to meet.

ACKNOWLEDGEMENTS

The completion of this dissertation was a long and arduous process of self-discovery and resiliency that was only possible thanks to the love and support from my family, friends, advisors and of course, from my wife, Sahid Rosado.

To Professor Barbara Minsker, my advisor, I will always be grateful for recognizing my potential to be a scholar and for taking a chance on me after reading a random email from a young and idealistic Puerto Rican. It was your caring personality and your humane approach to advising that allowed me to grow as an academic, but more importantly, as a person. To Professor Arthur Schmidt, my co-advisor, I thank you for adopting me into your research group, for nurturing my scholarly ideas, and for supporting me as an independent researcher. I thank you and Professor Minsker for teaching me that there is another way to an academic career and that living in the moment is as important as achieving your goals.

To Professor Julie Cidell and Dr. Morgan Grove, I thank you for your guidance and contributions to the work. I am very grateful for your dedication and all the time you devoted while advising me.

To Michal Ondrejcek, Jong Lee, and Kenton McHenry from the National Center for Supercomputing Applications (NCSA) for providing me with financial support, guidance, and a wonderful environment to work and study. All your help is greatly appreciated.

To my research group colleagues, Erhu Du, Ankit Rai, Wenzhao Xu, Tingting Zhao, Bardia Heidari, Pongsakorn (Tum) Suppakittpaisarn, and Fabian Neira for providing many valuable comments to improve the work and for serving as a support system throughout all these years. I will cherish our friendships.

To Professor Dan Work and Dr. Evan Coopersmith, your support and encouragement were instrumental in the completion of this degree. You were always there for me when needed and I will forever be a better person because of you both. You are an inspiration.

To Ave Alvarado and the Office of Diversity, Equity, and Access at the University of Illinois at Urbana-Champaign for providing me the support and professional development opportunities that allowed me to be successful as a Latino student in a foreign country.

To the team at Optimatics, who provided me with the financial support that allowed me to finish my dissertation and provided me with the corporate perspective I lacked in academia. I thank you for offering me your friendships and acceptance.

To my family, wife, and friends, Ricardo Sepulveda, Pedro Fernandes da Costa, Maria Godoy, and Regina Cattai whose friendships carried me through the hardest times. It was your unconditional support and love what provided me with the energy and motivation I needed to complete my Ph.D. studies.

To Bardia Heidari and Tetra Tech, I thank you for providing me the calibrated SWMM model for the Dead Run 5 (DR5) watershed.

Finally, the completion of this degree would not have been possible without the financial support of the College of Engineering's Support for Under-Represented Groups in Engineering (SURGE) Fellowship program, the Department of Civil and Environmental Engineering at the University of Illinois at Urbana-Champaign, the US National Science Foundation (NSF) Graduate Research Fellowship Program (GRFP), the NSF National Socio-Environmental Synthesis Center (SESYNC) which supported me by an award from the NSF (Grant # DBI-1052875), the University of Maryland, the Metropolitan Water Reclamation District of Great Chicago, and the NSF Cyber-Innovation for Sustainability Science and Engineering (CyberSEES [Award Number:1331807]).

TABLE OF CONTENTS

CHAPTER 1. INTRODUCTION AND BACKGROUND LITERATURE

1.1 Motivation & problem statement

Climate change and increasing populations in urban areas present new challenges for planning, design, and prioritization of infrastructure in our cities. More frequent, intense, and longer heat waves, droughts, and high-intensity rainfall events are some of the hazards that are being intensified by climate change and could potentially have disastrous effects on vulnerable communities (Karl et al. 2008; Strzepek et al. 2010; Dierauer et al. 2012; Andersen et al. 2013; Burian et al. 2013; Kunkel et al. 2013). The potential risks of these hazards have been aggravated by increasing rates of urbanization (Cutter et al., 2003; Turner II, 2003a & 2003b; Cutter & Finch, 2008; IPCC, 2007 & 2012; Kenett & Portugali, 2012). In addition, reductions in available funding have prevented the retrofitting and construction of new infrastructure needed to mitigate these natural hazards (ASCE, 2013; Minsker et al., 2015). Increasing urbanization has increased loads from stormwater runoff and pollutants, reduced ecosystem nutrient retention, and created poor water quality and ecosystem health downstream (NRC, 2008; Wendel et al., 2011). Furthermore, loss of tree canopy and expansion of impervious areas and storm sewer systems have significantly decreased infiltration and evapotranspiration and increased streamflow velocities, flood risk, and urban heat island impacts (Price, 2000 & 2011; Burian et al. 2013; Fletcher et al., 2013; Norton et al., 2015). All of these problems have brought increasing implementation of green stormwater infrastructure (GSI; e.g., rain gardens, green roofs, and pervious pavements) to reduce stormwater management problems (e.g., poor water quality, increased flood risk, etc.) while also benefitting human and ecosystem health.

Many municipalities across the United States are now implementing GSI practices to meet stormwater management goals (e.g., Benedict & McMahon 2006; NRC, 2008; Roy et al., 2014; Pennino et al., 2016; US EPA, 2018) by protecting, restoring, and mimicking natural landscapes and pre-development hydrology. The main objective for their implementation has varied from alleviating flooding and combine sewer overflows during heavy precipitation events (Montalto et al., 2007; Autixier et al., 2014; Lennon et al., 2014), to addressing water quality issues and restoring stream baseflows and aquatic ecosystems at the catchment scale (Walsh et al., 2005; Filoso & Palmer, 2011; Burns et al., 2012). Nevertheless, as components of the natural urban landscape, GSI projects, particularly those designed to include and support native vegetation, have

additional socio-ecological benefits that extend beyond local storm water control. GSI has shown great potential to mitigate heat island effects by providing shading and changing land surface albedos; to improve air quality by reducing nitrogen dioxide, particulate matter, and ozone levels; to restore ecological habitats and their connectivity; and to reduce energy consumption and noise pollution (Pincetl, 2007; Dunn, 2010; Pataki et al., 2011; Demuzere et al., 2014). Furthermore, urban green spaces exert significant positive impacts on individuals and communities by encouraging people to walk, run, cycle, play, and engage in recreation that provides healthy physical activity, reduces physiological symptoms of stress (Morris, 2003; Chang & Chen, 2005; Maas et al., 2006; Thompson et al., 2012), and increases life expectancy (Takano et al., 2002; Mitchell & Popham, 2008). Because of this multifunctionality, GSI is considered to be a no-regret strategy for climate change mitigation (Mees et al., 2011; Cheng, 2016), especially when compared to traditional single-purpose gray stormwater infrastructure (e.g., piped drainage and water treatment systems).

Despite the growing attention to large-scale (i.e., watershed, city, regional) implementation of GSI, its strategic spatial planning and implementation has been limited. Large-scale spatial planning of GSI has suffered from ambiguity in the term *green infrastructure* (i.e., whether it refers to all landscape urban features such as parks or just street/building level features such as rain gardens and green roofs). Furthermore, GSI implementation has followed an opportunistic, piecemeal approach, particularly with a lack of integrated planning methods that consider its full multifunctionality (Matthews et al., 2015; Kuller et al., 2017). Most spatial planning of GSI has been limited to site-scale designs that only consider stormwater reduction benefits. In cases where large-scale initiatives have been proposed, these have often received significant stakeholder resistance and have faced significant funding constraints that have limited evaluation of where GSI would be most beneficial (Clean Water America Alliance, 2011; Montalto et al., 2013; Baptiste et al., 2015).

Current planning and design methodologies have often concentrated only on hydrologic modeling and assessment of site-specific designs and thus do not adequately integrate site-scale design decisions with catchment-scale impacts (Golden et al., 2017; Jefferson et al., 2017; Kuller et al., 2017). Furthermore, current methods for assessing the benefits of GSI have often limited their use/applicability to a specific spatial scale (e.g., household, neighborhood) and are only intended for the evaluation of a specific objective (e.g., heat island effect mitigation, flood risk

reduction, water quality improvements, etc.) from a particular stakeholder (e.g., homeowners, governmental and non-governmental organizations, etc.). As such, planning and design decisions have often been based on limited information about where different types of GSI will be most effective and have disregarded the potential impacts of GSI to the entire suite of socio-ecological systems and the risks associated with multiple hazards (e.g., flash flooding, urban heat island). These limitations have made it difficult to translate the analysis and information between spatial scales and to consider the opinions of multiple stakeholders, thus creating a disconnect between regional assessments and city/neighborhood planning. More importantly, this lack of strategic planning disregards the significant implications that GSI siting decisions have for environmental and social justice, especially considering the coping capacity and hazard exposure of different communities to multiple hazards (i.e., their vulnerability).

These limitations suggest the need for more effective tools and methods that enable a more participatory and integrated assessment of sites and types of GSI projects at multiple scales, from regions to plots. Furthermore, there is limited understanding of how the opportunistic site-scale implementation of GSI and limitations in its spatial planning have affected the delivery of GSI benefits to the most vulnerable, and thus in ultimately understanding GSI's social justice ramifications (Lovell et al., 2013; Meerow, et al., 2017). Additionally, there is a need to understand how these limitations have affected the evaluation of spatial tradeoffs and synergies among the benefits of potential GSI installations to maximize their multifunctionality under multiple objectives (e.g., reducing flash flooding risk while increasing ecologic connectivity). All of these shortcomings suggest the need for more integrated and interdisciplinary approaches that include the concepts of vulnerability science, hazard risks, and human-environmental systems (Abunnasr, 2013; Locke et al., 2013; Norton et al., 2015).

The central premise of this study is to explore the use of vulnerability of socio-ecological systems as a driver for prioritizing locations and types of GSI installations in urban settings. More specifically, this work seeks to answer two primary research questions: (1) Have current approaches used for the quantification of socio-ecologic vulnerability and spatial planning of GSI affected the delivery of GSI benefits to areas of highest vulnerability? and (2) How can different locations and types of GSI installations be prioritized at multiple scales in order to maximizes its mitigation potential in the most socio-ecologically vulnerable areas to address multiple hazards?

It is hypothesized that the aforementioned limitations have prevented GSI projects from being strategically planned and sited in areas where their benefits are maximized for the most vulnerable community members, especially considering their full multifunctionality. Finally, it is expected that different spatial allocations and distributions of GSI could have significant impact on the socio-ecological vulnerability of systems without significantly reducing stormwater management benefits at the watershed scale.

1.2 Related work

One of the major challenges facing the adoption of GSI today is differences in conceptualization of the term itself. Different disciplines have used diverse biophysical, cultural, economic, political and socio-ecological characteristics to define GSI. This ambiguity in the interpretation and definition of the term has led to differences in methods and assumptions for spatial planning of GSI.

Existing methods used for spatial planning of GSI can be divided into two broad categories: (1) those that define GSI as *"planned open space"* and (2) those that define GSI as part of the stormwater management infrastructure system (Matthews et al., 2015; Sussams et al., 2015). Planning methods in the former category often consider political and/or ecological perspectives. Their objective is to improve management of the natural landscape by creating, preserving, or rehabilitating networks of multifunctional green spaces that provide a range of ecological, social and economic benefits (e.g., parks, green open fields, urban forests, etc.). Additionally, previous studies in this category have often guided policies and regulations for improving ecological integrity of the natural landscape, issues associated with social and environmental justice, and sustainable management of ecological services (Chang et al., 2012; Pearsall, et al., 2012; Cheng, 2013; Hansen & Pauleit, 2014; Heckert & Rosan, 2016; Calderón-Contreras et al., 2017). Due to the nature of the problems being addressed, spatial scales at which these methods have been used have ranged from countries to large regions (e.g., river basins to U.S. counties).

On the other hand, planning methods in the latter category have approached GSI planning from an engineering perspective as a rational exercise. Related to this topic, an abundant body of literature has been generated over the last 30 years about the hydrologic performance of GSIs under different hydro-climatic conditions, the most appropriate methods for its modeling and monitoring, and different frameworks for its localized planning and design. Illustrated by recent

literature reviews presented by Golden et al. (2017), Jefferson et al. (2017) & Kuller et al. (2017), previous studies have ranged from modeling and experimental performance assessment of different GSI to the development of frameworks that use simulation-optimization approaches to optimize the location, type, and design parameters of different GSI options. The spatial scale of analysis in these studies have varied from 1-200 km^2 watersheds to individual city blocks (Jefferson et al., 2017), and most of them have concentrated on either assessing the GSI capacity to reduce stormwater runoff problems (e.g., increase in infiltration and reduction in runoff volume and/or a time lag and reduction of peak discharge) or to improve the water quality via increased in-situ treatment of stormwater (e.g., reduction of phosphorous/nitrogen loads). These studies have been the basis for our current scientific understanding of the capabilities of GSI to address stormwater management problems, and have enabled initial buy-in from stakeholders for installation of numerous experimental/pilot projects. Nonetheless, recent findings suggest that these studies: (1) have not properly addressed the benefits of localized projects at the watershed scale, either from a volume/peak discharge reduction or water quality perspective, and (2) have failed to account for the full multifunctionality of GSI (Lovell et al., 2013; Golden et al., 2017; Jefferson et al., 2017; Kuller et al., 2017).

In particular, consolidation of the concepts and spatial scales used in these two aspects has received little attention, particularly as a component of the engineered stormwater management system. One approach that has been considered in urban watersheds is the idea of prioritizing areas for investment and implementation of GSI (e.g., Randhir et al., 2001; Perez-Pedini et al., 2005; Lee et al., 2012; Claro et al., 2013; Shuster & Rhea, 2013; Kuller et al., 2017). The central idea of these approaches is that detailed data at smaller scales can be used as *proxy* indicators of the aggregated benefits of GSI at larger scales. By spatially aggregating these indicators, larger areas can then be ranked based on the availability of suitable locations for GSI installation, the need of the communities to receive the GSI benefits, and the potential benefits of the GSI projects at the watershed scale. Moreover, by collecting data and hydraulic results at smaller watershed scales, these studies have then aggregated these indicators within larger administrative boundaries and integrated other types of data and methods to explore socio-ecological issues, policy regulations, and city-wide investment plans. Methods for these analyses have ranged from simple overlays of different spatial data layers to more complex analyses that use multi-criteria decision-making

frameworks and simplified hydrologic models (Norton et al., 2015; Heckert & Rosan, 2016; Chan et al., 2017; Kuller et al, 2017; Meerow et al., 2017).

Given the flexibility and simplicity of these GSI prioritization techniques and current concerns about the impacts of climate change, particularly to the most vulnerable communities, these methods have recently been of great interest for informing long-term GSI investment plans at large scales. This trend has been particularly significant in the last two decades when the concept of vulnerability has been increasingly adopted for planning and assessment of urban infrastructure projects (Damm, 2010; Abunnasr, 2013; Locke et al., 2013; Norton et al., 2015). Previously dominated by only exposure risk assessment (i.e., probability and intensity of a hazardous event), the process of infrastructure planning and design has evolved to now consider susceptibility and resilience (i.e., coping capacity) of the affected systems, particularly socio-ecological systems (Cutter 1996; Thywissen, 2006; Jones & Andrey, 2007; Damm, 2010).

Broadly defined, vulnerability refers to the potential to suffer loss or harm from some actual or potential hazardous event and the ability to recover from that loss. In the hazard literature, vulnerability is argued to be multidimensional, where the exposure to the hazard (i.e., risk) and the characteristics of the exposed system both function as co-determinants of the systems' vulnerability (McCarthy et al., 2001; Cutter et al., 2003; Turner II, 2003a; Mueller & Dooling, 2011; Kappes et al., 2012). Within this context, the concept of vulnerability is often used to guide analysis to enhance social and ecological well-being by reducing risks to different hazards. Urban infrastructure is often designed to provide a specified level of hazard risk reduction. Therefore, integrated planning, design, and prioritization of GSI that considers the concept of vulnerability should maximize risk reduction of the most vulnerable communities (i.e., provide the greatest reduction in potential to suffer loss or harm from some actual or potential hazardous event and maximize the ability to recover from that loss), and thus maximize potential benefits of the investment (Cheng, 2016; Meerow et al., 2016a).

At this time only a few studies have proposed analytical frameworks that integrate the concept of vulnerability into planning, prioritization, and design of GSI (Susilo et al., 2006; Claro et al., 2013; Locke et al., 2010 & 2013; Norton et al., 2015; Chan et al., 2017; Meerow et al., 2017). Among the most recent and complete analytical frameworks for the prioritization of GSI is the work presented by Locke et al. (2010 & 2013). Locke et al. (2010) proposed an urban tree canopy prioritization framework that integrated geographic information system (GIS) methods to

prioritize tree planting sites based on *need* (i.e., the capacity of trees to address a specific issue in the community) and *suitability* (i.e., biophysical constraints and tree-planting target goals). The method integrated a set of variables at the neighborhood level to identify communities with the greatest need to receive the tree canopy benefits associated with air quality, noise reduction, biodiversity, public health, water, urban heat island, and socio-economic metrics. The final prioritization of the neighborhoods used a standardized aggregated index for the need and suitability components and ranked them based on their position within a sorted list. This work was further expanded by Locke et al. (2013) and used in a collaborative planning process to achieve a tree canopy target in Baltimore, MD. Through surveys and preference solicitations, the study explored overlaps among public agency programs and stakeholders' preferences for tree planting prioritization criteria using a hierarchical clustering tree. The study concluded that tree planting initiatives should align with neighborhoods' motivations, capacities, and interests in order to improve adoption of better urban forestry practices.

A more recent study by Norton et al. (2015) presents a multi-scale (i.e., neighborhood, street, and street canyons scales) framework for prioritization and selection of urban green infrastructure when its intended use is urban heat mitigation. The framework integrates the concepts of social vulnerability, behavioral exposure, and the cooling benefits of GSI to prioritize the placement and type of GSI. The framework was applied to a case study in Port Phillips in Melbourne, AU, and the results were presented to a group of stakeholders during a workshop. The participants of the workshop recognized the utility of the approach in prioritizing neighborhoods but highlighted its lack of consideration of the multi-functionality of GSI. Finally, the workshop participants highlighted the implementation challenges associated with competing factors (e.g., high priority locations for GSI with underground electrical and water utility lines) and interactions between private and public spaces.

Previous studies have shown the importance of using planning methods that consider both small-scale impacts and larger-scale socio-ecological issues (Demuzere et al., 2014; Norton et al., 2015; Cheng, 2016; Jefferson et al., 2017; Kuller et al., 2017; Meerow et al., 2016a & 2017). In particular, they showed how spatial planning of GSI can be guided by disparities in different communities' abilities to mitigate the impacts of climate change. Furthermore, they have provided a much-needed conceptual framework for integrating the concept of vulnerability into decision making. Nevertheless, these studies have limited quantification of vulnerability to a specific

system and a particular hazard. Moreover, these studies have limited prioritization analyses to the spatial scale of neighborhood/Census Tract and a specific type of GSI (i.e., trees). If GSI is to be planned as a climate risk mitigation strategy, its prioritization must consider the full range of GSI benefits to the entire socio-ecological system. Moreover, it should consider the potential tradeoffs among benefits provided by different types of GSI under different hazard mitigation goals. Furthermore, with the exception of Locke et al. (2013), who attempted to consolidate stakeholder opinions by taking the mean of the results, most approaches have neglected potential impacts of opinions from multiple stakeholders (e.g., competition for space when considering multiple hazards and different types of GSI).

In order for GSI to be more widely adopted and implemented, recent studies have suggested that GSI planning tools should allow different groups of stakeholders to consolidate their different definitions of GSI and assess their planning objectives within their distinct institutional and administrative boundaries (Matthews et al., 2015), while translating the information gathered from the analysis across multiple scales. Furthermore, it has been argued that the use of planning tools that allow for the conceptualization of GSI as climate adaption strategies within a *"learn-by-doing"* framework might be the most suitable strategy to enable large-scale implantation of GSI (Matthews et al., 2013 & 2015). Additionally, studies have suggested the need for development of new frameworks that conceptualize cities as socio-ecological systems composed of a continuous matrix of multifunctional landscapes, including their synergistic interactivity (Lovell et al., 2013).

1.3 Contributions and thesis outline

Participatory and integrated assessment of GSI projects at multiple scales remains one of the grand challenges for their effective implementation (Matthews et al., 2015; Kuller et al., 2017). Previous approaches for prioritizing GSI have predominately only considered GSI stormwater management benefits. Furthermore, previous studies have only focused on the evaluation of a specific type of GSI and have ignored the synergies and tradeoffs among GSI multifunctionality. The primary objective of this work is to begin addressing these limitations through a new spatially scalable analytical framework (Figure 1.1) that uses socio-ecological vulnerability for prioritizing locations and types of GSI installations in urban settings. The framework considers the multiple benefits offered by different types of GSI and, more importantly, prioritizes GSI implementation by considering the geo-location of communities in most need of the GSI benefits (i.e., the most

vulnerable communities). The proposed framework achieves these objectives by integrating three primary components: (1) identification of vulnerable communities for which GSI would provide the greatest benefits, (2) identification of suitable sites for different types of GSI, considering local regulations and design criteria, and (3) a multi-criteria evaluation to explore spatial tradeoffs and synergies associated with the potential benefits of GSI.

The first step of the framework quantifies the vulnerability of different components of the urban system (i.e., social, ecological, and infrastructure). This is achieved by aggregating susceptibility indicators that represent vulnerabilities associated with different hazards. The method then combines these vulnerability scores into a relative vulnerability index (RVI) with different degrees of vulnerability (e.g., high, medium, low) in each area. Using screening rules associated with different design criteria and planning regulations, the methodology then identifies areas with the greatest suitability for GSI implementation. Lastly, a spatially scalable optimization approach is used to maximize the multifunctionality of these different locations and types of GSI project when considering multiple objectives (e.g., reducing flash flooding risk while increasing ecologic connectivity). The proposed framework uses a graph-based approach with a simplified distributed hydrologic model and mixed-integer linear programming to execute a multi-objective optimization to maximize potential delivery of GSI benefits to the most vulnerable areas. The framework can also incorporate opinions of multiple stakeholders by specifying varying importance to the mitigation of different hazards, weighting given to socio-ecologic systems, and preferences associated with GSI types and their geo-locations.

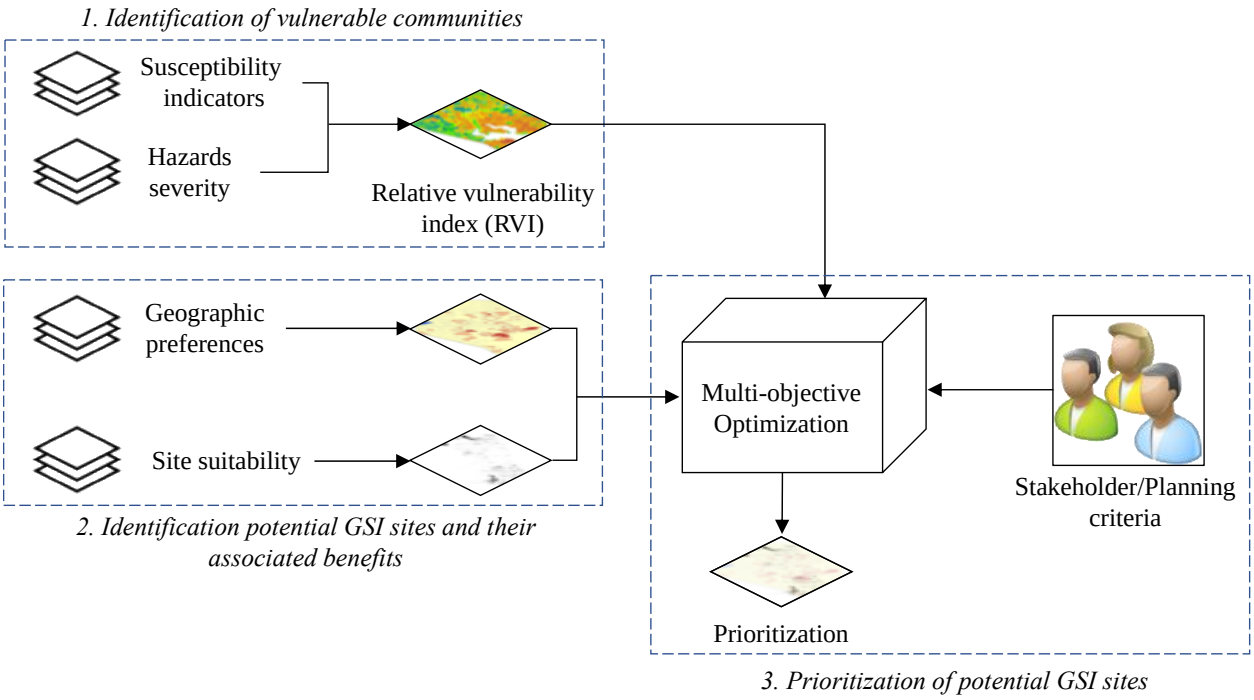

Figure 1.1: Conceptual overview of the GSI prioritization framework.

1.3.1 Thesis outline

To implement and test the framework given in Figure 1.1, several research questions are addressed:

- How should vulnerability be defined and quantified within the context of GSI planning?
- How should the multiple benefits of GSI be spatially quantified and represented?
- How can this information be integrated in a multi-criteria analysis to inform the spatial planning of GSI at multiple scales?

The first question focuses on whether current approaches for quantifying socio-ecological vulnerability can be used for spatial planning of GSI. Traditional methods used for quantification of social susceptibility create disconnects between the spatial scale at which GSI projects are planned (e.g., city blocks, tax lots, or small watersheds under 2-10 km^2) and the spatial scale used for quantifying vulnerability (Carr et al., 2015). As such, the work presented in Chapter 2 explores how current approaches for the quantification of social susceptibility may have limited the delivery of GSI to the most vulnerable communities by misdiagnosing the spatial correlation of vulnerability and using spatial units of analysis that can produce large variabilities in the final

results. To address these challenges, this chapter also presents a new analytical framework that downscales the vulnerability indicators to site scale (i.e., 10 m) and associates the vulnerability indicators with the potential benefits of GSI. The chapter concludes by presenting a spatial analysis of the most common spatial patterns of socio-ecologic vulnerability in four cities in the United States and their potential implications for spatial planning of GSI.

Having an approach for quantifying vulnerability, the second research question focuses on how the potential benefits of GSI to reduce vulnerability could be spatially quantified. Thus, in Chapter 3, the concepts of "service-benefiting" and "service-needing" areas (Fisher et al. 2009) are adopted to relate the multiple benefits of GSI to the vulnerability of socio-ecologic systems. This framework is then used to explore the spatial patterns of vulnerability and current GSI installations in the City of Philadelphia, PA. The goal of this chapter is to: (1) demonstrate the utility of the method as a planning tool and (2) better understand the extent to which vulnerable communities have benefited from the installation of GSI projects. These analyses provide insight into the potential limitations of current GSI planning's delivery of benefits to the most vulnerable communities.

Chapter 4 then presents a spatially scalable prioritization framework that optimizes the potential delivery of GSI benefits to the most vulnerable communities, building upon the knowledge gained in previous chapters. The framework spatially relates GSI mitigation potentials to vulnerability levels of different communities using the methods developed in Chapter 2 to identify the most vulnerable communities and the methodology presented in Chapter 3. The primary contribution of this chapter is the development of a multi-objective optimization framework that uses a graph-based approach with a simplified distributed hydrologic surrogate model and mixed-integer linear programming to maximize the potential delivery of GSI benefits to the most vulnerable areas. The framework is applied to three watersheds within the City of Baltimore, MD, the City of Philadelphia, PA, and the City of Dallas, TX, to test the utility and robustness of the prioritization method in diverse hydro-climates and explore the locations and distributions of different types of GSI at multiple scales. Furthermore, the impacts of different weights representing different hazard mitigation goals and/or planning criteria (i.e., different opinions from stakeholders) are explored. The chapter concludes with a discussion of the potential implications of the observed patterns on future planning and design of GSI.

Finally, Chapter 5 concludes the dissertation by summarizing the most significant findings of this work and discussing its limitations. Moreover, future research questions are proposed to guide further development of advanced tools and methods for quantifying GSI benefits and enable more integrated assessment and a participatory planning process.

CHAPTER 2. QUANTIFICATION OF SOCIO-ECOLOGICAL VULNERABILITY WITHIN A GREEN INFRASTRUCTURE PLANNING FRAMEWORK

2.1 Introduction

If green stormwater infrastructure (GSI) is to be used as a climate adaptation strategy, it is important that its spatial planning and design be considered within a vulnerability framework. To do so, the urban landscape needs to be conceptualized as a socio-ecologic system and consider the potential impacts that GSI could have on improving sustainability and resilience. Therefore, in this chapter we explore the literature on socio-ecologic vulnerability to investigate the following question: How should vulnerability be defined and quantified within the context of GSI planning?

The conceptual use of vulnerability, particularly of social vulnerability, to make informed planning and design decisions has been in practice for decades (Fekete, 2009; Burton, 2010; Zebardast, 2013; Guillard-Gonçalves et al., 2015). Particularly in the hazard and socio-environmental justice literature, the concept of vulnerability has often been presented as the risk of being exposed to a certain hazard severity (Fekete et al., 2010; Burian et al., 2013; Carr et al., 2015). More recently though, the definition of vulnerability has been expanded to include not only the risk of exposure to a hazard, but also the susceptibility and resilience of the exposed system (Cutter et al., 2003; Cutter & Finch, 2008; Damm, 2010; Kappes et al., 2012). Conceptually, resilience is often defined as the capacity of the system to adapt to or recover from a shock introduced by exposure to a stressor (Cutter et al., 2008; Meerow et al., 2016a & 2016b). On the other hand, susceptibility represents the intrinsic properties of the system that increase the likelihood of harm or loss when exposed to a stressor (Cutter et al., 2003; Kappes et al., 2012). Within this new conceptual definition, vulnerability is thus seen as a combination of risk of exposure to a hazard and the capacity of the system to remain undisturbed and/or quickly recover to its original state (Turner II, 2003a & 2003b; Kappes et al., 2012; Carr et al., 2015).

This reframing of the concept of vulnerability has brought challenges associated with its quantification. Particularly, the quantification of susceptibility and resilience has received a lot of attention in the last two decades (Tate, 2013; Carr et al., 2015; Meerow et al., 2016a & 2016b). Quantification of the probability of being exposed to a certain hazard severity (e.g., flooding return period) is a scientific exercise in which physical models and statistical tools used to predict exposure risk can be validated by the use of abundant historic data. However, there are currently

no models that can capture the complexities associated with intra- and inter-dependencies of socio-ecologic systems. More importantly, there are very little to no data to validate these vulnerability quantification methods (Bakkensen et al., 2017). Given these limitations, vulnerability quantification methods have concentrated on the identification of proxy metrics that attempt to capture the most critical characteristics associated with the susceptibility and resilience of socio-ecologic systems.

To date, most vulnerability quantification approaches predominantly rely on the use of indicators (i.e., hazard risk, susceptibility, and resilience). Traditionally, these assessments use a composite index (metric) to represent the *relative* vulnerability between different areas/communities in the system (i.e., the likelihood that a community will suffer more harm or loss when compared to another). This concept of relative vulnerability is used in the absence of validation data to create and/or corroborate the "*true"* degrees of vulnerability and the complexities associated with capturing cause-effect relationships and/or inter-system dependencies. Instead, the assumption is that given a spatial extent, one can identify areas that are more vulnerable than others. To create these relative vulnerability indices, a list of susceptibility and resilience indicators (e.g., for flooding, preparedness, awareness, and travel time) is aggregated into a single metric and associated with a hazard severity level. Using these metrics, different ranking/ordering approaches are then used to assign a nominal degree (e.g., low, moderate, high) of vulnerability. These vulnerability indicators simplify the complexities associated with quantifying system vulnerability, thus making vulnerability a more understandable and accessible concept to decision makers (Turner II, 2003b; Cutter & Finch, 2008; Damm, 2010; Locke et al., 2013; Norton et al., 2015).

However, the data, the spatial scale of analysis, and the method of aggregation/quantification of vulnerability indices have varied between quantification methods. Moreover, very often the definition of vulnerability itself has been drastically different, where the concept has been used to describe the marginality, adaptability, susceptibility, fragility and/or risk of the system to some threat, which is sometime "hypothetical" (Füssel, 2007). Furthermore, traditional approaches for quantifying vulnerability have failed to consider the spatial scale at which disaster risk-reduction interventions are designed and implemented (Carr et al., 2015).

These limitations have been shown to produce incomplete explanations of the variance in vulnerability outcomes and have suggested a risk of misdiagnosing community-specific

vulnerability and the effects of different intervention programs (Cutter & Finch 2008; Schmidtlein et al. 2008; Carr et al., 2015). This spatial attribution problem (i.e., where the sources of information or conceptualization do not align with the spatial scale and needs of those using the information [Birkmann et al., 2010; Fekete et al., 2010]) has been particularly prevalent in methods used for the quantification of social vulnerability (Fekete et al., 2010; Carr et al., 2015). Social vulnerability has been defined as the characteristics of the population that influence the likelihood of loss given a particular event. These characteristics are often associated with limited access to resources and political power, social capital, beliefs and customs, physical limitations of the population, and different characteristics of the built environment (Cutter et al., 2003; Schmidtlein et al., 2008). As such, social, economic, demographic, and housing data are often used to construct social vulnerability indicators. Because these data are often collected within administrative boundaries (e.g., county, U.S. Census Tracts) the spatial scale of analysis used to inform infrastructure planning and design decisions is often limited to those boundaries.

Depending on how large the discrepancy between the spatial resolution at which the data are available and the spatial unit of analysis of infrastructure projects (e.g., a watershed), correctly assessing where and what disaster-risk reduction interventions are most urgently needed can become very challenging and, more importantly, assessing who will be the beneficiaries of their implementation. To be effectively implemented, GSI is typically designed and constructed at small spatial scales (e.g., city parcel, tax lot, or subwatershed of 0.01-10 km^2) (Golden et al., 2017; Jefferson et al., 2017). This is because its engineering design depends on the calculation of fine-scale rainfall-runoff estimates in order to ensure an efficient and acceptable performance (e.g., flood mitigation goal, nutrient reduction threshold). In addition, it has been argued that many of the co-benefits associated with GSI (e.g., increase in productivity, reduction in stress, improved air quality, and urban heat island mitigation) only affect people that are in close proximity (e.g., distances less than 1.6 km [~1 mile]) (Lee & Maheswaran, 2011; James et al., 2015). Thus, if the concept of vulnerability is to be used to identify communities in need of GSI benefits, the quantification of social susceptibility should be done at the smallest spatial resolutions at which the data are available.

The objective of this work is to address these limitations through the development of a new method for quantifying social susceptibility at the smallest resolution for which data are available (i.e., Census Blocks). More specifically, this study seeks to evaluate the variability in the social

susceptibility indicator (SoSI) due to the use of dasymetric mapping techniques (i.e., areal aggregation/disaggregation) and different methods used for its calculation. The hypothesis to be tested is that the use of smaller scales of analysis will result in lower sensitivity to the calculation method, but a higher sensitivity to data uncertainty. Moreover, it is expected that calculation of the indicator at different spatial scales will result in changes to spatial patterns of vulnerability and better identification of the most vulnerable communities.

The method is applied to four cities in the United States to test the reproducibility of any observed changes in the variability of the social susceptibility indicator. This also allows investigation of the applicability and utility of the proposed framework to show common trends in spatial patterns of vulnerability in different regions.

2.1.1 Related work

Although there is neither a single definition nor a single measure of social susceptibility, the social vulnerability index (SoVI), introduced by Cutter et al. (2003), has been one of the most widely accepted and used (Fekete, 2009; Burton, 2010; Zebardast, 2013; Guillard-Gonçalves et al., 2015). SoVI is a metric composed of different indicators that represent a community's ability to respond to, cope with, recover from, and adapt to environmental hazards. Note that while Cutter et al. (2003) and others have defined and used SoVI as a metric to quantify vulnerability, they assume an equal probability of exposure to *any* environmental hazard. Under the most recent conceptual definition of vulnerability, this metric more suitably represents the susceptibility and/or resilience of a community. In this study, vulnerability is defined as a combination of the ordinal values that represent hazard exposure risk and susceptibility. Having noted this distinction, in this study SoVI will be referenced as the social susceptibility indicator (SoSI).

Particularly in the United States, the SoSI has been used and integrated in many studies and urban planning methods and for different purposes ranging from disaster planning to socio-environmental justice. For example, SoSI has been applied to compute the relative vulnerability of different populations under alternative infrastructure scenarios and to prioritize the location of new trees in urban settings (e.g., Jones & Andrey, 2007; Cheng, 2013; Tate, 2013; Norton et al., 2015; Cheng, 2016; Meerow et al., 2017). However, to date, the use of the SoSI as part of infrastructure planning and prioritization assessments has been very limited due to a lack of data for validation and variability of the results as a consequence of methodological choices (Jones &

Andrey, 2007; Tate, 2013; Carr et al., 2015). Furthermore, while previous studies have had an appropriate spatial scale of analysis (i.e., counties and Census Tracts), the discrepancy between the spatial scales at which SoSI has been calculated and analyzed and the spatial resolution needed to effectively plan and design GSI (e.g., small neighborhoods of 5- 6 street blocks) has been identified as a limitation (Birkmann & Von Teichman, 2010; Carr et al., 2015).

Openshaw & Taylor (1979) identified the *scale problem* and the *aggregation problem* as part of the Modifiable Areal Unit Problem (MAUP) of a aereally aggregated data at different scales. The scale problem refers to the ecological fallacy in which the scales of analysis change the relationship between the studied variables. The aggregation problem refers to the fact that this relationship between the variables can be equally likely from the intrinsic relationship between the variables or a product of the aggregation scheme. Current methods used for the construction and utilization of the SoSI suffer from both of these problems. As such, quantifying the impact of different methodological choices and the use of different spatial scales on the variability of the SoSI have been the primary focus of past studies.

As an initial step to address some of these problems, previous studies have concentrated on quantifying the sensitivity of the SoSI to different construction methods and its application at different spatial scales and in different geographic contexts. Jones & Andrey (2007) provided a critical review on the methods used for construction of the SoSI and were among the first to show their impact on the resulting indicators of relative vulnerability. Schmidtlein et al. (2008) evaluated the sensitivity of the SoSI to changes in its construction, the spatial scale at which is applied, and different geographical contexts. Their results demonstrated that the predominant factor influencing the variability of the results is the manner in which the components of a principal component analysis (PCA) are combined to create the final index value. Additionally, the authors found that a decrease in the scale of aggregation caused a decrease in the variability of the data explained by the PCA, and increased the variance of the resulting SoSI indexes.

Tate (2012) performed a sensitivity analysis on the change in final SoSI ranking using different structural designs and analysis of scale within a Monte Carlo simulation framework. The analysis suggested that the structural designs and scales accounted for 58 to 86% of the variance in the results. Most recently, Tate (2013) performed a very similar analysis with different construction methods and spatial scales. The results showed a high magnitude of uncertainty and

statistical bias in areas of high vulnerability. Additionally, the results suggested that the selected weighting scheme had the most influence in the uncertainty/variance of the final results.

To date, none of these previous studies has explored the sensitivity of the SoSI to the use of dysametric methods that allow calculation at smaller scales than Census Block Groups and the impact of data uncertainty at these smaller scales (i.e., American Community Survey, 2012). Nor have they evaluated the impact that the observed variability in SoSI could have on spatial patterns associated with another metrics (e.g., hazard exposure). This lack of understanding of the variability of social susceptibility indicators at smaller scales deters its use for local decision making (Birkmann & Von Teichman, 2010; Carr et al., 2015).

2.2 Methodology

The methodology used in this study consists of three main components: (1) calculation of the SoSI using the new method (Section 2.2.1), (2) aggregation of indicators to represent infrastructure susceptibility, ecological integrity, and hazard exposure severity associated with flooding and urban heat island (Section 2.2.2); and (3) spatial analysis of the variability in socio-ecologic vulnerability (Section 2.2.3).

2.2.1 Quantification of social susceptibility

The proposed approach to computing the SoSI follows the methods used in most previous studies but introduces a new uniform dasymetric mapping to populated areas as a way of transferring information about susceptibility between spatial scales. The method used to construct the SoSI largely consists of 5 main steps: (1) selection of model structure, (2) selection and data collection for the indicators, (3) transformation and normalization of the input data, (4) weighting and aggregation methods to combine the data into a single metric, and (5) allocation of the SoSI results to a set of vulnerability classes (i.e., ranking scheme). However, as will be discussed in Section 2.2.1.5 below, in this study the aggregation of the indicators differs from previous studies by using data collected at different spatial scales. The choices made by the index developer in each of these steps involve conceptual assumptions and have been demonstrated to have significant impacts in the final rankings of vulnerability (Jones & Andrey, 2007; Tate, 2013). Figure 2.1 presents an overview of these steps and the variability analysis implemented in this work.

In this section, some of the most common approaches used in each of these steps are highlighted, including their conceptual and/or theoretical assumptions. For a more detail discussion and review of the steps and assumptions used to quantify social susceptibility, the reader can refer to Jones & Andrey (2007), Schmidtlein et al. (2008), and Tate (2012 & 2013).

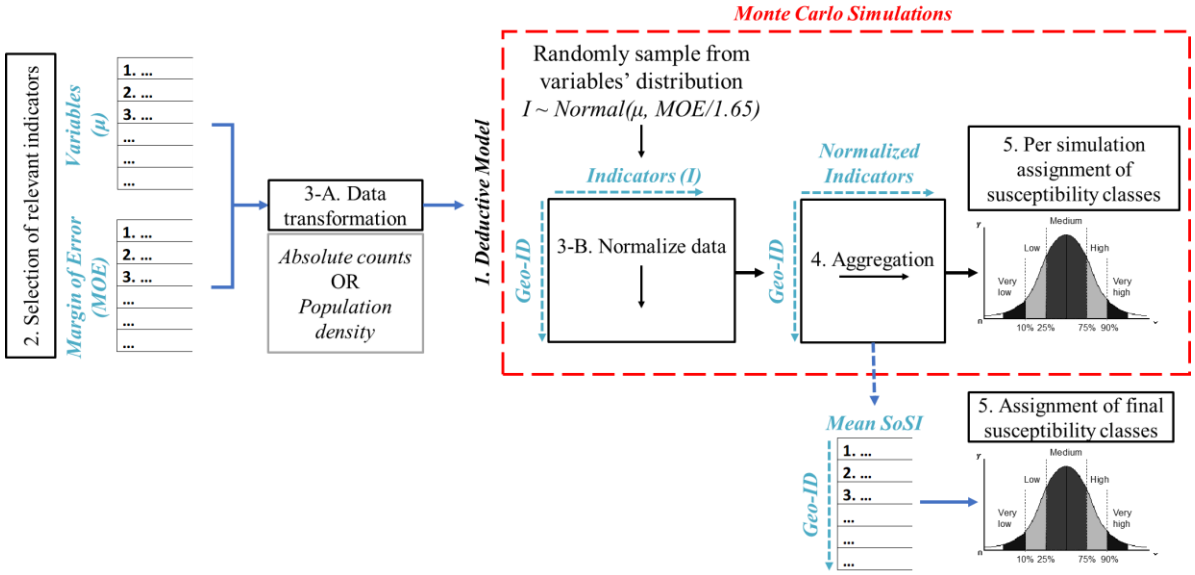

Figure 2.1: Overview of steps used to calculate the SoSI and assess its variability to different methodological choices. Geo-ID refers to the unique identifiers assigned to Census Blocks and Census Block Groups.

2.2.1.1 Model selection

The process of quantifying social susceptibility begins by selecting a model to be used to represent vulnerability. The deductive model (Tate, 2013), which commonly uses a short (e.g., 10) list of variables that are normalized and combined to obtain the social susceptibility indicator, is selected for this work. This model was chosen because it is the most widely used, because of its ease of implementation and interpretation, and because of the flexibility it provides to add/remove variables. Some studies have raised concerns that the deductive model introduces double counting (Cutter et al., 2003; Tate, 2012 & 2013), which is the idea that results might be biased towards populations for which more than one variable is highly correlated. This study argues that double counting is not a significant limitation when the intended use is to inform the prioritization of GSI projects. This reasoning stems from the idea that all things being equal, populations with a higher susceptibility in one indicator should be deemed as such even if highly correlated with other

indicators. This assumption seems reasonable given the lack of supporting literature and lack of consensus to justify assigning relative importance to the different indicators, which would be necessary for methods such as PCA. Furthermore, because the data used in this study is collected at different spatial scales, the existence of this correlation might be beneficial in transferring social susceptibility information between scales. Nevertheless, in an effort to reduce this problem, attention was paid to the selection of the indicators such that a similar number of indicators represents each dimension of social susceptibility.

2.2.1.2 Selection of indicators

The objective of the indicator selection step is to choose a set of indicators as proxy metrics of the multidimensional and complex dimensions of social susceptibility. The major considerations in the selection of indicators are: (1) the dimensions of vulnerability that are intended to be represented when combined with the exposure to a hazard, (2) the correlation between indicators, and (3) the availability and cost of obtaining the data. When selecting indicators, one must consider whether these are related to the susceptibility of people when exposed to the hazard(s) of interest. For example, while a variable such as "air conditioning in home" is relevant to calculating the vulnerability to extreme heat, it is not relevant when considering the exposure to flooding. Additionally, consideration must be given to how these indicators were collected as it might not be possible to spatially aggregate/ disaggregate to other spatial units. The availability of the data and its uncertainty often play a major role in which indicators are finally selected.

The social susceptibility indicators used in this study are presented in Table 2.1. These are the most common indicators used in studies of social susceptibility to multiple hazards, particularly flooding and extreme heat events, the two hazards for which GSI is most often used as a mitigation strategy. The data used to calculate the indictors are collected from the U.S. Census and the American Community Survey at three different spatial scales: Census Tracts, Census Block Groups, and Census Blocks. Census Blocks are the smallest spatial unit at which the U.S Census reports its decennial data and thus represent the smallest scale of analysis that could be used to calculate the SoSI (U.S. Census SF1, 2010). Census Block Groups have been used in some of the most recent sensitivity studies and thus serve as a base of comparison to the results at the smaller scale of Census Blocks. Lastly, Census Tracts are statistical subdivisions of counties, having population sizes between 2,500 and 8,000 people[2].

It should be noted that the social susceptibility indicators are collected only at the spatial scale(s) for which a representative sample of the population can be obtained. While Census Blocks provide total counts of demographic data (i.e., total number of people or households), at this level the dissemination of data related to wealth, health, and education are limited due to privacy concerns. Therefore, these data are collected at the Census Block Group and Census Tract levels for which a more representative sample of the population is available.

Table 2.1: List of social susceptibility indicators with their respective cardinality, data sources, and spatial resolution.

			Spatial Resolution			Source	
System	Indicators	Cardinallity	Blocks	Block Groups	Tracts	SF1	ASC5
Social vulnerability (SoVI)	Total Population	+	✓	✓		✓	
	% Population under 5 yrs	+	✓	✓		✓	
	% Population over 60 yrs	+	✓	✓		✓	
	% of Females	+	✓	✓		✓	
	Median Age		✓	✓		✓	
	White alone		✓	✓		✓	
	% Black or African American	+	✓	✓		✓	
	% American Indian and Alaska Native	+	✓	✓		✓	
	% Asian	+	✓	✓		✓	
	% Native Hawaiian and Other Pacific Islander	+	✓	✓		✓	
	% Hispanic or Latino	+	✓	✓		✓	
	Number of housing units	+	✓	✓		✓	
	Number of occupied housing units	+	✓	✓		✓	
	Number of vacant housing units	-	✓	✓		✓	
	Number of housing units- owned with a mortgage or a loan		✓	✓		✓	
	Number of housing units - owned free and clear		✓	✓		✓	
	Number of housing units - renter occupied	+	✓	✓		✓	
	Mean person per household	+	✓	✓		✓	
	% of occupied housing units	+	✓	✓		✓	
	Family households: Female householder, no husband present	+	✓	✓		✓	
	Nonfamily households: Female householder, no husband present	+	✓	✓		✓	
	Institutionalized population - Nursing	+	✓	✓		✓	
	Household Income - >= $100,000	-		✓			✓
	Per capita income in the past 12 months	-		✓			✓
	Median family income in the past 12 months	-		✓			✓
	Median gross rent	-		✓			✓
	Median gross rent as a percentage of household income	+		✓			✓
	Median Value (Dollars) for Owner-Occupied Housing Units	-		✓			✓
	Median contract rent	-		✓			✓
	People with education <= 12 high school diploma	+		✓			✓
	Median number of rooms	-		✓			✓
	Mobile home	+		✓			✓
	No vehicle available	+			✓		✓
	Income in the past 12 months below poverty level	+			✓		✓
	People with a disability	+			✓		✓
	Women who had a birth in the past 12 months	+			✓		✓
	Unemployed people	+			✓		✓
	English Proficiency (Less than very well)	+			✓		✓

**SF1 – U.S. Census Summary File 1, 2010 [www.census.gov/2010census/news/press-kits/summary-file-1.html].*

**ASC5 – American Community Survey 5-year estimates, 2012 [www.census.gov/programs-surveys/acs/guidance/estimates.html]*

2.2.1.3 Transformation of the data

The next step in the process of constructing the indicator is to consider whether the data will be transformed or not. The two most common transformations used to date are the absolute count or the use of a relative proportion of the population. An *absolute count* refers to the use of the total population count associated with a particular socio-economic characteristic and the assignment of its corresponding cardinality (i.e., +/- add or reduces susceptibility as the value of the variable increases). For example, when examining the indicator for age one might consider higher counts of older populations to represent a higher level of susceptibility. On the other hand, a higher total count of the population in private residences might represent a lower level of susceptibility. The transformation of the data using *relative proportion* divides the total count by a normalizing value and is intended to represent the relative disadvantage between population groups. The two most common metrics used to create relative proportions are the total population in the area of study and population density (i.e., total count of people per area). Because of the popularity of these two transformation methods (i.e., absolute counts and population density) in the literature and the documented impact they can have on the final values of the SoSI, both of them are considered in the analysis of variability.

2.2.1.4 Normalization, aggregation, and ranking

The last three steps of the process include the normalization (also known as standardization) of the indicators to a dimensionless scale (i.e., normalization), the aggregation of these into a single metric and the assignment of some ranks or categorical values intended to represent different levels of susceptibility. In order to understand the impact of different methodological choices on social susceptibility at the smaller scale of Census Blocks, the following normalization methods are considered: linear scaling (i.e., min-max), standard score (i.e., z-score) and ordinal values (i.e., percentiles) (Schmidtlein et al., 2008; Tate, 2013). The aggregation methods considered in this work include the summation of the normalized values (sum) and the weighted summation of susceptibility categories (i.e., wrank). In the wrank method, susceptibility categories (i.e., normalization by using nominal values) are assigned to the raw data and then a weighted sum is computed of the total number of indicators that are assigned the same nominal category. The SoSI value for spatial unit *i* is thus calculated by:

$$SoSI_i = \sum_{j=C_{min}}^{C_{max}} \frac{C_j}{C_{max}} * X_{C_j} \quad (2.1)$$

where C_j represents the nominal degree of social susceptibility (e.g., Low = 2), C_{max} represents the maximum nominal value that could be assigned (e.g., Very High = 5) and X_{Cj} represents the total number of indicators that received a nominal value equal to C_j when using the ranking scheme on the raw data.

The wrank method seeks to reduce the problems of sensitivity to outliers present when using multiplication methods, and to reduce the issues of compensability (i.e., low values in one indicator can mask high values in another) associated with summation. However, because of the use of nominal categories, the method produces a loss in the measurement of relative differences, and thus a loss of information, and continues to use the assumption of interaction (i.e., all groups behave statistically similar) used by previous methods.

Finally, the assignment of categorical levels of susceptibility uses the percentiles of the resulting SoSI. As such, the resulting SoSI values are allocated to susceptibly categories defined as: (1) Very low ([0%- 5%]), (2) Low ([10%-25%]), (3) Moderate ([25%-75%]), (4) High ([75%-90%]) and, (5) Very high ([90% - 100%]).

2.2.1.5 Spatial disaggregation

This work proposes a modification to prior work with a spatial disaggregation method that allows the use of data collected at different spatial scales. Spatial disaggregation, most commonly known as dasymetric mapping, is a technique used to distribute attribute data more accurately within a larger or arbitrary area unit by the overlay of geographic boundaries that exclude, restrict, or confine the attribute in question[1]. The techniques are more often used for the spatial redistribution of population counts from the spatial areas at which the data were collected, or source zones (e.g., Census Tracts), to smaller areal units that usually fall within boundaries of the source zone (i.e., target zones) defined by smaller administrative boundaries (e.g., city parcels or tax lots). Dasymetric methods have varied from the use of simple areal weighting estimations that

[1] Retrieved February 22, 2016 from: http://support.esri.com/en/knowledgebase/GISDictionary/term/dasymetric%20mapping

use land cover as ancillary data to the use of probabilistic models that make use of different data sources for the total population counts and an array of ancillary datasets (e.g., land cover, residential point data, tax lot datasets, etc.) (Su et al., 2010; Nagle et al., 2014).

In this study however, the proposed spatial disaggregation method is much simpler. Rather than redistributing population counts to the target zones, the corresponding SoSI associated with the source zone is assumed to be uniform in all populated areas of the target zones. In short, the SoSI is computed at the spatial scale at which the data are available, and the resulting values are assumed to be constant in all corresponding smaller areas that had a population count (see Figure 2.2 for reference).

Additionally, rather than using the area of land reported by the U.S. Census data, land cover data are used to calculate the total inhabited area. Inhabited area is assumed to be only those areas classified as *developed* (i.e., open space, low intensity, medium intensity and high intensity) in the 2011 National Land Cover Data (NLCD) from the U.S. Geological Survey (USGS). All other classes are assumed to be unpopulated regions. This approach assumes that all communities in the target zones have the same level of susceptibility associated with the indicator collected at the source zone. This assumption, while limited, does not produce biases or introduce uncertainties by using more complex dasymetric methods (Su et al., 2010; Nagle et al., 2014). For example, the method does not make assumptions about how to distribute the total count associated with the indicators, particularly those associated with minority groups (e.g., people with a disability).

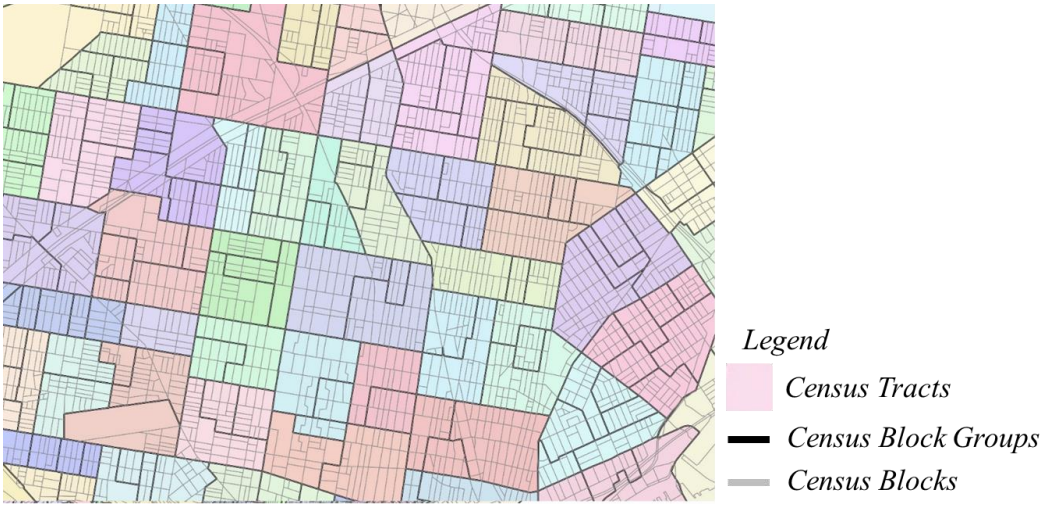

Figure 2.2: Spatial relationship of U.S. Census spatial units. SoSI values of the source zone are assumed to be uniform in all populated areas of the target zones.

2.2.2 Overview of vulnerability framework

The second component of the methodology relates the susceptibility of socio-, ecological- and infrastructure systems to multiple hazards, taking into consideration the potential benefits that GSI could offer as a mitigation strategy. Following a prior approach commonly used in risk-hazard assessments (Kappes et al., 2012; Carr et al., 2015), this study uses the relationship between exposure to a hazard and susceptibility of the exposed systems to define different levels of relative vulnerability. As such, the proposed approach has two primary components: (1) the aggregation of susceptibility indicators for social, ecological, and infrastructure systems, and (2) the designation and mapping of different levels of hazard severity.

The subsections below present descriptions and a table of indicators (Table 2.2) selected from the literature to represent the susceptibility of infrastructure systems, the ecologic integrity of the urban landscape, and exposure severity to the hazards of flooding and urban heat island. These indicators have: (1) good consensus about their significance to represent the intended dimension of vulnerability, and (2) a spatial scale of quantification that is similar or smaller than Census Blocks (i.e., a resolution of raster data). Additionally, the metrics represent the dimensions of the systems in which implementation of GSI could be beneficial (e.g., ecologic connectivity) and use commonly available data in most cities.

2.2.2.1 Ecological integrity / susceptibility

Some forms of GSI have shown great potential to address issues of ecologic susceptibility, also referred to as ecologic integrity (Chang et al., 2012; Lovell et al., 2013; Zhao et al., 2013). Ecological susceptibility is a complex, often case-specific, concept with many definitions and no standard set of metrics for its quantification. Broadly defined, it refers to the capacity of the ecosystem to withstand and adapt to stressors over time and space (Williams & Kapustka, 2000). The concept of ecological susceptibility has been applied extensively in many land conservation planning and watershed policy studies. In these previous studies, the quantification of ecosystem susceptibility has often concentrated on measuring exposure to hazards that threaten the integrity of ecosystems and/or habitat integrity at various scales of species organization (for a detailed review, refer to De Lange et al., 2010). As such, many of these studies have been conducted at a regional scale and have considered long time periods (i.e., months to decades).

The potential benefits of GSI to the ecosystem are however much more localized (Weber et al., 2006; Chang et al., 2012; Tannier et al., 2012; Yu et al., 2012; Tannier et al., 2016). The use of GSI to increase ecological connectivity and restore habitat integrity has often been cited (Tzoulas et al., 2007; Chang et al., 2012; Yu et al., 2012; Zhao et al., 2013). Ecologic connectivity is broadly defined as the degree to which the landscape facilitates or impedes the movement of natural resources and species, considering both structural and functional connectivity. Functional connectivity takes into account the behavior of the species, while structural connectivity is used to define the spatial configuration of habitat patches. Given the diversity of species that one could consider in the urban landscape, the indicators selected in this study focused only on metrics for structural connectivity (Mallarach et al., 2006; Chang et al., 2012; Yu et al., 2012; Meerow et al., 2017). More specifically, the metrics selected are intended to represent the level of connectivity between ecologic cores, their habitat integrity and the resistance of the landscape to facilitate its connectedness (McRae et al., 2008; Shirk & McRae, 2013).

In addition, when GSI is implemented within riparian areas, it has shown potential to improve the health of aquatic ecosystems in streams and large water bodies (Zhao et al., 2013). Moreover, many municipalities today have implemented GSI with the primary objective of complying with restrictions on pollutant loads from stomwater runoff (e.g., MS4 permits). Therefore, an additional set of indicators is also included that identify water bodies susceptible to significant increases in pollutant load due to stormwater runoff. These indicators include water bodies with a large percentage of impervious drainage area and/or streams close to road intersections, as well as water bodies identified by the U.S Environmental Protection Agency (EPA) as impaired waters.

2.2.2.2 Infrastructure susceptibility

Unlike ecosystem and social susceptibility, the concept of infrastructure susceptibility has been well defined and various methods exist for its quantification. Infrastructure susceptibility refers to the ability of the infrastructure (the system or individual components) to withstand and/or absorb the shock of a hazard without compromising its structural integrity, without affecting human well-being, and while continuing to provide its intended functionality/service (Kappes et al., 2012; Evans et al., 2014; Mazzorana et al., 2014). As shown in Table 2.2, a basic list of indicators from the literature is used to represent both the structural and functional vulnerabilities

of buildings. The indicators represent characteristics of buildings associated with their structural vulnerability to flooding events and, critically, with their intended functions for human well-being.

Table 2.2: List of indicators for ecological integrity and infrastructure susceptibility

System	Indicators	Cardinallity	References
Ecological integrity (EcOS)	Normalized Difference Vegetation Index (NDVI)	-	Weber et al., 2006 De Lange et al., 2010 Tran et al., 2010 Zhao et al., 2013 Sherrouse et al., 2014 Behling et al., 2015 Tannier et al., 2016
	% of impervious surfaces near streams and wetlands (riparian zones) (i.e., buffers of 10m, 30m and 100m)	+	
	% of tree canopy near streams and wetlands (riparian zones) (i.e., buffers of 10m, 30m and 100m)	-	
	Barren land	+	
	Continous patches of tree canopy	-	
	Continous patches of impervious surfaces	+	
	% of roads buffers (Urparian zones) (10 m, 30 m, 100 m)	+	
	Impervious surfaces with slope > 3%	+	
	Landscape resistance to ecologic connectivity	-/+	
	NDBI (Normalized Difference Building Index)	+	
	Road crossing streams	+	
	U.S. EPA impaired waters	+	
Infrastructure susceptibility (InFraS)	Buffer zones around schools, hospital, community centers and nursing homes (i.e., 0.5 mi, 1 mi and 3mi)	+	Peduzzi et al., 2009 Jordan & Javernick-Will, 2012 Kappes et al., 2012 Evans et al., 2014 Mazzorana et al., 2014
	Year of construction of buildings (i.e., <1950 (highest vulnerability), 1950<year<1990, >1990 (lowest vulnerability))	+	
	Residential structures (i.e., homes, apartment complex, etc.)	+	
	Building with only one floor	+	

2.2.3 Hazard exposure severity

Among the most common hazards for which GSI has been used as a mitigation strategy are air quality, noise pollution, water quality, urban heat island, flooding, drought, wildfires, and human health problems (Demuzere et al., 2014; US EPA, 2018). Among all of these hazards, flash flooding, river flooding, and urban heat island (UHI) have been the primary hazards driving the implementation of GSI and are the focus of this work (Demuzere et al., 2014).

GSI has been shown to potentially mitigate flooding by reducing the velocity and volume of stormwater runoff, thus reducing the peak discharge from small to moderate rainfall events. For large storms, GSI has demonstrated mixed performance and thus often is not considered as a mitigation strategy (US EPA, 2014; Golden et al., 2017; Jefferson et al., 2017). Nevertheless, the reduction of impervious surfaces and the increase in infiltration and evapotranspiration associated with implementation of GSI has made flood mitigation one of the primary reasons for its implementation (Golden et al., 2017; Jefferson et al., 2017).

GSI has also been used as a mitigation strategy for the effects of UHI by replacing impervious surfaces, increasing infiltration rates, and providing shading (Norton et al., 2015; Park

et al., 2017). All of these benefits contribute to reduction in risk of mortality due to extreme heat and increase thermal comfort (Tzoulas et al., 2007; Wang et al., 2016; Pincetl et al., 2016; Park et al., 2017; Zhang et al., 2017).

To quantify the level of exposure and/or risk associated with each these hazards, there are many methods ranging from deterministic to probabilistic models (e.g., Demuzere et al., 2014; Kuller et al., 2017). However, most of these methods require very detailed data and their analytical capability on large spatial scales is often limited. A simplification that is often used is to employ a proxy measurement (e.g., land surface temperature to represent urban heat island) and/or assignment of different categorical values that represent the degree of exposure severity using risk thresholds commonly reported in the hazard literature. Given this study's scale of analysis and effort to use commonly available data, a simplified quantification method is implemented to represent different levels of hazard exposure severity. The subsections below discuss the steps used to construct the categorical severity values (0 – no exposure/risk, 5-maximun exposure/risk) for the hazards of flash flooding, river flooding, and urban heat island.

2.2.3.1 River flooding and flash flooding

The risk associated with exposure to river flooding is measured using the National Flood Hazard Layer (NFHL) from Federal Emergency Management Agency (FEMA) maps. NFHL FEMA flood maps assign a nominal value to the results of hydrologic modeling. Although deterministic and uncertain, these maps have been used extensively in assessing flood risk. The assigned categorical severity values used in this study follow general guidelines for assessing flood risks (Table 2.3).

The risk of exposure to flash flooding is measured using the modified version of the Flash Flooding Potential Index (FFPI) developed by the National Oceanic and Atmospheric Administration (NOAA) and National Weather Service (NWS) (Ceru, 2012; Zogg & Deitsch, 2013). This FFPI index indicates which areas are more likely to produce large and fast volumes of runoff. The index is generated using four empirical formulas that consider infiltration capacity of different soils, the land cover, and the topographic slope (Zogg & Deitsch, 2013).

However, the application of the FFPI in urban environments has been limited and it has typically been used to analyze large regions (e.g., counties or states). As such, the metrics do not account for differences in exposure risk between communities upstream and downstream of the

watershed outlet. Moreover, the metrics do not account for potential exposure to flash flooding in communities located near tributaries and small streams. In order to consider these criteria for application in urban watersheds, the index is modified in this work to include three additional indicators: the topographic wetness index, the height above nearest drainage, and the height above the watershed outlet.

The topographic wetness index (TWI) has been used in previous studies to identify flat areas with low infiltration and large drainage areas (Babbar-Sebens et al., 2013; Martin-Mikle et al., 2015; CMAP, 2017). The TWI is a steady state wetness index that is a function of the topographic slope and the drainage area. As such, areas with a high TWI value are more likely to experience high flow accumulation, and therefore a higher likelihood of flooding. The height above nearest drainage (HAND) has been used extensively to identify areas likely to experience flooding by accounting for the difference in elevation between an area within the watershed and the nearest stream (Nobre et al., 2011 & 2015; CMAP, 2017). Similarly, the height above the watershed outlet represents the higher likelihood of flash flood in communities near the watershed outlet versus those upstream. The inclusion of these two metrics accounts for local (i.e., HAND) and regional differences in exposure of downstream versus upstream communities.

One limitation of these two indicators (i.e., HAND and height above watershed outlet) is the need to delineate the watershed and/or have a good representation of the stream network. Furthermore, the indicators are a relative measure of potential to flood and thus are defined by the spatial extent of the analysis. To address these limitations, height above the outlet is calculated using the watershed boundaries delineated by the National Hydrography Dataset (NHD) with a hydrologic unit code of HUC12 and the height above nearest drainage is calculated using smaller watershed boundaries delineated by the ArcHydro Tool. Lastly, it should be noted that the transfer of water between watersheds is not accounted for when considering the height above the outlet. This could be considered a limitation as the HUC12 watersheds themselves have a relative risk to experience flooding. However, due to the large extent of the HUC12 as compared to the spatial extent of city limits, this assumption is considered reasonable.

Finally, the value of the FFPI is computed by adding the mean of the four equations in the NOAA FFPI to the TWI, HAND, and height about watershed outlet indices. The resulting FFPI values are then scaled 0-1 and the assignment of categorical severity values is defined as: (0) Very

low ([0%- 5%]), (1) Low ([10%-25%]), (2) Moderate ([25%-75%]), (3) High ([75%-90%]) and, (4) Very high ([90% - 100%]).

Table 2.3: Severity categories assigned to FEMA flood types.

Severity class	***Description***	***FEMA Codes***
Very high	1% annual chance flood	A, AE
High	River or stream flood	AO
Moderate	Shallow ponding	AH
Low	Increase flood risk due to development	AR
Very low (No risk)	No Flooding	X, B

2.2.3.2 Urban heat island

The risk of exposure to extreme heat caused by urban heat island (UHI) is measured using mean land surface temperatures (LST) as a representative metric. LST has been extensively used in previous studies to represent UHI and its relationship to land cover and urban form, as well as risk of exposure to extreme heat experienced by communities with different socio-economic profiles (Liu et al., 2011; Connors et al., 2013; Xu & Guo, 2014; Mirzaei, 2015). The mean LST temperatures are estimated using Landsat 8 data during the hottest months of the year (May to September) for multiple years in each city. The data are converted from radiance measurement of the satellite's infrared and red bands to LST (Liu et al., 2011; Connors et al., 2013; Xu & Guo, 2014). Additionally, the cloud coverage of any given dataset is limited to less than 5%. Lastly, categorical severity values are assigned using the maximum mean annual relative humidity (~ 60 to 70 %) for a particular city and the categories of extreme heat suggested by NOAA (Figure 2.3).

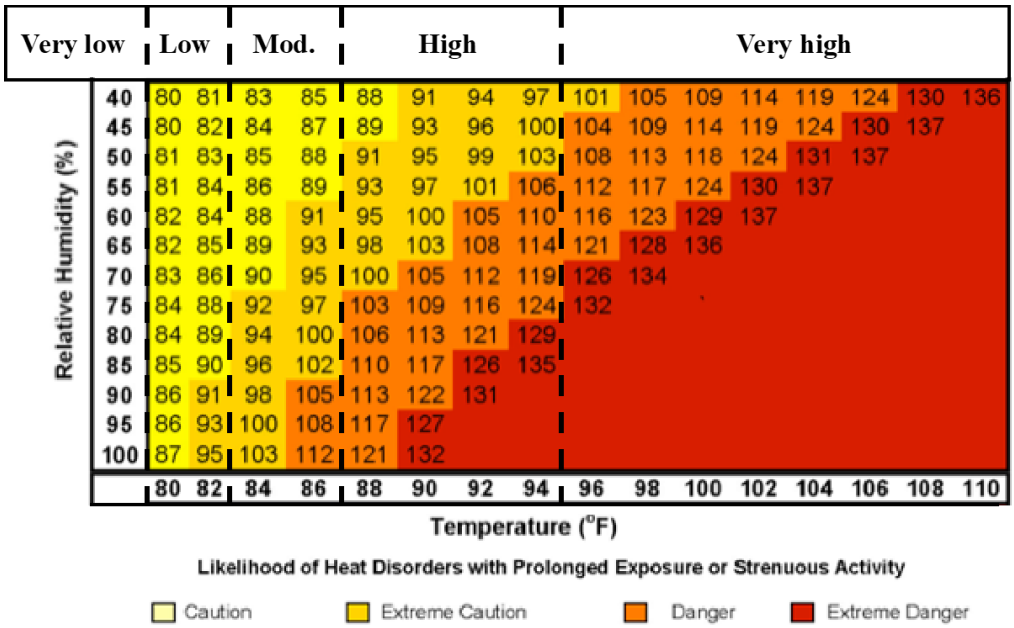

Figure 2.3: NOAA's heat index and exposure severity classes.

2.2.4 Variability analysis of social susceptibility

The last part of the methodology consists of: (1) assessing the variability of social susceptibility to the influence of data uncertainty and the use of different methodological choices for its construction, and (2) quantifying the variability in the spatial patterns of hazard vulnerability caused by using different spatial scales and handling of unpopulated areas in the SoSI calculation. Unpopulated areas are either considered to have very low social susceptibility or are excluded from the analyses.

The SoSI variability analysis uses a Monte Carlo approach for each of the 12 possible combinations of methodological choices presented in Table 2.4. The simulations are conducted by sampling data for each of the individual indicators associated with the ACS5 data, following guidelines for using the Margins of Errors (MOE) published by the 2012 American Community Survey (ACS) 5-year summary (refer to U.S. Census Bureau, 2009 for more details). During the sampling process, all indicators with negative values are replaced by a zero. A total of 500 simulations were used since the running average of all Census Block Groups and Census Blocks reached convergence at this value. Results of the variability due to methodological choices are analyzed by comparing the correlation between the resulting SoSI values. Lastly, the effects of

data uncertainty to the variability in the susceptibility categories are analyzed using the consistency of the category throughout all Monte Carlo simulations.

Table 2.4: Methodological choices considered in the SoSI variability analysis.

Data transformation	Normalization	Aggregation
Absolute	min-maz	equal weight sum (sum)
Population density	z-score	weighted ranks (wrank)
	percentiles	

In order to explore the impact of SoSI variability on the spatial patterns of vulnerability, a univariate and bivariate spatial autocorrelation analysis is performed using the method of Local Indicator of Spatial Association (LISA) (Anselin et al., 2006; Lloyd, 2006), with the spatial weights defined by queen contiguity (i.e., consideration of all immediately contiguous units/neighbors). The univariate analysis investigates the variability in spatial correlation of social susceptibility and the location of spatial clusters of highly susceptible communities. The bivariate analysis explores the spatial relationship of social susceptibility with the dependent variables of infrastructure susceptibility, ecologic integrity, and hazard severity exposure categories for urban heat island, river flooding, and flash flooding. The bivariate analysis uses the mean of the SoSI obtained from the Monte Carlo simulations for each of the respective spatial units of analysis and the average value of the dependent variables, calculated using the raster cells within each of the Census Block Groups or Census Blocks.

Lastly, particular consideration is given to the treatment of unpopulated areas. The LISA method uses the difference between the values in a defined neighborhood to their mean in order to calculate the spatial correlation. Therefore, the treatment of unpopulated areas as areas with no-susceptibility (i.e., null value) or very-low susceptibility (i.e., zero) can have significant impacts on the mean in these neighborhoods. More specifically, depending on the distribution of the dependent variable associated with these non-populated areas, the spatial autocorrelation can skew towards more positive or negative correlations, depending on whether these unpopulated areas are included or excluded from the analysis. This study shows the implications of using either of these two assumptions below.

2.3 Case studies and data – 4 cities

The proposed framework is applied in four US cities to explore the spatial patterns of vulnerability: Philadelphia, PA, Chicago, IL, Baltimore, MD, and Dallas, TX. These cities are selected to represent humid to semi-arid hydro-climatic regions that are more likely to use green features, as well as many of the different hazards for which GSI has been identified as a mitigation strategy. Furthermore, each of these cities has different institutional structures, policies and regulations that drive the urban form, and socio-economic and socio-ecological profiles, a needed diversity to assess the contributions of the study. Figure 2.4 presents the spatial extent considered in each of these cities. Note that although the extent used for Baltimore, MD, and Dallas, TX, encompasses the city boundaries, the spatial limits used are more representative of the County because of data availability and the hydrologic properties of the region.

The data collected for each of these cities and their respective sources are presented in Table B.1 (Appendix B). In order to calculate all hydrologic indicators (e.g., TWI, HAND, etc.) the hydrologic data are collected for the entire HUC12 watersheds that contain the city limits. All of the collected data are pre-processed to the same spatial reference system (i.e., North American Datum [NAD] 1983 with corresponding zones) and a raster resolution of 10 meters. Lastly the data used to calculate the SoSI variables are gathered from two sources published by the US Census Bureau: Summary File Level 1 (SFL1) data (2010) and the American Community Survey for 5-years prediction (ACS5) (2012).

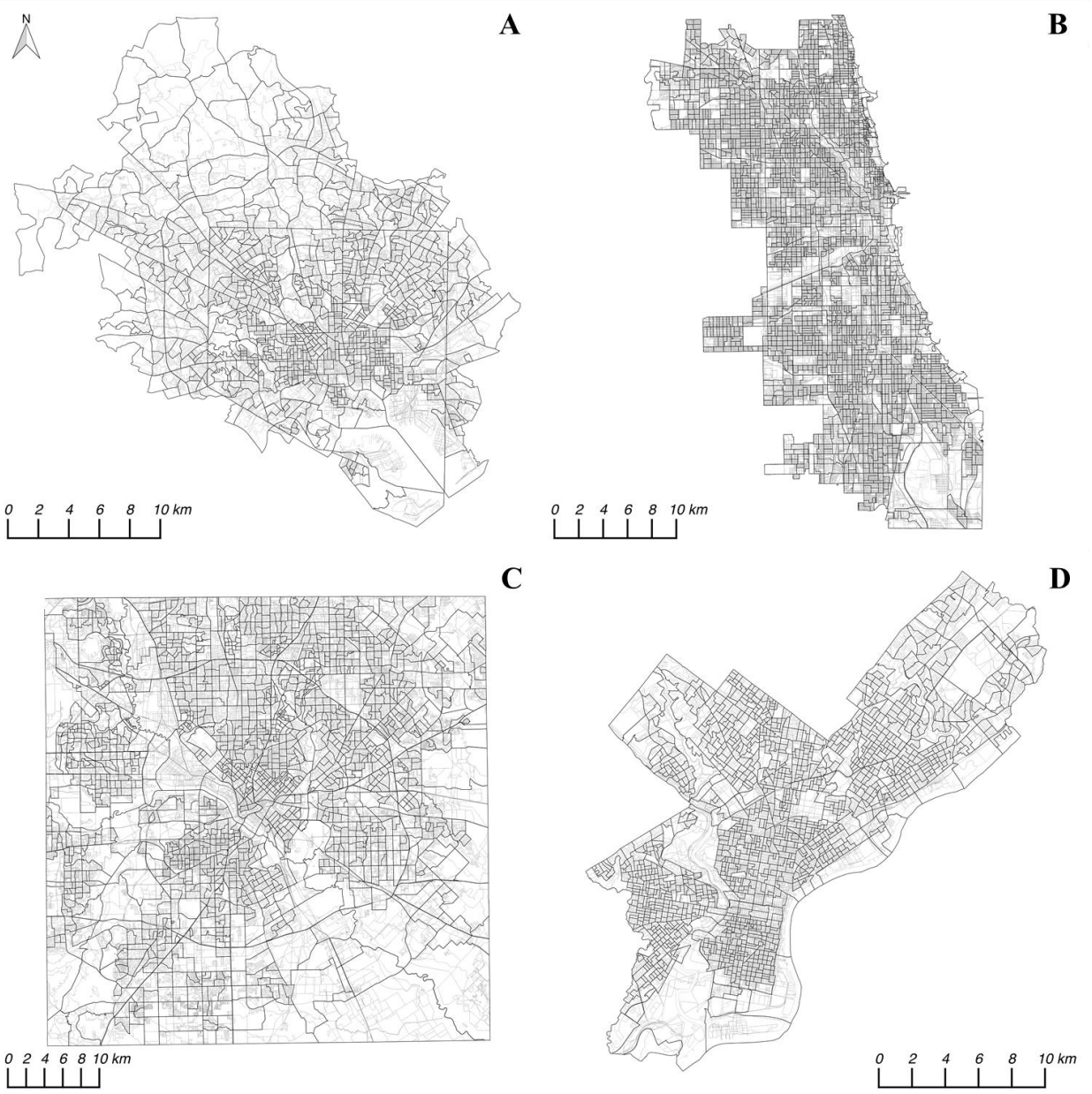

Figure 2.4: Spatial extent of cities included in the case studies, including Census Block Groups (darker lines) and Census Blocks (light gray lines), for: A) Baltimore, MD, B) Chicago, IL, C) Dallas, TX and D) Philadelphia, PA.

2.4 Results and discussion

The results presented in this study include: (1) an analysis of SoSI variability to data uncertainty and different methodological choices, and (2) a spatial correlation analysis of the observed spatial patterns of vulnerability.

Figure 2.5 presents the mean value of the Pearson's correlation coefficient for SoSI values calculated using the methods from Table 2.4. The results show that at the scale of Census Block Groups, there is a marked difference in SoSI values using different data transformation methods. More specifically, there is a reduction in the mean correlation for methods that use an absolute count versus those that use population density. However, this was the only step of the indicator construction process that seemed to cause a significant change in the correlations. Except for the City of Chicago, all other cities have a SoSI correlation larger than 0.9 regardless of the combination of construction steps used after the data transformation. In Chicago, in addition to the influence of different data transformation methods, using population density with an ordinal normalization causes a reduction in the correlation.

However, methodological choices seem to have a larger influence on the variability of correlations at the Census Block scale. At this scale, the transformation of the data is also the most influential methodological step. However, in contrast to the Census Block Groups scale, other methodological choices also affect the correlations. The use of different aggregation methods appears to cause most of this variability, particularly when population density is used. In contrast, the min-max normalization method causes the largest variability in the correlations when absolute counts are used. In fact, these aforementioned combinations of methods have a greater correlation with all other combinations. In other words, the use of absolute counts and the min-max normalization method seem to compromise the correlation of the SoSI with other methodological combinations that use the same data transformation, resulting in higher correlations with all combinations of methods.

In Figures 2.6 and 2.7, the effects of data uncertainty for each combination of methods is presented. Figure 2.6 presents the percent consistency in susceptibility classes identified in the Monte Carlo simulations. Percent consistency is defined as the percent of Monte Carlo simulations for which a spatial unit (e.g., Census Block) receives the same susceptibility class. Figure 2.7 presents the percent of Census Block Groups and Census Blocks that have consistency in their susceptibility classes across 80% or 90% of all Monte Carlos simulations. These two figures suggest that data uncertainty has a larger effect on the variability of the susceptibility categories at the Census Blocks level, particularly when using population densities and the z-score or min-max normalization.

Additionally, the results suggest that the use of the sum of weighted ranks aggregation method or ordinal normalization resulted in a larger number of Census Block and Census Block Groups achieving the same consistency threshold, thus suggesting a lower sensitivity to the data uncertainty. This higher consistency in susceptibility categories for a larger number of spatial units is not surprising as these two methods reduce the relative difference between SoSI values and thus reduce changes in susceptibility categories caused by data uncertainty.

Lastly, it is worth noticing that the City of Chicago resulted in a very small number of Census Block Groups and Census Blocks with consistency in their susceptibility categories larger than 80% when using population densities and z-score or min-max normalization. Nevertheless, in all other cities the results show similar variability in susceptibility classes due to data uncertainty regardless of the methods used for the SoSI calculation.

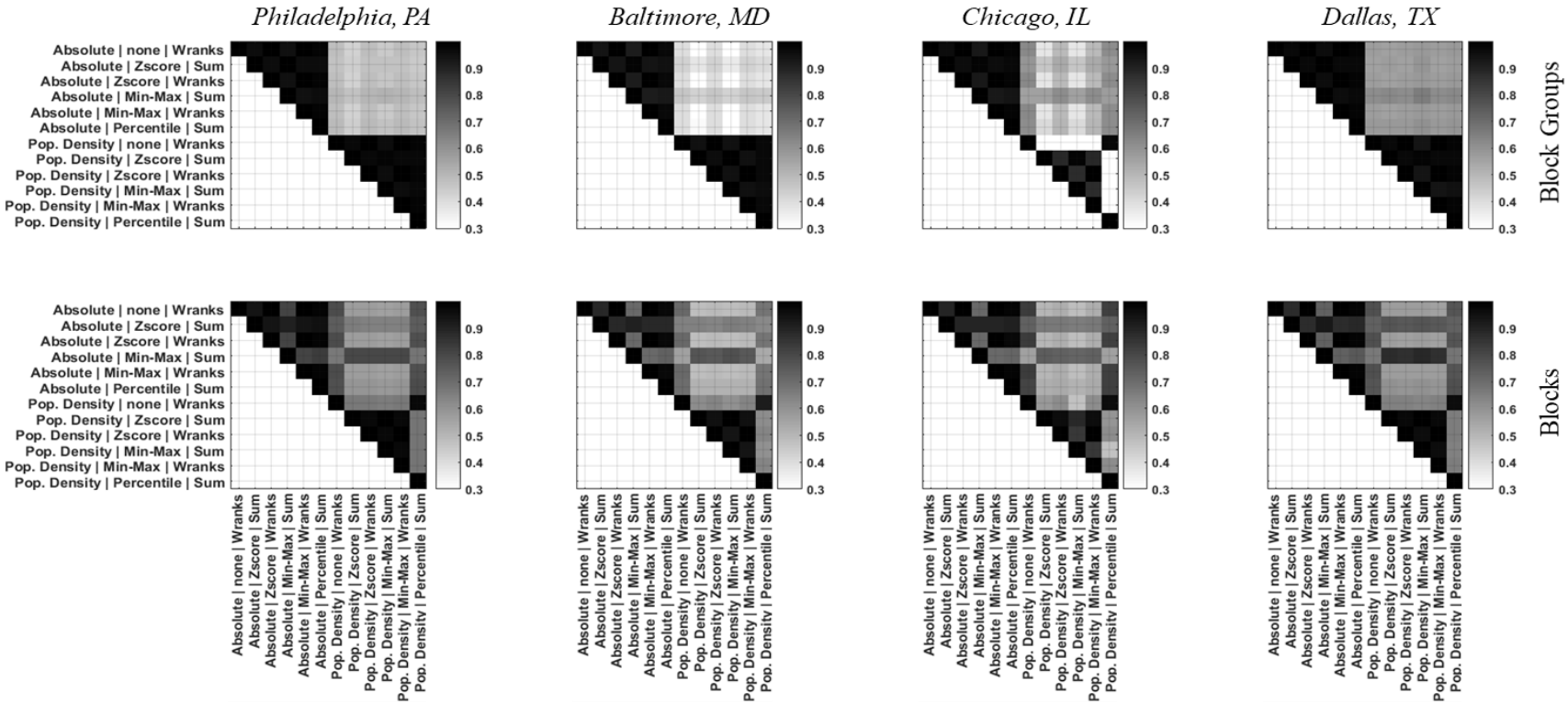

Figure 2.5: Correlation matrices of the SoSI values obtained using different methods from Table 2.4. Axis labels show the combination of methods used for transformation | normalization | aggregation.

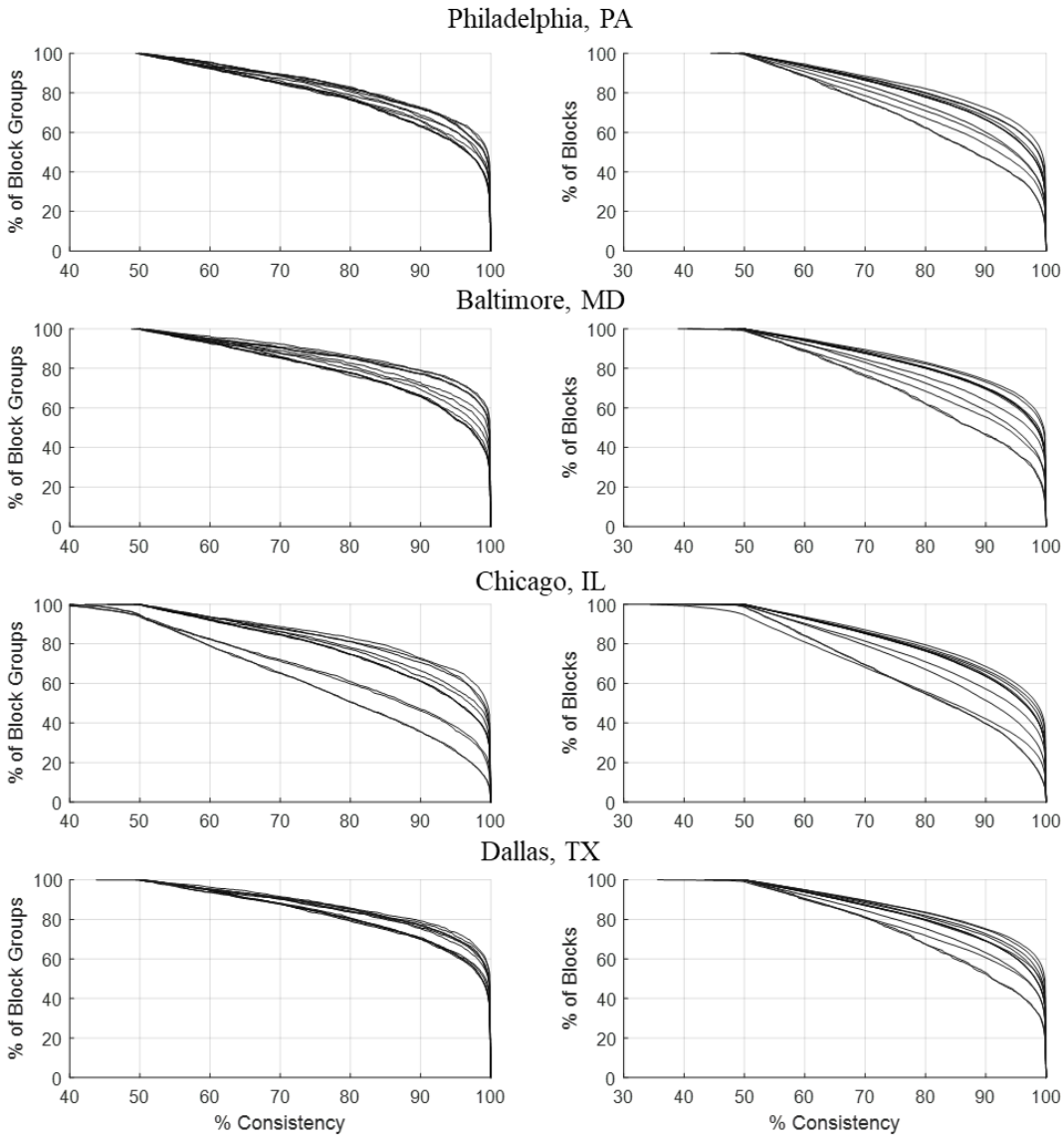

Figure 2.6: Percent consistency in social susceptibility category when considering all Monte Carlo simulations. Each line represents a different combination of methods.

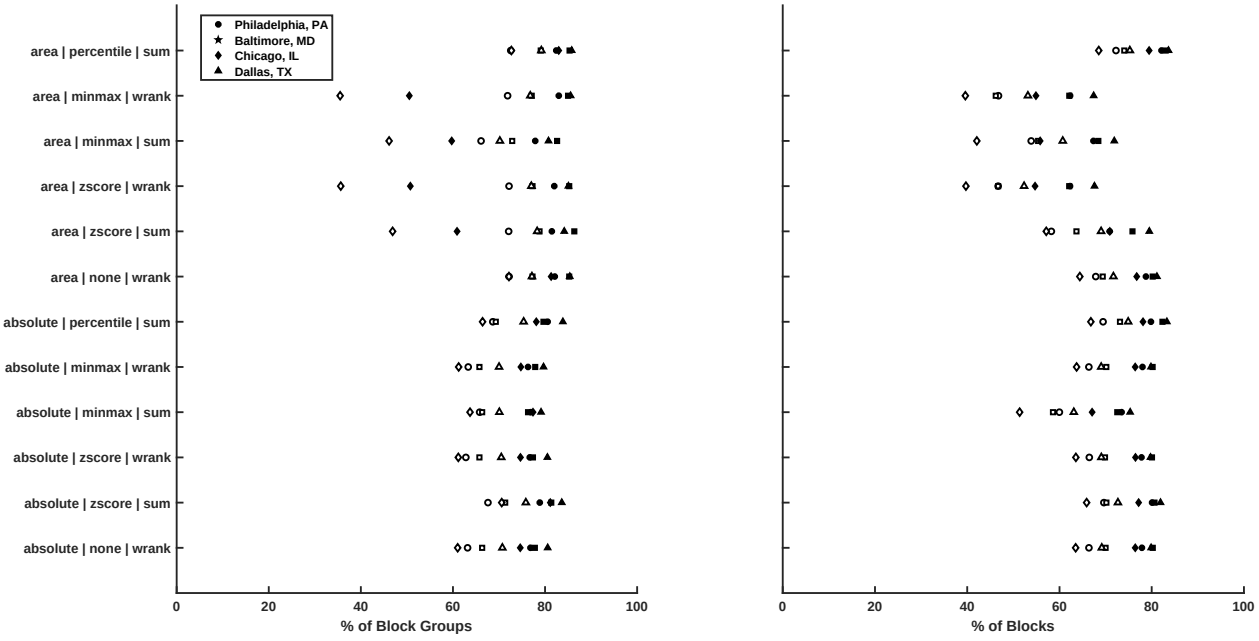

Figure 2.7: Percent of Census Block Groups and Census Blocks with consistency in susceptibility categories larger than 80% (white markers) and 90% (black markers).

The results presented in this section suggest that the most critical step in the construction of the SoSI is the data transformation, regardless of the spatial unit. These results are consistent with other studies and are not surprising given that conceptually the use of absolute counts versus relative ratios have different meanings. Furthermore, given that 47% (16 of the 34) of the indicators used to construct the SoSI are not available at the Census Block scale, the observed dominance of the data transformation method on SoSI variability may be due to the influence of data transformation methods at larger spatial scales. The observed increase in SoSI correlation at the Census Block scale for some combinations of methods seems to support this hypothesis, suggesting that at these smaller scales, choices in construction steps become less important to the variability of the results. However, in order to test this hypothesis, the indicators used for the analysis would need to be collected at all spatial scales. Finally, the results suggest that the use of ordinal normalization could increase consistency of the SoSI categories when data uncertainty is considered, while reducing the impact in SoSI variability due to other methodological choices.

2.4.1 Variability in the spatial patterns of vulnerability

Figures 2.8 and 2.9 present the distribution of the resulting spatial correlations obtained using different data transformation methods in the SoSI calculation (i.e., absolute count or population density) and each treatment of unpopulated areas (i.e., A-excluded from the analysis, B-considered to have SoSI equal to zero). There are three main observations that can be made from these results. First, in using Census Block Groups to compute the SoSI, different data transformation methods had a significant impact on the spatial correlation of social susceptibly. In particular, when population density is used, the correlation increases to larger positive values. These results suggest that the use of area as a normalizing variable reduces the spatial variability of the computed SoSI. On the other hand, the variability in spatial correlation due to the use of different data transformation methods is lower at the Census Block scale. Only for the case when population density is used, and unpopulated areas included in the analysis, are large variabilities observed in the spatial correlation. However, upon further investigation, the z-score or min-max normalization, regardless of the aggregation technique, had high positive correlation values (close to 0.8), which caused the observed large variability. Lastly, Census Blocks have more consistent values of spatial correlation regardless of how the unpopulated areas are treated.

Second, in order to further investigate the variability in the SoSI spatial correlation, the spatial clusters identified by the LISA method are analyzed. These spatial clusters of autocorrelation are obtained from the scenario in which unpopulated areas are excluded from the analysis and only clusters with statistical significance ($p \leq 0.01$) are considered. Figures 2.10-A and 2.10-B presents a series of maps of spatial autocorrelations for the different data transformation techniques at both the Census Block Groups and the Census Blocks spatial scales. For the purpose of simplifying the illustrations, only the cities of Dallas, TX (Figure 2.10-A), and Chicago, IL (Figure 2.10-B), are presented, but all maps are available in Appendix B (Figure B.1). Using these maps, the influence of the choice in data transformation method at the Census Block Groups can be seen more clearly. In Chicago, IL, some of the large clusters of high and low social susceptibility are somewhat consistent between data transformation methods at the Census Block Groups scale. However, in Dallas, TX, the opposite behavior is observed, with no good spatial correlation between clusters of high or low social susceptibility. A possible explanation for this behavior is the relative difference in the extent of Census Block Groups in Dallas versus in Chicago. By visual inspection, the Census Block Groups in Chicago seem to be more consistent

in size when compared to the Census Block Groups in Dallas. Thus, when transforming the data to population densities, variability in the area of the Census Block Groups in Dallas creates a completely different relationship between the indicators used to construct the SoSI. At the Census Blocks scale, this relative difference between the areas is reduced and thus a better spatial match of the cluster is observed. This is particularly true for Chicago, in which the spatial clusters identified using both data transformation methods are very similar. In Dallas, while there is still some significant differences in the spatial patterns of the clusters, a much better match is observed for clusters of high social susceptibility.

Finally, the third observation relates to the general trends in the patterns of how social susceptibility spatially relates to hazard exposure and susceptibility of the ecological and infrastructure systems. Figure 2.8 shows that in all cities, when unpopulated areas are excluded from the analysis, social susceptibility is positively spatially correlated with areas of lower ecological integrity and higher infrastructure susceptibility. These results are consistent with previous studies that have concluded that communities with lower socio-economic status are often spatially close to areas of higher imperviousness and urban green spaces of low quality, and have limited accessibility to parks and other open spaces (Nicholls, 2001; Pham et al., 2012; Heckert, 2013; Hoffimann et al., 2017). Furthermore, the use of population density at the Census Block Groups scale results in a large positive correlation between social susceptibility and both ecologic and infrastructure susceptibility. The large discrepancy of this result with the spatial correlations obtained in all other scenarios suggests that the large positive spatial autocorrelation of social susceptibility is biasing these results towards larger correlation values. Lastly, it should be noted that at the Census Block scale, the choice of data transformation method has a lower impact on the variability of the correlation values. The largest influence comes from the consideration or exclusion of unpopulated areas.

With regards to the spatial relationship with hazards exposure, socially susceptible communities are more likely to be located in areas prone to flash flooding and at higher risk of exposure to extreme heat (Figure 2.9). More specifically, the results presented in Figure 2.9 illustrate that when using absolute counts, there is a “weak” but positive correlation between these factors. This suggests that areas with a larger number of susceptible people, as opposed to a higher density of susceptible people when population density is used, are more likely to be exposed to higher degrees of hazard severity.

Finally, it is worth noticing that there are some exceptions to these patterns and that the consideration of unpopulated areas can have significant impacts in diagnosing these vulnerabilities. For example, the City of Chicago shows no spatial correlation between social susceptibility and urban heat island when unpopulated Census Blocks are eliminated from the analysis. However, when these unpopulated Census Blocks are assigned a social susceptibility category, an increase to a positive spatial autocorrelation is observed. This discrepancy is caused by two problems when using the LISA method: (1) the elimination of neighbors that have a high hazard severity category around areas of high social susceptibility when unpopulated areas are excluded from the analysis and (2) the assignment of a value of zero to the social susceptibility of these unpopulated areas when these are considered in the calculation of spatial correlation.

In Chicago, this discrepancy occurs because some of the unpopulated areas have higher severity classes for urban heat island. In fact, when unpopulated areas are excluded from the analysis, the univariate spatial autocorrelation of urban heat island in Chicago is 0.8. However, when these unpopulated areas are considered, the spatial autocorrelation increases to 0.88. By eliminating unpopulated areas from the spatial correlation analysis, adjacent Census Blocks are assumed not to be exposed to these higher hazard severity categories and thus report a lower correlation. A similar phenomenon is observed for the City of Dallas. When unpopulated Census Blocks are eliminated from the analysis, the social susceptibility seems to dominate the spatial correlation due to the large numbers of highly susceptible areas with a high number of neighbors that were eliminated. However, when these unpopulated areas are considered in the analysis not only the variability of the spatial correlation is reduced, and the difference between using absolute counts versus population density is negligible, but there is a slight increase in the correlation that suggest a “weak” but positive correlation.

Regardless of the treatment of unpopulated areas, using the proposed quantification method at the Census Block scale is more consistent in identifying spatial clusters of high social susceptibility and high hazard severity. In fact, even when the spatial autocorrelations are significantly different, the High-High areas remain somewhat invariable. For example, Figure 2.11 presents the Census Block Groups and Census Blocks identified by the bi-variate LISA analysis as clusters of high social susceptibility and high exposure severity to flash flooding and urban heat island (i.e., High-High clusters) in the City of Philadelphia, PA. Figure 2.11 shows the percent of all methods that identified the same High-High areas (i.e., percent of agreement).

As seen in Figure 2.9, the treatment of unpopulated areas has significant impacts on the spatial autocorrelation. However, areas identified as High-High in Figure 2.11 remain somewhat unchanged. Furthermore, while the use of both spatial units identify similar High-High areas for both hazards, at the Census Blocks scale a larger portion of the area has a higher percentage agreement. Moreover, the use of Census Blocks allows identification of additional High-High areas that are obscured when using the larger spatial scale of Census Block Groups.

Figure 2.12 offers a summary of these findings in all cities by presenting a matrix of percent agreement between methods in identifying High-High areas. More specifically, the row value in a column represents the percentage of High-High areas (i.e., Census Block Groups or Census Blocks) identified by the column method that were also identified by the row method. The results show that the influence of different methodological choices becomes less significant when using Census Blocks as the spatial unit of analysis, providing smaller variability in identifying High-High areas. For Census Block Groups, the High-High areas identified by methods using absolute counts were also identified as High-High areas by methods using population density. The opposite, however, is not shown to be true.

All of these results indicate robustness of the proposed method to inform decision making, since regardless of the assumptions made during the construction of the SoSI and the treatment of unpopulated areas, the areas in most need of receiving GSI benefits can be identified.

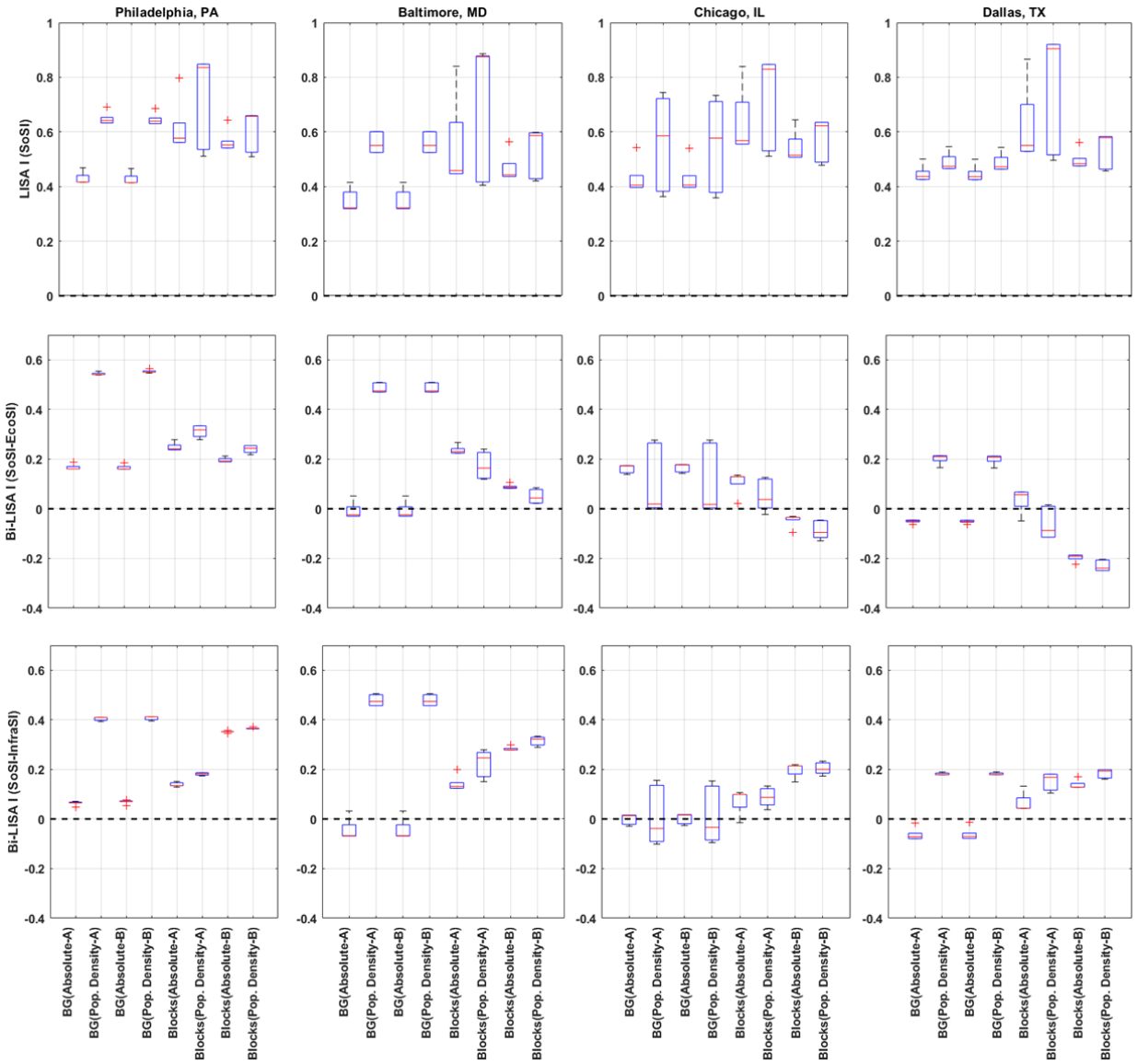

Figure 2.8: Variability in the spatial autocorrelation of social susceptibility and its spatial relationship to ecologic integrity (EcoS) and infrastructure susceptibility (InfraS).

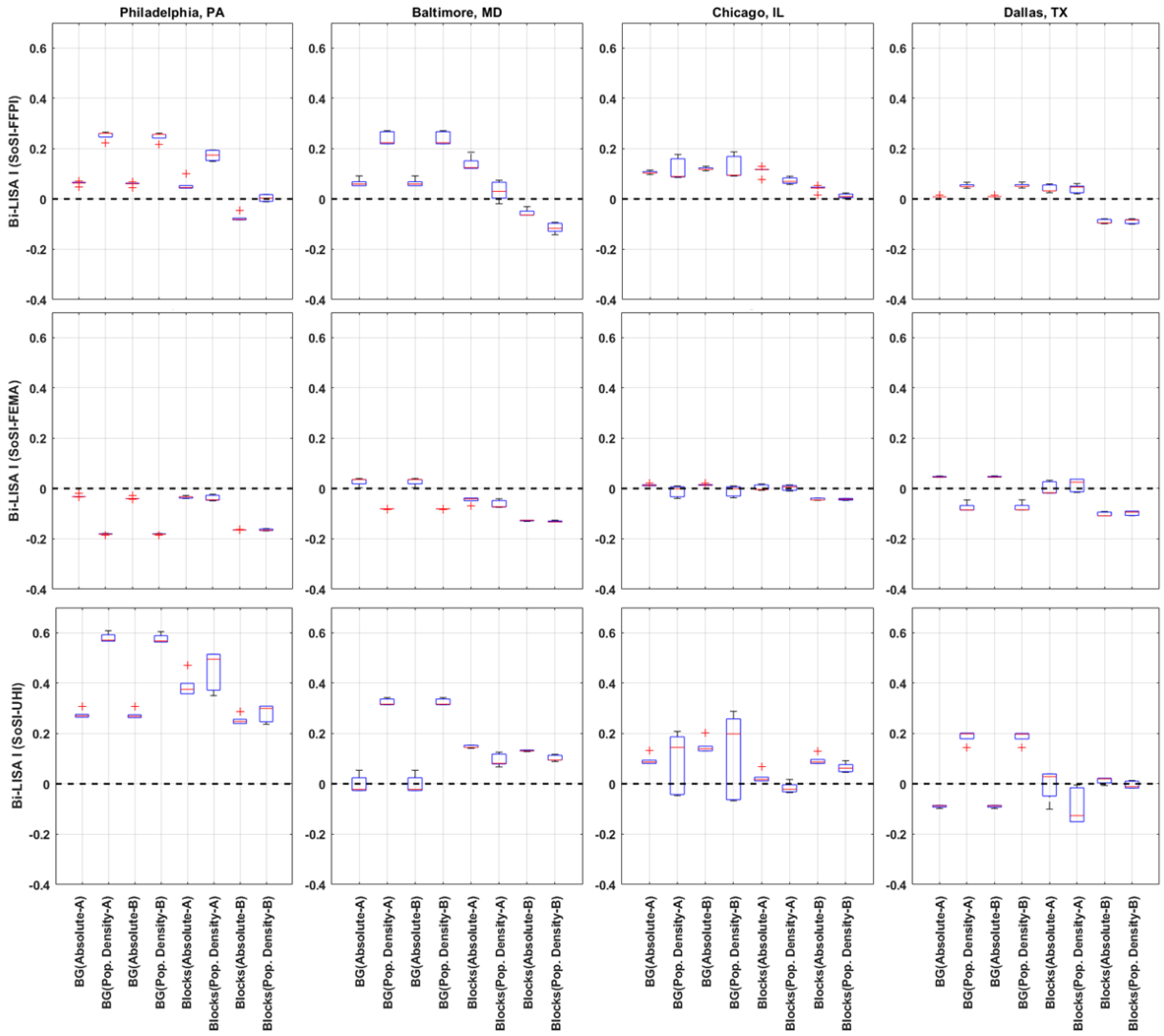

Figure 2.9: Variability in the spatial autocorrelation of social susceptibility and its spatial relationship to the exposure severity of urban heat island (UHI), flooding (FEMA) and flash flooding (FFPI).

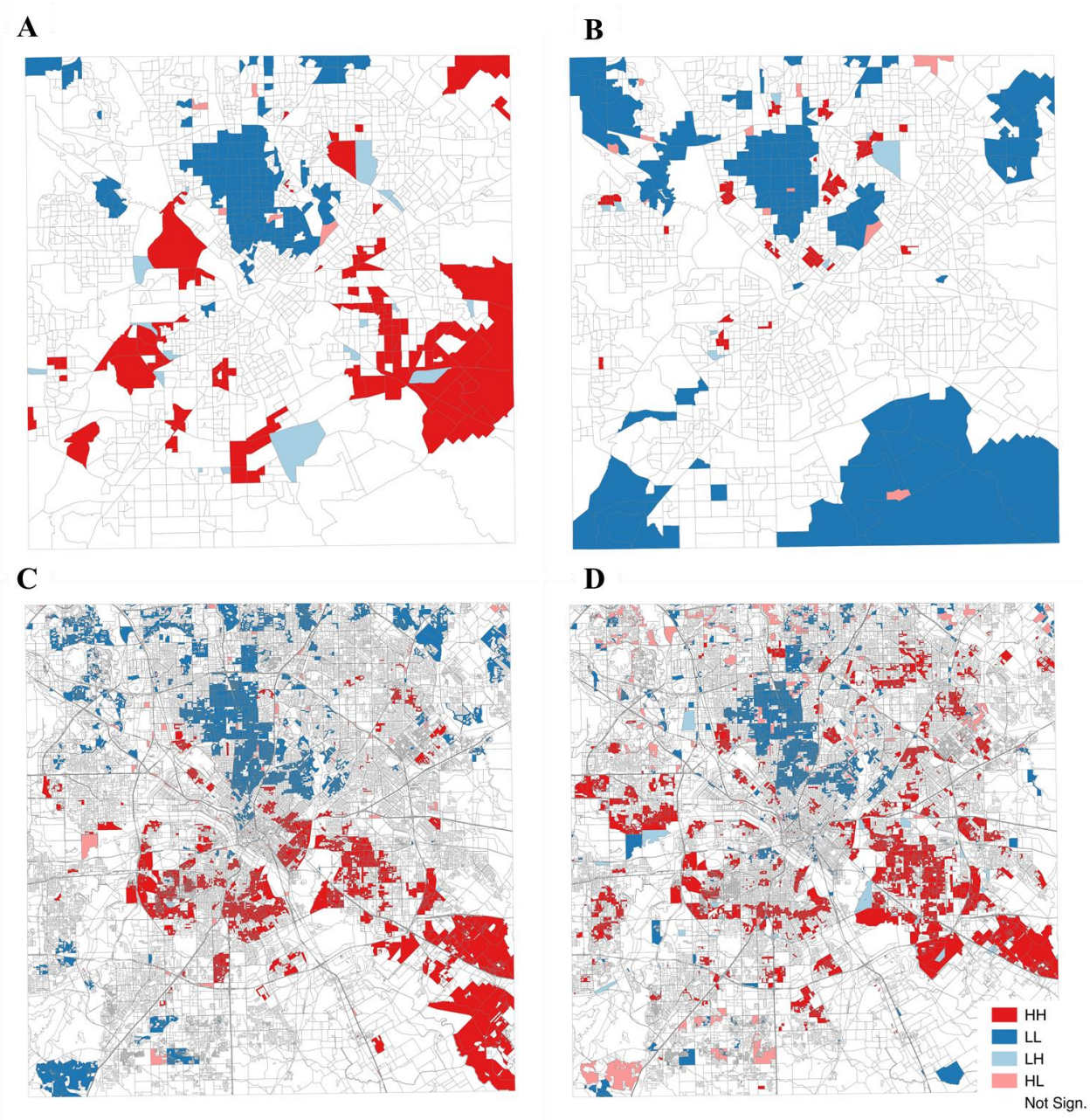

Figure 2.10-A: Spatial cluster of autocorrelation as identified by LISA for Dallas, TX. The four scenarios presented include: A-absolute counts/Census Block Groups, B-population density/Census Block Groups, C-absolute counts/Census Blocks, and D-population density/ Census Blocks.

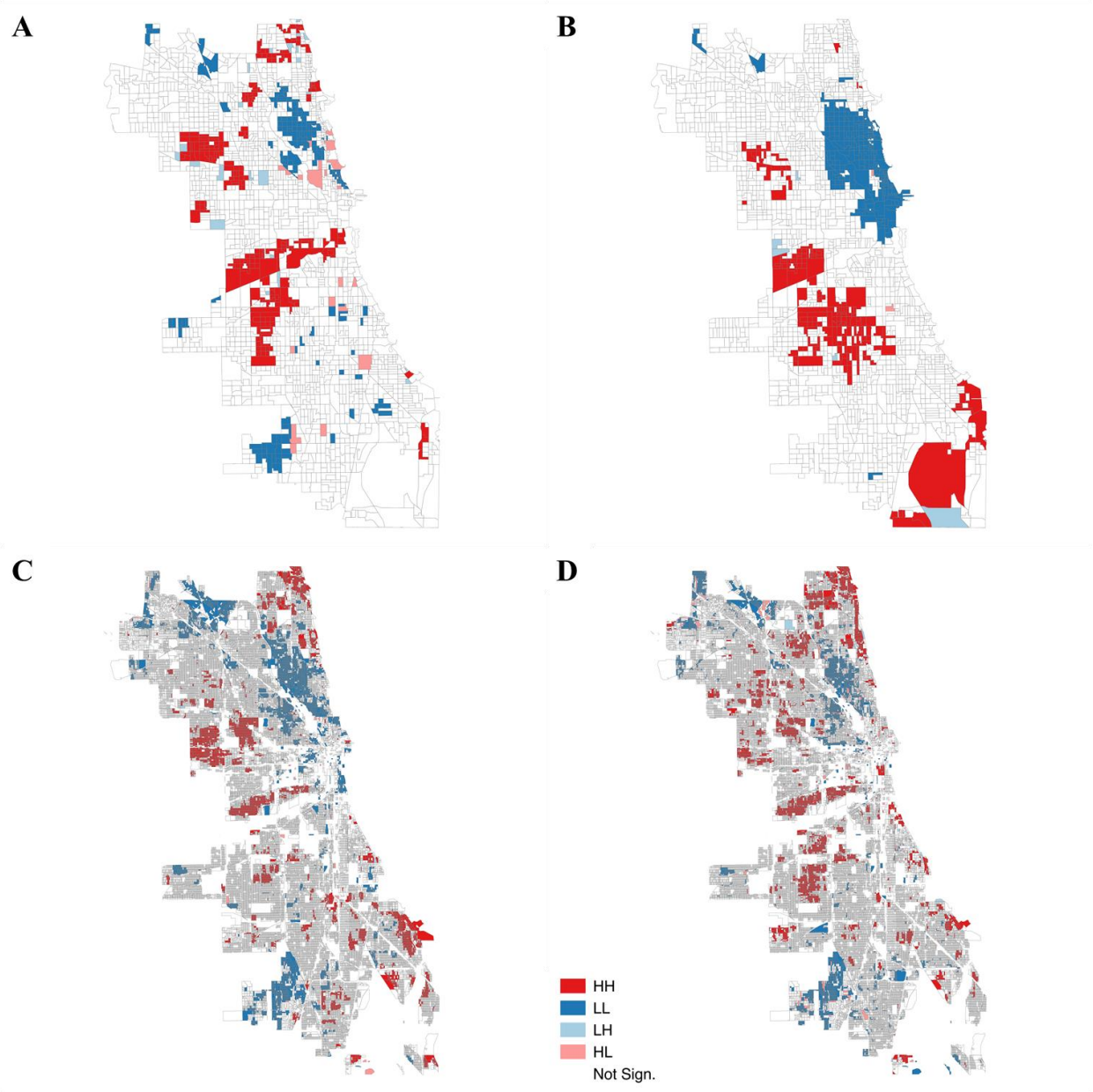

Figure 2.10-B: Spatial cluster of autocorrelation identified by LISA method for Chicago, IL, using: A-absolute counts/Census Block Groups, B-population density/Census Block Groups, C-absolute counts/Census Blocks, and D-population density/ Census Blocks.

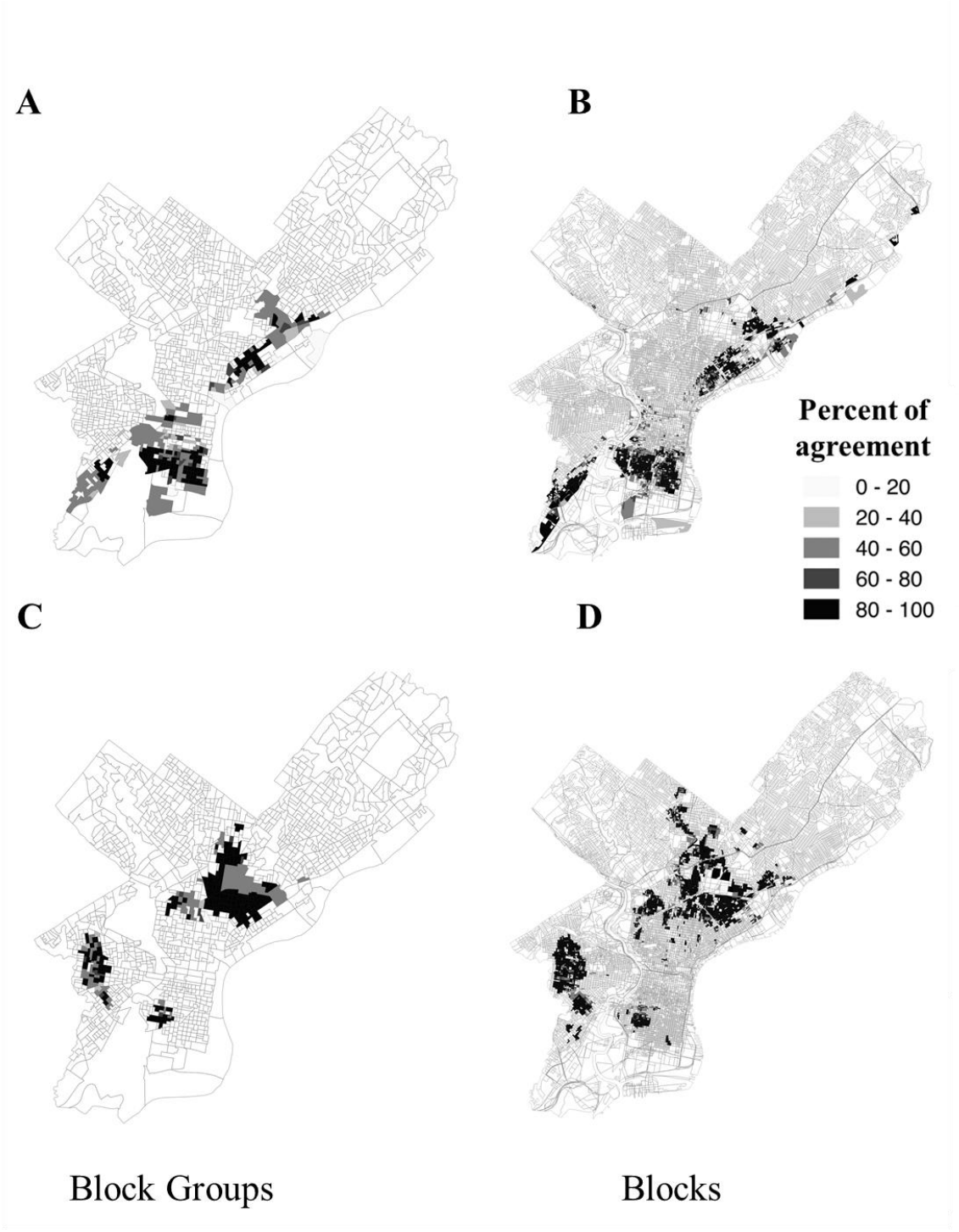

Figure 2.11. Spatial clusters of high social susceptibility and high potential exposure to flash flooding (FFPI) (A & B) and urban heat island (C & D) in Philadelphia, PA. Gray scale represents the percentage of social susceptibility methods that identified the same Census Block Groups (A & C) or Census Blocks (B & D) as High-High clusters in the bi-variate analysis when excluding unpopulated areas from the analyses.

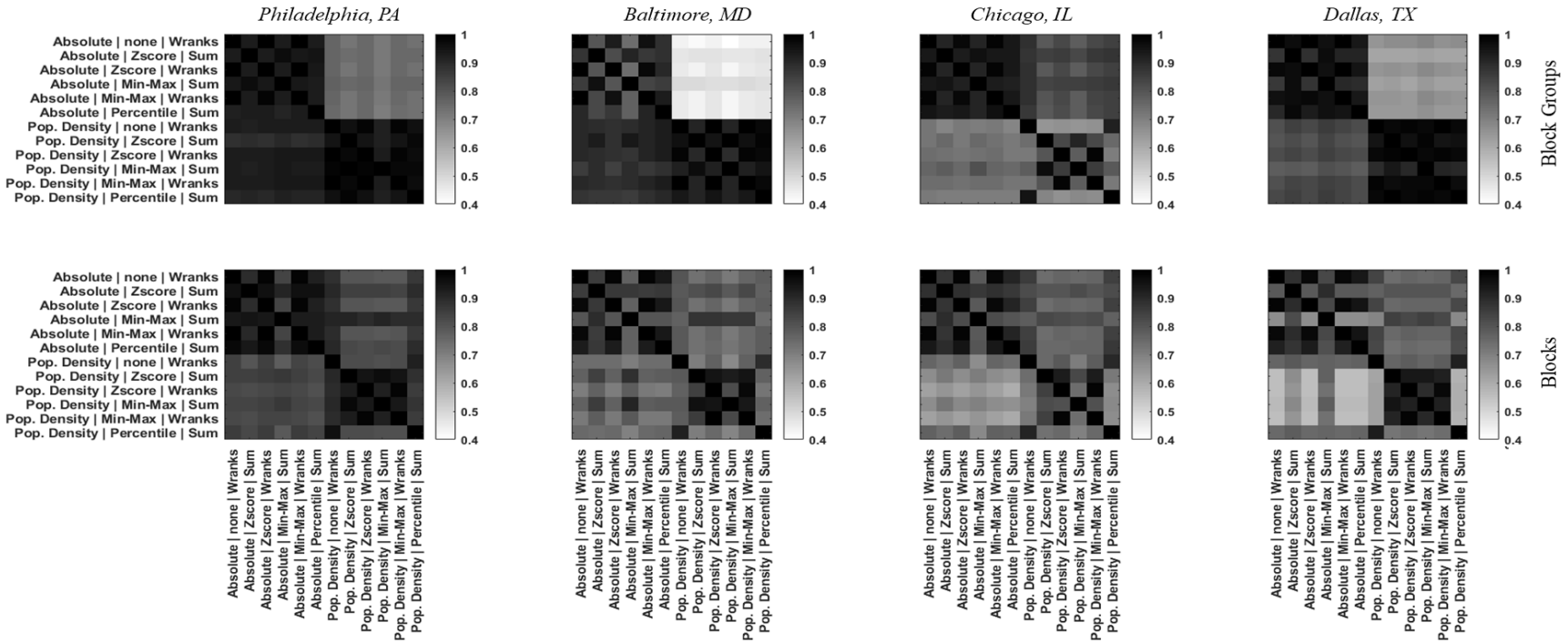

Figure 2.12. Percent of agreement between methods in identifying High-High areas. The row value in a column represents the percentage of High-High areas (i.e., Census Block Groups or Census Blocks) identified by the column method that were also identified by the row method.

2.5 Conclusions and limitations

To fully integrate the concept of vulnerability in the planning and design of GSI, a more systematic and flexible approach is needed that defines what constitutes vulnerability (what parameters should be measured), the appropriate scale at which it should be quantified (spatial unit at which the benefits will be received), and how these different metrics should be interpreted/aggregated to represent relative vulnerability). This study addresses this problem with a new framework for quantifying vulnerability at a spatial scale that is useful for planning GSI.

While prior methods have proposed quantification of vulnerability at the Census Track and Census Block Groups, this study shows that the spatial patterns of vulnerability observed at these scales can be largely influenced by the data transformation method selected. By using the proposed approach to quantify social susceptibility at the Census Blocks scale, the influence of methodological choices on the spatial patterns of vulnerability is reduced. Additionally, the results suggest that computing social susceptibility at the Census Block Groups scale eliminates small clusters of highly susceptible communities that are exposed to high hazards severity, an important feature for decision making.

Furthermore, this study concludes that the data transformation step is the most critical in contributing to the variability of social susceptibility. Ordinal normalization allows for a reduction in variability due to data uncertainty and produces similar spatial patterns of vulnerability, regardless of the data transformation used. As such, an absolute count data transformation with an ordinal normalization appears to be the most appropriate method for calculating social susceptibility in the context of spatial GSI planning. The use of absolute counts produces lower variability in identifying spatial clusters of high vulnerability.

Previous studies have noted that using absolute counts has often given the SoSI a positive correlation with higher population areas (Jones & Andrey, 2007; Tate, 2013). As such, it has been suggested that this method should be used only when: (1) the difference in population between spatial units is low, in order to avoid skewing the SoSI values by population size, and/or (2) when the objective for using SoSI is to identify the total number of vulnerable people (e.g., use in evacuation planning). As with any other infrastructure investment, the implementation of GSI should maximize the population that will be positively affected while reducing costs. Thus, using an absolute count may be beneficial in identifying areas where there are large numbers of vulnerable people for whom small investments in GSI could have a large impact.

Finally, this study uses the traditional risk-hazard analytical framework in which the relationship between the natural phenomenon that constitutes a threat and the impact that the threat could have on each of the systems is addressed. While it is the most widely used approach in the hazard literature, the approach is limited by not accounting for the multiple interactions that exist between ecological and social systems. Additionally, it does not consider threats that are processes rather than events (e.g., climate change, land use change). Finally, the approach does not consider the relationship between the magnitude of the stressor and the sensitivity of the social, ecological, and infrastructure systems, which would determine the potential risk and coping capacity of each system. More accurate and complete data are needed to better understand the validity of the indicators used to represent these processes and for the proposal of method that could allow to quantify them.

CHAPTER 3. SPATIAL PATTERNS OF VULNERABILITY AND GREEN STORMWATER INFRASTRUCTURE: ARE WE MAXIMIZING BENEFITS?

3.1 Motivation & related work

Building upon the work presented in the previous chapter, this study addresses the question of how current and planned GSI implementation relate spatially to the areas of highest vulnerability. As the greening of cities continues to become a popular way to mitigate the impacts of climate change, the creation and preservation of urban green spaces have become an environmental justice concern. There has been longstanding interest and work devoted to understanding and quantifying the spatial relationship between urban green spaces and the socio-economic conditions of urban populations (Pham et al., 2012; Nicholls, 2001; Sister et al., 2009; Heckert, 2013; Wen et al., 2013). These studies have usually defined *green infrastructure* as a broad range of multifunctional green spaces that provide ecological, social and economic benefits (e.g., parks, green open spaces, urban forests, green-way trails, etc.).

Spatial relationships between green infrastructure and different sociodemographic groups have often been explored from a perspective of *"access"* to green spaces (where *access* is defined as the spatial density of green spaces in each of the administrative boundaries (e.g., Census Tracts), the use of distance buffers around these green spaces, or the travel time and/or road distance to the nearest green space) (Landry et al., 2009; Pearsall et al., 2012; Pham et al., 2012; Kabisch et al., 2014; La Rosa et al., 2014; Wolch et al., 2014; Schwarz et al., 2015; Ambrey et al., 2017; Ekkel et al., 2017). More recent studies have done similar analyses using a more narrowed definition of GSI that only includes engineered systems specifically designed and/or installed for on-site treatment and infiltration of stormwater runoff (e.g., green roofs, rain gardens, bioswales, etc.). For example, Chan et al. (2017) investigated the spatial relationship (i.e., co-location) between street tree and green roof density in Portland, OR, and the sociodemographic factors of different Census Block Groups. The study found that Census Block Groups with a higher percentage of minorities, people of lower median age and income, and people with a lower level of education had, in general, a higher green street density. Census Block Groups with a lower median age and median income also had a higher density of green roofs.

Given GSI's utility as a climate change mitigation strategy, the focus of more recent studies is on the relationship between urban green spaces and vulnerability of socio-ecologic systems.

These studies have explored the spatial relationships between social susceptibility to flooding or urban heat hazards and the spatial co-location of urban green spaces (e.g., Fekete, 2009; Cheng, 2013; Johnson et al., 2012; Yoon, 2012). The objective of the studies has been to either: (1) demonstrate how the concepts of vulnerability can be used to identify communities in need of mitigation strategies (i.e., vulnerable communities with a lack of green spaces), or (2) to identify what characterizes the most vulnerable communities within the study area (e.g., lower income, lower education levels, higher median age, etc.) and how these are related to the location of green spaces (Huang et al., 2011; Bradford et al., 2015; Cheng, 2016). These studies have found that vulnerable socio-economic groups tend to be in areas with more imperviousness and *"low quality"* green spaces (e.g., small parks with only grass). Additionally, these studies have concluded that vulnerable socio-economic groups tend to have a higher risk of exposure to severe floods and heat waves.

These prior studies have only considered urban green spaces rather than engineered GSIs, and have disregarded their multifunctionality as a mitigation strategy for multiple hazards. The distinction between *urban green spaces* and engineered GSIs is particularly important because the benefits of engineered GSIs are often more localized than those from larger urban green spaces (e.g., parks), their cost of installation and operation/maintenance is often not shared by everyone, and their main functionality is the management of stormwater. Furthermore, these studies have analyzed GSI in terms of their spatial density or co-location, but GSI benefits are not confined to an administrative boundary and should be analyzed considering the entire spatial extent to which GSI benefits are received. This is a particularly critical distinction when assessing stormwater management benefits, as hydrologic processes and land surface temperatures can vary drastically within large administrative boundaries (e.g., Census Tracts).

To begin addressing these limitations, recent studies have begun to explore the challenges of considering more localized GSI and their spatial relationship with social vulnerability. For example, Heckert & Rosan (2016) proposed an "Equity Index" for the identification of areas in need of GSI installations. Using Philadelphia, PA, as a case study, the index was used to identify Census Block Groups that are in need of GSI installation based on their socio-economic profiles and the spatial density of playgrounds and vacant lots. Meerow et al. (2016a) proposed a three-phase process for resilience planning in which the "five Ws" (i.e., for whom, what to what, where, when, and why) could be negotiated collectively in order to achieve greater consensus among

stakeholders, considering the significant implications that resilience planning decision could have on equity. The study showed that the large spatial variability in prioritization of different areas for GSI development is a consequence of using different spatial scales of analysis and different planning criteria. The authors acknowledge the heterogeneity that exists within Census Tracts and the limitations of using administrative boundaries for the planning of green spaces, which could hinder the correct identification of green space beneficiaries.

A more recent study by Meerow et al. (2017) began to address some of these limitations by focusing on more specific engineered/planned GSIs and their multiple benefits. Using Pearson correlation as the metric of evaluation, the study revealed the synergies (positive correlation) among places with high priority for improvements in urban heat island, stormwater management, and air quality, and also highlighted the tradeoffs (a negative correlation) between these places and those with a high need for habitat connectivity. Additionally, the study revealed that while current and planned GSI projects in Detroit have been located in places with high *"park poverty",* they have not been sited in Census Tracts with high priority for social vulnerability, urban heat island, stormwater abatement, habitat connectivity, and air quality (i.e., all of these metrics had a negative correlation), even when accounting for stakeholder preferences.

To date, the inclusion of socio-ecologic vulnerability and its relationship to the location of engineered GSI has been limited. The few previous studies that have investigated this relationship have used a spatial scale of analysis that is too large to account for the true beneficiaries of the GSI or to identify which communities are most in need of GSI. By using a spatial analysis comparable to Census Tracts (very few at Census Block Groups scale) the assumption has been that everyone within these administrative boundaries is equally benefiting from the co-location of GSI in these areas. However, the socio-economic profiles and exposure to different hazard severities within these large administrative boundaries can be highly heterogeneous.

Furthermore, in previous studies, no differentiation has been made between the benefits associated with different types of GSI. Instead, it has been assumed that all GSI, regardless of size or type, could provide the same level of service. This is mostly because previous studies have concentrated on the broader definition of urban green open spaces. This definition might be appropriate for exploring social and environmental justice issues related to accessibility within larger administrative boundaries (e.g., Census Tract), but for engineered stormwater management practices, a closer examination of potential benefits is needed (e.g., permeable pavements have a

negligible impact on providing habitat restoration and human health benefits). Moreover, because the primary goal of engineered GSI is abatement of stormwater runoff, their benefits need to be quantified considering the hydrologic connectivity of the landscape. Lastly, the conclusions of previous studies could have been biased by the modifiable areal unit problem (MAUP) (Openshaw et al., 1979; Lloyd, 2006; Wong, 2009): As the area used for spatial aggregation increases, the correlation between the variables tends to increase as well (i.e., this is particularly true for socio-economic variables).

3.1.1 Contributions

To our knowledge, no other studies have explored the relationship between socio-ecologically vulnerable communities and the location of GSI at a spatial scale closer to their benefits (i.e., 10 meter raster). Furthermore, no other study has examined these relationships for GSI specifically engineered for stormwater management. As such, the main contribution of this study is to develop an analytical approach that uses the concepts of "service-needing and service-benefiting areas" to spatially relate the potential benefits offered by engineered GSI and the vulnerability of different communities. The approach integrates the vulnerability framework presented in Chapter 2 with a multiple flow direction algorithm to better understand where the beneficiaries of GSI are located, as well as the communities in most need of GSI. Lastly, this study investigates the spatial synergies and tradeoffs associated with GSI benefits, particularly impacts on immediate surroundings versus downstream areas, for identifying areas of high priority for GSI implementation.

The hypothesis to be tested in this study is that GSI installations have not been sited in areas that would maximize their multifunctionality to communities that need the benefits of GSI the most (i.e., the most vulnerable communities). Additionally, it is expected that the use of a smaller spatial unit of analysis, a fuller concept of vulnerability that includes engineered and ecological systems, and the consideration of hydrologic connectivity will provide new insights on social and environmental justice issues.

3.2 Methodology

In order to investigate the spatial relationship between vulnerability and the benefits provided by GSIs, this study adopts the concept of service areas for the assessment of ecosystem

services. This concept was introduced by Fisher et al. in 2009, used by Syrbe & Walz in 2012, and highlighted recently by Hansen & Pauleit (2014) and Kuller et al. (2017). In this conceptual framework, the spatial aspects of ecosystem services are analyzed by dividing and categorizing the landscape into service–providing, -connecting and –benefiting areas. Service-providing areas (SPAs) are defined as those with the potential to offer one or multiple ecosystem services. These ecosystem services are then provided to service-benefiting areas (SBAs) by service-connecting areas (SCAs). Finally, SPAs and SBAs can have one of four possible spatial relationships: in-situ, omnidirectional, directional – slope dependent (i.e., downslope), and directional without strong slope dependence.

In order to apply this concept to the planning of GSI, SPAs are defined as areas where GSIs are installed and SBAs are defined as areas receiving the potential benefits offered by these GSI projects. In addition, this study introduces the concept of service-needing areas (SNAs) to define those areas with the highest need to receive a particular GSI benefit (i.e., those most vulnerable). Unlike previous studies that have often defined SNAs as areas with low spatial density of green spaces or trees and larger disadvantaged populations, in this study SNAs are defined as the areas with higher vulnerability of social, ecological, and infrastructure systems. As such, SNAs are highly dependent on the susceptibility of the systems to the exposure severity of different hazards and therefore will vary spatially depending on the hazard and system considered (i.e., less confined to administrative boundaries).

Using this conceptual framework, the methodology consists of three primary components: (1) quantification of the vulnerability of socio-ecologic systems using susceptibility and hazard exposure severity indicators, (2) definition and identification of service-needing areas, and (3) definition and identification of GSI's service-benefiting areas. The quantification of vulnerability is completed using the susceptibility and hazard exposure severity indicators discussed in Chapter 2 and will not be repeated in this chapter. However, the sub-sections below extend Chapter 2 by addressing how susceptibility and hazard exposure indices are combined to reflect different levels of vulnerability in order to define and identify SNAs. Finally, the last step of the methodology differentiates between the benefits of GSI that are perceived locally from spatial proximity and those that must consider the hydrologic connectivity of the topography.

3.2.1 Susceptibility and hazard exposure indicators

The susceptibility and hazard severity exposure indicators used in this study follow the methods and indicators presented in Chapter 2. Based on the findings of Chapter 2, the SoSI analysis uses an absolute count for each of the indicators and nominal normalization of the data (specifically weighted sum of ranks), which resulted in the least variability due to data uncertainty and spatial unit of analysis. Lastly, the SoSI is calculated at both the Census Block Groups and Census Block level in order to investigate the impact of different spatial scales on the observed patterns of vulnerability and GSI projects.

3.2.2 Definition and identification of service-needing areas

As previously mentioned, SNAs are defined by the location of vulnerable communities. Although many have argued that vulnerability is an intrinsic characteristic of a system, most analysts acknowledge that the vulnerability of a system only becomes relevant under the potential risk of a hazard (Cutter et al., 2003; Cutter & Finch, 2008; Damm, 2010; Kappes et al., 2012). Therefore, the quantification of vulnerability should consider both the likelihood of exposure to a particular hazard and the potential effects of the hazard on each of the social, ecological and infrastructure systems (e.g., flooding events affect all three systems, while extreme heat events only affect social and ecological systems). In this study, SNAs are thus identified by using the spatial co-location of different levels (i.e., nominal categories) of susceptibility and hazard exposure.

This approach recognizes that not all hazards affect urban systems equally, thus exposure severity categories of a hazard are only associated with susceptibility of relevant sub-systems. More specifically, SNAs are defined using the various combinations of susceptibility and exposure severity to urban heat island and flooding. For example, one vulnerability level to urban heat island might be described by a *high* social susceptibility and a *very high* exposure severity to extreme heat. By using the severity associated with each of these two dimensions of vulnerability, the decision as to which combination of susceptibility categories and degrees of hazard exposure merits attention is left to the index user. Lastly, as discussed in Chapter 2, no assumptions are made about the impact of hazards on the ecological system and therefore ecological susceptibility is not associated with a hazard.

This definition of SNAs avoids assumptions about how the two dimensions of vulnerability should be aggregated into a single metric, a common method used in previous studies. In the hazard literature, most studies have used summation or multiplication methods to relate these two metrics, resulting in an index of relative vulnerability. While easy to interpret and implement, the use of these aggregation methods assumes a particular type of relationship between the degree of vulnerability changes and a unit change in either the hazard exposure severity or the susceptibility of the system. Summation methods assume a linear relationship, while multiplication methods assume more complicated relationships that could reduce compensability problems (i.e., low values in one indicator can mask high values in another).

Proposed approaches have often also combined the vulnerability to multiple hazards by adding up the resulting values of vulnerability, and therefore have assumed that the degree of vulnerabilities to different hazards is the same. Both of these assumptions are problematic, especially when the degree of vulnerability is being used to guide decision making. To date, there is no consensus as to which of these approaches should be used and very little evidence to support either assumption. The use of either of these aggregation methods introduces an additional level of uncertainty. Furthermore, preliminary analyses in this study showed that the assumed relationships between susceptibility and hazard exposure can have significant impacts on the spatial patterns of relative vulnerability.

3.2.3 Definition of service-providing and service-benefiting areas

In a recent review by Demuzere et al., 2014 the author emphasizes the need for a framework that accounts for the multi-scale and multi-functional nature of GSI as a climate mitigation strategy. The study suggests that the benefits of GSI associated with stormwater management (i.e., flood mitigation and improvements to water quality), human and restorative capacities, and CO_2 reductions can be perceived and reasonably quantified at three spatial scales (site-scale/ city-block, neighborhood/district, and city region). However, the literature review also highlighted the lack of supporting evidence to suggest that GSI benefits associated with other air quality improvements (e.g., NO_2, PM_{10}), thermal comfort, reduction in energy use, and other ecologic services are well understood and quantified at scales larger than the site-scale/city-block (e.g., Ekkel et al., 2017; Park et al., 2017).

The lack of consensus and empirical evidence to support the quantification of non-stormwater GSI benefits at scales larger than site-scale/city-block suggest the need for different quantification methods in their assessment. As such, this study relates the GSI benefits to vulnerable areas by differentiating between the stormwater management benefits (i.e., hydrologic benefits) and the GSI benefits that are provided to the immediate surroundings (i.e., localized). This differentiation is done by using two spatial relationships: the hydrologic connectivity of the topography and an omnidirectional spatial relationship.

3.2.3.1 Localized benefits

In this study, the localized benefits of GSI are defined as those that require the beneficiaries to be in spatial proximity (i.e., Euclidian distance of ≤ 1 mile) in order to receive benefits. Among the most common and well-recognized localized benefits associated with GSI are thermal comfort, reduced energy use, human health, provision of micro-habitats, and improvements in air quality (mostly CO_2 sequestration) (Pakzad et al., 2017).

The individual cooling capacity of site-specific GSI has been reported to be dependent on its type and structure and has often been limited to its immediate surroundings. This cooling capacity is most often associated with changes to the surface albedo from replacing impervious surfaces and providing shade with trees. Trees, for example, can have a radius of influence between 3-12 m (Akbari et al., 1992; Troxel et al., 2013) which is most often associated with the height and width of the tree crowns (i.e., shading potential and evapotranspiration) (Wang, 2016; Park et al., 2017). Gardens have shown to be capable of having a surface temperature of 4 °C lower than the immediate surrounding surfaces (Cameron et al., 2012). Green roofs have been observed to reduce daytime roof temperatures by as much as 3 °C (Sharma et al., 2016). However, more recent studies have demonstrated that the cooling capacity of larger, more centralized green spaces (e.g., parks) can have larger regions of influence. For example, Vaz Monteiro et al. (2016) concluded that green spaces between 3-5 hectares (ha) could have cooling benefits that extend a distance of 70-120 meters. Lin et al. (2015) found that 2 km^2 parks could affect the temperature of surrounding areas up to a distance of ~250 meters.

Similar to the urban heat island mitigation potential, the potential of GSI to improve ecologic connectivity and habitat integrity at the site-scale is often limited. Studies often report an increase in biota (i.e., insects, birds and small reptiles) near or within GSI (Cameron et al., 2012).

However, when analyzed at the larger scale, connected GSI can help reduce the landscape resistance to movement of different species, thus improving ecologic connectivity. GSI has also been shown to provide mental health benefits (i.e., stress, depression, anxiety), improve cognitive abilities, encourage physical activity and serve as an educational tool (Morris, 2003; Chang & Chen, 2005; Maas et al., 2006; Tzoulas et al., 2007; Lee & Maheswaran, 2011; Thompson et al., 2012). For people to receive these health benefits, the quality of the green spaces (e.g., degree of visual stimulation) and access and proximity to the GSI (e.g., positive interactions with nature) are arguably among the most critical factors (Lee & Maheswaran, 2011; James et al., 2015). Studies have also found that urban green spaces that are poorly maintained and in disrepair are less likely to be visited due to a perceived lack of safety.

In order to account for differences in spatial extent of each of these benefits and avoid assumptions about appropriate distance thresholds, this study adopts the concept of spatial proximity. The approach follows Tobler's first law of geography (Tobler, 1970; Lloyd, 2006), which assumes that those in closer proximity to the GSI will have a higher likelihood of perceiving its benefits. Additionally, no assumptions are made about how the presence of GSI affects the degree of vulnerability in surrounding areas. Therefore, the analysis solely computes the distribution of vulnerability around the GSIs.

Under these assumptions and generalizations, spatial proximity is measured using Euclidean-ring buffers (Figure 3.1) around each of the GSI projects up to a distance of 1800 meters (a maximum distance threshold used in previous studies addressing issues of accessibility to urban green spaces) (Wendel et al., 2011; Heckert, 2013). Ring buffers define the area of analysis by taking the difference between an inner and outer circular buffer of different diameters. As such, ring buffers are selected over circular buffers because they allow exploration of how the distribution of vulnerability changes as the distance from the GSI increases. While the use of circular buffers would also allow exploration of the change in vulnerability as the distance from the GSI increases, it would only provide the cumulative vulnerability of the areas surrounding the GSI. The use of ring buffers allows more explicit observation of how areas at different distances from the GSI contribute to total cumulative vulnerability (i.e., the difference between the cumulative vulnerability at two different distances when using circular buffers).

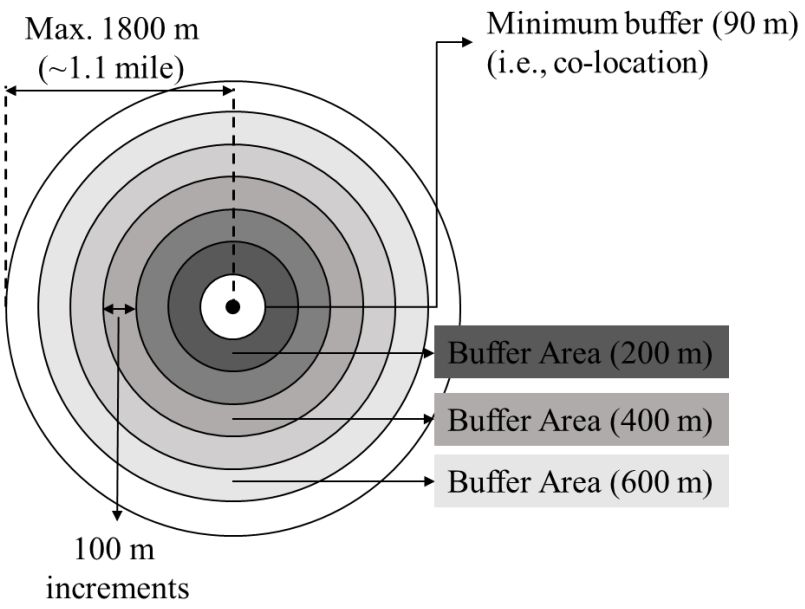

Figure 3.1. Illustration of Euclidean ring buffers used to assess the change in vulnerability as a function of the distance from the GSI. Ring buffers are incremented using distance steps of 100 meters. The minimum and maximum buffer diameters are 90 meters and 1800 meters, respectively.

3.2.3.2 Stormwater management benefits

The main goal for the implementation of engineered GSI has been improved management of stormwater runoff. These benefits have often been quantified by a reduction in peak discharge at the watershed outlet and/or in the total volume of surface water runoff, especially from impervious surfaces. In order to estimate the impact of GSI on these two criteria, a hydrologic model is needed to consider complex rainfall-runoff processes in urban watersheds (e.g., infiltration, water routing, performance of hydraulic structures such as storm sewer systems, surface and subsurface water interactions, etc.). A large array of urban hydrology models are available to model these processes (see reviews by Jefferson et al., 2017 and Kuller et al., 2017). However, the models usually require very detailed data about the properties of the watershed and the stormwater management infrastructure (e.g., drainage and sewer system, location of pervious and impervious surfaces, soil properties, etc.) that may not be readily available. Furthermore, calibration data are needed in the form of discharge values at a gauging station near the outlet or downstream of the watershed, which are not available in many watersheds.

In lieu of these very detailed models, at larger scales (i.e., city, regional) approximate hydrological analysis of a watershed is often completed using digital elevation models (DEMs), which can identify watershed boundaries, sub-catchments, channel and stream networks, stream lengths, and many other parameters (for reference, see Maidment, 2002, and Dixon & Uddameri, 2016). To conduct these analyses, two of the most important watershed characteristics are flow direction and flow accumulation. Broadly defined, these two parameters describe how the total amount of surface water flows across the terrain, assuming each terrain cell receives a rain drop. As such, these parameters have been the foundation for flooding analyses, assessment of geomorphological processes, and modeling of overland flows (e.g., Maidment, 2002; Khaleghi et al., 2011; Dixon & Uddameri, 2016; Zhang et al., 2017).

Acknowledging the complexities that dominate hydrological processes in urban watersheds, and because of its common use in large-scale hydrological analysis, this study uses the metric of flow accumulation to represent the hydrological connectivity of the landscape (i.e., potential water flow that exists between different areas of the watershed). The use of flow accumulation accounts for potential flow paths that the stormwater runoff retained at GSIs could have followed and thus aids in identifying areas downslope of the GSI project to which a large portion of this retained volume of water would have drained. These areas are then assumed to be the beneficiaries of the GSI stormwater management benefits.

However, not all cells downslope of GSI projects have an equal likelihood of receiving these benefits. To account for these differences, this study makes use of the multiple flow direction method (MFD) proposed by Freeman (1991) & Quinn et al. (1991), called FD8, to calculate flow accumulation. The FD8 method allocates the outflow of a terrain grid cell to its neighboring downslope grid cells using the slope between cells to proportionally distribute the flow. Using the FD8 method, it is assumed that each individual GSI grid cell has the potential to reduce flow accumulation of its downslope cells by 1 unit of runoff/grid cell area (i.e., maximum runoff potential of a grid cell). Because no rainfall is assumed and the resolution of the grid cell is constant, the estimation of how much of this 1 unit of runoff/grid cell area is received by downslope cells (i.e., potential reduction to flow accumulation because of the GSI) is dependent on the terrain topography and the allocation of flow calculated using the FD8 method.

The advantage of using a multiple flow direction method is that it provides a more conservative estimate of the downslope and upstream areas by not constraining the potential water

flow to a single flow path downslope, as in the steepest descent method [D8]. A conservative estimate is appropriate given the uncertainties in the DEM, the exact geo-location of the GSI, and errors/uncertainty in the land cover data. Furthermore, it allows conclusions that are statistically significant by not reducing the number of downslope samples to a single cell.

The disadvantage of using an MFD method is that a decision needs to be made as to how flat regions will be handled. Allocating the potential water in a terrain grid cell of a flat region using differences in slope is not possible as all surrounding cells have the same terrain elevation. In this case, the algorithm needs to assume an allocation of the water flow, otherwise no allocation of the water is made and the hydrologic connectivity is discontinued (i.e., the flat region is interpreted as a sink – no outlet). There are two possible solutions to this problem: (1) pre-processing the DEM so that there are no flat areas and/or sinks, or (2) using a different approach to allocate the flow in these situations. Solutions in the latter category include the assumption of an equal likelihood, and thus an equal allocation of the water to all neighboring cells (i.e., deterministic), the random allocation of the water to a specific number of cells (i.e., random), and the allocation of the water to all neighboring cells with some introduced noise (i.e., randomized).

Once again, in an effort to be conservative and draw conclusions about the vulnerability in downslope areas of the GSI project that are insensitive to these limitations, this study considers two different resolution DEMs and two approaches to water routing over flat areas. The DEMs evaluated include a 10-meter resolution DEM obtained from the National Elevation Dataset (NED) and the 30-meter resolution hydrologically-corrected DEM provided in the National Hydrography Dataset (NHDPlus), both owned by the United States Geological Survey (USGS). The NHDPlus DEM is resampled to a 10-meter resolution using bilinear interpolation in order to match the resolution of the data to the susceptibility and hazard exposure severity indicators. The two approaches to water routing over flat areas are: (1) treating flat areas as sinks and (2) deterministic allocation. Treating flat areas as sinks assumes that none of the areas downslope of flat areas are hydrologically connected, thus no benefits can be perceived. On the other hand, the deterministic approach assumes that all areas downslope of flat areas would receive water flow allocation (i.e., no restriction on hydrologic connectivity).

3.3 Case study – Philadelphia, PA

In order to investigate the utility of the proposed approach, the City of Philadelphia, PA is used as a case study to explore the spatial patterns between vulnerability and engineered GSI. The Philadelphia Water Department (PWD) has committed to invest $1.6 billion dollars in GSI as a means to reduce stormwater runoff and prevent occurrences of combined sewer overflows (Philadelphia Water Department, 2009). As part of their *Green City, Clean Waters* project (Philadelphia Water Department, 2009), PWD began implementing numerous GSI projects around the city in 2009. More importantly, the PWD has compiled and validated detailed information about implemented and planned GSI projects, data that is currently scarce in most U.S. cities. This information includes types of GSI and a polygon representation of their geo-locations, which allows a more accurate definition of GSI parameters for benefits estimation and comparison with vulnerability.

PWD has also committed to active engagement with the private sectors to achieve their stormwater mitigation goals, as they acknowledge that using public lands alone will be insufficient. Considering the opinion of diverse stakeholders in the planning and design of GSI projects has been argued to be critical for successful and efficient implementation (Heckert & Rosan, 2016; Meerow et al., 2017; Kuller et al., 2017). However, it has also been argued that GSI stakeholder incentive programs (e.g., tax rebates) can reinforce social and environmental inequalities (Perkins et al., 2004; Heynen and Perkins, 2005; Heynen et al., 2006). Sectors that receive incentives to implement GSI are often those with more economic resources, that own private land, and that have more available space on their properties. Furthermore, there is often lack of confidence in effective long-term maintenance of GSI when implemented in communities with a lack of economic resources (Heckert et al., 2016). As such, GSI projects implemented in the City of Philadelphia provide an opportunity to investigate whether these challenges have caused disparities in the mitigation of vulnerabilities and to illustrate how the proposed approach could inform more equitable and just GSI implementations.

The PWD GSI project data are available at the OpenDataPhilly portal (https://www.opendataphilly.org/). The data include a list of different types of implemented and planned GSI projects from both public and private owners. Data associated with implemented GSI projects include year of installation, from 2000 to 2016, (Figure 3.2) and whether they are on public or private land. Data provided for planned GSI (i.e., in design, waiting approval, or in

construction) is in the form of point locations and includes a general description of the selected site and a list of the different types of GSI that are intended to be constructed. Because of their point location format, the data for planned GSI are only used to investigate how these locations spatially relate to areas with a high potential for benefits and needs. Finally, PWD's data on type of GSI is related to types of benefits as shown in Table 3.1. Based on the descriptions provided by PWD for each listed GSI, it is assumed that infiltration/storage trenches and pervious pavements, which have no vegetation, provide little to no benefits associated with habitat preservation/improvement, reduction of urban heat island, or human health.

The spatial co-location of GSI and SNAs is explored by using a minimum buffer distance of 90 meters and a maximum distance of 1800 meters (refer to Figure 3.1 for reference). A minimum buffer distance of 90 meters is used because at least 98% of the landscape has land surface temperatures that do not vary by more than 5 °F (Figure B.2 in Appendix B), and thus it is assumed that the hazard exposure severity to urban heat island would not vary much within such a short distance. Lastly, Euclidian - ring buffers are created using a 100-meter increment.

Table 3.1: Potential benefits of different types of GSI

GSI Types	**Potential Benefit (Mitigation/Restoration)**			
	Hydrologic	**Ecologic**	**Urban heat island**	**Human health**
Infiltration/Storage trench	✓			
Bumpout	✓	✓	✓	✓
Rain garden	✓	✓	✓	✓
Wetland	✓	✓	✓	✓
Basin	✓	✓	✓	✓
Tree trench	✓	✓	✓	✓
Planter	✓	✓	✓	✓
Pervious pavement	✓			
Swale	✓	✓	✓	✓
Green roof	✓	✓	✓	✓

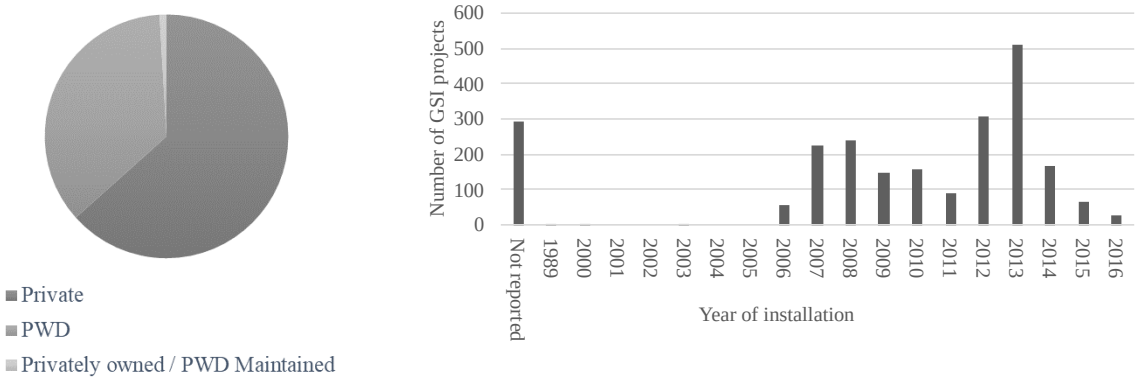

Figure 3.2: Summary of ownership and year of installation for GSI projects

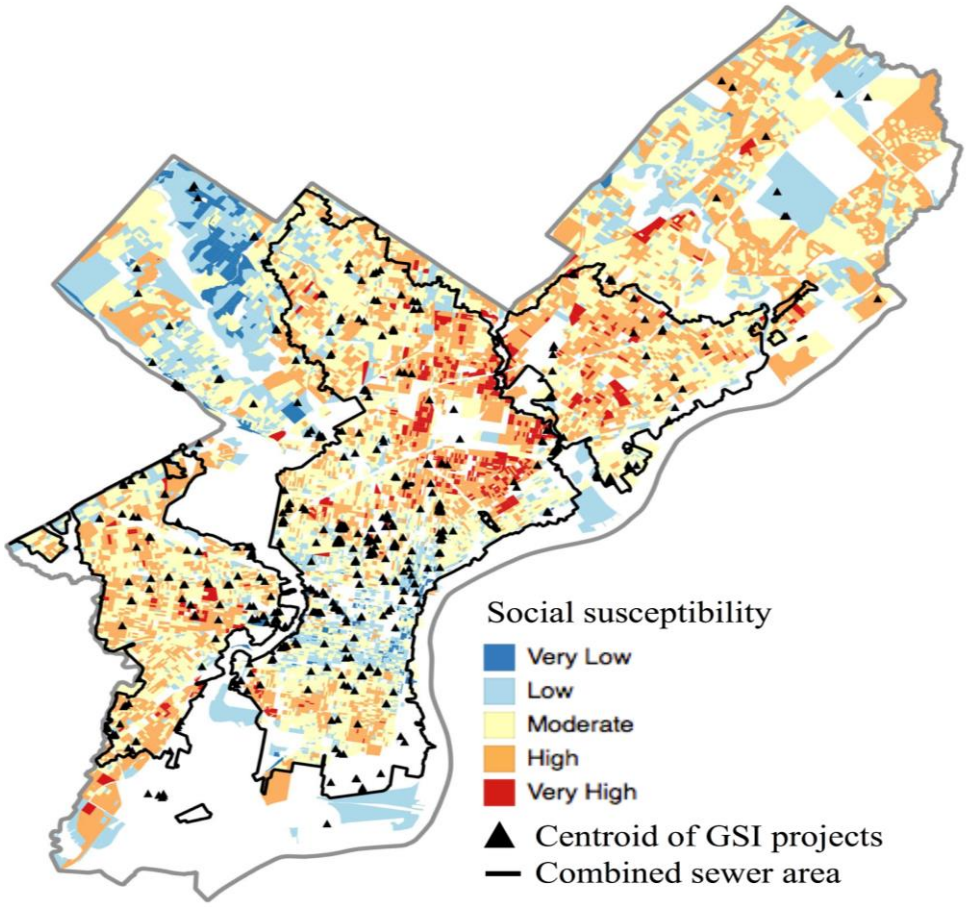

Figure 3.3: PWD GSI projects and social susceptibility.

3.4 Results and discussion

This section presents the spatial patterns among GSI projects in the City of Philadelphia, PA and the identified SNAs and SBAs. The analyses are restricted to the combined sewer service area, shown in Figure 3.3, where PWD has concentrated GSI implementation. The results include:

(1) spatial proximity of GSI projects to SNA for ecological susceptibility and social vulnerability related to urban heat island, (2) distribution of social vulnerability to flash flooding in areas downslope of the GSI projects, and (3) spatial synergies between SNAs that could represent missed opportunity for maximizing multifunctionality of GSI.

3.4.1 Spatial patterns of susceptibility and urban heat island vulnerability

3.4.1.1 Spatial co-location

Figure 3.4-A presents the distribution of susceptibility categories with spatial co-location (i.e., 90 meter concentric circle buffers) of GSI projects. Figure 3.4-A suggests that most GSI projects are associated with areas of moderate susceptibility, with few projects located in very low or very high susceptibility areas. Only a spatial co-location of GSI projects with areas of high infrastructure susceptibility are observed.

Note that in Figure 3.4-A, the percentages of the total buffer area associated with infrastructure susceptibility are generally low (i.e., less than 10%). This is because non-building areas are excluded from the infrastructure susceptibility calculations (i.e., rather than assigning a very low susceptibility, non-building areas are assigned a null score). Therefore, a large percentage of the total buffered areas is associated with null infrastructure susceptibility. Nevertheless, the results show that most buildings around the GSI (i.e., a higher percentage of the total buffered area) have higher infrastructure susceptibility. These results are likely due to almost 2/3 of all GSI projects being implemented on privately owned land. Due to data limitations, infrastructure susceptibility in this study considers only building use and buffer zones around buildings with the highest need for protection (i.e., schools, hospitals, community centers, senior centers, and residences). Thus, given the PWD goal of targeting schools and privately owned land for GSI implementation (Philadelphia Water Department, 2009), it is not surprising that higher infrastructure susceptibility is observed.

Furthermore, one of the main goals of the PWD is the reduction of impervious surfaces and greening of the combined sewer service area. Thus, it is not surprising that many of the GSI projects are located near areas with moderate to high ecological susceptibility. Lastly, one of the indicators used to calculate social susceptibility is the ownership status of the household. Areas with a higher number of owned households receive a lower susceptibility score. To investigate whether the observed distributions of social susceptibility were due to biases introduced by land

ownership, the results were recalculated considering only GSI projects located on public land. No significant changes to the results were observed, thus suggesting that even those projects that have been located on public lands have been located in areas of moderate social susceptibility.

Another possible explanation for the observed distributions of susceptibility was the introduction of biases from assigning susceptibility categories. Moderate susceptibility is associated with all values that between 25^{th} and 75^{th} percentiles, and thus account for a larger percentage of the data. In order to test the hypothesis that the observed distributions in Figure 3.4-A were not a caused by a category bias (i.e., a larger percentage of the total area associated with a susceptibility category was within the buffers), the total area contained in the 90-meter buffers for each susceptibility category was divided by their respective total areas in the combined sewer service region. Figure 3.4-B presents the result of these calculations. It can be seen that, in general, all susceptibility categories had a similar percentage of their total area within the buffered area and thus it can be assumed that no category biases were introduced to the susceptibility patterns.

Note that when using Census Blocks, the distribution of GSI located in areas with very low social susceptibility changes significantly (i.e., about 20%) when compared to results obtained using Census Block Groups. This change in distribution is mostly due to the siting of GSI in unpopulated areas. On the other hand, GSI distributions in areas with high social susceptibility did not change significantly when using either Census Blocks or Census Block Groups for the social susceptibility calculation. The small differences observed for the high and very high social susceptibility categories were due to the small number of GSIs that were spatially co-located in these areas. Such results further highlight the biases that can be introduced when using Census Block Groups to calculate social susceptibility. As such, all other results are presented in this section at both spatial scales to illustrate the impacts of this assumption on the observed spatial patterns.

Figure 3.5 presents the results of the spatial co-location of GSI and socially vulnerable areas for urban heat island exposure. The results suggest that GSI projects with heat island mitigation potential have mostly been located in areas of low to moderate vulnerability and not in areas with the highest degree of exposure severity. When accounting for categorical biases, some of these findings become even more significant. Figure 3.5-B presents the *stacked* percentages of the total vulnerability area included within the buffers (i.e., each combination of susceptibility and hazard exposure severity is one partition in the bars, thus the theoretical maximum of the y-axis is

500%). Figure 3.5-B shows that although 52% of the total area associated with a high to very high hazard severity are included within the buffer areas, thus spatially co-located with the GSI, only 11% was co-located with areas of high to very high social susceptibility. This finding is more significant in areas with very high social susceptibility and very high hazard severity at the Census Block scale, since 0% of these areas were included within the buffers. In short, while it seems that GSI projects have been located in areas with high degree of exposure severity to urban heat island, the results suggest that there has been no consideration of the susceptibility of the communities in these areas. Therefore, those more vulnerable to urban heat island are not the most likely beneficiaries of the urban heat island mitigation potential offered by the GSI projects in Philadelphia.

Lastly, one possible explanation for the observed distributions of susceptibility and vulnerability in Figures 3.4 and 3.5 is that these patterns are caused by the assumptions made in assigning susceptibility categories. First, it is assumed that the location of the GSI and the assignment of the susceptibility and hazard exposure categories are not independent spatial processes. In other words, it is assumed that the location of the GSI projects should be influenced by the degree of vulnerability. Second, the observed distributions of vulnerability are analyzed by considering both the percentage of buffered areas and the percentage of total area associated with a susceptibility category and different degrees of hazard exposure severity.

Therefore, under these two assumptions, if the planning of GSI has targeted the most vulnerable areas, then the buffer area around the GSI should account for a large percentage of the total area associated with the higher vulnerability categories. This would be true even though the total area might be small compared to the areas associated with other degrees of vulnerability (e.g., moderate susceptibility with moderate hazard exposure severity). However, such patterns are not observed in Figures 3.4 and 3.5, and instead GSI projects are located in areas of moderate to high hazard severity with low to moderate susceptibility (i.e., low to moderate vulnerability). Therefore, the results suggest that the PWD has not targeted the most vulnerable communities and the assignment of high to very high susceptibility categories does not have a significant impact on the results.

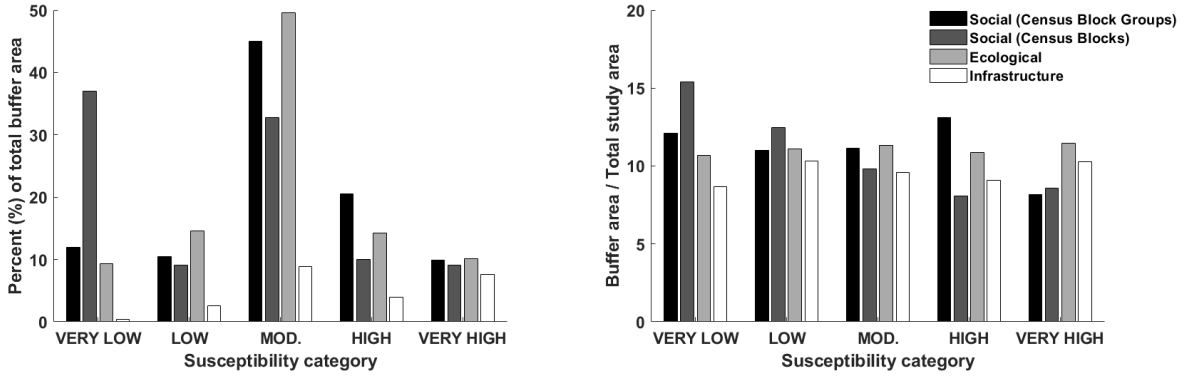

Figure 3.4: Left (A): Distribution of the social, ecological and infrastructure susceptibility categories of areas where GSI was located. Right (B): Percent of the total area associated with a susceptibility class included within the buffered areas.

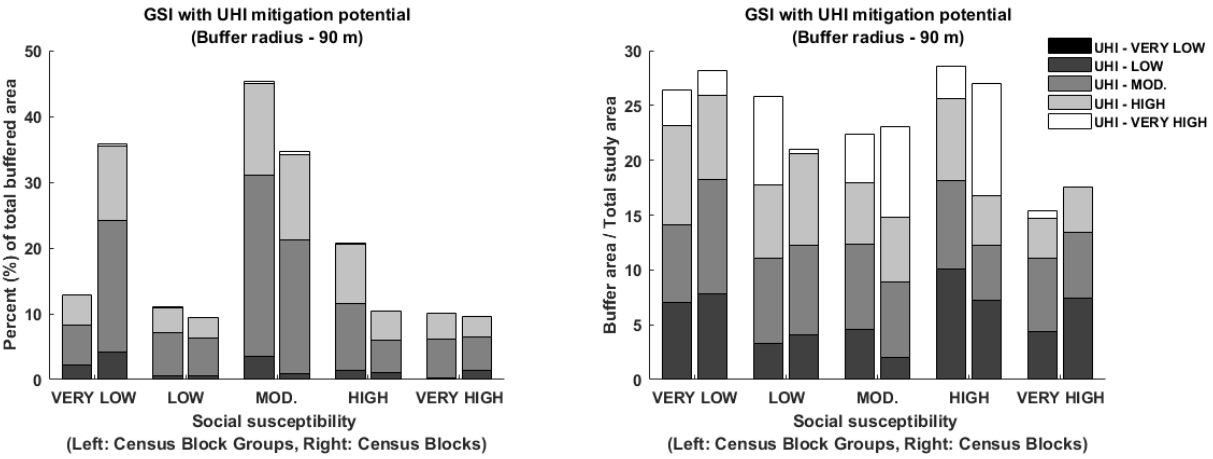

Figure 3.5: Left (A): Distribution of social vulnerability to urban heat island for areas where GSI was located. Right (B): Percentages of the total area associated with UHI vulnerability classes within the buffered areas. Legend shows the hazard severity categories for UHI.

3.4.1.2 Changes in vulnerability with spatial proximity

Having explored the distribution of susceptibility and vulnerability as it relates to the spatial co-location of GSI projects, the next step was to investigate how these distributions changed with distance from the GSI. Figure 3.6 shows the change in susceptibility and hazard exposure severity for each of the areas covered by the Euclidian ring buffers. It can be observed that as the distance from the GSI increases, the percentage of buffer area corresponding to higher social susceptibility categories increased. However, the maximum percentage of buffered area was observed to still be less than 20% at a distance of 1000 meters from the location of the GSI projects.

On the other hand, no changes were observed in the distribution of ecological susceptibility and infrastructure susceptibility decreases with distance. These patterns suggest that a very small number of GSI projects have been located in areas surrounding communities with higher social susceptibility. Furthermore, the decrease in infrastructure susceptibility with distance from GSI confirms the hypothesis that many of these projects were sited in residential, school, or hospital areas.

Figure 3.7 shows the change in social susceptibility and severity of urban heat island as a function of distance to GSI projects. In this case, only the change in vulnerability using Census Blocks is illustrated as a more significant variability was observed than when using Census Block Groups (Figure B.3 in Appendix B). Similar to the results of spatial co-location, when considering only the percentage of buffered areas corresponding to different degrees of vulnerability, no significant change is observed (Figure 3.7-A). The most notable trends are the decrease in percentage of area associated with moderate social susceptibility and increase in very low susceptibility, and the increased percentage of the buffered area corresponding to a very high hazard severity category. These results suggest that the areas surrounding GSI tend to have lower social susceptibility and a higher degree of exposure severity. When the total area within the buffers is divided by the total area corresponding to a particular degree of vulnerability, Figure 3.7-B shows that this increase in hazard severity is quite significant. At a distance of 900 to 1000 meters from the GSI, the percentage of the total area associated with very high exposure severity and high and very high social susceptibility are 60% and 35%, respectively. In other words, if GSI projects had been located within these areas, they would be in much closer proximity (< 100 meters) of 95% of the area with the highest vulnerability (i.e., very high exposure severity and high to very high social susceptibility). These results suggest that urban heat island mitigation and/or social susceptibility were not one of the major drivers in PWD's selection of potential GSI locations.

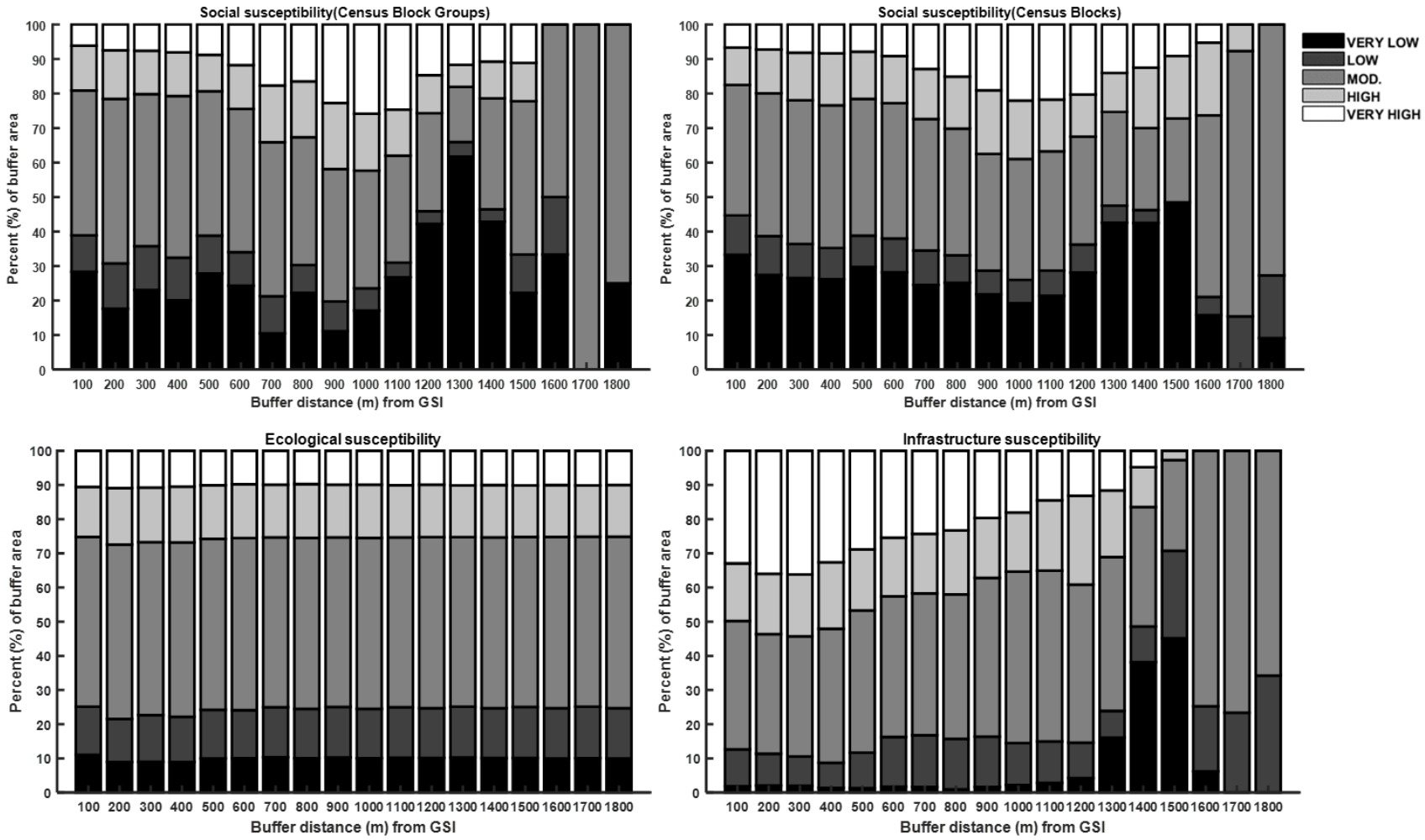

Figure 3.6: Changes in the distribution of susceptibility as a function of distance from the GSI.

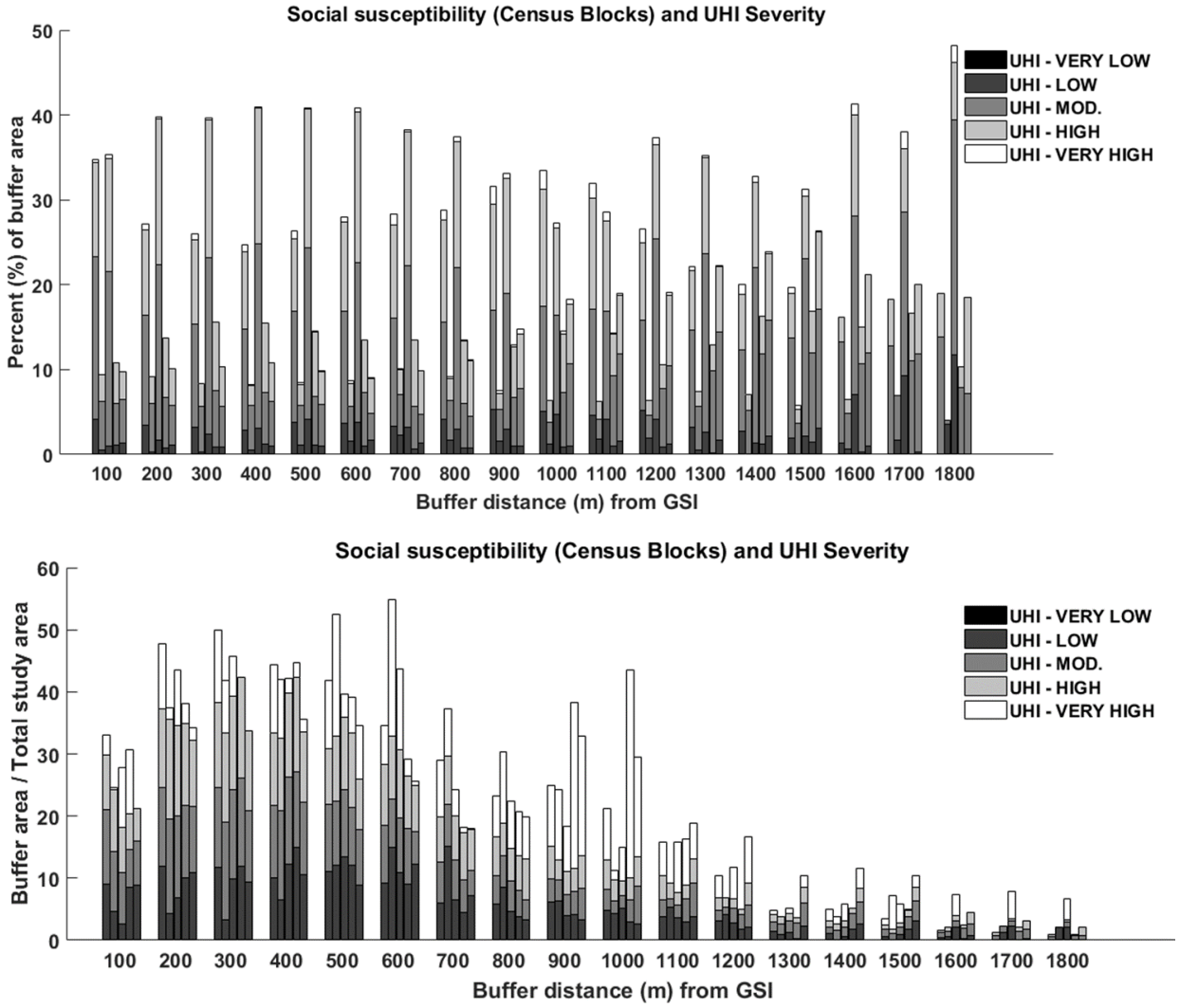

Figure 3.7: Changes in distribution of hazard exposure severity and social susceptibility as a function of distance from the GSI. For each ring buffer distance, the plotted bars represent the different categories of social susceptibility [i.e., Left: Very Low to Right: Very High]. Top graph (A) presents the change in distribution relative to the area of the ring buffer. Bottom graph (B) presents the change in distribution relative to the total area associated with each of the potential combinations of vulnerability.

3.4.2 Spatial patterns of flood vulnerability and stormwater management benefits of GSI

The analysis of GSI SBAs and SNAs for stormwater management benefits are presented in a similar fashion to those in the previous subsection. Figure 3.8 shows the distribution of social susceptibility categories and corresponding degrees of exposure severity to flash flooding of areas

downslope of the GSI projects. However, unlike the results in the previous section, the total area associated with a vulnerability category is calculated using the total downslope area of the GSI project, as opposed to the total area within the buffered area as for the localized benefits. The results are again presented for both Census Block Groups and Census Blocks to illustrate the importance of accounting for non-populated areas and small "hot-spots" of high social susceptibility (as presented in Chapter 2).

Additionally, Figure 3.9 shows the distributions of vulnerability to flash flooding for different potential stormwater benefits (i.e., the percentage of potential reduction to the flow accumulation caused by the GSI projects). Lastly, the results are shown using both DEM sources (i.e., NHDPlus and USGS) and the two approaches discussed for handling flat areas in the calculation of flow accumulation (i.e., No Flats – considered flats as sinks, Flats – used deterministic approach to estimate direction and allocation of the flow).

The results in this section show that, in general, the GSI projects tend to be located upstream of areas with high flash flooding potential (i.e., high to very high exposure severity categories). This is not a surprising result since the abatement of stormwater runoff has been the major driver in PWD's GSI implementation. However, GSI projects are located in no particular social susceptibility category, suggesting that vulnerability of downslope areas was likely not taken into consideration. In Figure 3.8-A, most GSI projects were located upstream of areas with very low (probably unpopulated) and moderate social susceptibility. When evaluating the category biases (Figure 3.8-B), most categories had similar percentage of their total area included within these downslope areas, although those associated with very low and very high social susceptibility consistently had the highest percentages. Given that highly vulnerable areas are not more likely to be downslope of the GSI and that the total area by vulnerability category was similar, it suggests that observed patterns are more a function of the approach used to assign nominal categories of susceptibility and hazard exposure severity and that GSI projects were not sited with the intention of reducing vulnerability.

Lastly, the observed patterns were consistent regardless of the DEM used or the treatment of flat areas in the flow accumulation calculation. Although different combinations of DEMs and flat area approaches had an impact in estimating total downslope areas (as expected), the relative differences between vulnerability categories remained consistent, providing a higher degree of robustness to these findings.

The most vulnerable areas are also less likely to receive a larger portion of the stormwater reduction benefit provided by the GSI projects. Figure 3.9 presents the reduction in flow accumulation by vulnerability category. The observed patterns of vulnerable communities having low likelihood to receive GSI benefits were more pronounced by taking into account flow accumulation reduction in these areas. Furthermore, areas that are benefiting the most from the GSI projects are those associated with moderate exposure severity and moderate social susceptibility.

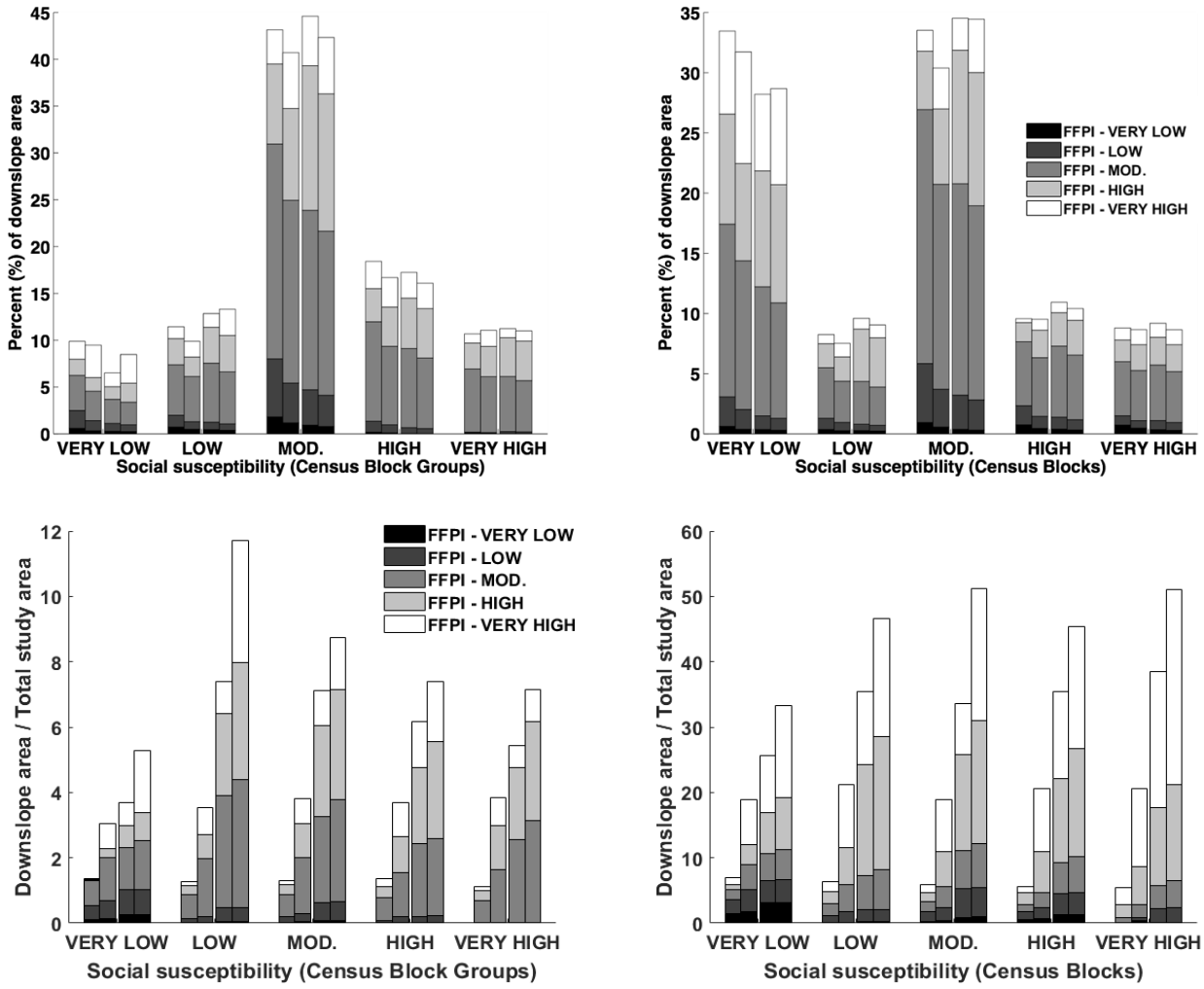

Figure 3.8: Top graphs (A): Vulnerability of downslope cells from the GSI projects. Bottom graphs (B): Percent of total area associated with each vulnerability class. [Left: Census Block Groups, Right: Census Blocks]. The bars in each susceptibility category correspond to the use of (left to right) USGS DEM-No Flats, USGS DEM-Flats, NHD DEM-No Flats and NHD DEM-Flats.

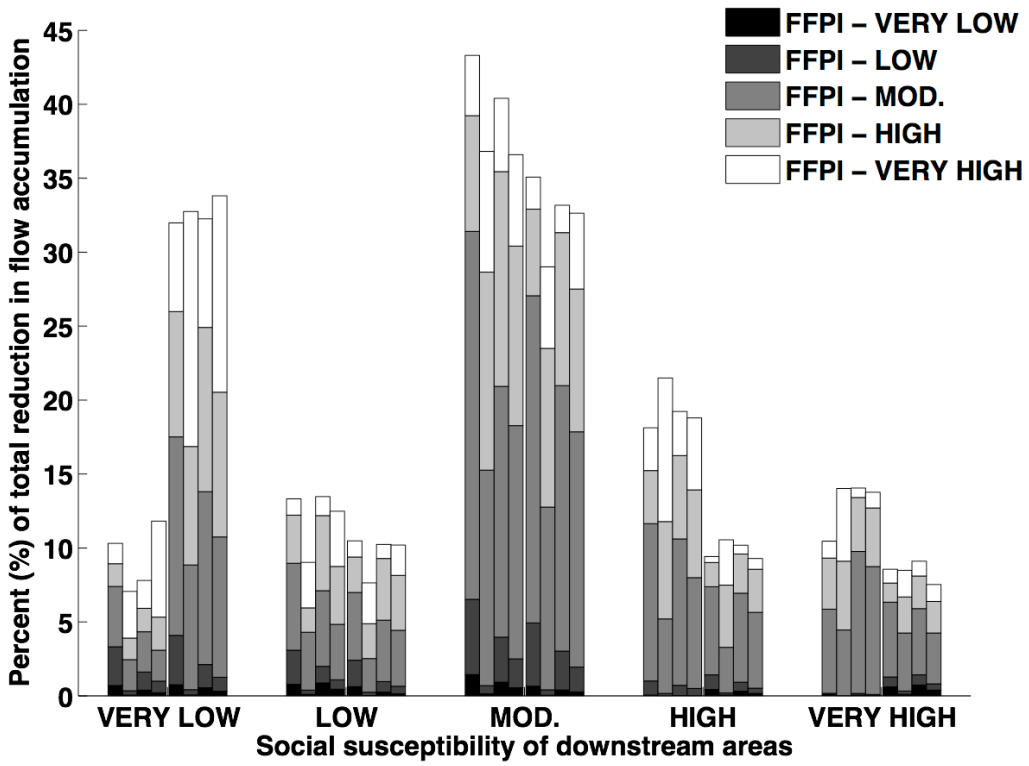

Figure 3.9: Total reduction in flow accumulation in downslope areas. The bars in each susceptibility category correspond to the use of (left to right): Block Groups / USGS DEM-No Flats, Block Groups / USGS DEM-Flats, Block Groups / NHD DEM-No Flats, Block Groups / NHD DEM-Flats, Blocks / USGS DEM-No Flats, Blocks / USGS DEM-Flats, Blocks / NHD DEM-No Flats and Blocks / NHD DEM-Flats.

3.4.3 Spatial patterns of planned GSI and SNAs: Are we maximizing opportunities?

Having observed that most implemented GSI projects have not been sited in areas that benefit the highest vulnerable areas, the next step is to examine planned GSI projects. The spatial intersection of the nominal categories of high and very high susceptibility and hazard exposure severity is used to identify: (1) areas upslope of communities with high vulnerability to flash flooding, (2) vulnerable communities to urban heat island, (3) areas upslope of impaired water bodies, and (4) areas with high social and ecological susceptibility. These areas offer the maximum potential benefits for GSI. Upslope areas are calculated using the USGS DEM, since it has a higher grid resolution, and considering both approaches for treatment of flat areas.

Figure 3.10 presents visual representation of areas with high to very high synergy potential and planned GSI. Visual inspection of these patterns suggests that most of the planned GSI projects

seemed to be surrounding these high synergy areas, rather than located within them. Moreover, a significant portion of the planned GSI are located near the central-east boundary of the combined sewer service area, which has very little synergy potential. In order to quantify these spatial patterns, Figure 3.11 presents the change in distribution of the synergy potential as a function of distance to the planned GSI projects. Between 400 and 500 meters from the location of the planned GSI projects, the percentage of areas with high synergy potential could be larger.

A possible explanation for the observed patterns is PWD's goal to install GSI projects on public land associated with parks and schools and on private properties. Figure 3.10 shows that 34% of the planned GSI projects are confined to schools or parks. The rest of the projects were intended to be installed in identified green streets or other vacant lots. While this approach has benefits for reducing the cost of implementation (e.g., land acquisition, construction and maintenance/operation, etc.), it may hinder siting GSI in areas that could increase return on investment by improving the vulnerability of several systems simultaneously.

Another hypothesis was that perhaps these locations were chosen to address areas not being served already by regulation projects in private properties (i.e., required by PWD in any new development) (Philadelphia Water Department, 2018). The PWD requires new development to treat "the first 1.5 inches of runoff from all directly connected impervious area (DCIA) within the limits of earth disturbance." To test this hypothesis, a clustering analysis using the cross-L function was done. The cross-L function is a measurement of repulsion (no clustering) or attraction (clustering) between different point sets (Appendix A.2). As such, the tested hypothesis is: the planned PWD GSI projects would show repulsion (no clustering) with respect to GSI regulation projects that were already implemented or planned. The results (Figure 3.12) suggest that there is a statistically significant clustering (i.e., p-value ≤ 0.01 for 100 simulations of complete spatial randomness [CSR]) around planned regulation projects at a distance of approximately 400 meters and no statistically significant pattern with currently installed regulation projects.

These results suggest that most of the planned PWD GSI projects have been located near areas of new development where GSI projects are now required under current regulations. However, the results also show that no significant spatial pattern is observed between the locations of planned PWD GSI projects and current regulation projects. Further research and engagement with the PWD is needed to better understand these conflicting results and the policies and strategies driving future GSI projects. Nevertheless, the results presented in Figures 3.11 and 3.12 confirm

the hypothesis that planned PWD GSI projects have not been located in areas of most need for GSI benefits.

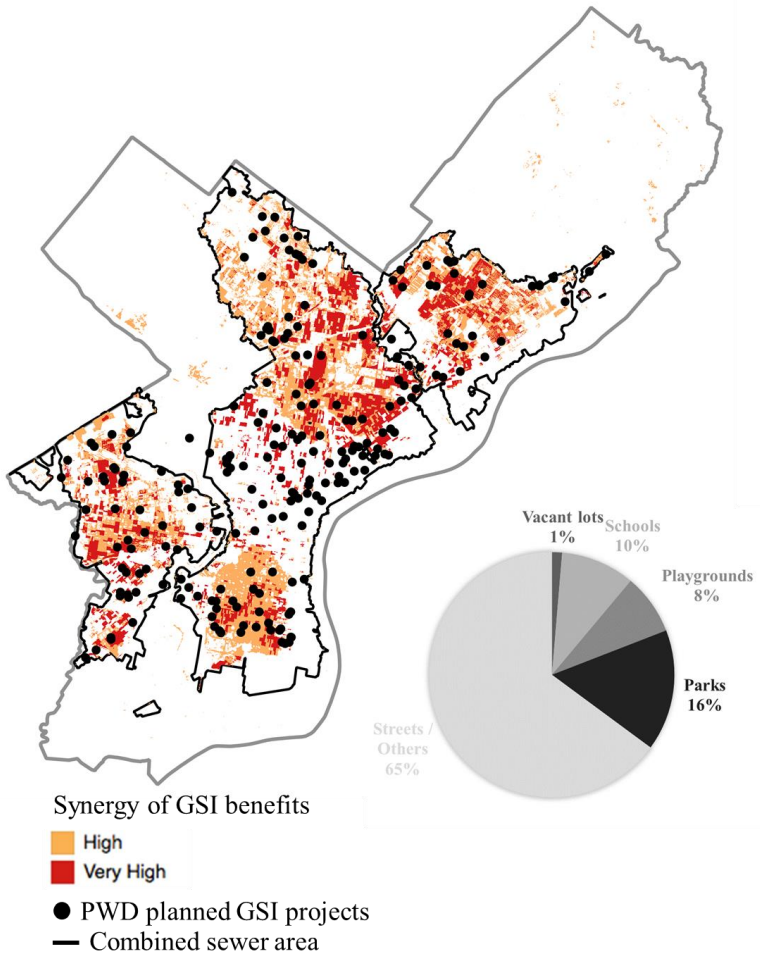

Figure 3.10: Types of locations for planned GSI projects and their spatial relationship with areas of high synergy.

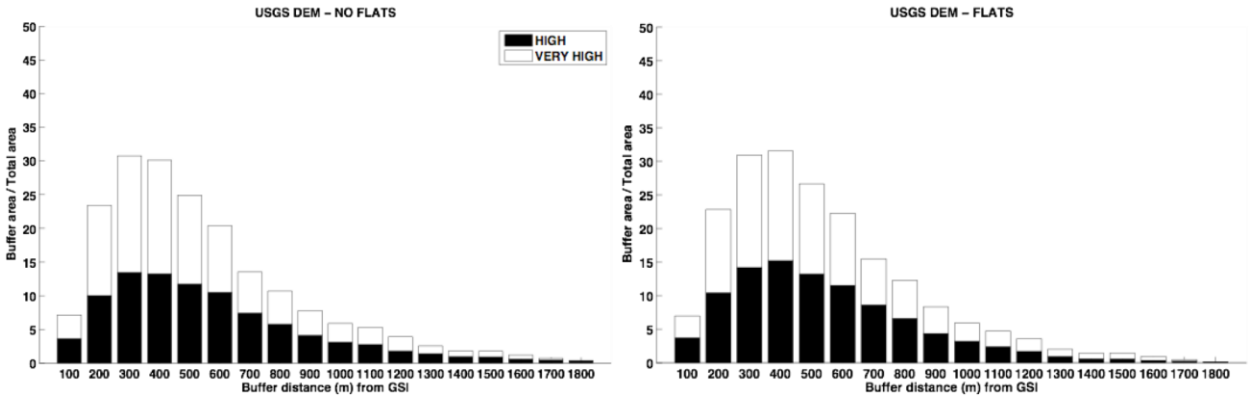

Figure 3.11: Synergistic potential of areas surrounding the planned GSI projects.

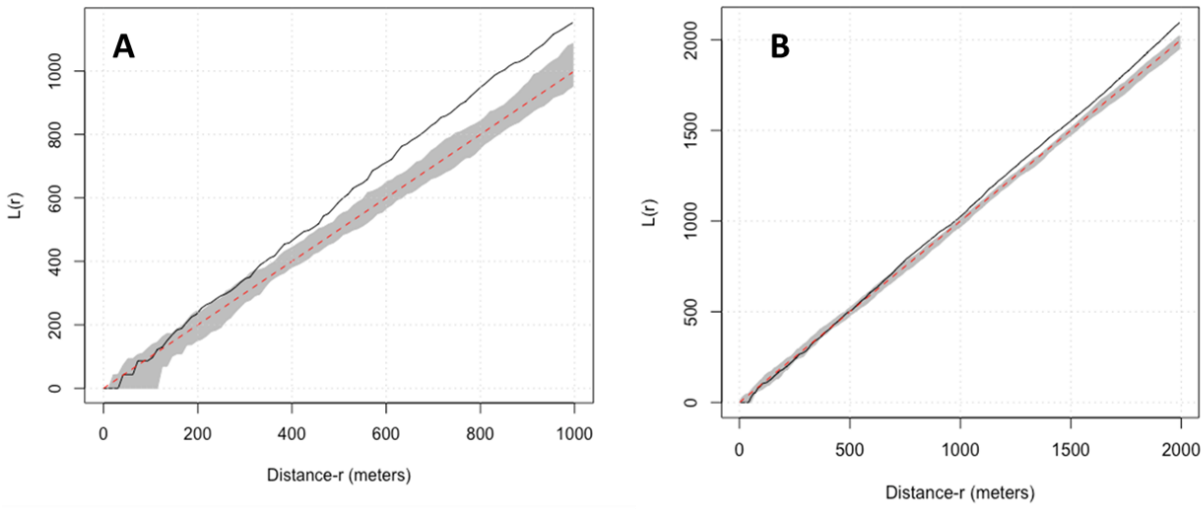

Figure 3.12: Cross-L functions for PWD planned GSI projects with respect to: (A) planned regulation GSI projects and (B) current regulation GSI projects. Solid black lines represent the values of the L-function, the gray region shows the envelope of statistical significance for the simulations of complete spatial randomness, and the dashed red line represents the theoretical Poisson L-function.

3.5 Conclusions

With growing popularity of GSI in cities, it is important that planning decisions consider the social and environmental justice implications of siting decisions. This study explores the spatial relationships between green infrastructure and socio-ecological vulnerability using a new analytical method for more spatially explicit assessment of GSI benefits.

The results from the spatial analysis of current and planned GSI projects and vulnerability in the City of Philadelphia suggest that GSI projects could be more strategically placed to maximize multifunctionality for the most vulnerable communities. Current GSI projects have most often been co-located in areas of low to moderate socio-ecologic susceptibility and UHI vulnerability. Additionally, most of these GSI projects are upslope of areas with very low to moderate vulnerability to flash flooding, and a portion are upslope from unpopulated areas.

Finally, by using the spatial intersection between different SNA, the method identifies areas with high synergistic potential for GSI implementation that are within 500 – 1000 meters of current GSI projects. Additionally, future planned PWD projects are in close proximity, but not

within, these areas of high priority for GSI implementation. Most of these planned GSI projects are clustered around private regulatory projects, suggesting that siting decisions are most likely based on land ownership criteria.

The findings of this study concur with previous studies that have highlighted the need for planning tools to represent more spatially explicit GSI benefits (Kuller et al., 2017). By calculating the results at both the Census Block Group and Census Blocks, this study shows that, particularly for stormwater abetment benefits, the spatial scale of analysis has a significant impact on the results. Such findings suggest that previous studies exploring the spatial relationship of GSI and vulnerability might have misestimated the true beneficiaries of GSI and overestimated the spatial correlations between the location of GSI and the vulnerability of those communities.

The findings of this study however, are limited to the analysis of GSI projects in the City of Philadelphia and should be tested in other cities. Rai (2018) has developed GSI detection tools that can be used to identify GSI locations, since most cities do not have complete inventories of GSI. Furthermore, the conclusions presented in this study are limited by the assumption that all GSIs have the same effectiveness to reduce/retain stormwater runoff. In reality, the runoff reduction potential varies among different types of GSI; exploring these differences might provide new insights about the magnitude of benefits experienced by communities in service needing areas. Finally, more investigation is needed on the spatial relationship of GSI and vulnerability under different organizational, institutional and governmental structures. For example, do GSI projects planned by non-profit organizations show a different relationship with vulnerable areas? How different are the spatial patterns of vulnerability and GSI benefits in cities with required GSI implementation (e.g., Baltimore City) versus voluntary programs? Such analysis would provide a much richer understanding of the factors that may prevent GSI implementation in the most vulnerable locations.

CHAPTER 4. AN INTEGRATED AND SPATIALLY SCALABLE PRIORITIZATION FRAMEWORK FOR GREEN STORMWATER INFRASTRUCTURE SITING

4.1 Introduction & problem statement

As discussed in Chapter 1 and confirmed with the case study in Chapter 3, current methods for large-scale spatial planning of GSI lack consideration of multiple benefits at multiple scales. Additionally, only a few studies have considered the vulnerability of socio-ecologic systems for prioritization of future GSI implementation. This chapter presents a new planning support system (PSS) for prioritization of GSI siting to address these limitations.

Planning support systems (PSS), a term introduced and defined by Harris (1989), are information frameworks that integrate a diverse set of criteria, information technologies, and data. PSS need to be interactive, adaptable, flexible, integrative, and allow for a participatory process (Harris, 1989; Malmqvist et al., 2006; Geertman & Stillwell, 2012; Chandio et al., 2013; Brown et al., 2015; Kuller et al., 2017). More specifically, for PSS to be successful in guiding the decision-making process, they need to: (1) provide a deeper and richer understating of the problem at hand and (2) allow translation of ideas into actionable plans by aiding their formulation and communication between stakeholders (Ashley et al., 2004; Geertman & Stillwell, 2012; Malczewski et al., 2015; Kuller et al., 2017). When used for spatial planning, PSS need to explicitly represent the spatial problem, translate information between different data sources and scales of analysis, and enable the spatial analysis and production of highly visual and easily interpretable results (Geertman & Stillwell, 2012; Malczewski et al., 2015).

To date, the use of PSS for spatial planning of GSI has focused solely on estimating stormwater management benefits. Kuller et al. (2017) review an extensive list of PSS used for spatial planning of GSI in practice and research. The study concludes that most of the available PSS for spatial planning of GSI have rarely been used for planning purposes, especially at large spatial extents (e.g., city scale). The primary reasons for this *implementation gap* (Kuller et al., 2017) are: (1) methods that are too generic, complex, inflexible, and technology-oriented, and (2) tools that require specific and detailed data and trained personnel to use them (Klosterman, 1997; Geertman & Stillwell, 2004; Vonk et al., 2005; te Brömmelstroet & Bertolini, 2008; Viavattene et al., 2008; Kuller et al., 2017). These limitations have prevented PSS from being used for evaluating GSI implementation scenarios, story-telling and translation of vision plans, and providing

transparency to decision processes. Additionally, the use of GSI hydrologic models has been hindered by their complexity (distributed parameter models) and lack of spatial explicitness (lumped parameter models) needed to integrate with other GSI multi-criteria decision analysis at multiple scales (Kuller et al., 2017).

The quality of the PSS and their use during the planning process have great influence over the success of the implemented GSI (Montalto et al., 2013; Kuller et al., 2017). Using current PSS could lead to technologically optimized plans that fail to provide the full range of benefits in practice. To address these problems and increase the use and uptake of PSS in the spatial planning of GSI, new tools are needed. In particular, previous studies suggest that new PSS should consider reframing the spatial planning of GSI as a *location choice* (Locke et al., 2010; Norton et al, 2015; Kuller et al., 2017). As a location choice, the goal becomes identifying locations in which GSI could be most *efficient* (i.e., suitability of the site to implement GSI) and *effective* (i.e., delivering benefits to areas with the greatest need). For this goal, it has been suggested that new PSS should sacrifice some of the complexity associated with correctly modeling the hydrologic behavior of the GSI in order to provide user friendly, flexible, and heuristic but methodologically competent tools that generate easily interpretable results (te Brömmelstroet & Bertolini, 2008). Planning tools tend to lose transparency and user friendliness with increasing complexity. On the other hand, disregarding this complexity can diminish the accuracy and comprehensibility of the results. Therefore, finding a balance between these competing factors is an active area of research.

Other than the evidence-based framework proposed by Kuller et al. (2017), in which the authors present a list of indicators that have been used in practice or research to represent the *efficiency* and *effectiveness* of different types of GSI, to the author's knowledge, no other study has proposed an analytical framework that considers the spatially explicit assessment/integration of these two components. Moreover, no other PSS considers a wide range of socio-ecological factors nor, more importantly, the vulnerability of these systems to multiple hazards (Kuller et al., 2017). *The central premise of this chapter is to develop and test a new spatially scalable multi-objective optimization framework as an improved PSS for spatial planning of GSI. The framework considers multiple GSI benefits, provides flexibility to consider opinions of multiple stakeholders, and incorporates vulnerability of socio-ecological systems.*

The framework is applied to three watersheds in the City of Dallas, TX, the City of Philadelphia, PA, and Baltimore County, MD, to test the utility and robustness of the prioritization

method in diverse hydroclimates and at multiple spatial scales (11 km^2, 5 km^2, and 1 km^2 watersheds). The watershed in Baltimore County, MD, is used to test the utility of the proposed framework to inform decisions at the scale at which GSI is typically planned (i.e., small neighborhood, sub-watersheds $\leq$ 2 km^2; Golden et al., 2017; Jefferson et al., 2017). The case studies in Philadelphia, PA, and Dallas, TX, explore the impact of different hazard mitigation goals and planning criteria (i.e., different stakeholder opinions) on the spatial distribution of different types of GSI and their impact on the vulnerability of socio-ecologic systems. The study concludes with a discussion about the implications of GSI siting decisions on vulnerability and how the proposed framework could be used as a PSS to guide future decision making towards more socially just implementations.

4.2 Methodology

The GSI prioritization framework consists of three main components, shown in Figure 1.1: (1) identification of suitable GSI sites given local regulations and design criteria, (2) quantification of geographical preferences based on the potential of these GSI to mitigate multiple hazards, improve ecological integrity and human health, and consider different planning policies, and (3) identification of locations and types of GSI using geographical information systems (GIS) multi-criteria decision analysis (GIS-MCDA). Using screening rules associated with different design criteria and planning regulations, the methodology begins by identifying areas with the greatest suitability for GSI implementation. These areas are then subdivided into potential spatial arrangements and sizes for different types of GSI. Each of these spatial arrangements is then assigned a geo-preference score that estimates the potential of GSI to provide different benefits in these locations. Finally, a multi-objective optimization framework is used to maximize the potential of GSI to reduce stormwater runoff volume from impervious surfaces while considering other benefits, including improvement of socio-ecological vulnerability. The following subsections define these steps in more detail.

4.2.1 Identification of suitable sites

The process of identifying suitable sites for implementing GSI is often dominated by two main factors: (1) the biophysical properties of the potential site and design criteria associated with the GSI, which depends on the main driver for its implementation (e.g., stormwater runoff

reduction, reduction in urban heat island, etc.), and (2) institutional and organizational policies and regulations that dictate availability of urban spaces for different types of GSI. In practice, the site identification process is often time consuming and costly, as a holistic analysis of site suitability requires a large amount of data, approval of many government agencies, and consideration of the opinions of many different stakeholders. Furthermore, this process is often conducted at the neighborhood or sub-watershed scale, as large-scale planning (e.g., city or county scale) would significantly increase costs and planning duration (e.g., Shoemaker, 2009; Marney, 2012). To address these challenges, rule-based methods have been developed to rapidly and inexpensively identify potentially suitable sites for GSI installation using predetermined thresholds for different design criteria (e.g., Viavattene et al., 2008; Marney, 2012; Lee et al., 2012; Locke et al., 2013).

One of the most well-known and widely used rule-based methods for GSI planning is the EPA BMP Siting Tool (Shoemaker, 2009; Lee et al., 2012), which is a component of the workflow implemented in the EPA SUSTAIN tool (US EPA SUSTAIN, 2018). EPA SUSTAIN is best known for its capacity to optimize a portfolio of different types of GSI using an evolutionary algorithm that maximizes reduction in runoff volume and improvements to water quality while minimizing the project's total cost. To generate an array of different alternatives for evaluation, SUSTAIN first identifies potential locations for implementing GSI using the EPA BMP Siting Tool's design and policy criteria, for which thresholds are defined (e.g., distance from building > 10 feet). In addition, the tool allows users to rank potential locations based on user preference for soil type. Locations meeting all criteria are then evaluated as potential sites for implementing a specific type of GSI.

The siting methodology used in this work takes a similar approach to the EPA BMP Siting Tool. The method selects sites based on how their features compare to different design and policy thresholds, and selects sites meeting all criteria as potential locations for GSI implementation. Table 4.1 presents this framework's list of criteria, which were selected based on recommendations from the literature (Lee et al., 2012; Kuller et al., 2017) and design manuals shown. Many of these criteria and their recommended thresholds are used in the EPA BMP Siting Tool and the GSI design guidelines listed for several U.S. cities. However, unlike the EPA BMP Siting Tool, the proposed approach also includes ranges for the site's percent of tree canopy and percent of imperviousness. These ranges prevent GSI from being placed in locations with high tree canopy coverage or high degrees of perviousness, since these sites already provide some of the same

benefits as GSI. Additionally, GSI is not placed in highly impervious locations given that implementation is often costly and/or impractical in these areas. Finally, the EPA BMP Siting Tool reports the results as vector features (i.e., polygons), while the proposed approach identifies sites at the 10-meter raster cell level (i.e., grid cells). This enables integration with the other steps of the framework and different spatial aggregations (e.g., total surface area of GSI). Furthermore, it enables the use of grid-based distributed hydrologic models for more detailed evaluation of GSI implementation scenarios.

This methodology for identifying suitable areas is robust and adaptable, as it enables adding or removing additional criteria for different types of GSI. Additionally, the use of thresholds reduces the computational cost of analyzing large spatial extents and a large array of different GSI.

Table 4.1: Criteria for identifying potential GSI implementation sites.

Siting criteria	Small GSI (retention)	Large GSI (retention)	Trees	References
Drainage Area (acres)	< 5	10 < DA < 25	-	EPA SMP Siting Tool
Slope (%)	<= 5	<= 15	<= 30	
Imperviousness (I) (%)	30 < I < 80	30 < I < 80	30 < I < 80	
Soil Group	A-D (with ranking)	A-D (with ranking)	-	
Road buffer	< 100 ft	> 100 ft	-	
Stream buffer	> 100 ft	> 100 ft	-	
Building buffer	> 10 ft	> 60 ft	> 10 ft	
Tree Canopy (TC) (%)	TC < 60	TC < 30	TC < 60	Design manuals from multiple cities
Outside 100yr floodplain	Yes	-	-	
Land cover (NLCD, 2011)	Developed, barren, shrubland, herbaceous	Developed, barren, shrubland, herbaceous	Developed, barren, shrubland, herbaceous	
Min. Surface Area	8% of impervious area	30% of impervious area	-	
Links to Design Manuals				
Santa Clara Valley County	http://www.scvurppp-w2k.com/pdfs/1112/c3_workshop/c3_workshop_track_2_sizing_calcs_6-5-12.pdf			
City of Seattle	http://ascelibrary.org/doi/pdf/10.1061/41009%28333%2961			
City of Portland	https://www.portlandoregon.gov/bes/71127			
City of Sacramento	https://www.cityofsacramento.org/-/media/Corporate/Files/DOU/Specs-Drawings/SWQ_DesignManual_May07_062107.pdf?la=en			

4.2.2 Assessment of different spatial configurations for infiltration structures

Once suitable areas for implementing GSI have been identified, the next step in the methodology is to assess how these areas can be used to implement different spatial configurations and different sizes of infiltration and retention structures. The spatial configuration of the GSI refers to the many potential options for spatial clustering of grid cells to make up the GSI surface

area. The assessment of potential spatial configurations is especially needed when considering large areas that have significant numbers of grid cells.

The assessment of potential spatial configurations of infiltration structures begins by assuming that every grid cell within a suitable area could potentially be used to implement GSI. For the purposes of this discussion, the total spatial extent associated with an identified suitable area will be referred to as $Area_i$, where i is an index between 1 and the total number of suitable areas, and the total number of grid cells within $Area_i$ will be referred to as M_i. Using this notation, a single grid cell is the smallest type of GSI that could be considered for implementation within $Area_i$, and its maximum surface area is considered to be equal to the area of the grid cell.

The algorithm then sorts the grid cells by their flow accumulation (i.e., the proxy metric use to represent the total amount of surface water flow across the terrain, as introduced in Chapter 3) and identifies the grid cell with the largest flow accumulation within $Area_i$. It is assumed that the grid cell with the largest flow accumulation is the location with the highest likelihood of receiving the most stormwater runoff and thus the most desirable location to implement GSI. From the grid cell with the largest flow accumulation, an iterative process begins in which directly connected grid cells (i.e., contiguous in all directions) with the largest flow accumulation are added recursively. In the case that multiple cells have the same flow accumulation value, each of them is considered as a different spatial configuration with the same surface area. This process continues until no more grid cells are directly connected or the total extent of the $Area_i$ is accounted for. Lastly, the process is repeated $M_i - 1$ times within the same $Area_i$ to account for potential spatial configurations with other upslope cells considered as the starting cell of the algorithm.

The described approach could yield a very large number of potential GSIs, especially if the spatial extent of $Area_i$ is large. To address this issue, a data tree structure is used to associate the different spatial configurations to the grid cells that were used as starting points of the recursive process described above. The use of a data tree structures the decision space of potential GSIs by their surface area. Thus, the root node of the data tree for $Area_i$ represents the largest possible GSI that could be implemented within it (i.e., theoretically, that area would be equal to $Area_i$). The child nodes of the root nodes would then be the second largest GSI that could be implemented, and so forth. Every time a level is added to the tree, multiple child nodes could be created if different spatial configurations have the same surface area. This process continues growing the data tree up to the point at which all child nodes are assigned a single grid cell. As such, the parent

nodes of the tree structure represent different spatial configurations of GSI, all with the same surface area. These different levels of the data tree will be denoted by the subscript *j* and the different spatial configurations for that level will be differentiated by the subscript *k*. Therefore, $Area_{ijk}$ represents the *k* spatial arrangement with a surface area associated with level *j* for $Area_i$.

This approach considers a significant number of different GSI implementation scenarios, a needed capability of any GSI planning tool. Furthermore, it provides the user with great flexibility to consider potential implementation of specific types of GSI (i.e., small infiltration structures with a specified surface area), or to explore the solution space by considering all possible scenarios. Moreover, because the approach is done for each $Area_i$, a specific type of GSI for which the stakeholders have a strong preference could be evaluated in one area, while in another $Area_i$ the full envelope of potential GSIs could be considered (e.g., a network of smaller GSI or a large retention structure such as a wetland).

4.2.3 Assignment of geo-preferences

Having identified potential GSIs that could be implemented, the next step of the methodology is to quantify the potential benefits of these GSIs to mitigate exposure severity to multiple hazards, improve ecological integrity and human health, and associate their geo-location with different planning policies. As noted earlier, this framework adopts the concept of geographical preferences (i.e., geo-preferences) for both the *efficiency* and *effectiveness* of potential GSI sites.

Geo-preference, a term often used in urban planning, represents a set of qualitative or quantitative levels of preferences associated with specific criteria (e.g., Locke et al., 2013; Norton et al., 2015; Jankowski et al., 2016; Kuller et al., 2017). The value used to indicate preferences can represent the magnitude of marginal preference of some locations over others or can simply define the preference order (i.e., rank). These geo-preferences are often extracted from the knowledge gathered from previous studies conducted at smaller and more detailed spatial scales. For GSI, these geo-preferences should identify the optimal location for the intended use and multi-functional benefits. Previous studies can inform the assignment of geo-preferences associated with the desired implementation location, given a particular objective (e.g., Marney, 2012; Locke et al., 2013; Norton et al., 2015; Kuller et al., 2017). Moreover, these geo-preferences should relate

vulnerability to the GSI's hazard mitigation potential, such that the most preferable locations are those that could provide the greatest benefits to the most vulnerable communities.

In this study, geo-preferences are limited to the specific effects that GSI can have on human health, hydrological performance (potential runoff retention), ecological and habitat restoration, and urban heat island (UHI) mitigation, as these are the benefits considered most important in the case study cities. Additionally, this study considers the geo-preferences associated with cities' policies and regulations, and the community's preferences for the types of GSI. The use of geo-preferences in this study highlights the capability and flexibility of the prioritization framework to consider multiple benefits, but other criteria may also be important in some regions.

The prioritization framework assumes that potential GSI sites are the service-providing areas (SPAs) described in Chapter 3. Thus, geo-preference scores are assigned to GSI sites based on their potential to deliver different localized benefits and stormwater management benefits to the respective service-needing areas (SNA). A geo-preference score for GSI *i* associated with the criteria *k* (i.e., g_{ik}) is then calculated by aggregating (i.e., summation or multiplication) normalized metrics derived using these methods. Geo-preference scores associated with criteria *k* are finally scaled between zero (i.e., very low preference) and one (i.e., very high preference). A brief discussion of the quantification of these geo-preference scores is provided in the sub-sections below.

4.2.3.1 Human health and ecological benefits

For people to receive human health benefits from GSI, access and proximity are considered the most critical factors (Lee & Maheswaran, 2011; James et al., 2015). Although there are no clear guidelines for locating GSI to maximize human health benefits, most studies suggest that the potential to walk, feel safe, and enjoy the aesthetics of green spaces motivate most people to make use of them (Morris, 2003; Maas et al., 2006). In urban planning, especially in transportation planning, it is often accepted that people are willing to walk between 0.25-0.50 miles, with a maximum of 1 mile, to their destination. As such, the geo-preference assigned to potential GSI sites for human health benefits consider 0.25, 0.5, 0.75 and 1-mile circular buffer zones around schools, hospitals, community spaces, parks, and green open spaces. Specifically, 0.25 mi buffers are assumed to have very high preference [1], while 1 mi buffers have low preference [0.25]. All buffer layers are then added (i.e., a GSI site that is 0.25 miles from school [score = 1] and 0.5 miles

from a hospital [score = 0.75] would receive a score of 1.75), and the resulting values are scaled between zero and one.

Additionally, sites that have high to very high social susceptibility within a 90-meter buffer are given higher priority. Geo-preference values for this criterion are then calculated by considering the percentage of the buffer area that has high to very high social susceptibility. Finally, the human health geo-preference score for a GSI site is calculated by adding the values obtained from both of these buffer analyses (Appendix A.3).

Similarly, the potential of GSI to restore ecological connectivity and provide habitat restoration has been associated with creating ecological cores in areas with little to no vegetation or in areas that have high resistance to the flow of species between ecological cores (McRae et al., 2008; Chang et al., 2012; Tannier et al., 2012). Additionally, GSI has been shown to improve the health of aquatic ecosystems by reducing pollutant loads to receiving waters, mimicking more natural stream flows, and recharging the groundwater (Zhao et al., 2013; Golden et al., 2017). The framework uses the indicators of ecologic susceptibility described in Chapter 2 and the methods from Chapter 3 for identifying areas with the highest need for ecological restoration/protection, and thus the areas with the highest need to receive these GSI benefits. GSI sites that are located near areas with high ecologic susceptibility (within a buffer of 90 meters as described in Chapter 3) or upslope of the most impaired water bodies (i.e., moderate to very high susceptibility) receive a higher geo-preference. Geo-preference scores of GSI sites are then calculated by taking the mean of the ecologic susceptibility within a 90-meter buffer and normalizing the resulting values between zero and one. Finally, if the GSI sites are upslope of water bodies with moderate to very high susceptibility a one is added to their geo-preference score (Appendix A.3).

4.2.3.2 Policy and planning criteria

Policy geo-preferences are those associated with the city's regulations for using and developing urban spaces. When planning and designing GSI, different regulatory mandates dictate the use and intended use of the land and/or the specific type of permitted development. These regulations can often be very strict and can deter the completion of a proposed project. Thus, when planning GSI installations, geo-preference should be given to those locations that either are in compliance or have the least potential for conflict. In this study, the preference associated with zoning regulations and the use of vacant lots were considered because of their common use in

planning GSI projects. Even though zoning and land use preferences differ between cities, design guidelines (see Table 4.1) indicate a high preference for locating GSI in residential and/or open urban areas (i.e, geo-preference score equal to 1), followed by a moderate preference for commercial/business areas (i.e., geo-preference score equal to 0.75-0.5), and very low preference for manufacturing/industrial sites (i.e., geo-preference score equal to 0.25 - 0), with some cities not even considering manufacturing/industrial sites as an option. Additionally, vacant lots, especially those owned by the city, are always a preferred location for GSI because the cost of acquisition and redevelopment is typically low. Thus, the geo-preference score of a GSI site for policy and planning criteria is calculated by adding up the normalized values of preferences associated with land use/zoning and a binary variable that indicates if the potential GSI is located within a vacant lot.

4.2.3.3 Urban heat island mitigation index

The quantification of UHI mitigation potential by different types of GSI remains a highly active area of research (Mirzaei, 2015). While models exist to estimate UHIs (Liu et al., 2011; Connors et al., 2013; Xu & Guo, 2014; Mirzaei, 2015), these are generally complex and require detailed spatio-temporal data for a large number of variables that are often not readily available. More importantly, no models were identified that could estimate the reduction in UHI due to implementation of different types of GSI and/or their spatial configuration. While the majority of previous studies have concentrated on site-scale measurement of the reduction in air and surface temperatures produced by trees, gardens, or green roofs, the impact of different levels of GSI implementation at larger scales is still unclear. Nevertheless, a significant number of studies have explored the spatial relationship between land surface temperatures (LST) and land cover and the cooling benefits of green spaces of different sizes and types (e.g., Chen et al., 2006; Connors et al., 2013; Myint et al., 2013; Maimaitiyiming et al., 2014; Zheng et al., 2014; Lin et al., 2015; Zhang et al., 2017). Therefore, the geo-preferences associated with the UHI mitigation potential of GSI followed the general recommendations and findings of these studies, as outlined below.

In general, larger and more concentric clusters of green spaces, especially those containing a higher percent of tree canopy, have been found to produce a stronger cooling effect than scattered, dispersed green spaces (Zhang et al., 2009; Myint et al., 2013; Maimaitiyiming et al., 2014; Lin et al., 2015). In addition, numerous studies (e.g., Chen et al., 2006; Connors et al., 2013;

Myint et al., 2013; Maimaitiyiming et al., 2014; Zheng et al., 2014; Zhang et al., 2017) have demonstrated how increases in impervious surfaces and loss of tree canopy are largely responsible for increases in LST and have demonstrated the positive effect of increasing vegetation coverage. Zheng et al. (2014) showed the importance of the spatial configuration of anthropogenic land cover features on the LST. The results suggest that city planners should target areas with a large continuous patch of paved surfaces and/or open areas with minimum vegetation for UHI mitigation. Additionally, optimization of the spatial arrangement of trees to provide maximum shading over these paved surfaces was recommended for significant UHI mitigation.

Following these general guidelines, geo-preference scores associated with the potential of GSI sites to mitigate UHI are assigned by considering four indicators: (1) surface area, (2) eccentricity, (3) mean LST, and (4) difference between mean LST within the potential GSI site and mean LST of the surrounding area. Potential GSI sites with a larger surface area and located in areas with higher LST are assumed to have higher cooling potential, especially if tree canopy is increased in these areas. The eccentricity, which measures the deviation of an area from a perfect circle (where 0 represents a perfect match and 1 represents a spatial arrangement close to a line), is used to give preference to GSI arrangements that are concentric. Finally, following the recommendations by Zhang et al. (2017), the difference in mean LST in the potential GSI area and the mean LST of surrounding areas is used as a geo-preference associated with GSI potential cooling capacity. It is assumed that GSI sites with higher mean LST than surrounding areas would have more significant impact in reducing LST.

Using these four indicators, the geo-preference score of every potential GSI site is calculated by taking the average of the normalized values of the indicators (Appendix A.3). Note that no GSI site is given a geo-preference score of 0, since it is assumed that reducing impervious surfaces will always help to mitigate UHI, even if it is small. Additionally, it is assumed that trees, particularly those with shading potential, are the preferred strategy for UHI mitigation over green open spaces and/or GSI that are *not* intended to retain large volumes of water (e.g., detention ponds) (Norton et al., 2015; Zardo et al., 2017). Finally, when taking into consideration social susceptibility of the communities where potential GSI are located, a higher geo-preference score is given to those sites in highly vulnerable areas. Highly vulnerable areas are identified by a binary variable and defined as those having any combination of the nominal categories of high to very high for social susceptibility and UHI exposure severity (refer to Chapter 3 for more details).

Finally, the UHI vulnerability is considered in the geo-preference score by multiplying the previously-calculated normalized indicator by the percentage of a 90-meter buffer area around the GSI deemed vulnerable to UHI.

It should be noted that the indicators used in this study to represent the cooling benefits of GSI sites should only be used as general guidelines, as the cooling effects of continuous green spaces are highly variable and will depend largely on the patch size and the characteristics of the surrounding area (Connors et al., 2013; Lin et al., 2015). As such, the use of these indicators to represent the potential of GSI projects to mitigate UHI has two main limitations. First, it assumes a linear relationship between the indicators and the cooling benefits of GSI. Previous studies have shown that this might be a valid assumption for areas smaller than 1-2 ha, but the relationship becomes non-linear for larger areas (Lin et al, 2015, suggested an exponential relationship.).

Secondly, these indicators do not account for the additional cooling benefits that a GSI project could provide when another nearby GSI project is also implemented. To what degree the cooling benefit of an area is affected by additional implementation of nearby GSI is not clear or well documented to date (Zhang et al., 2017). Lastly, the cooling benefits of specific types of GSI could be maximized by following different and more detailed guidelines for their optimal geo-location. For example, large trees tend to provide the greatest cooling benefits by providing shade; thus, the recommendation is that they be placed next to buildings and/or over streets where shade can have the largest impact (Locke et al., 2010; Norton et al., 2015). However, implementing many of these guidelines at the watershed scale can be challenging, as high spatial resolution data (e.g., tree locations, building height, road width, etc.) are needed to assess not only the potential impact on land surface temperature but also the watering needs of the infrastructure itself (Norton et al., 2015).

4.2.3.4 Hydrological performance: Potential runoff retention index

The stormwater management benefits of GSI are undoubtedly the primary driver for their implementation. Any PSS proposed to aid in the spatial planning of GSI should therefore reflect the heuristics used for stormwater design and planning and use appropriate performance indicators. In this study, the hydrological performance of GSI sites, and thus their potential for mitigating the risk of flooding, is approximated using the potential runoff retention index. The index serves as a proxy for the potential of different locations and types of GSI to reduce the volume of runoff

produced at these sites and/or from their contributing upslope area. Volume of runoff was selected as the metric of interest, instead of peak discharge reduction, because several well documented indices exist for its estimation. Additionally, considering only the dampening of peak flow in GSI design could have the negative effects of producing longer peak flows (due to superposition of the resulting hydrographs) if done without careful consideration of the hydrologic connectivity of the sub-watersheds (McCuen, 1979; Emerson et al., 2005; Goff & Gentry, 2006; Petrucci et al., 2013). Careful assessment of the potential effects caused by peak discharge reduction requires the use of hydrologic models and their calibration with gauge data, which is a level of complexity that the proposed planning framework is intended to avoid.

The calculation of the potential runoff retention index in this study relies on two primary assumptions: (1) the hydrologic connectivity of the landscape can be quantified by using a multiple flow direction method, and (2) the concept of a design capture ratio. As discussed in Chapter 3, the use of the multiple flow direction method (MFD) proposed by Freeman (1991) and Quinn et al. (1991) [FD8] is used to represent the hydrologic connectivity of the landscape, and the metric of flow accumulation is used to represent the likelihood of this connectivity. In this chapter, the same assumptions and methods are used to integrate the concept of capture ratio.

GSI capture ratio is a proxy metric that is used to represent the efficiency of the GSI in reducing stomwater runoff given its total surface area, its design ponding depths and infiltration rates, and the amount of runoff from contributing upslope area (Lee et al., 2012). Its calculation varies depending on the available information and the intended use, but it is most commonly represented by the ratio between the water storage capacity of the GSI and the expected volume of runoff that will drain to it. The capture ratio has been used in many planning and design guidelines for quick assessment of potential GSI sites (e.g., design guidelines in Table 4.1). In particular, it is most often used as a sizing criterion where the surface area of the GSI needs to be greater than a percentage of the total impervious area it treats. In some cities, the proposal for any new GSI must meet a predefined minimum threshold for the capture ratio. For example, the City of Portland, OR, requires that the surface area of proposed infiltration structures be at least 6-9% of the total drainage area (City of Portland, 2018). Hydrologic tools such as the EPA National Stormwater Calculator (SWC) (US EPA SWC, 2018) have also used this metric for the sizing of GSI and for estimation of the expected reduction in runoff by different types of GSI. In the SWC manual, capture ratios of 5-6% of the total contributing impervious area are recommended (p. 47).

Using the MDF method and the concepts discussed above, the potential runoff retention index of a GSI is quantified as the ratio between its surface area (e.g., number of connected cells [$Area_{ij}$]) and its contributing drainage area. The potential runoff from the contributing drainage area for any GSI is calculated by adding up the runoff potential of all grid cells that are upslope from it. The potential runoff of each grid cell caused by 1 in of rainfall is quantified using the NRCS TR-55 composite curve number for connected impervious areas. Curve numbers are one of the most extensively used methods for estimation of the potential runoff from areas with different land uses, land cover, and soils. Its long history of use and investigation have shown that it is a reliable proxy metric to the estimation of runoff potential, although it is well known that it tends to overestimate the runoff volumes (Paudel et al., 2009). The curve numbers used in this study are those associated with the land cover categories from the National Land Cover Database (NLCD, 2011; Homer et al., 2015), and were gathered from the most common values in the literature (NRCS TR-55, 1986; WSDOT, 2014). Finally, the adjusted curve numbers for a given land cover with a percentage of impervious area are estimated with the following equation (NRCS TR-55, 1986):

$$CN_c = CN_p + \frac{P_{imp}}{100}\left(98 - CN_p\right) \tag{4.1}$$

where CN_c is the runoff curve number for the entire land use, CN_p is the pervious runoff curve number and P_{imp} is the percent imperviousness. This equation is used when the runoff from impervious areas is directly connected to the drainage system or the runoff occurs as a shallow concentrated flow that runs over the pervious area and then into the drainage system. These two assumptions are usually valid for urban and/or residential land where GSI are often implemented. Within this framework, this equation was used to account for the different imperviousness found within the same land cover category, and therefore assumes that those grid cells with higher imperviousness will have a higher potential to produce runoff.

Using equation 4.1, the total drainage area of a GSI (i.e., DA_i) is then calculated by adding the runoff potential (i.e., CN) of all contributing cells as determined by the MFD. As previously discussed, the MFD method partitions the flow coming out of a grid cell to its downslope neighbors by using the slope between cells to proportionally distribute the flow. Therefore, the contribution of runoff from a grid cell upslope from a GSI site is calculated by multiplying the percentage of

contributing flow, determined by the MFD, and the CN of that grid cell. The total drainage area of a GSI is thus the sum of the potential runoff of all grid cells upslope.

The proposed potential runoff retention index has several properties that make it desirable for the prioritization of GSI sites. By using this index, GSI sites with a contributing area with low tree canopy cover and a large area of impervious surfaces receive a higher geo-preference for GSI because these areas are assumed to be the most influential in producing larger runoff volume whose mitigation will result in a larger reduction in vulnerability. Additionally, GSI that are upslope in the watershed are preferred given the likelihood of these sites to have larger capture ratios. Upslope GSI sites are often desirable given their larger potential to retain and reduce the velocity and volume of stormwater runoff as the volumes and velocities of water in these areas are often lower than in downhill areas. Finally, as will be presented in the section below, this metric also gives higher preference to GSI that have the potential to form a connected hydrologic network of GSI over isolated GSI sites.

4.2.4 Multi-criteria prioritization of GSI projects

The final prioritization of the location and types of GSI is performed by using a GIS multi-criteria decision analysis (GIS MCDA). GIS MCDA is the process of analyzing spatially explicit multi-criteria geographical information by coupling geographical information systems with methods of multi-criteria analysis (Malczewski & Rinner, 2015). GIS MCDA methods are commonly employed in PSS due to their ability to synthesize complex processes using proxy indicators and for their ability to explicitly consider the spatial component of the problem at hand. GIS MCDA has been widely applied to mapping the suitability of GSI implementation and for determining optimal spatial locations; among the most common techniques is multi-objective optimization algorithms based on GIS MCDA.

Multi-objective optimization, or multi-objective decision analysis, is the process of framing decisions based on a model described by a set of objectives and constraints. When based on GIS MCDA, the most commonly used methods include those that generate non-dominated solutions (weighting and constraint methods), distance-based methods (e.g., goal programming and reference point methods), and interactive methods. (Malczewski & Rinner, 2015, provide more detailed descriptions of each of these methods.) The selection of which method to use is often dictated by the problem being solved, the planning process, and/or the need for the model to

consider multi-criteria and the opinions of multiple stakeholders. Regardless of the method used, this type of analysis enables identification of the tradeoffs and synergies among the objectives (often expressed as marginal costs or benefits).

Moreover, previous studies have demonstrated the importance of engaging and involving stakeholders in GSI planning and design to avoid unsustainable solutions, resistance from stakeholders, and future rejection of GSI projects (Clean Water America Alliance, 2011; Montalto et al., 2013; Baptiste et al., 2015). Furthermore, one of the major challenges is considering competing stakeholder opinions in evaluating different GSI alternatives (Montalto et al., 2013; Norton et al., 2015). Multi-objective optimization presents a viable option to address these challenges by allowing different levels of importance to be given to different objectives and presenting a Pareto front of tradeoffs among multiple objectives to facilitate reaching consensus.

Therefore, this study uses multi-objective optimization to identify the location and types of GSI that should be implemented to maximize runoff volume reduction from impervious surfaces while considering other benefits (i.e., geo-preferences) and the vulnerability of socio-ecologic systems. To this end, two primary concepts are used to model runoff: (1) the concept of a spatially distributed hydrograph, and (2) the use of a directed graph to represent the hydrologic connectivity of GSI.

In general, two main conceptual approaches have been used for developing spatially distributed hydrographs. One approach is based on the idea of a spatially distributed *unit* hydrograph. First introduced by Maidment (1993) and then further developed and tested by Muzik (1996a & 1996b), this approach derives a time-area diagram. Using a single flow direction method to estimate the flow directions derived from a DEM, a flow distance to the outlet can be determined. Assigning flow velocity to each cell, a flow time to the outlet can then be calculated. Using these flow times, isochrones of flow time at a specified time interval can then be laid out on a grid and the time-area diagram for a watershed can be calculated by considering the number of cells between isochrones.

The second conceptual approach for spatially distributed hydrographs conceptualizes the grid cells as a combination of linear reservoirs and linear channels. Introduced by Dooge (1959), and extended by Wang et al. (1996) to provide an analytical solution, this approach divides a watershed into sub-watersheds, each assumed to have an approximately uniform precipitation excess (i.e., volume of rainfall available for direct surface runoff) and geographical conditions.

The spatially distributed hydrograph is then represented by the numerical convolution of the hydrologic response of each cell and the unequal inputs to each cell. This concept has been the foundation of many surface rainfall-runoff distributed models (Zellner et al., 2016), including the EPA Soil and Water Assessment Tool (SWAT) model (US EPA SWAT, 2018).

The concept of the spatially distributed hydrograph is used in this study to estimate the potential reduction in volume and peak discharge of stormwater runoff caused by the hydrologic connectivity of GSI projects. The assumption is that if the convolution of the hydrographs of each grid cell represents the hydrologic response at the outlet of the watershed, maximizing the hydrologic connectivity of the GSI or the capacity of the GSI network would result in the greatest improvement at the watershed scale. In other words, the retention of runoff by GSI in series would maximize their efficiencies (i.e., higher capture ratios) and therefore provide the largest retention of runoff volume. This idea has been proposed and explored by previous studies on the optimal spatial allocation of retention basins (Travis et al., 2008; Shen et al., 2013; Sebti et al., 2016). Furthermore, recent literature reviews have highlighted the need to consider the hydrologic connectivity of GSI sites in the development of distributed hydrologic models that could scale the impact of GSI to the watershed scale (Jefferson et al., 2017; Golden et al., 2017). However, to the author's knowledge, no other studies have integrated this concept within a multi-objective optimization framework for spatially explicit planning of GSI.

Using the concept of spatially distributed hydrographs, the hydrologic connectivity of the GSI, and thus the added benefits due to superposition of GSI hydrographs, can be represented by a directed graph. Directed graphs are a common method used to represent flow networks where the edge connecting two nodes is usually assigned a flow capacity and the nodes connected by this edge are distinguished between sources and sinks (see Saha Ray, 2013). Commonly used to represent transportation networks, directed graphs are useful for simplifying complex spatial processes by using a matrix to represent the transfer of flow between sources and sinks. Such representation of the spatial problem enables the use of linear and non-linear optimization techniques, a desirable feature in any multi-criteria analysis due to the low computational cost and convergence of these methods. The use of a directed graph to represent the hydrologic connectivity of the GSI assumes that each GSI site is a node in the graph and the edges between nodes represent the reduction in the volume of stormwater runoff to downslope GSI by implementing GSI upslope. More specifically, the reduction in the runoff volume to a GSI located downslope of another GSI

is proportional to its surface area (i.e., potential runoff retention index) (see Appendix A.4 for an illustrative example). Finally, the directed graph of GSI hydrologic connectivity is represented by a matrix in which each row is a potential GSI and each column contains the potential reduction in runoff volume draining to this GSI (i.e., surface area of GSI that are upslope). This matrix is subsequently referred to as *CB* (i.e., connectivity benefit).

4.2.4.1 Optimization formulation

In order to simplify the discussion of the optimization formulation, in this section a GSI associated with $Area_{ijk}$ (Section 4.2.2.) will be referred to by simply using the subscript i. It is assumed that the user/stakeholder has already decided which type of GSI will be considered in the optimization, has extracted their spatial arrangement and surface area from the data tree structure (Section 4.2.2), and has calculated their respective upslope drainage areas. Mathematically, this problem can be represented as:

$$\max_{x} \sum_{i=0}^{N} x_i * DA_i \; + \sum_{i=1}^{N} y_i \tag{4.2}$$

$$Total\ area = \ Budget\ (Bc) = \frac{\sum_{i=1}^{N} Area_i * x_i}{\sum_{i=1}^{N} Area_i} \leq Bc \tag{4.3}$$

$$Capture\ Ratio\ Lower\ Limit\colon (DA * y_i - CB * x_i) * \alpha \leq Area_i * x_i \tag{4.4}$$

$$Capture\ Ratio\ Upper\ Limit\colon (DA * y_i - CB * x_i) \geq Area_i * x_i \tag{4.5}$$

$$S_E * y_i \leq 1 \tag{4.6}$$

$$x_i - \ y_i \leq 0 \tag{4.7}$$

$$0 \ \leq \ x_i \ \leq 1 \tag{4.8}$$

$$y_i \geq 0 \tag{4.9}$$

where x_i is the decision variable that represents the percentage of the area for a particular site (i.e.$Area_{ijk}$) that will be used to implement the GSI, N is the total number of spatial arrangements of GSI being considered, DA_i represents the total upslope drainage area of GSI i, Bc is the percentage of the total available area suitable for implementing GSI that can be used, CB is the hydrologic connectivity matrix that represents the reduction in drainage area due to implementation of GSI networks, α is the required capture ratio, and S_E is a matrix that prevents

GSI from sharing the same grid cells in their spatial arrangements (described in more detail below). Equation 4.5 assumes that GSI with a capture ratio larger than 1, which implies accumulating less runoff volume than their intended design storage capacity, are not desirable.

The binary variable y_i is used to implement the capture ratio constraint when an infiltration or retention GSI is implemented (i.e., $y_i = 1$). Lastly, an additional constraint can be added when different sizes and spatial arrangements of GSI can be considered for implementation within the same $Area_{ij}$. Consider, for example, the scenario in which an entire $Area_{ij}$ could be used for the construction of a wetland, or a smaller portion can be used to implement a number of smaller bio-retentions in series, both of which are defined by a spatial arrangement of grid cells. In this scenario, if the wetland is considered for implementation, the option to implement smaller bio-retentions has to be disregarded as the area (or shared space) has already been committed. To account for this problem of sharing the same space, the constraint shown in Equation 4.6 is added. The matrix S_E in this constraint [Equation 4.6] represents the competition for space between different GSI. Each row of S_E is associated with a potential GSI and a one is allocated to the columns of said row for each other GSI with the same grid cells in their spatial arrangement. As such, the total sum of each row should be equal to one, implying that only one of the GSI that share grid cells in their spatial arrangements can be implemented (e.g., if the wetland is implemented, the smaller bio-retentions cannot be considered).

The above formulation maximizes the interception of runoff from impervious surfaces (represented by the drainage area calculated using the adjusted CN values [Equation 4.1]) given a threshold of capture ratio and total area to be used to implement GSI projects. Intuitively, Equation 4.2 maximizes the capture of runoff from areas upslope of the GSI while ensuring that the capture ratio design criteria are met. While x_i represents the percentage of a GSI's area that will be used, its multiplication by DA_i in Equation 4.1 translates to maximizing potential runoff capture. The use of *CN* for the calculation of DA_i [Equation 4.1] identifies those upslope areas from the GSI that have the potential to produce the largest volumes of runoff. Maximizing the sum of $DA_i * x_i$ in Equation 4.2 therefore can be interpreted as *finding* which GSI sites have the potential (enforced by the capture ratio constraint) to provide the largest reduction in runoff volume. However, by considering the hydrologic connectivity of the GSI using the matrix *CB*, the formulation also finds the network of GSI that has the largest runoff reduction potential. Lastly, the closer x_i is to one, the higher the GSI capture ratio and therefore the higher the efficiency.

Up to this point, the optimization formulation has only considered the stormwater management benefits of infiltration structures. In order to consider the other benefits and geo-preferences of GSI, the ϵ-constraint method is used. Introduced by Haimes et. al. (1971), the ϵ-constraint method is a commonly used approach in multi-objective optimization in which one of the objectives is optimized while the others are restricted to a user-specified value (ϵ). The main advantages of this method are its applicability to convex and non-convex problems and the elimination of the need for a normalization approach and weights to represent importance given to the different objectives.

For each geo-preference considered as part of the multi-criteria analysis, the following constraint is added to the optimization formulation:

$$\sum_{i=1}^{N} g_{ik} * x_i \geq \lambda_k G_k \tag{4.10}$$

where g_{ik} is the geo-preference score of GSI i associated with the criteria k, G_k is the maximum score that can be achieved for this criterion, obtained by solving the optimization problem with the associated geo-preference scores, and λ_k is the percentage of that maximum value that is required to be met. Conceptually, this approach forces the optimization to select areas that might not be hydrologically optimal but that have great potential to meet some of the other criteria. By using the constraints of the original formulation when maximizing the total score associated with a particular geo-preference, the capture ratio constraint is also invoked.

One of the most significant limitations of the ϵ-constraint method is that the range of feasible values for the objectives used as constraints needs to be known in advance. Furthermore, in order to find the Pareto front, a thorough investigation of the solution space is needed with many secondary objectives as constraints. If the range of feasible solutions is not known by the user, the use of the ϵ-contraint method will give an optimal solution for the user-specified constraint values, but cannot ensure that said solution is fully Pareto optimal. As a solution to this problem, it is often recommended that the user begins exploration of the solution space by attempting to find a feasible solution using the bounds of the secondary objectives. This ensures that at least the anchor points (i.e., the optimal solution with only one additional secondary objective) of the Pareto front are found.

Finally, in this optimization formulation the variable z_i [Equation 4.11] is used to represent those GSI that do not have to meet the capture ratio constraint, such as trees, or to consider the use of these areas for other purposes (e.g., recreational spaces, open green areas, etc.). While most engineered GSI are designed and intended for the retention and infiltration of stormwater runoff, trees are often a more desirable alternative to reduce UHI and provide ecological services. Therefore, the inclusion of trees in the optimization formulation preserves areas with a high need to receive tree benefits by maximizing potential runoff reduction using other areas first. Additionally, the use of trees can reduce the potential runoff from contributing upslope areas to GSI sites (i.e., a lower value of *CN* and thus a lower DA_i [Equation 4.1]) that initially do not meet the capture ratio constraint. By adding trees in upslope areas, these GSI sites can become feasible options.

For non-engineered GSI such as trees, the potential runoff reduction benefit φ [Equation 4.11] is calculated using a rainfall interception rate (i.e., storage capacity) obtained from field observations, empirical models, and/or physical models. In this study, the storage capacity of these non-engineered GSI is computed using curve numbers from the literature (Sample, et al., 2001; Engel & Hunter, 2009; Ahiablame et al., 2012 & 2013; Liu et. al., 2015; WERF, 2017).

Lastly, depending on the spatial planning scale, it might be desirable to restrict the use of $Area_{ij}$ to only one type of GSI (e.g., rain gardens or trees). To account for this restriction, an additional constraint [Equation 4.13] needs to be considered. Mathematically, these modifications to the optimization formulation can be represented by:

$$\max_x \sum_{i=1}^{N} x_i * DA_i + \sum_{i=1}^{N} y_i + \sum_{i=1}^{N} z_i * \varphi * Area_i \tag{4.11}$$

$$\frac{\sum_{i=1}^{N} Area_i * x_i + \sum_{i=1}^{N} Area_i * z_i}{\sum_{i=1}^{N} Area_i} \leq Bc \tag{4.12}$$

$$\sum_{i=1}^{N} g_{xik} * x_i + \sum_{i=1}^{N} g_{zik} * z_i \geq \lambda_k G_k \tag{4.13}$$

$$y_i + z_i \leq 1 \ (optional) \tag{4.14}$$

where z_i is the percentage of $Area_{ij}$ used by the non-engineered GSI, φ is the percentage of rainfall interception, and g_{xik} and g_{zik} represent the geo-preference scores associated with criteria *k* [previously presented in Equation 4.12] for infiltration structures and trees, respectively.

The use of Equation 4.14 as a constraint in this optimization formulation should be given careful consideration given the main goal of the analysis and the spatial extent and type of GSI under consideration. This constraint prevents the use of a single GSI location ($Area_i$) to be used simultaneously for infiltration structures and trees. When planning a large spatial extent (e.g., 10-20 km^2 watershed), the goal of the multi-objective optimization should be to identify the $Area_i$ that have the largest potential to provide the desired benefits (e.g., reduction of runoff or mitigation of UHI), with less concern for specific types and spatial arrangements of GSI. When the spatial scale of analysis focuses on smaller regions (i.e., identified $Area_i$ at the larger scale, such as 1-2 km^2 watersheds), this constraint becomes more important to identify a specific type of GSI and where should it be located. The available space to implement different types of GSI within the same $Area_i$ also becomes limited. For example, the implementation of both trees and retention ponds within a single grid cell in a 3-meter grid is unlikely.

4.2.4.2 Weighting scheme

To provide a high level of flexibility in the different spatial planning criteria, two methods are used to account for differences in stakeholder opinions and preferences: (1) sum of weights, to consider the importance given to mitigation of flooding versus UHI, and (2) multiplication by a preference factor to reflect the degree of preference given to sites that meet planning criteria and/or are located in areas of high social or ecologic susceptibility.

The sum of weights approach is implemented using four different weights for: (1) the reduction of total volume of runoff at the watershed outlet (W_{DA}), (2) the mitigation of UHI (W_{UHI}), and (3,4) the mitigation of urban heat island and flash flooding in the most vulnerable communities (W_{UHIV}, W_{FFPI}, respectively). To ensure that the sum of the weights equal one, the weights are calculated as follows:

$$W_{FFPI} = (1 - W_{DA}) * W_{ffpi} \tag{4.15}$$

$$W_{UHIV} = (1 - W_{DA}) * \left(1 - W_{ffpi}\right) \tag{4.16}$$

$$W_{UHI} = W_{DA} * \left(1 - W_{ffpi}\right) \tag{4.17}$$

$$W_{DA}, W_{ffpi} \in [0, 1] \tag{4.18}$$

where W_{DA} represents the importance given to maximization of runoff reduction at the watershed outlet, and thus gives less importance to the location of vulnerable communities, and W_{ffpi}

represents the relative importance given to the mitigation of flash flooding over the mitigation of UHI. These weights are incorporated into the optimization formulation through the parameter λ_k [Equation 4.13], which is used to constrain the percentage of the maximum attainable score for a given geo-preference. This sum of weights method is chosen because: (1) it is intuitive and easily interpretable by the stakeholders, (2) it shows the tradeoffs that exist when accounting for different objectives and (3) it reduces the number of potential combinations of weights that could be used.

The second method for representing stakeholder preferences is multiplication by a preference factor (i.e., a penalty weight), which represents how much one site is preferred over others given its compliance with planning criteria and siting in areas of high social and ecologic susceptibility. As such, the magnitude of the factor can be interpreted as the relative importance given to these criteria over those associated with the performance of the GSI (i.e., mitigation potentials), as shown below:

$$wg_{i,NoINF} = \sum_{k=1}^{K} g_{i,k} * \left(1 - W_{INF,k}\right) * F_k \tag{4.19}$$

$$wg_{i,INF} = \sum_{k=1}^{K} g_{i,k} * W_{INF,k} * F_k \tag{4.20}$$

$$W_{INF,k} \in [0, 1] \tag{4.21}$$

where $wg_{i,k}$ is the multiplier associated with GSI site i and criteria k, $g_{i,k}$ is the normalized geo-preference score, F_k is the preference factor used for criteria k (i.e., large value relative to the range of g_k), and $W_{INF,k}$ represents the marginal preference for infiltration structures over non-infiltration structures at GSI site i (e.g., the marginal benefit of having trees versus rain gardens when considering improvement to human health or ecologic restoration).

By separating these criteria from the geo-preference indicators associated with the performance of the GSI, the approach rewards sites with a high geo-preference score while meeting the performance constraints (specified by λ_k [eq. 4.13]). Moreover, the approach is methodologically flexible, equitable, and transparent, characteristics argued as crucial to any participatory process (Geertman & Stillwell, 2012; Nordstrom et al., 2012; Kuller et al., 2017).

One limitation of the proposed weighting scheme is that the magnitude of the preference factor [F_k] needs to be large enough to account for the range of values associated with the objective

function. In other words, the preference factor has to be large enough that when multiplied by the values of the objective function a clear preference is given to those GSI that meet the intended criterion. The selection of the magnitude of the preference factor is therefore a trial-and-error process.

An additional limitation of the presented weighting scheme is that it does not guarantee that the optimized solutions will be Pareto optimal if: (1) the implementation of different types of GSI in the same space (i.e., $Area_i$) is not allowed [Equation 4.14] and (2) two or more secondary objectives (i.e., at least two ϵ-constraints) are considered *at the same time.* This limitation is created because the weighting method requires that the sum of the weights has to equal one, and the use of Equation 4.14 prevents simultaneous maximization of multiple benefits gained by implementing different GSI in the same $Area_i$.

This limitation is most significant in the scenario where a small percentage of the area to implement GSI is considered [Equation 4.12] and both the vulnerability to flash flooding and UHI are considered as part of the analysis. When these two objectives are considered, the implementation of infiltration structures or the planting of trees will depend largely on the importance given to the hazard mitigation goals. Therefore, if the benefits associated with implementing GSI in $Area_i$ are restricted to only those provided by one of these two types of GSI, the current weighting method would produce a linear tradeoff between hazard mitigation objectives. Depending on the spatial scale of analysis, and the GSI being considered, such tradeoff might not reflect the true Pareto front.

Finding the true Pareto front in this case would require relaxing the requirement that the sum of the weights has to equal one. For low levels of GSI implementation, it might be possible to find a solution that achieves the full benefits associated with these secondary objectives [Equation 4.13 is met when $W_{UHIV} = 1$, and $W_{FFPI} = 1$]. This process, however, introduces a large computational cost, particularly for planning problems that consider a large number of solutions, and disregards the relative importance given by the stakeholders to each objective. Thus, rather than trying to find the exact Pareto front, this weighting method allows for a rapid representation of the solution space with Pareto optimal anchor points. Once consensus has been built among the stakeholders about which scenarios are worth exploring in more detail, a fuller consideration of the weights can be given to find the exact Pareto optimal solutions.

4.2.4.3 Testing and sensitivity analysis

The last step of the methodology involves testing how well the optimization results perform at stormwater capture via a hydrologic model, as well as conducting a sensitivity analysis of the most significant parameters in the optimization formulation. For this step, the LandLab open-source toolkit (Bates et al. 2010; Hobley et al., 2017) is used to calculate the peak discharge and runoff volume associated with the prioritized GSI projects. LandLab uses an overland shallow water two-dimensional storage cell inundation model to derive a simplified and explicit solution for the routing of overland flow. The model considers water acceleration (thus reducing the rapid reversals of water flow referred to as *chequerboard oscillations*) and propagation of the shallow water wave. The model was extended by De Almeida et al. (2012) to improve stability in low friction areas and since then has been used in several flooding studies (De Almeida, et al., 2013; Sampson et al., 2013). This model was selected for this study because of its similarity to the hydrologic assumptions of the prioritization framework (i.e., multiple flow directions), its flexibility to manipulate the properties of grid cells as needed, and its low computational cost. Landlab uses a topology of grid cells represented as nodes and the flow of water between grid cells is represented by links. This implementation allows routing in multiple flow directions and estimation of results by grid cell, a desirable feature for analyzing the reduction of runoff in specific areas (e.g., vulnerable areas).

In this study, the LandLab overland flow model is modified to account for differences in the roughness of different land covers and their initial abstractions (i.e., rainfall depth after which runoff begins) are estimated using the curve number method. Different Manning roughness coefficients are assigned to the grid cells using typical values from SWMM for pervious (η=0.1) and impervious (η=0.01) surfaces and weighting the values by the percent of imperviousness (e.g., 80% impervious would result in a η=0.028). Additionally, curve numbers are assigned to each grid cell using Equation 4.1 and the storage capacity (S) and initial abstractions (Ia = 0.2*S) of the grid cell are calculated. Therefore, it is assumed that until the initial abstractions are met a grid cell will not generate runoff.

It is acknowledged that this is a significant simplification to the process of infiltration, not only because the soil infiltration rates are ignored, but also because it treats rainfall and incoming runoff produced by upslope cells equally. However, this method allows consideration of the differences in timing that can occur because of these infiltration processes without adding any

computational cost (e.g., as opposed to solving Green and Ampt's [1911] equations for each grid cell at each time step).

Finally, the modeling of infiltration structures is done by assuming a storage capacity of 2 inches and a Manning's roughness coefficient of $\eta = 0.1$. The properties of the grid cell in which GSI is considered for implementation are changed by using the area average value of the existing conditions and the percentage of the grid cell [$Area_i$] dedicated to implementation of GSI as obtained from the optimization results (i.e., x_i).

Next, the sensitivity analysis considers: (1) the impact of a Euclidian distance threshold between grid cells to limit the hydrologic connectivity and contributing drainage area of distant GSI sites, (2) the use of different values to represent the potential of infiltration structures to mitigate urban heat island, and (3) the potential of trees to prevent stormwater runoff (i.e., volume of rainfall intercepted by trees). The sensitivity to potential UHI mitigation of different types of GSI considers common guidelines found in the literature. As previously discussed, trees have much higher mitigation potential to land surface temperatures than vegetated open spaces (Zheng et al., 2014; Norton et al., 2015; Zardo et al., 2017). However, there is very little evidence as to the marginal benefits associated with this difference. In a recent article by Zardo et al. (2017) the authors present a framework for assigning scores of cooling capacity to different combinations of tree canopy coverage, land cover, and total surface area. The results suggest that the cooling capacity of grass and other vegetated areas can be between 0.1 – 0.3 of those areas with high tree canopy coverage. These suggestions align with the differences in land surface temperatures (LST) observed in this study between areas with impervious surfaces greater than 50% and no trees versus higher tree canopy percentage (Figure B.4 in Appendix B). Therefore, the sensitivity analysis compares the results with the cooling capacity of infiltration structures to be 10% or 30% of trees [parameter $g_{xik} = 0.1\text{-}0.3 * g_{zik}$ in Equation 4.13].

Similarly, no clear guidelines exist to suggest the percentage of rainfall that can be captured by trees, or cluster of trees, in urban areas. Studies that have investigated this question have reported the results as the interception of annual rainfall volume, not at the level of individual storm events (e.g., Xiao et al., 2002; Inkiläinen et al., 2013). Furthermore, the results of the studies have varied significantly since the capacity of trees to capture rainfall and slow runoff will depend on many intrinsic properties of different tree types (e.g., leaf area index, tree canopy area, height, trunk width, etc.). Nevertheless, trees have been represented in previous studies (e.g., Mccutcheon,

2003; Fan et al., 2013; see NRCS TR-55, 1986) using curve number values ranging from 65 to 77. When compared to typical curve number values used to represent engineered GSI (i.e., 35-40) the capacity of trees to produce runoff is approximately twice the potential of infiltration structures. If the storage capacity is compared using these curve numbers, the rainfall interception capacity of trees has an upper limit of 20% of engineered GSI. Therefore, the sensitivity analysis considers 5%, 10% or 20% rainfall interception ratios for trees [parameter φ in Equation 4.11].

4.3 Case studies – Three watersheds

To test the feasibility, utility, and robustness of the proposed approach for prioritization of GSI projects, three watersheds with different areas and land cover distributions are considered as case studies. The three watersheds are located in the City of Dallas, TX, the City of Philadelphia, PA, and Baltimore County, MD (Figure 4.1; Figure B.5, B.6 and B.7 in Appendix B). The watershed located in Baltimore County, MD, is known as Dead Run 5 (DR5) watershed and is a tributary of the Dead Run watershed located on the outskirts of Baltimore City. The 1.6 km^2 watershed has mixed land cover with 36% impervious areas, and has mostly residential land use. Because of its inclusion within the Gwynns Fall watershed, which is part of the Baltimore Ecosystem Study Long Term Ecological Research site (BES LTER [https://beslter.org/]), DR5 has been the subject of numerous previous studies (e.g., Smith, 2010; Smith et al., 2013; Miles et al., 2014 & 2015; Bhaskar et al., 2016). This provided high resolution data for the locations identified as potential sites for implementation of rain gardens (i.e., infiltration structures) and a calibrated SWMM model (provided by Tetra Tech) to compare the results of the overland flow model. As such, in DR5 the prioritization of trees is not considered. Furthermore, UHI mitigation is also not considered because the UHI hazard exposure severity ranges from very low to low in this watershed.

The watersheds located in Philadelphia, PA, and Dallas, TX, are also mostly residential and have high needs for GSI implementation based on the analyses presented in previous chapters. The watershed in Philadelphia has a total area of 11 km^2 with 76% impervious area and 1.6% tree canopy, along with a high density of planned PWD GSI projects. The watershed located in Dallas, TX, is a “hot spot” for vulnerability to both urban heat island and flooding. This is the largest of the three watersheds, with an area of 24.8 km^2, including 34% impervious areas and 28% tree canopy. Table 4.2 summarizes the properties of each watershed.

Lastly, the analyses presented in the section below assume that a capture ratio of α = 8% is required for infiltration structures [Equation 4.4], that the rainfall interception capacity of trees is φ = 5% [Equation 4.11], and the urban heat island mitigation potential of infiltration structures is 10% of UHI mitigation for trees (i.e., 10% of the urban heat island mitigation geo-preference score of a site) [$g_{xik} = 0.1 * g_{zik}$ in Equation 4.13]. It is also assumed that the hydrologic connectivity of sites extends to the total area of the watershed (i.e., infinite hydrologic connectivity). An infinite hydrologic connectivity implies that the potential runoff of a grid cell (i.e., flow accumulation) is equal to the potential runoff produced by said grid cell plus the allocation of runoff from all upslope grid cells as determined by the MFD method.

Table 4.2: Summary of the most prevalent features for the case study watersheds

Watershed	Area (km^2)	Imperviousness (%)	Tree canopy (%)	Potential area for GSI (% of watershed area)
Dead Run 5 (Baltimore, MD)	1.60	36.0	22.0	19.8
Sub-watershed of PWD CSO service area (Philadelphia, PA)	11.0	74.0	1.60	17.6
Sub-watershed of Turtle Creek (Dallas, TX)	24.8	34.0	28.0	21.8

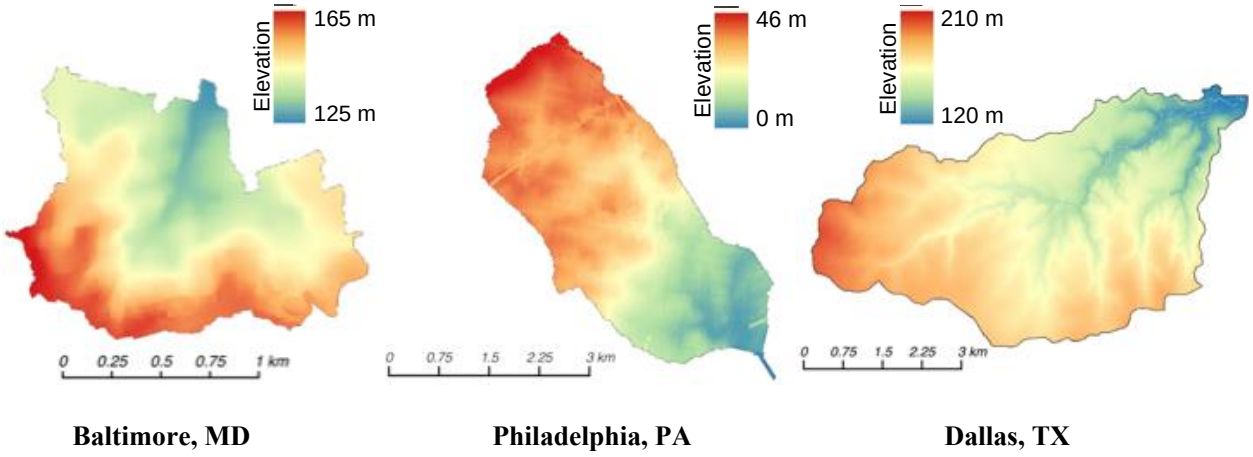

Figure 4.1: Spatial extent and elevation of the three case study watersheds.

4.4 Results and discussion

The results of this study include (1) evaluation of the optimization solutions with the overland flow model for the DR5 watershed (the only watershed for which a validated SWMM model was available), (2) the analysis of spatial tradeoffs and synergies that exist between potential GSI projects when considering different hazard mitigation goals in the Philadelphia and Dallas watersheds, and (3) a sensitivity analysis of these spatial patterns. The analysis of spatial tradeoffs and synergies that exist between potential GSI projects and hazard mitigation goals was only completed in the Philadelphia and Dallas watersheds that have more heterogeneous spatial patterns of flash flooding and urban heat vulnerability than those observed in DR5. Furthermore, the larger spatial extent of these two watersheds provides a more complete representation of the Pareto fronts for different levels of GSI implementation.

4.4.1 Evaluation of optimized solutions with the overland flow model in DR5 watershed

Evaluation of the GSI prioritization in DR5 with the overland flow model followed two main steps: (1) a comparison of the discharge at the watershed outlet obtained from the overland flow model and the EPA SWWM model, and (2) evaluation of the hydrologic response (i.e., peak flow discharge and runoff volumes) produced by the optimized spatial allocation of infiltration structures in the watershed for different budget constraints (i.e., total available area to implement GSI).

4.4.1.1 Assessment of overland flow model

Using the EPA SWMM model provided by Tetra Tech, continuous design storms associated with a 2-year return frequency and storm durations of 5, 15, 30, and 60 minutes, as well as 2 hours, were evaluated to identify the critical storm for this return period. A 2-year design storm is most often used for the design of small GSI (see design manuals in Table 4.1). For a 2-year return period, the 30-minute storm with a rainfall intensity of 2.1 inches/hour produced the largest peak discharge, with a value of 38.4 cubic feet per second (cfs). This 2-yr, 30-min continuous design storm was then used as inputs into the overland flow model in order to obtain a discharge curve that could be compared to the SWMM results.

To assess the match between the models, the Nash–Sutcliffe model efficiency coefficient (E) and the coefficient of determination (r^2) were used (for reference see Krause et al., 2005) to

compare discharges at the watershed outlet. The Nash–Sutcliffe efficiency metric quantifies the sum of squared differences between the predicted and observed values normalized by the variations in the observed values. The coefficient of determination (r^2) is used to quantify how much of the observed dispersion in the discharge values is due to the prediction model and the observed discharge values. For comparison purposes with the simplified overland flow model, the results obtained from the SWMM model are assumed to be the *true* representation of the hydrologic response of DR5 to the evaluated design storm (i.e., observed values).

The resulting values for the Nash–Sutcliffe model efficiency coefficient and coefficient of determination for the hydrographs were 0.9 and 0.91, respectively. Figure 4.2 shows that the largest discrepancy between the models was the magnitude and timing of the peak discharge, which occurs at a later time in the simplified overland flow model. Nevertheless, these results suggest that both models have similar results and therefore that the simplified overland flow model can reasonably represent hydrologic responses.

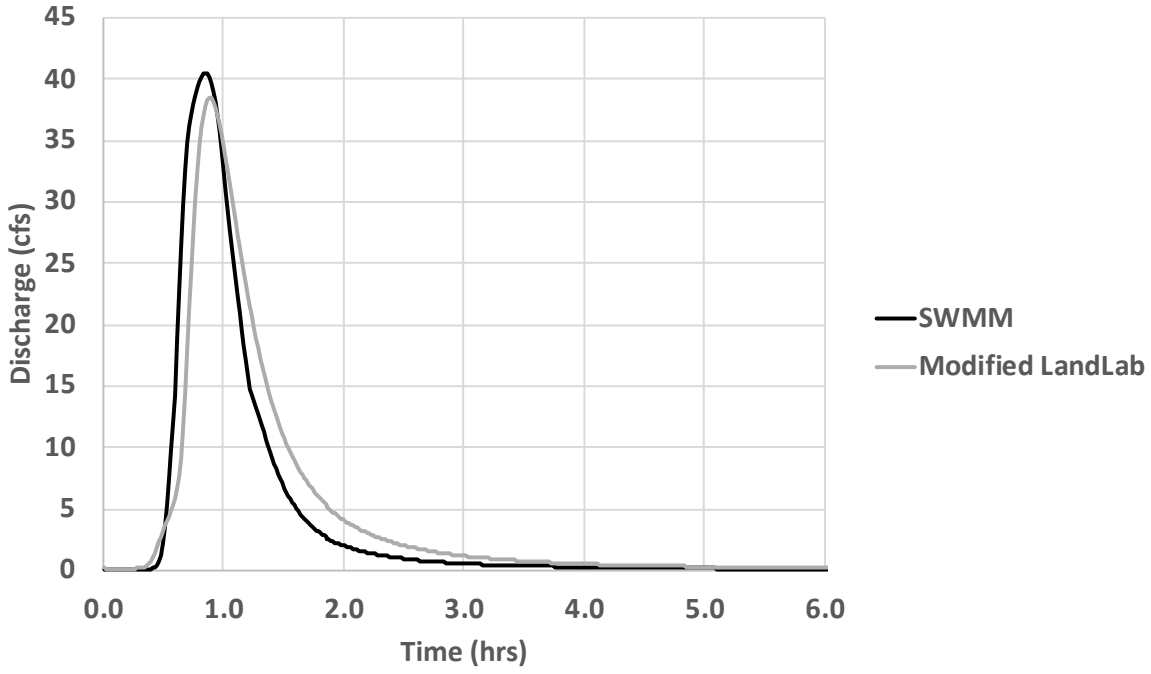

Figure 4.2: Resulting hydrographs from SWMM and the modified overland flow model for a 2-year, 30-minute continuous storm (intensity 2.1 inches/hour).

4.4.1.2 Assessment of the hydrologic response of the optimized allocation of GSI

Having tested the ability of the overland flow model to represent hydrologic response, the next step was to investigate the hydrologic response of the optimized GSI implementation scenarios. Prioritization of potential sites for infiltration structures was done by considering each suitable grid cell to be a potential GSI (i.e., GSI surface area is equal to grid cell size [100 square meters]) and maximizing the reduction in total runoff volume at the watershed outlet and the total runoff volume to those areas with higher vulnerability to flash flooding. At the spatial scale of DR5, social susceptibility was not observed to be significantly different between areas and thus the definition of the most vulnerable areas considered only residential buildings that had high to very high exposure severity to flash flooding. In addition, given the small extent of the watershed, a capture ratio of 1% is used. The identified vulnerable areas can be observed in Figure 4.3.

The multi-objective optimization of GSI locations in DR5 was completed for eight different budget constraints (i.e., 5% to 20% of the area available for infiltration structures). Additional scenarios were not evaluated as it was observed that no additional potential reduction of flow accumulation (i.e., runoff volume) in the most vulnerable areas was achievable. Figure 4.3 presents the Pareto fronts for each of the implementation scenarios and Figure 4.4 shows the locations of the prioritized GSI for the scenarios in which 5% and 10% of the total GSI area was used. The results suggest that for a low level of GSI implementation there is a tradeoff between reducing volume of runoff at the outlet and the reduction of runoff volume in the vulnerable areas. Moreover, it can be seen that the spatial locations of the prioritized GSI projects are distinctly different. As the area used for GSI is increased, the competition between the objectives becomes less prevalent up to the point in which no additional implementation of GSI would produce further benefits in the vulnerable areas.

Because the highest level of competition between objectives was observed for lower levels of implementation, the optimal solutions for 5% and 10% of the GSI area were then used as inputs to the overland flow model. The peak discharge at the watershed outlet and runoff volumes in the vulnerable areas (i.e., reported per grid cell) were then calculated as presented in Figures 4.5 and 4.6. It can be seen that the hydrologic results show similar patterns to the tradeoffs observed in the optimization results. As discussed in the methodology section, the reduction of flow accumulation from the most impervious areas and the hydrologic connectivity of the GSI are assumed to have the largest impact on the peak discharge given the spatially distributed hydrographs. The results

presented in Figure 4.5 suggest that this is a reasonable assumption for this watershed and overland flow model.

When analyzing peak discharge in Figure 4.5, the optimization formulations that weighted the reduction of flow accumulation to the watershed outlet more heavily had the lowest values of peak discharge, as expected. However, it can also be noted that when the implementation level of infiltration structures was increased to 10%, the differences in peak discharge between prioritization scenarios was reduced. In fact, other than the optimization formulation in which the maximum achievable reduction of flow accumulation to the vulnerable areas was used as a constraint, all other prioritization scenarios had similar peak discharges. This relationship is suggested in the Pareto fronts given the small values obtained for the total reduction of flow accumulation when the optimization formulation was required to meet 100% of the achievable reduction of flow accumulation to the vulnerable areas. For all other scenarios, as the level of GSI implementation increased, the difference between flow accumulation reduction at the watershed outlet became negligible, thus suggesting a similar peak discharge.

Analyzing the runoff volume reduction in the vulnerable areas, similar conclusions can be made. Figure 4.6 shows that the total runoff volume reported by the overland flow has a positive relationship with the prioritization scenarios that used a higher weight for reduction of flow accumulation in the most vulnerable areas. Moreover, it can be observed that the difference in total runoff volume between scenarios that consider only the runoff to the outlet and the scenario that considered only runoff to vulnerable areas increased with higher levels of GSI implementation. The results presented in Figure 4.6 and the Pareto fronts presented in Figure 4.3 suggest that neglecting vulnerability in prioritizing infiltration structures could aggravate disparities unless a minimum level of GSI implementation is met. For DR5 watershed, the optimization results suggest that this level would be 0.0632 km^2, or 4% of the total area of the watershed (i.e., 20% of the available area for GSI implementation).

Note that while Figures 4.3, 4.5, and 4.6 suggest a tradeoff between the optimization objectives, the magnitude of these tradeoffs are significantly different. The maximum percent difference between peak discharges was ~ 3% when only considering reduction of flow accumulation to the watershed outlet [W_{FFPI} = 0] versus the vulnerable areas [W_{FFPI} = 1]). In addition, the mean percent difference between W_{FFPI} = 0 and other weightings of the objectives were 1% and 0.2% when using 5% and 10% of the total GSI area. On the other hand, the mean

percent difference between the total volume of runoff in vulnerable areas was 50% (standard deviation of 10%) for W_{FFPI} = 0 versus W_{FFPI} = 1. Intuitively, these results suggest that prioritization of GSI locations for the most vulnerable communities has a small impact on stormwater benefits at the outlet. On the other hand, disregarding vulnerable areas in GSI planning can have a significant impact on hazard impacts.

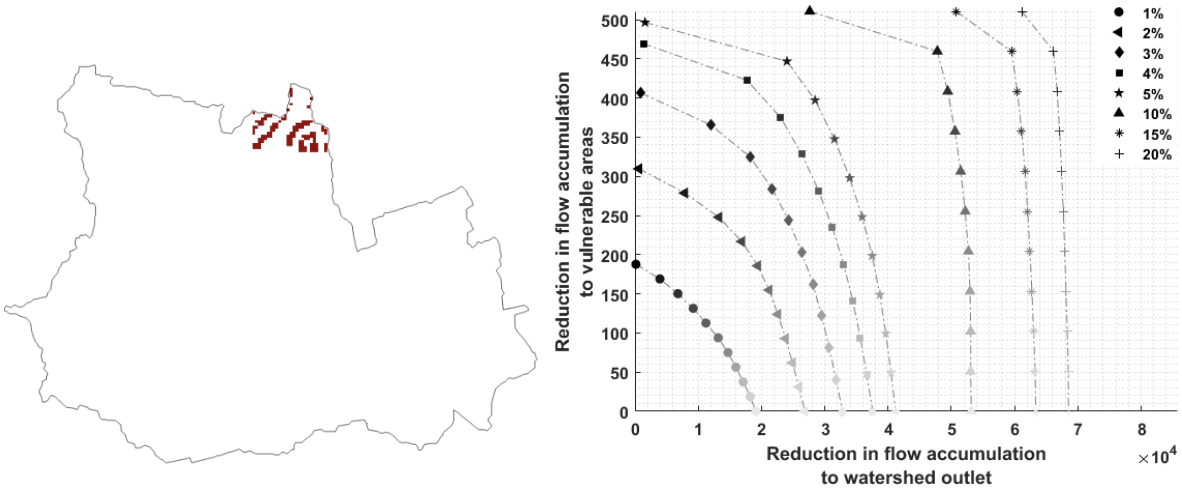

Figure 4.3: Left: Location of the most vulnerable areas in DR5. Right: Pareto fronts for DR5 with different percentages of GSI implementation (symbols) and weightings used for W_{FFPI} (i.e., percent of maximum achievable reduction in flow accumulation to vulnerable areas) [Light gray: W_{FFPI} = 0; Black: W_{FFPI} = 1].

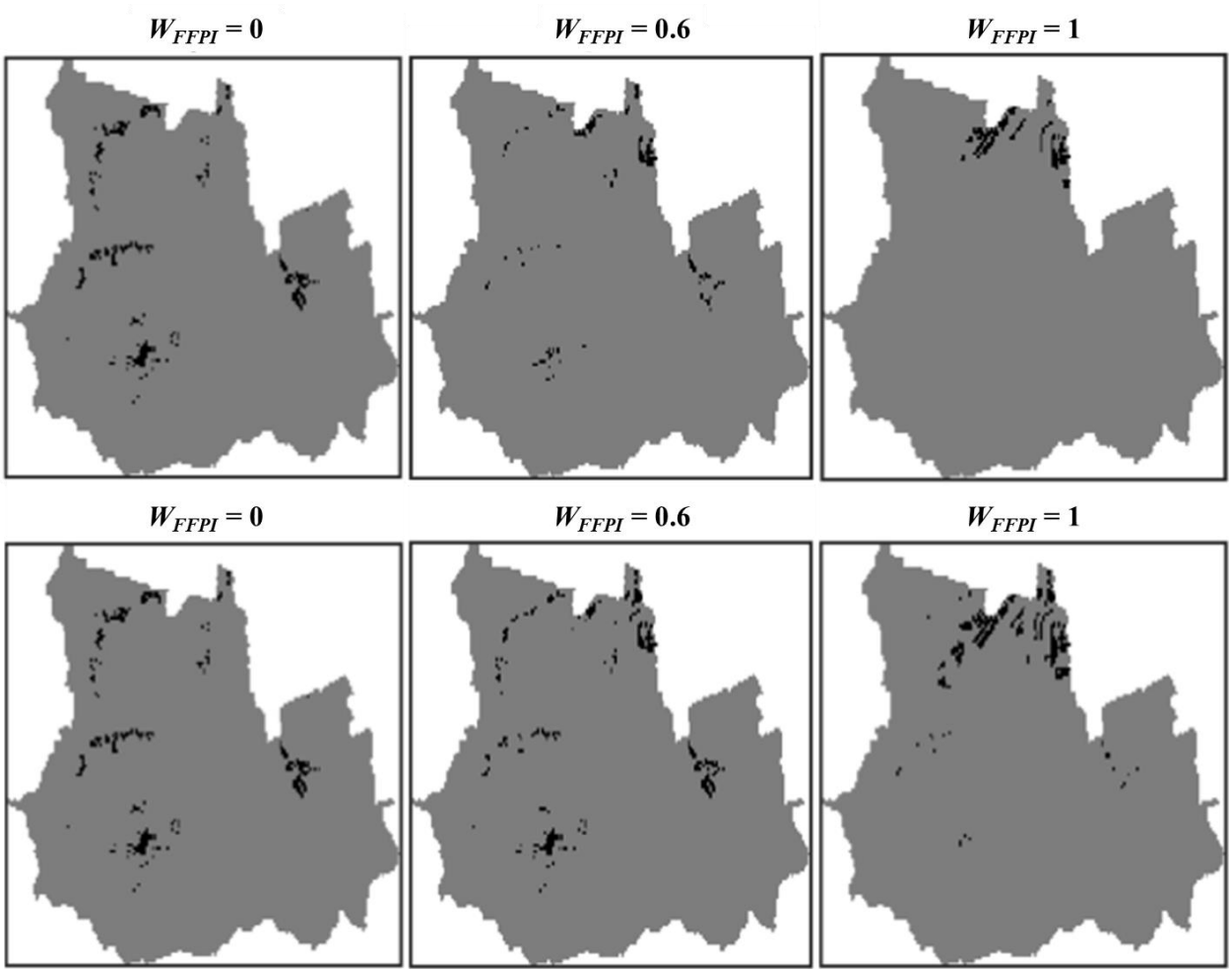

Figure 4.4: Spatial representation of prioritized infiltration structure locations with no consideration of vulnerability (left) and full consideration of vulnerability (right). Top row represents the prioritization when considering only 5% of the available area and the bottom row shows results for 10% of the available area.

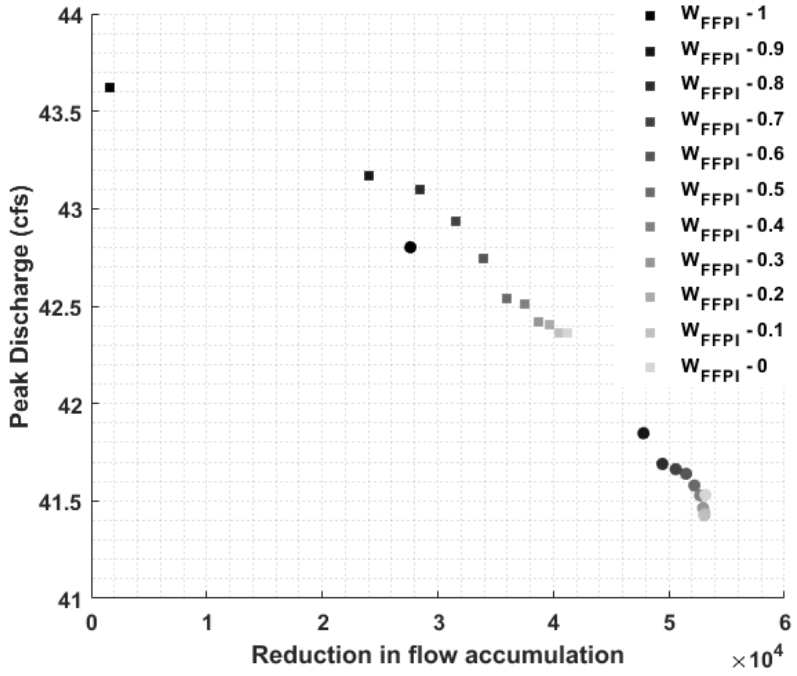

Figure 4.5: Observed relationship between the optimized flow accumulation values and the peak discharge reported by the overland flow model. The color of the markers in the plot symbolize the weights used for W_{FFPI} (i.e., percent of the maximum achievable reduction in flow accumulation to vulnerable areas) [Light gray: $W_{FFPI} = 0$; Black: $W_{FFPI} = 1$]. Additionally, squares represent 5% of available area for GSI; circles represent 10% of available area for GSI.

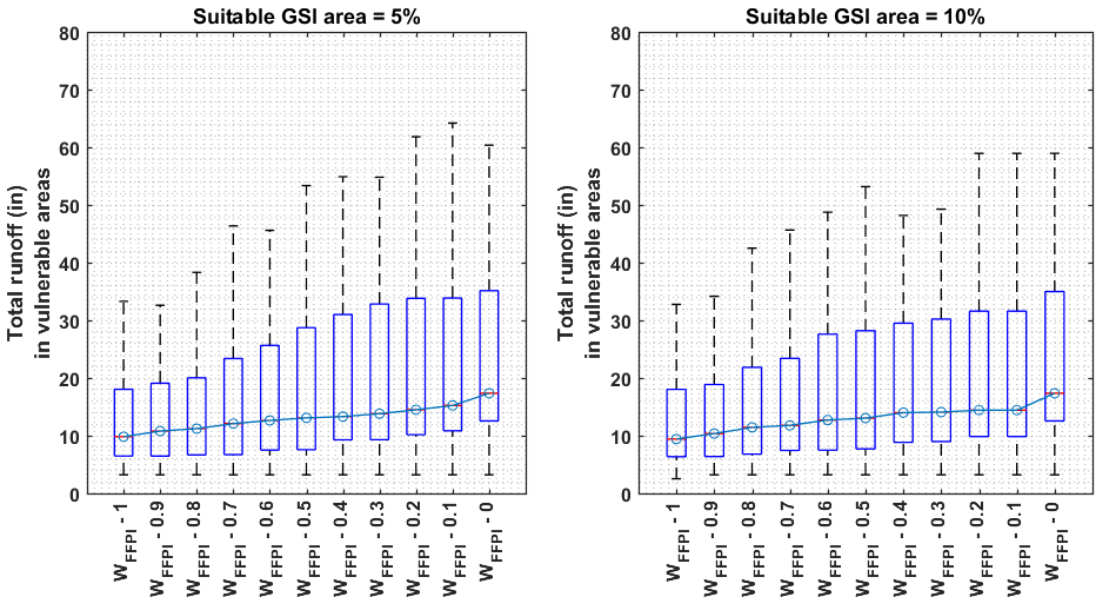

Figure 4.6: Total runoff volume in vulnerable areas reported by the overland flow model for different implementation scenarios and weighting of the objectives.

4.4.2 Prioritization of GSI given different mitigation goals: Philadelphia, PA and Dallas, TX

The second part of the analysis considers the tradeoffs and synergies observed when prioritizing infiltration structures and trees in the cities of Philadelphia, PA and Dallas, TX. To conduct the analysis, it is assumed that a capture ratio of α = 8% is required for infiltration structures [Equation 4.4], that the rainfall interception capacity of trees is φ = 5% [Equation 4.11] and the urban heat island mitigation potential of infiltration structures when compared to that of trees is 10% (i.e., 10% of the urban heat island mitigation geo-preference score of a site) [g_{xik} = 0.1 * g_{zik} in Equation 4.13]. It is also assumed that the hydrologic connectivity of sites extends to the total area of the watershed (i.e., infinite hydrologic connectivity). An infinite hydrologic connectivity implies that the potential runoff of a grid cell (i.e., flow accumulation) is equal to the potential runoff produced by said grid cell plus the allocation of runoff from all upslope grid cells as determined by the MFD method. Four scenarios are analyzed with different weights to represent the importance given to mitigation of urban heat island and flash flooding and to assign a higher preference to ecologic and human health benefits and/or planning criteria (refer to Equations 4.15 to 4.20):

(1) Runoff reduction in watershed outlet and mitigation of UHI (i.e., W_{DA} = 1 and W_{ffpi} varies between 0 and 1 in increments of 0.2)

(2) Runoff reduction at the watershed outlet and in the most vulnerable areas to flash flooding (i.e., W_{ffpi} = 1 and W_{DA} varies between 0 and 1 in increments of 0.2)
(3) Mitigation of flash flooding and UHI vulnerability (i.e., W_{DA} = 0 and W_{ffpi} varies between 0 and 1 in increments of 0.2)
(4) Consideration of ecologic, human health benefits, and planning criteria in the previous three weighting scenarios (i.e., $W_{INF,k}$ = 0.5 and F_k = 100).

Figure 4.7 presents the Pareto fronts for the mitigation of urban heat island and the reduction of runoff volume at the watershed outlet (i.e., weighting scenario 1). In both watersheds, the Pareto front shows a competition for space between hazard mitigation objectives. As UHI mitigation is given higher importance, the implementation of trees is preferred and thus the potential to reduce runoff at the watershed is reduced. The opposite relationship holds true given higher preference for flood mitigation, for which infiltration structures are more effective.

When both objectives are considered, a higher importance given to UHI mitigation results in an increase in the marginal benefits of increased GSI investment for both of these objectives. Trees can only offer UHI mitigation benefits when located in areas with high land surface temperatures. On the other hand, infiltration structures are less spatially restricted, as many locations can offer similar potential for runoff reduction. However, the performance of infiltration structures can improve from implementing trees in their upslope areas that reduce the potential volume of runoff (i.e., total impervious area) draining into these sites (i.e., higher capture ratios). The results also suggest that neglecting either of these objectives can have significant impacts on the potential mitigation benefits that could otherwise be achieved if both are considered. Planting trees in areas with higher UHI mitigation potential should thus be given priority over the use of infiltration structures in these areas, as it is likely that other sites could be used to implement infiltration structures and achieve similar runoff reduction benefit at the watershed scale.

When comparing the Pareto fronts of these watersheds, two noteworthy observations can be made. First, one of the most notable differences between the Pareto fronts is the marginal benefit in the geo-preference scores of UHI with an increase in budget. When the UHI mitigation potential is given full consideration [Equation 4.17 W_{UHI} = 1], the Pareto fronts for the watershed in Philadelphia suggest that ~85% of the total achievable UHI mitigation potential can be obtained by using only 25% of the potential area for GSI. In Dallas, 50% of the potential area for GSI is needed to reach a similar UHI mitigation potential.

A possible explanation for this difference is that the watershed in Dallas has a larger percent of its area with high to very high UHI hazard exposure severity, and therefore a higher percentage of its area is needed for GSI to gain a similar UHI mitigation objective. However, only 38.8% of the watershed area had high to very high UHI hazard exposure severity in Dallas, versus 56.2% in Philadelphia. Further, the percentage area suitable for planting trees within these areas of high to very high UHI hazard exposure severity is 33.9% in Dallas and 12.1% in Philadelphia. More importantly though, only 6.4% of the GSI area in Philadelphia provided 50% of the total UHI mitigation geo-preference score, while in Dallas 18.6% of the GSI area is needed. These results highlight the importance of considering both the *efficiency* and *effectiveness* of potential GSI sites. The identification of a large percentage of the watershed area as suitable sites for GSI implementation does not necessarily translate to a large UHI hazard mitigation benefit. This is because the UHI mitigation potential of a GSI site depends on the composition of its surrounding areas (e.g., consider the example of locating a tree in the middle of a large parking lot). Furthermore, the low percentages of the GSI area need to achieve at least half of the UHI mitigation potential highlight the competition for space that could exist when considering different hazard mitigation objectives. For a low level of GSI implementation, if the GSI sites with large UHI mitigation potential are also among the most desirable locations for flood mitigation, this results in a tradeoff as previously discussed.

The second notable difference between the Pareto fronts of these two watersheds is the marginal increase in UHI mitigation benefit at low UHI weighting levels (i.e., $W_{UHIV} = 0.2$). The Pareto fronts for the Dallas watershed suggest that mitigation of UHI as an objective in the optimization formulation needs an importance weight of at least $W_{UHIV} = 0.4$ (almost equal to the importance given to the reduction of runoff at the watershed outlet) in order to observe a significant marginal increase in UHI mitigation benefits (i.e., geo-preference score). In Philadelphia, this trend is not observed and the marginal benefits increase more uniformly. These results suggest that many of the potential GSI sites in Philadelphia have high UHI mitigation potential as well as high potential to reduce runoff volume at the watershed outlet, while in Dallas a competition for space is less prevalent and the Pareto fronts are dominated by how much of the potential GSI area is dedicated to the mitigation of each separate hazard (i.e., importance weights represented by parameter λ_k and used in eq. 4.13).

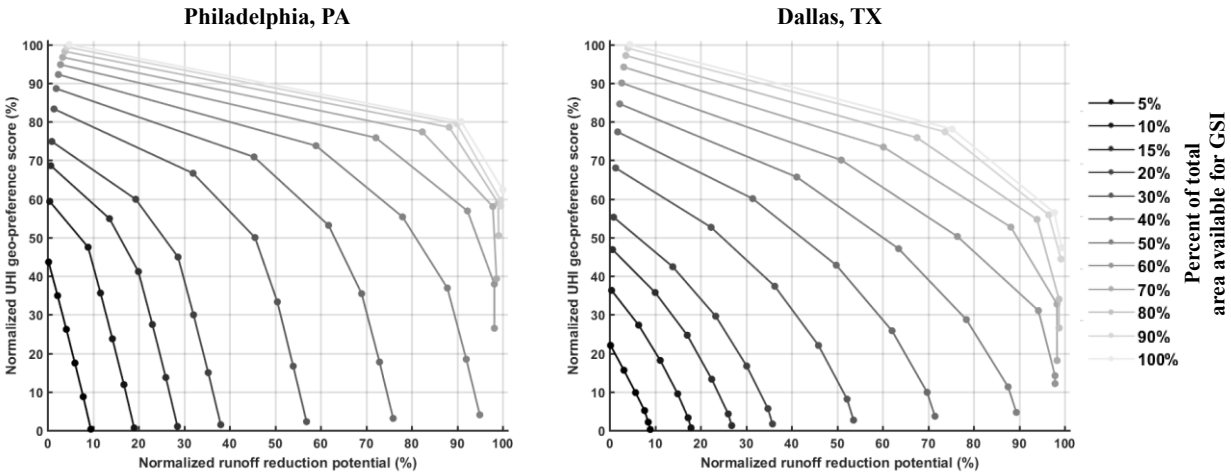

Figure 4.7: Pareto fronts for Philadelphia and Dallas watersheds when considering mitigation of urban heat island and runoff volume at the watershed outlet. Each line represents a different GSI implementation scenario (i.e., percent of total area available for implementing GSI). Round markers in lines represent different degrees of importance given to optimization objectives. Weighting scenarios increase W_{DA} by 0.2 starting from $W_{UHI} = 1$ / $W_{DA} = 0$ [Equations 4.15-4.18].

Similar results are observed when the vulnerability of different communities to these two hazards is considered. Figure 4.8 presents the observed tradeoffs when different degrees of importance are given to reducing the volume of runoff at the watershed outlet and to the reduction of runoff volumes in areas with the highest flash flooding vulnerability. Figure 4.9 (A and B) presents the locations of the prioritized sites for several levels of GSI implementation. Similar to the patterns observed in DR5, as higher importance is given to runoff volume reduction in vulnerable areas, a spatial clustering of GSI occurs upslope of said areas. This is particularly significant in the scenarios where a small percentage (i.e., < 20%) of the available area for GSI implementation is used. Similar to the patterns observed in DR5, prioritization of sites to reduce flash flood vulnerability did not have a negative impact on the potential reduction in runoff volume at the watershed outlet. However, it should be noted that a larger number of GSI sites is needed to achieve said levels of runoff reduction in vulnerable areas.

Furthermore, the difference in the total number of sites considered for implementation between weighting scenarios decreased with an increase in the watershed area. For the watershed in Philadelphia, a larger number of infiltration structures is needed to provide maximum runoff reduction benefits to the vulnerable areas while maintaining the same level of runoff reduction at

the watershed outlet. This difference is negligible in the watershed located in Dallas, in which regardless of the importance given to the protection of the vulnerable communities the number of sites and the reduction of runoff at the watershed outlet remain very similar. One possible explanation for the observed results is that they are caused by the assumptions of infinite hydrologic connectivity. By assuming that hydrologic connectivity extends over the whole watershed, the increase in area creates additional opportunities for sites that could benefit the vulnerable areas and thus creates less competition for space.

The results in Figure 4.8 also show that as the percentage of the area used for implementing GSI increases, the reduction in runoff volume to the vulnerable areas plateaus at about 60-70% of the total potential benefits in both cities, suggesting that no additional benefit could be obtained. Upon further investigation of the results, it was concluded that the unattainable 30-40% of the potential benefits are associated with GSI sites that do not meet the capture ratio constraint and therefore are prioritized for the planting of trees. Related to this limitation, when full consideration is given to the reduction of runoff in vulnerable areas ($W_{FFPI} = 1$), the runoff reduction benefits at the watershed outlet decreased after a certain percentage of the available area for GSI is used. The decrease in benefits at the watershed outlet is caused by the prioritization of trees in areas upslope from the vulnerable communities (e.g., Figure 4.9-A). In short, by requiring the optimization problem to meet the maximum achievable level of runoff reduction to the vulnerable areas, GSI sites that do not have a hydrologic connectivity to these vulnerable areas are not considered as potential sites for GSI implementation until said level of benefit is achieved. As such, a higher preference is given to the use of trees in order to reduce the potential runoff from areas that drain to the vulnerable areas but that do not meet the capture ratio constraints for infiltration structures.

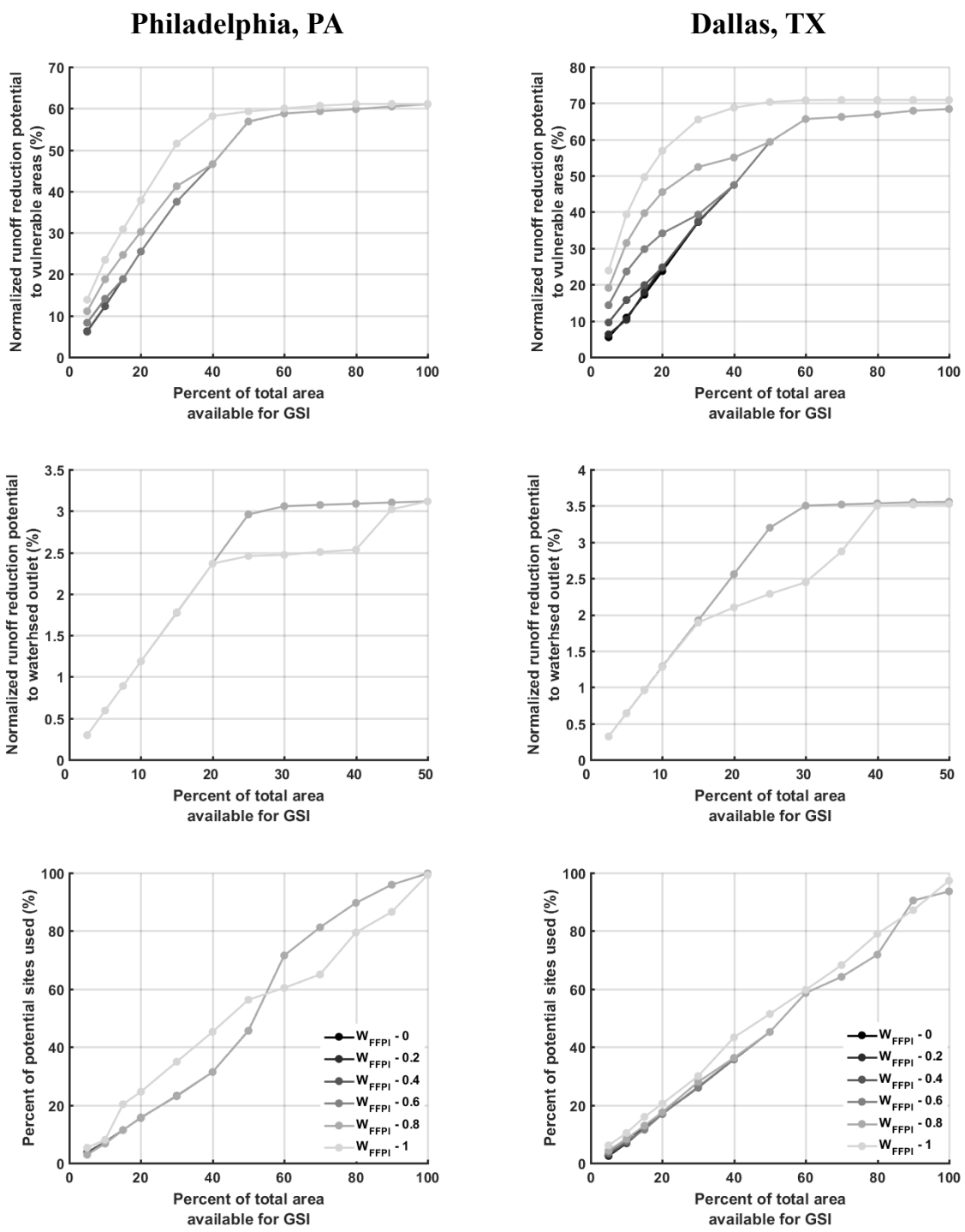

Figure 4.8: Potential runoff reduction benefits in vulnerable areas [light gray: $W_{FFPI} = 1$] and at the watershed outlet [black: $W_{FFPI} = 0$] as a function of the total area used for implementing GSI. The different lines represent different degrees of importance given to the two runoff reduction objectives (i.e., percentage of the maximum achievable reduction in flow accumulation to vulnerable areas).

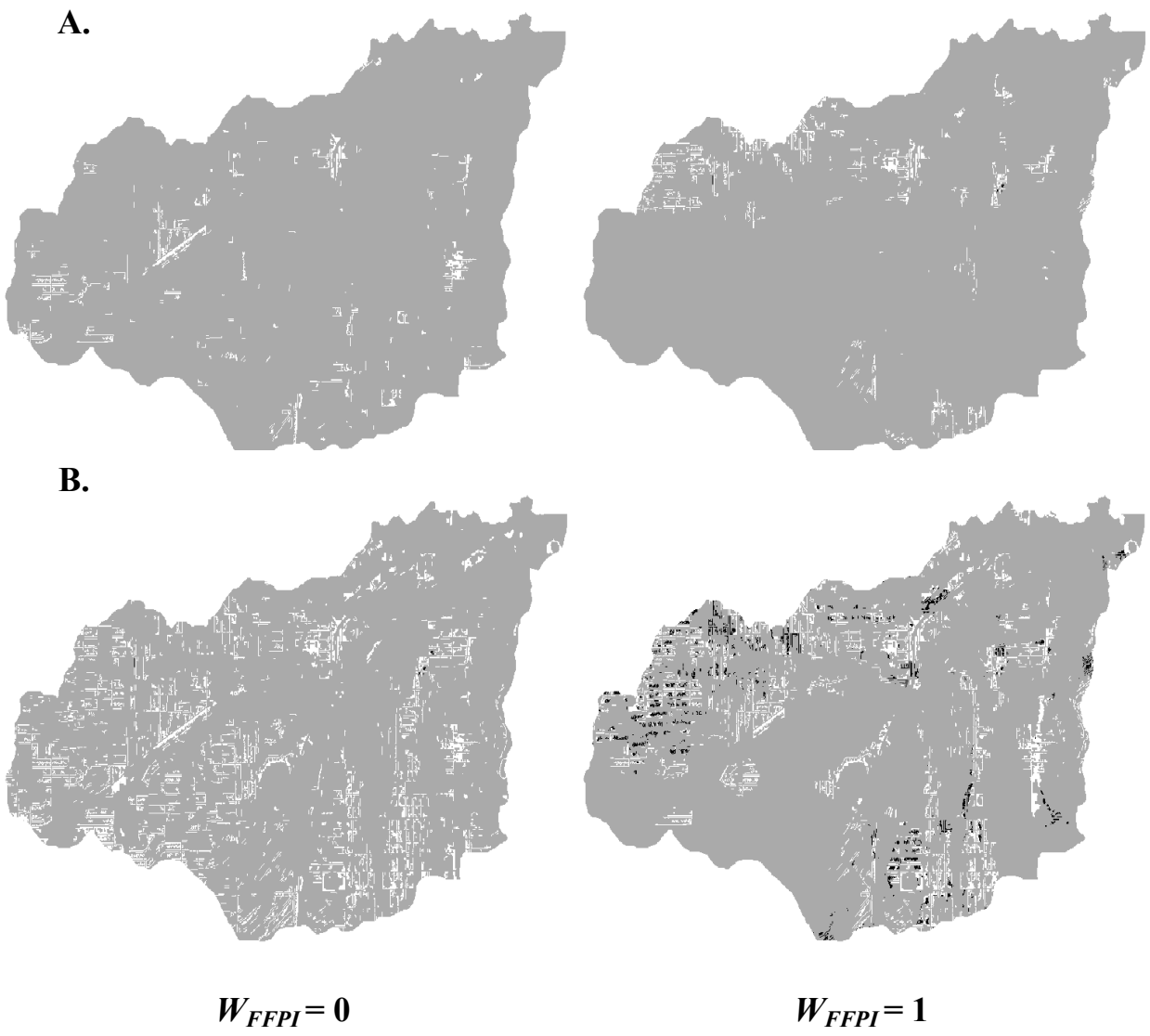

Figure 4.9-A: Optimized spatial allocation of trees (black) and infiltration structures (white) when optimizing to reduce runoff reduction in vulnerable areas [W_{FFPI} = 1] and at the watershed outlet [W_{FFPI} = 0] in Dallas, TX., with: (A)10% and (B) 40% of the potential GSI area implemented.

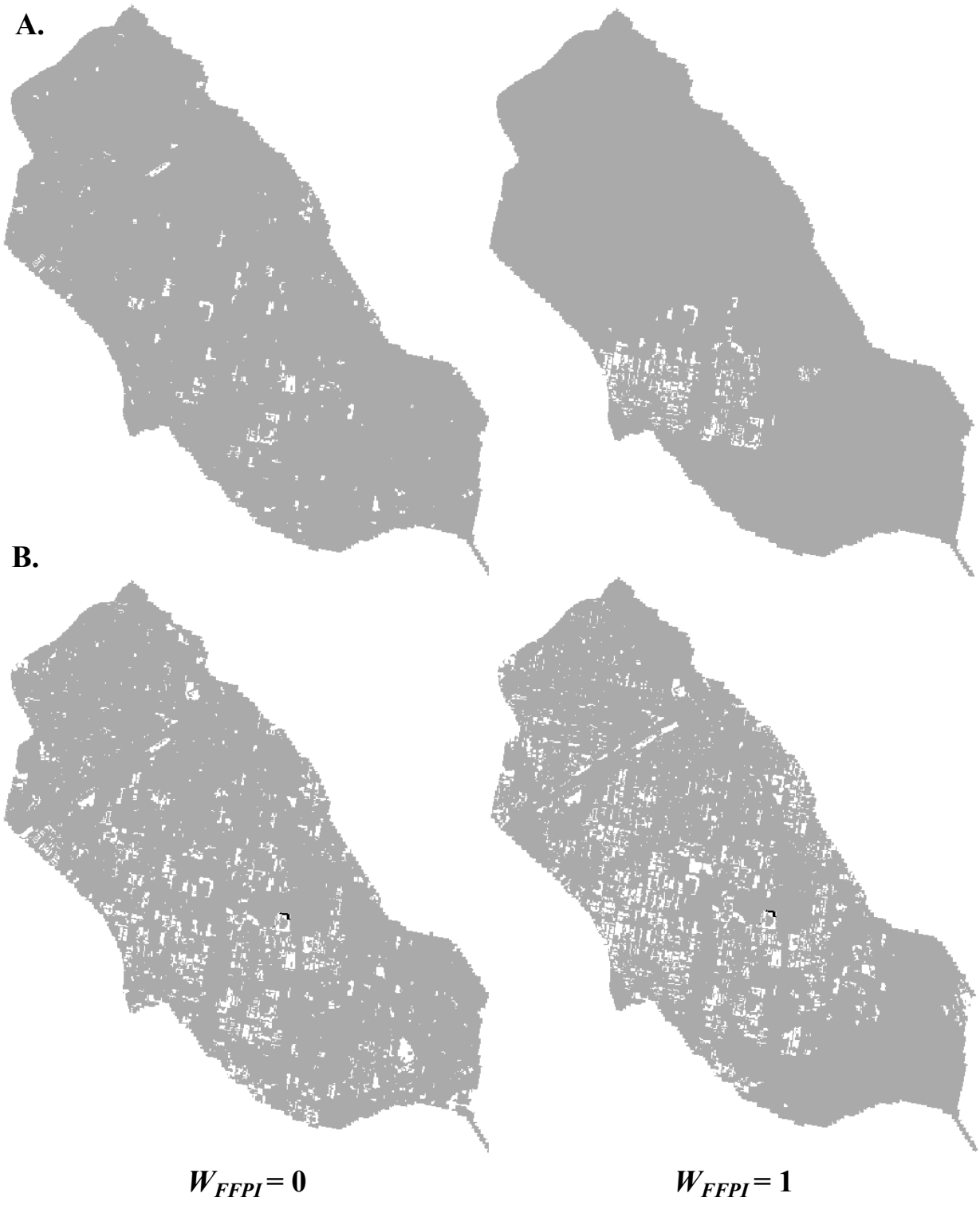

Figure 4.9-B: Optimized spatial allocation of trees (black) and infiltration structures (white) when optimizing to reduce runoff reduction in vulnerable areas [$W_{FFPI} = 1$] and at the watershed outlet [$W_{FFPI} = 0$] in Philadelphia, PA, for: (A)10% and (B) 40% of the potential GSI area implemented.

Figure 4.10 presents a graph for the same parameters as discussed in the previous paragraph but for the scenario in which different degrees of importance are given to the mitigation of flooding and urban heat island vulnerability. Other than the scenario in which only the mitigation to urban heat island is considered, small changes to the curves are observed (when compared to those presented in Figure 4.8). When prioritizing sites solely for the objective of mitigating urban heat island vulnerability, the planting of trees is preferred in the vulnerable areas. Thus, the optimization solution does not include implementation of infiltration structures until all sites with the potential to mitigate urban heat island vulnerability are used to plant trees. This has severe impacts on both the runoff reduction benefits in areas of flash flood vulnerability and at the watershed outlet.

As the importance given to mitigation of flash flooding in vulnerable areas increases (and thus the importance UHI mitigation decreases), the changes in the curves are less significant. Nevertheless, the results show that inclusion of flash flooding vulnerability as an optimization objective has significant impact on potential runoff reduction, even if given small importance. When small importance is given to flash flooding mitigation (e.g., $W_{FFPI} = 0.2$), the optimization formulation is required to meet at least 80% of the total UHI mitigation potential (i.e., geo-preference score; $W_{UHIV} = 0.8$ is used in Equation 4.13 as λ_k). In Philadelphia, the small shifts in the curves associated with this weighting scenario suggest that there are a low number of GSI sites that have large and similar mitigation potential for both hazards in vulnerable areas. For the watershed in Dallas, the magnitude of differences between weighting scenarios is larger, suggesting that a higher number of potential GSI sites have large and similar mitigation potential for both hazards in vulnerable areas. As suggested before, this might be due to the assumption of infinite hydrologic connectivity and the larger watershed area. Overall, the results in Figure 4.10 suggest that neglecting either of the hazard mitigation objectives could result in significant losses of potential vulnerability reduction and that GSI prioritization should consider both objectives.

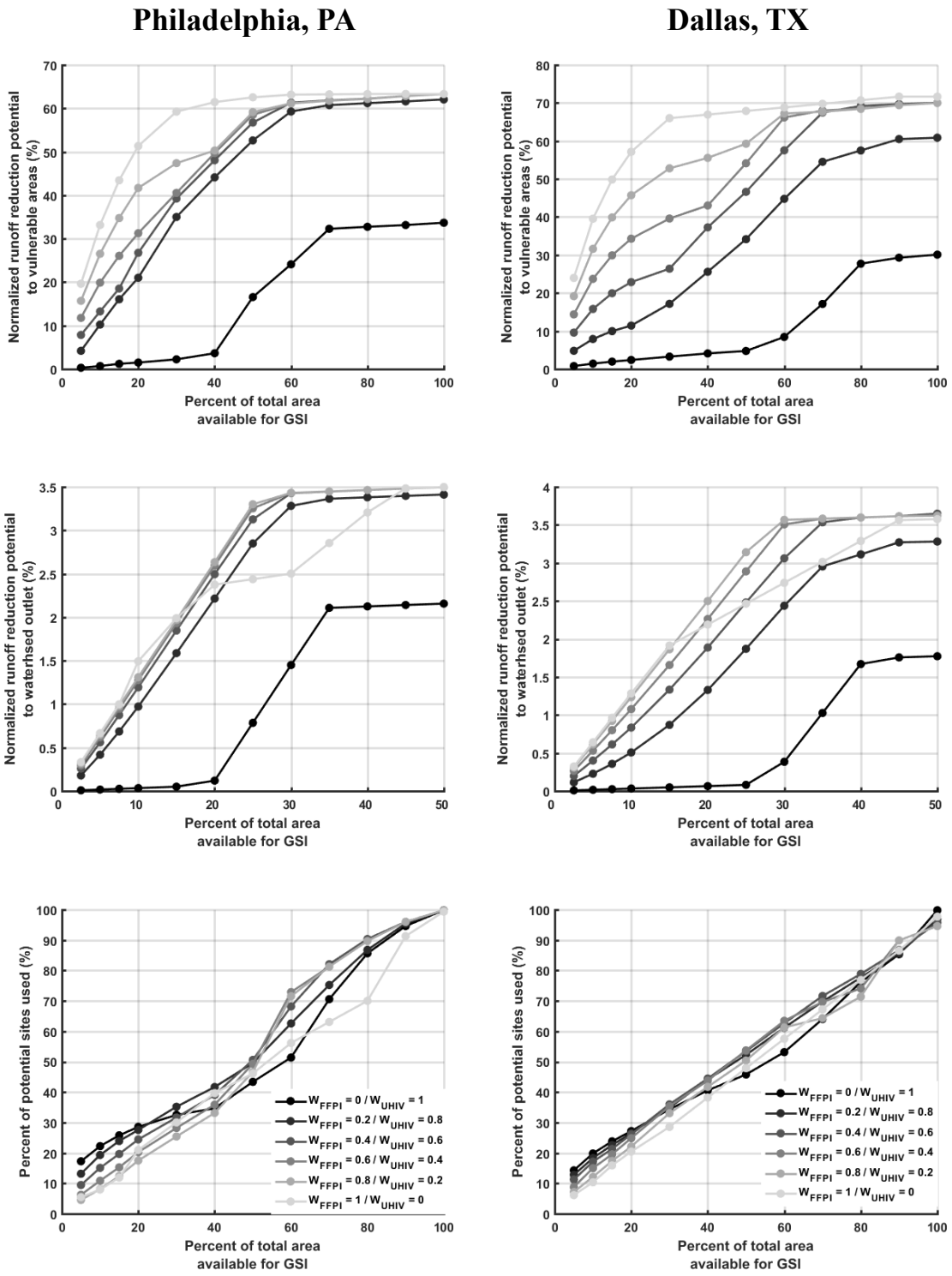

Figure 4.10: Potential runoff reduction benefits in vulnerable areas and at the watershed outlet as a function of the total area used for implementing GSI. Each line represents different degrees of importance given to UHI mitigation [black: W_{FFPI} = 0] and flash flood vulnerability [light gray: W_{FFPI} = 1].

Lastly, the influence of higher weighting for ecologic and human health benefits and/or planning criteria was investigated. Figures 4.11 & 4.12 presents a comparison of the total geo-preference score associated with prioritized sites when including/excluding these criteria and consideration of different hazard mitigation objectives. While a small increase in the geo-preference score for a particular level of GSI implementation is observed when these criteria are considered, the shape of the curves is dominated by the performance constraints (e.g., capture ratio, minimum runoff reduction to vulnerable areas).

Nevertheless, there are two noteworthy observations. First, the prioritization of sites based on their potential to reduce runoff at the watershed outlet produced higher total geo-preference scores, thus suggest that many of the sites prioritized by considering only said objective have higher potentials to provide ecologic and human health benefits, and/or are preferred by planning criteria. Secondly, the consideration of vulnerability in the prioritization process reduced the variability of the curves for different weightings of the objectives. This suggests that regardless of the mitigation objective, sites with a higher potential for mitigating urban heat island and flash flooding vulnerability have similar geo-preference scores associated with these other criteria.

The observed trends suggest that the traditional engineering approach that only considers the stormwater abetment at the watershed outlet could have the largest impact on ecologic restoration and human health as defined in this work. However, UHI mitigation has human health benefits that are not reflected in the results of Figure 4.11. Future work is needed to better understand how a reduction in UHI could be reflected in human health risk reduction.

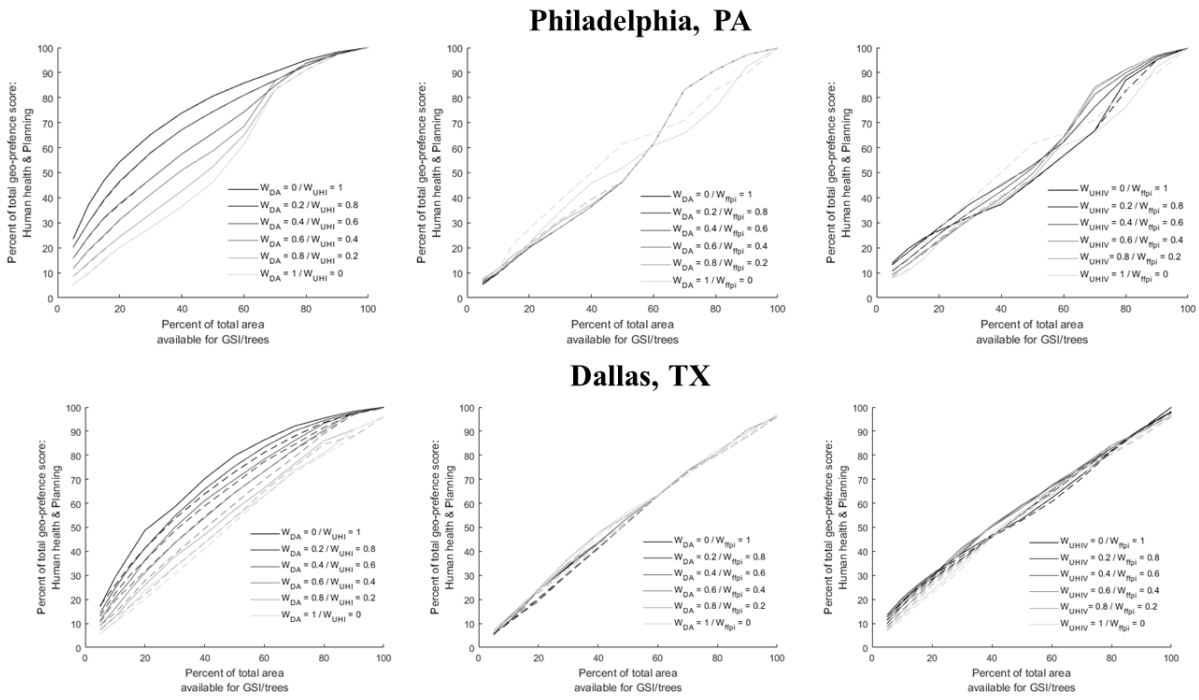

Figure 4.11: Total geo-preference scores for human health and planning criteria when considering different prioritization objectives. Solid lines represent the inclusion of said criteria in the prioritization process; dashed lines represent its exclusion.

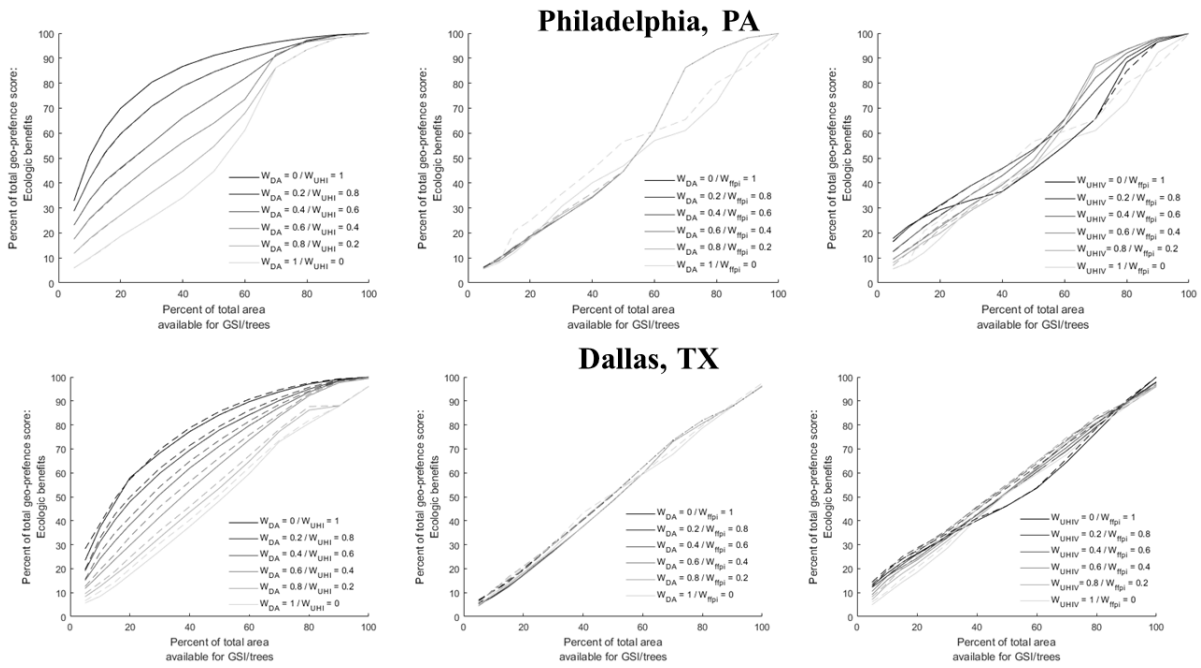

Figure 4.12: Total geo-preference scores for ecologic benefits when considering different objectives. Solid lines represent the inclusion of said criteria in the prioritization process; dashed lines represent its exclusion.

4.4.3 Sensitivity analysis results

The results of the sensitivity analysis show that the observed patterns and conclusions discussed in the previous section are not significantly affected by changes in the values used to represent cooling capacity of infiltration structures or rainfall interception rate of trees. While the use of different values produces some small shifts in the coordinates of the Patero curves, the tradeoff and patterns previously discussed remained unchanged. This is not surprising given that regardless of the range of values used, the cooling capacity of infiltration structures is always lower than trees and the rainfall interception rate of trees is always lower than the runoff reduction potential of infiltration structures.

Moreover, the sensitivity analysis showed that the observed patterns are not significantly affected by a distance restriction in hydrologic connectivity. Figures 4.13 and 4.14 present the runoff reduction in vulnerable areas and at the watershed outlet when considering mitigation of flash flooding and UHI vulnerability. Comparing the trends of the curves in Figures 4.13 and 4.14 with those in Figures 4.8 and 4.10, in which no restriction to hydrologic connectivity was imposed,

it can be seen that the trends remain largely unchanged. Furthermore, when comparing the spatial location of prioritized areas, no significant changes were observed. Such results highlight the robustness of the prioritization framework and its spatial scalability.

Additionally, these results invalidate the hypothesis that the assumption of infinite hydrologic connectivity caused the previously discussed differences in the Dallas watershed. It was hypothesized that the small difference in the number of GSI sites needed to achieve different runoff reduction benefits (Figure 4.8) and the competition for space observed when considering the vulnerability to different hazards (Figure 4.10) could have been caused by the assumption that any upstream GSI located within the watershed area could provide runoff reduction benefits to the vulnerable areas. However, the similarity of the results presented in Figures 4.13 and 4.14 suggest that this assumption of infinite hydrologic connectivity had no significant impact on the observed trends, implying that many of the optimal locations have a hydrologic connectivity of 200 meters or less. These results suggest that the observed differences for the Dallas watershed are caused by its larger watershed area. A larger watershed area provides a larger number of potential GSI sites, each with different runoff and UHI mitigation potential.

Finally, only the graphs showing the total number of sites used as a function of the total available area in Figures 4.13 and 4.14 are seen to have a noteworthy change with restrictions in hydrologic connectivity. The previously noted increase in the total number of sites used for mitigation of flash flooding vulnerability was reduced and all curves followed a similar trend regardless of the importance given to this objective. Restricting the hydrologic connectivity has the most significant impact when considering low levels of GSI implementation for the scenario where only runoff reduction to the watershed outlet is considered. This is not an unexpected result, given that the restriction imposed on hydrologic connectivity forces the prioritization framework to consider locations that are spatially close, thus resembling the clustering behavior observed when the reduction of runoff in vulnerable areas is given the most importance.

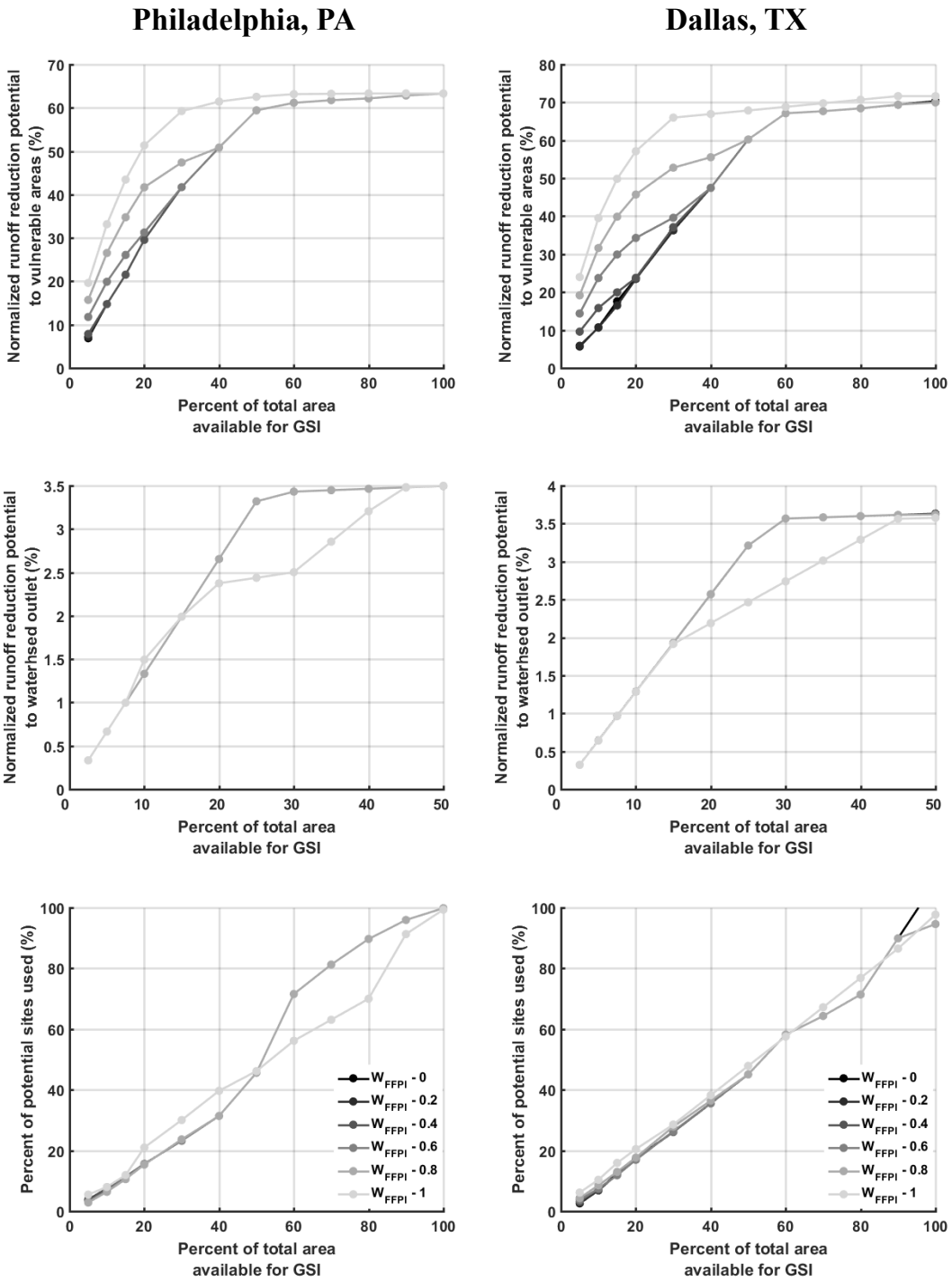

Figure 4.13: Potential runoff reduction benefits in vulnerable areas [light gray: W_{FFPI} = 1] and at the watershed outlet [black: W_{FFPI} = 1] as a function of the total area used for implementing GSI, with a distance threshold of 200 meters to restrict hydrologic connectivity. Each line represents different degrees of importance given to the two runoff reduction objectives (i.e., percent of the maximum achievable reduction in flow accumulation to vulnerable areas).

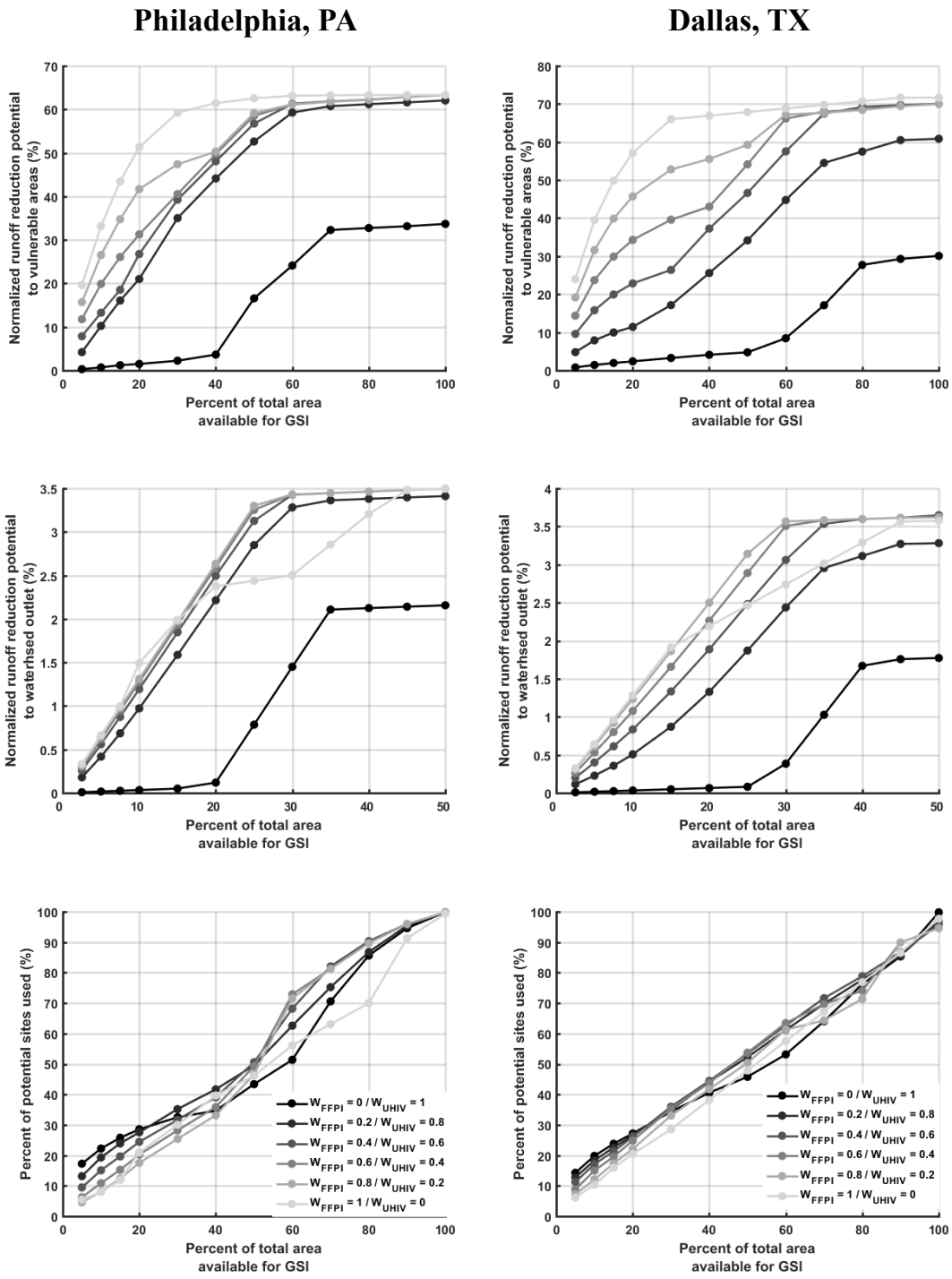

Figure 4.14: Potential runoff reduction benefits in vulnerable areas and at the watershed outlet as a function of the total area used for implementing GSI, with a distance threshold of 200 meters to restrict hydrologic connectivity. Each line represents different degrees of importance given to the mitigation of urban heat island [black: $W_{FFPI} = 0$] and flash flood vulnerability [light gray: $W_{FFPI} = 1$].

4.5 Conclusions and limitations

This chapter proposes an integrated and spatially scalable PSS for spatial planning of GSI. Using the concepts of spatially distributed hydrographs, the capture ratio of infiltration structures, and commonly used indicators and guidelines for the calculation of geo-preference scores associated with GSI benefits, the locations and types of GSI are prioritized based on their potential to address different design and planning objectives. Additionally, the framework considers the vulnerability of socio-ecological systems to enable a spatial planning process that maximizes GSI benefits in the most vulnerable communities.

Results obtained from the prioritization framework have good representation of an overland flow hydrologic model and show the impact of considering spatially explicit representation of GSI, particularly in the reduction of flash flooding vulnerability. Application of the framework in two urban watersheds highlights its ability to explore tradeoffs between mitigation of different hazards with various types of GSI. Results highlight the impact that GSI siting decisions can have in reducing vulnerability and suggest the need for its inclusion in the spatial planning process. Using vulnerability as a major driver for GSI prioritization is shown to have minimal impact on stormwater abetment benefits at the watershed outlet. More importantly, for these case studies, a potential space competition is identified between different hazard mitigation objectives and the various types of GSI.

The findings of this study highlight the need for better methods and approaches that more accurately quantify the multiple benefits of GSI. While the geo-preference scores used in this study simplify the quantification of GSI benefits, the approach has limitations in representing the real degree of tradeoffs between hazard mitigation objectives, especially when vulnerability is considered. Better data/models are needed to quantify all of the benefits from different types of GSI more accurately. Moreover, there is a need to understand the marginal benefits and costs with changes in the spatial scale of analysis, total area, spatial configuration, and combinations of types of GSI. This is particularly true for the estimation of UHI mitigation potentials, as the benefit associated with different levels of GSI implementation and its spatial arrangement is poorly understood. Lastly, the patterns observed in the prioritization of areas preferred by planning criteria and/or because of their potential to positively influence ecological and human health suggest the need for more integrated and participatory approaches with transparent and inclusive planning processes.

Future work is needed to better understand the persistence of the tradeoffs between mitigation objectives and to investigate the validity of the hydrologic assumptions used. Application of the prioritization framework in other cities and the inclusion of additional factors associated with spatial planning of GSI (e.g., cost and construction regulations) could provide new insights to propose more socially just plans. Additionally, the use of the proposed framework to explore GSI implementation scenarios that consider different policies and regulations, the cost of installation and operation/maintenance of GSI, and additional implementation objectives (e.g., in-situ treatment of runoff) would further elucidate the competing factors and areas that would provide the greatest return on investment.

Lastly, as previously discussed, the proposed spatial optimization framework neglects the temporal component of the rainfall-runoff process as well as the sub-surface processes that occur over longer time periods (e.g., recharge of groundwater, impact on base flows). This is, in part, due to the lack of distributed hydrologic models that can fully capture the complexities of urban stormwater processes. Using distributed hydrologic models would also involve a more computationally-intensive optimization process that may not be necessary for large-scale planning. Once the best areas and types of GSI are identified with this framework, more detailed hydrologic models can be developed for those areas if needed. Nonetheless, this multi-step process could be avoided if future research developed distributed hydrologic models that can account for urban rainfall-runoff processes and the complexities of modeling the GSI performance while maintaining a low computational cost and sufficient flexibility to be integrated into the PSS.

CHAPTER 5. LIMITATIONS AND FUTURE WORK

The findings presented in this dissertation suggest that the lack of integrated spatial GSI planning, particularly at large scales, have limited the delivery of GSI benefits to the most vulnerable communities. Application of the proposed prioritization framework shows that consideration of vulnerability in GSI planning significantly affects spatial allocation of GSI, which, if ignored, could aggravate social justice disparities. In this chapter, limitations of the approach are summarized and recommendations are made to further investigate the findings and overcome the limitations.

The proposed framework for the quantification of socio-ecological vulnerability assumes no interactions among the susceptibility indicators nor among the hazards and ignores the temporal component of said relationships. However, it has been argued that the vulnerability of socio-ecologic systems is not static nor system independent (Füssel, 2007; De Lange et al, 2010; Fekete et al., 2010). Threats to these systems occur over different time scales and their impact may reflect differently at multiple scales (e.g., urbanization). Additionally, when combined, spatio-temporal hazard processes may create different risks associated with exposure (e.g., a heavy rain during a drought period, while beneficial to some systems, could exacerbate the risk to extreme heat by increasing relative humidity). Moreover, there are intra- and inter-dependences that may influence the vulnerability of said systems and are ignored in the proposed framework. For example, economic stability can depend on the integrity of ecological services (Turner II, 2003a & 2003b).

More importantly, the proposed approach neglects the concept of resilience. Resiliency, a concept describing the recovery and adaptive capacity of the system, must be considered in order to have a full representation of all dimensions of vulnerability. Unfortunately, due to its fairly new uptake and consideration for decision making, insufficient indicators have been proposed for its quantification (Meerow et al., 2016a & 2016b). Furthermore, a recent literature review on urban resiliency identified significant tensions in finding agreement on its conceptual meaning, which has led to challenges in the proposal of frameworks (Meerow et al., 2016a & 2016b). Advances must be made in this area before resiliency can be integrated into the proposed vulnerability framework or used to guide decision-making. Moreover, there is a need for identification and collection of data that could serve as indicators of recovery and adaptive capacity of socio-ecologic and socio-technical systems.

To this end, it would be interesting to consider the development and use of data science techniques to develop resilience indicators. Data science techniques such as text mining, computer vision, and machine learning enable the extraction and analysis of large volume of data from many different sources (e.g., social media, news articles, images). Moreover, these techniques have showed to be less costly and time consuming than methods often used to collect survey data (e.g., Japec et al., 2015). In particular, new methods for the quantification of social susceptibility could be developed using social media data. For example, Klinenberg (1999) determined that a significant resilience indicator to UHI vulnerability is the level of neighborhood cohesion (i.e., the level of aid/help shared between neighbors). At the same time, other studies have shown how Facebook data could be used to estimate social networks (e.g., Adamic et al., 2005; Horvát et al., 2012). Therefore, data science techniques could potentially be used to estimate the level of neighborhood cohesion (i.e., resilience indicator to extreme heat) from Facebook data. Future research to extract and validate derived indicators of resilience using data science is needed.

The proposed approach for quantifying social susceptibility could be extended by considering the use of more complex and statistically rigorous dasymetric techniques. Recently proposed methods, such as the penalized maximum entropy dasymetric model proposed by Nagle et al. (2014), use high resolution spatial data and information from many data sources collected at different spatial scales (e.g., point location of households and satellite imagery) to provide estimates of population at very fine spatial scales (i.e., tax lots). These methods are computationally costly. Furthermore, their use has been limited to socio-demographic characteristics and not features related to income or physical disadvantage of the populations at risk. Due to privacy concerns, these features are often reported at the Census Tract or county level.

The use of Cloud computing and Web services to calculate social susceptibility presents an opportunity to solve these problems. The users could select which dimensions of social susceptibility will be considered, the method used for its quantification, and the data to be used, all while maintaining data privacy. To date, a few Web services for social susceptibility have been developed (e.g., NOAA's Digital Coast, US Army Corps of Engineers Social Vulnerability Index-Explorer). However, these are restricted to the use of a specific method and data, and do not provide the flexibility needed to accommodate conceptual assumptions that have significant impacts on the spatial patterns of vulnerability, as shown in Chapter 2. Moreover, these Web

services report social susceptibility at the spatial scale of counties or Census Tracts, which were shown to be too large for spatial planning of GSI.

Another limitation of this work is the variability analysis of the spatial patterns of social susceptibility and vulnerability, which is limited to methods and indicators most commonly used in the literature. It would be beneficial to understand the applicability of the proposed approach with other methods and for decision making related to other problems (e.g., evacuation planning).

The findings presented in this dissertation also suggest the need for methods that more accurately estimate the multiple benefits of GSI. The results in Philadelphia, PA, and Dallas, TX, suggest that a competition for space exists between hazard mitigation goals and for the protection of vulnerable areas to these hazards. Whether or not the geo-preference scores and indicators accurately reflect the full capacity of different GSI to provide the intended benefits is a question that needs further investigation. This would require the collection of more detailed data on these benefits at multiple scales and the development of models that accurately predict the full suite of GSI co-benefits and their impacts on vulnerability. This would allow stakeholders to decide how much, if any, they would be willing to sacrifice of one objective for the added benefit of another objective.

The findings presented in this dissertation also highlight the need for distributed hydrologic models that can estimate hydrologic benefits of GSI at multiple scales and are computationally efficient. This has been an area of recent interest, and recent studies have identified such needs (Golden et al., 2017; Jefferson et al., 2017). The results of this work also show that flow accumulation is a suitable proxy metric for representing rainfall-runoff processes in large-scale GSI planning. However, the presented analyses used only a simplified overland flow model and thus do not consider any of the complexities associated with the conveyance of stormwater runoff in urban environments. Given the significant impact that siting decisions can have on reducing flood vulnerability, a more thorough assessment of the appropriateness of using flow accumulation as a proxy metric or the development of new estimation models is need.

Furthermore, additional research is needed to understand the impacts of using different capture ratio values for different types of GSI. The analyses presented in Chapter 4 assume a capture ratio of 8% regardless of the area dedicated to implementation of infiltration structures. Nevertheless, the literature suggests that different infiltration structures should have different capture constraints (e.g., design guidelines in Table 4.1). Moreover, infiltration structures with the

same surface area could have different storage capacities, and thus require varying capture ratios, due to different design parameters (e.g., soil used, connection to sewer system, etc.). Therefore, the influence of using capture ratios that vary with the type of GSI and their design parameters on the optimal spatial allocation of GSI is an area of future research.

Another limitation of this work is the assumption of a static planning process in time, which is not valid in practice because the urban landscape and the opinion of stakeholders are constantly changing. Therefore, the prioritization process should account for shifts over time in the importance given to different objectives and changes in the availability of space to implement GSI. Models could take into account future land development plans, predictions of population growth and urban sprawl, and any regulatory/policy constraints that could affect future GSI implementation and effectiveness. Furthermore, the prioritization process should account for changes in spatial patterns of vulnerability caused by shifts in community susceptibility (e.g., displacement of lower-income families in gentrifying neighborhoods) or implementation of hazard mitigation strategies (e.g., new reservoirs with flood water capacity).

To address this limitation, the proposed prioritization framework could be coupled with urban growth and climate change models to yield more robust and cost-effective GSI implementation plans. Urban growth models allow prediction of spatio-temporal land use patterns and re-allocations of different communities (Cheng, 2013; Feng et al., 2016; Li & Gong, 2016; Musa et al., 2017). Similarly, climate models can estimate spatio-temporal changes in temperatures and rainfall patterns (Cheng, 2013; IPCC, 2012) that could affect GSI planning. Incorporation of these models would, however, require re-formulation of the multi-objective optimization and nonlinear solution methods to handle the added complexity.

Furthermore, while the presented framework facilitates the translation of information between multiple stakeholders, it does not provide the capability to find an optimal solution that maximizes the level of stakeholder consensus given different opinions. Future research is needed to include preference aggregation techniques or collaborative optimization models (e.g., Mysiak et al., 2005; Tippett, 2005; Babbar-Sebens & Minsker, 2008; Singh et al., 2008; Piemonti et al., 2013; Basco-Carrera et al., 2017; Choi et al., 2017) that maximize the needs of all stakeholders involved.

Finally, the proposed prioritization framework enables investigation of many other issues related to the spatial planning of GSI that were not considered in this work. Among the most critical

factors associated with GSI implementation, and not explicitly considered in this study, is the cost of construction and operation/maintenance. Different GSI can have economies of scale associated with their construction cost (i.e., larger projects could provide larger benefits for a low increase in the marginal costs) (Potts et al., 2015). Thus, the cost associated with GSI implementation scenarios could vary even if the total GSI area is the same, which is the proxy metric used in this work as a budget constraint in optimization formulation. Including monetary cost explicitly in the framework could improve understating of the tradeoffs between reducing vulnerability and the cost of implementing different types of GSI.

Moreover, different economic incentives programs could be explored to foster more equitable planning of GSI. One such idea would be to investigate different economic models that would share the costs of GSI among all beneficiaries. The cost of operation/maintenance and a percentage of the cost of construction are usually assumed by the owners of the land in which the GSI is installed. However, as demonstrated in this dissertation, the hydrologic benefits of GSI are not limited to its geo-location and not all areas downstream benefit equally from its implementation. Therefore, an economic model that shares the cost among all beneficiaries could help increase buy-in to implement GSI and aid in developing incentive programs that target sites providing the most benefit to the vulnerable communities.

Additionally, the proposed framework could be used to further investigate other issues such as equity and social justice, the impact of current and new policies and regulations on the design and management of GSI, and the impact that GSI could have in solving specific ecologic/environmental problems (e.g., preservation of salmon habitat in Portland, OR). By framing the spatial planning of GSI as a spatially explicit quantification of vulnerability, site suitability, and mitigation potential, the proposed framework allows integration of additional spatial data that represent these related issues.

While the results presented in this dissertation highlighted the impact that GSI siting decision could have on improving vulnerability, the analyses did not include an assessment of other aspects of social and/or environmental justice. Much like the concept of vulnerability, the concept of social justice is complex, multi-faceted, and multi-disciplinary, and thus its explicit consideration requires a discussion of its definition and the use of methods appropriate for its assessment. For example, future research could explore how GSI perceptions and willingness-to-

pay affect the implementation of GSI in the areas where GSI is needed the most, and thus its impact on improving vulnerability.

More specifically, the results presented in Chapter 3 suggest that a large portion of the available area for GSI in Philadelphia, PA, is private land. Thus, further research is needed to investigate the barriers associated with GSI implementation (e.g., aesthetics, maintenance cost, etc.) on private land and whether re-framing the problem with a vulnerability perspective could help overcome some of those barriers. In addition, many municipalities today have policies and regulations associated with the capture/reduction of stormwater runoff (e.g., stormwater credit programs) that could be re-evaluated from a social justice perspective. For example, should runoff generating areas upslope from vulnerable communities pay higher service charges? Should increasing trees around schools located in lower socio-economic educational districts, which was shown in recent studies (Matsuoka, 2010; Wu et al., 2014; Sivarajah et al., 2018) to significantly improve student performance, be prioritized over mitigation of urban heat island? The proposed framework enables investigating the impact of different polices and plans on these issues and could aid in the proposal of more equitable and just GSI implementation.

Lastly, generalization of the observed tradeoffs between mitigation objectives is limited by the application of the prioritization framework in two watersheds. Further research is needed to better understand how these patterns could change when different hydro-climatic conditions, types of urban form, and additional implementation objectives (i.e., removal of pollutants, groundwater recharge, etc.) are considered.

REFERENCES

Abunnasr, Y. F. (2013). *Climate Change Adaptation: A Green Infrastructure Planning Framework for Resilient Urban Regions*. Retrieved from http://scholarworks.umass.edu/open_access_dissertations/775/

Adamic, L., & Adar, E. (2005). How to search a social network. *Social Networks*, *27*(3), 187–203. https://doi.org/10.1016/j.socnet.2005.01.007

Ahiablame, L. M., Engel, B. A., & Chaubey, I. (2013). Effectiveness of low impact development practices in two urbanized watersheds: Retrofitting with rain barrel/cistern and porous pavement. *Journal of Environmental Management*, *119*, 151–161. https://doi.org/10.1016/j.jenvman.2013.01.019

Ahiablame, L. M., A. Engel, B., & Chaubey, I. (2012). Representation and Evaluation of Low Impact Development Practices with L-THIA-LID: An Example for Site Planning. *Environment and Pollution*, *1*(2), 1–13. https://doi.org/10.5539/ep.v1n2p1

Akbari H, Davis S, Dorsano S, Huang J & Winnett S. (1992). Cooling our communities: A guidebook on tree planting and light-colored surfacing. US Environmental Protection Agency, Washington, DC

Ambrey, C., Byrne, J., Matthews, T., Davison, A., Portanger, C., & Lo, A. (2017). Cultivating climate justice: Green infrastructure and suburban disadvantage in Australia. *Applied Geography*, *89*(February), 52–60. https://doi.org/10.1016/j.apgeog.2017.10.002

Andersen, T. K., Marshall Shepherd, J., Shepherd, J. M., & Marshall Shepherd, J. (2013). Floods in a Changing Climate. *Geography Compass*, *7*(2), 95–115. https://doi.org/10.1111/gec3.12025

Anselin, L., Syabri, I., & Kho, Y. (2006). GeoDa: An Introduction to Spatial Data Analysis. *Geographical Analysis*, *38*(1), 5–22. https://doi.org/10.1111/j.0016-7363.2005.00671.x

ASCE. (2013). *2013 Report Card for America's Infrastructure*. https://doi.org/10.1061/9780784478837

Ashley, R., Blackwood, D., Butler, D., & Jowitt, P. (2004). *Sustainable Water Services: A Procedural Guide*. Retrieved from https://books.google.com/books?id=rhacPn4aqAIC&pgis=1

Autixier, L., Mailhot, A., Bolduc, S., Madoux-humery, A., Galarneau, M., Prévost, M., & Dorner, S. (2014). Evaluating rain gardens as a method to reduce the impact of sewer over fl ows in sources of drinking water. *Science of the Total Environment, The*, *499*, 238–247. https://doi.org/10.1016/j.scitotenv.2014.08.030

Babbar-Sebens, M., Barr, R. C., Tedesco, L. P., & Anderson, M. (2013). Spatial identification and optimization of upland wetlands in agricultural watersheds. *Ecological Engineering*, *52*, 130–142. https://doi.org/10.1016/j.ecoleng.2012.12.085

Babbar-Sebens, M., & Minsker, B. (2008). Standard Interactive Genetic Algorithm—Comprehensive Optimization Framework for Groundwater Monitoring Design. *Journal of Water Resources Planning and Management*, *134*(6), 538–547. https://doi.org/10.1061/(ASCE)0733-9496(2008)134:6(538)

Bakkensen, L. A., Fox-Lent, C., Read, L. K., & Linkov, I. (2017). Validating Resilience and Vulnerability Indices in the Context of Natural Disasters. *Risk Analysis*, *37*(5), 982–1004. https://doi.org/10.1111/risa.12677

Baptiste, A. K., Foley, C., & Smardon, R. (2015). Understanding urban neighborhood differences in willingness to implement green infrastructure measures: A case study of Syracuse, NY. *Landscape and Urban Planning*, *136*, 1–12. https://doi.org/10.1016/j.landurbplan.2014.11.012

Basco-Carrera, L., Warren, A., van Beek, E., Jonoski, A., & Giardino, A. (2017). Collaborative modelling or participatory modelling? A framework for water resources management. *Environmental Modelling & Software*, *91*, 95–110. https://doi.org/10.1016/J.ENVSOFT.2017.01.014

Bates, P. D., Horritt, M. S., & Fewtrell, T. J. (2010). A simple inertial formulation of the shallow water equations for efficient two-dimensional flood inundation modelling. *Journal of Hydrology*, *387*(1–2), 33–45. https://doi.org/10.1016/j.jhydrol.2010.03.027

Benedict, M. A., & McMahon, E. T. (2006). *Green Infrastructure: Linking Landscapes and Communities*. *Urban Land* (Vol. June). https://doi.org/10.1007/s10980-006-9045-7

Bhaskar, A. S., Beesley, L., Burns, M. J., Fletcher, T. D., Hamel, P., Oldham, C. E., & Roy, A. H. (2016). Will it rise or will it fall? Managing the complex effects of urbanization on base flow. *Freshwater Science*, *35*(1), 293–310. https://doi.org/10.1086/685084.

Birkmann, J., & von Teichman, K. (2010). Integrating disaster risk reduction and climate change adaptation: Key challenges-scales, knowledge, and norms. *Sustainability Science*, *5*(2), 171–184. https://doi.org/10.1007/s11625-010-0108-y

Bradford, K., Abrahams, L., Hegglin, M., & Klima, K. (2015). A Heat Vulnerability Index and Adaptation Solutions for Pittsburgh, Pennsylvania. *Environmental Science and Technology*, *49*(19), 11303–11311. https://doi.org/10.1021/acs.est.5b03127

Brown, R. R., Deletic, A., & Wong, T. H. F. (2015). Interdisciplinarity: How to catalyse collaboration. *Nature*, *525*(7569), 315–317. https://doi.org/10.1038/525315a

Burian, S. J., Walsh, T., Kalyanapu, A. J., & Larsen, S. G. (2013). *Climate Vulnerabilities and Adaptation of Urban Water Infrastructure Systems*. (Elsevier, Ed.), *Climate Vulnerability: Understanding and Addressing Threats to Essential Resources* (Vol. 5). New York. https://doi.org/10.1016/B978-0-12-384703-4.00509-8

Burns, M. J., Fletcher, T. D., Walsh, C. J., Ladson, A. R., & Hatt, B. E. (2012). Hydrologic shortcomings of conventional urban stormwater management and opportunities for reform.

Landscape and Urban Planning, *105*(3), 230–240. https://doi.org/10.1016/J.LANDURBPLAN.2011.12.012

Burton, C. G. (2010). Social Vulnerability and Hurricane Impact Modeling. *Natural Hazards Review*, *11*(2), 58–68. https://doi.org/10.1061/(ASCE)1527-6988(2010)11:2(58)

Calderón-Contreras, R., & Quiroz-Rosas, L. E. (2017). Analysing scale, quality and diversity of green infrastructure and the provision of Urban Ecosystem Services: A case from Mexico City. *Ecosystem Services*, *23*(April 2016), 127–137. https://doi.org/10.1016/j.ecoser.2016.12.004

Cameron, R. W. F., Blanuša, T., Taylor, J. E., Salisbury, A., Halstead, A. J., Henricot, B., & Thompson, K. (2012). The domestic garden – Its contribution to urban green infrastructure. *Urban Forestry & Urban Greening*, *11*(2), 129–137. https://doi.org/10.1016/J.UFUG.2012.01.002

Carr, E., Abrahams, D., de la Poterie, A., Suarez, P., & Koelle, B. (2015). Vulnerability assessments, identity and spatial scale challenges in disaster-risk reduction. *Jàmbá: Journal of Disaster Risk Studies*, *7*.

Ceru, J. (2012). Flash Flood Potential Index for Pennsylvania. Proceedings, 2012 ESRI *Federal GIS Conference*. Available at: http://proceedings.esri.com/library/userconf/feduc12/papers/user/JoeCeru.pdf

Chan, A. Y., & Hopkins, K. G. (2017). Associations between Sociodemographics and Green Infrastructure Placement in Portland, Oregon. *Journal of Sustainable Water in the Built Environment*, *3*(3), 05017002. https://doi.org/10.1061/JSWBAY.0000827

Chandio, I. A., Matori, A. N. B., WanYusof, K. B., Talpur, M. A. H., Balogun, A. L., & Lawal, D. U. (2013). GIS-based analytic hierarchy process as a multicriteria decision analysis instrument: A review. *Arabian Journal of Geosciences*. https://doi.org/10.1007/s12517-012-0568-8

Chang, C.Y., Chen, P.K., (2005). Human response to window views and indoor plants in the workplace. *Hortscience, 40(5),* 1354-1359.

Chang, Q., Li, X., Huang, X., & Wu, J. (2012). A GIS-based Green Infrastructure Planning for Sustainable Urban Land Use and Spatial Development. *Procedia Environmental Sciences*, *12*(41001112), 491–498. https://doi.org/10.1016/j.proenv.2012.01.308

Chen, X.-L., Zhao, H.-M., Li, P.-X., & Yin, Z.-Y. (2006). Remote sensing image-based analysis of the relationship between urban heat island and land use/cover changes. *Remote Sensing of Environment*, *104*(2), 133–146. https://doi.org/10.1016/j.rse.2005.11.016

Cheng, C. (2013). Social vulnerability, green infrastructure, urbanization and climate change-induced flooding: A risk assessment for the Charles River watershed, Massachusetts, USA. *ProQuest Dissertations and Theses*, 181. https://doi.org/10.1016/j.gloenvcha.2004.12.005

Cheng, C. (2016). Spatial Climate Justice and Green Infrastructure Assessment: A case study for the Huron River watershed, Michigan, USA. *GI_Forum*, *1*, 176–190.

Chicago Metropolitan Agency for Planning (CMAP). (2017). *ON TO 2050 Water Resources Strategy Paper: Stormwater and Flooding*.

Choi, G. B., Kim, J. W., Suh, J. C., Jang, K. H., & Lee, J. M. (2017). A prioritization method for replacement of water mains using rank aggregation. *Korean Journal of Chemical Engineering*, *34*(10), 2584–2590. https://doi.org/10.1007/s11814-017-0191-1

Claro, A., Formato, T., Huyhua, S., Lock, R., Martineau, K., Moore, A., . . . Trotman, L. (2013). Leveraging the multiple benefits of green infrastructure: Sustainability management capstone project for New York City's department of environmental protection. Science in Sustainability Management, Columbia University.

Clean Water America Alliance. (2011). *Barriers and gateways to green infrastructure*. Clean Water America Alliance.

City of Portland (2018, March 22). 2016 Stormwater Management Manual. Retrieved from: https://www.portlandoregon.gov/bes/64040

Connors, J. P., Galletti, C. S., & Chow, W. T. L. (2013). Landscape configuration and urban heat island effects: Assessing the relationship between landscape characteristics and land surface temperature in Phoenix, Arizona. *Landscape Ecology*, *28*(2), 271–283. https://doi.org/10.1007/s10980-012-9833-1

Cutter, S. L. (1996): Vulnerability of environmental hazards. In: *Progress in Human Geography*. vol. 20, pp. 529 – 539.

Cutter, S. L., Barnes, L., Berry, M., Burton, C., Evans, E., Tate, E., & Webb, J. (2008). A place-based model for understanding community resilience to natural disasters. *Global Environmental Change*, *18*(4), 598–606. https://doi.org/10.1016/j.gloenvcha.2008.07.013

Cutter, S. L., Boruff, B. J., & Shirley, W. (2003). Social Vulnerability to Environmental Hazards*. *Social Science Quarterly (Wiley-Blackwell)*, *84*(2), 242–261. https://doi.org/10.1111/1540-6237.8402002

Cutter, S. L., & Finch, C. (2008). Temporal and spatial changes in social vulnerability to natural hazards. *Proceedings of the National Academy of Sciences of the United States of America*, *105*(7), 2301–2306. https://doi.org/10.1073/pnas.0710375105

Damm, Marion. (2010). *Mapping social-ecological vulnerability to flooding: a sub-national approach for Germany.* University of Bonn

De Almeida, G. A. M., & Bates, P. (2013). Applicability of the local inertial approximation of the shallow water equations to flood modeling. *Water Resources Research*, *49*(8), 4833–4844. https://doi.org/10.1002/wrcr.20366

De Almeida, G. A. M., Bates, P., Freer, J. E., & Souvignet, M. (2012). Improving the stability of a simple formulation of the shallow water equations for 2-D flood modeling. *Water Resources Research*, *48*(5), 1–14. https://doi.org/10.1029/2011WR011570

De Lange, H. J., Sala, S., Vighi, M., Faber, J. H., Lange, H. J. De, Sala, S., … Faber, J. H. (2010). Ecological vulnerability in risk assessment — A review and perspectives. *Science of the Total Environment*, *408*(18), 3871–3879. https://doi.org/10.1016/j.scitotenv.2009.11.009

Demuzere, M., Orru, K., Heidrich, O., Olazabal, E., Geneletti, D., Orru, H., … Faehnle, M. (2014). Mitigating and adapting to climate change: Multi-functional and multi-scale assessment of green urban infrastructure. *Journal of Environmental Management*, *146*, 107–115. https://doi.org/10.1016/j.jenvman.2014.07.025

Dierauer, J., Pinter, N., & Remo, J. W. F. (2012). Evaluation of levee setbacks for flood-loss reduction, Middle Mississippi River, USA. *Journal of Hydrology*, *450–451*, 1–8. Retrieved from http://www.scopus.com/inward/record.url?eid=2-s2.0-84862691727&partnerID=40&md5=2b3c09b0d8695d832d2f5642abd135d7

Dixon, B., & Uddameri, V. (2016). *GIS and Geocomputation for Water Resource Science and Engineering*. *GIS and Geocomputation for Water Resource Science and Engineering*. John Wiley & Sons, Ltd . https://doi.org/10.1002/9781118826171

Dooge, J. C. I. (1959). A general theory of the unit hydrograph. *Journal of Geophysical Research*, *64*(2), 241–256. https://doi.org/10.1029/JZ064i002p00241

Dunn, A. D. (2010). Siting green infrastructure: legal and policy solutions to alleviate urban poverty and promote healthy communities. *BC Envtl. Aff. L. Rev.*, 37, 41.

Ekkel, E. D., & de Vries, S. (2017). Nearby green space and human health: Evaluating accessibility metrics. *Landscape and Urban Planning*, *157*, 214–220. https://doi.org/10.1016/j.landurbplan.2016.06.008

Emerson, C. H., Welty, C., & Traver, R. G. (2005). Watershed-Scale Evaluation of a System of Storm Water Detention Basins. *Journal of Hydrologic Engineering*, *10*(3), 237–242. https://doi.org/10.1061/(ASCE)1084-0699(2005)10:3(237)

Engel, B.A., Hunter, J., 2009. L-THIA LID Long-term Hydrologic Impact Assessment Low Impact Development Model. Spreadsheet Version. West. Purdue University, Lafayette, IN.

Evans, C., Wong, A., Snow, C., Choate, A., & Rodehorst, B. (2014). Indicator-based vulnerability screening for improving infrastructure resilience to climate change risks. In *ICSI 2014: Creating Infrastructure for a Sustainable World - Proceedings of the 2014 International Conference on Sustainable Infrastructure* (pp. 215–228). https://doi.org/10.1061/9780784478745.019

Fan, F., Deng, Y., Hu, X., & Weng, Q. (2013). Estimating Composite Curve Number Using an Improved SCS-CN Method with Remotely Sensed Variables in Guangzhou, China. *Remote Sensing*, *5*(3), 1425–1438. https://doi.org/10.3390/rs5031425

Fekete, A. (2009). Validation of a social vulnerability index in context to river-floods in Germany. *Natural Hazards and Earth System Science*, *9*(2), 393–403. https://doi.org/10.5194/nhess-9-393-2009

Fekete, A., Damm, M., & Birkmann, J. (2010). Scales as a challenge for vulnerability assessment. *Natural Hazards*, *55*(3), 729–747. https://doi.org/10.1007/s11069-009-9445-5

Feng, Y., Liu, M., Chen, L., & Liu, Y. (2016). Simulation of Dynamic Urban Growth with Partial Least Squares Regression-Based Cellular Automata in a GIS Environment. *ISPRS International Journal of Geo-Information*, *5*(12).

Filoso, S., & Palmer, M. A. (2011). Assessing stream restoration effectiveness at reducing nitrogen export to downstream waters. *Ecological Applications, 21(6),* 1989-2006.

Fisher, B., Turner, R. K., & Morling, P. (2009). Defining and classifying ecosystem services for decision making. *Ecological Economics*, *68*(3), 643–653. https://doi.org/10.1016/J.ECOLECON.2008.09.014

Fletcher, T. D., Andrieu, H., & Hamel, P. (2013). Understanding, management and modelling of urban hydrology and its consequences for receiving waters: A state of the art. *35th Year Anniversary Issue*, *51*, 261–279. https://doi.org/http://dx.doi.org.proxy2.library.illinois.edu/10.1016/j.advwatres.2012.09.001

Freeman, T. G. (1991). Calculating catchment area with divergent flow based on a regular grid. *Computers and Geosciences*, *17*(3), 413–422. https://doi.org/10.1016/0098-3004(91)90048-I

Füssel, H.-M. (2007). Vulnerability: A generally applicable conceptual framework for climate change research. *Global Environmental Change*, *17*(2), 155–167. https://doi.org/10.1016/J.GLOENVCHA.2006.05.002

Geertman, Stan, Stillwell, J. (2012). *Planning Support Systems in Practice* (Second). https://doi.org/10.1007/978-3-540-24795-1

Geertman, S., & Stillwell, J. (2004). Planning support systems: an inventory of current practice. *Computers, Environment and Urban Systems*, *28*(4), 291–310. https://doi.org/10.1016/S0198-9715(03)00024-3

Golden, H. E., & Hoghooghi, N. (2017). Green infrastructure and its catchment-scale effects: an emerging science. *Wiley Interdisciplinary Reviews: Water*, *5*(February), e1254. https://doi.org/10.1002/wat2.1254

Guillard-Goncąlves, C., Cutter, S. L., Emrich, C. T., & Zêzere, J. L. (2015). Application of Social Vulnerability Index (SoVI) and delineation of natural risk zones in Greater Lisbon, Portugal. *Journal of Risk Research*, *18*(5), 651–674. https://doi.org/10.1080/13669877.2014.910689

Hansen, R., & Pauleit, S. (2014). From multifunctionality to multiple ecosystem services? A conceptual framework for multifunctionality in green infrastructure planning for Urban Areas. *Ambio*, *43*(4), 516–529. https://doi.org/10.1007/s13280-014-0510-2

Harris, B. (1989). Beyond Geographic Information Systems. *Journal of the American Planning Association*, *55*(1), 85–90. https://doi.org/10.1080/01944368908975408

Heber Green, W., & Ampt, G. A. (1911). Studies on Soil Phyics. *The Journal of Agricultural Science*, *4*(01), 1. https://doi.org/10.1017/S0021859600001441

Heckert, M. (2013). Access and Equity in Greenspace Provision: A Comparison of Methods to Assess the Impacts of Greening Vacant Land. *Transactions in GIS*, *17*(6), 808–827. https://doi.org/10.1111/tgis.12000

Heckert, M., & Rosan, C. D. (2016). Developing a green infrastructure equity index to promote equity planning. *Urban Forestry and Urban Greening*, *19*, 263–270. https://doi.org/10.1016/j.ufug.2015.12.011

Heynen, N., & Perkins, H. A. (2005). Scalar dialectics in green: urban private property and the contradictions of the neoliberalization of nature. *Capitalism Nature Socialism*, *16*(1), 99–113. https://doi.org/10.1080/1045575052000335393

Heynen, N., Perkins, H. A., & Roy, P. (2006). The political ecology of uneven urban green space: The impact of political economy on race and ethnicity in producing environmental inequality in Milwaukee. *Urban Affairs Review*, *42*(1), 3–25. https://doi.org/10.1177/1078087406290729

Hobley, D. E. J., Adams, J. M., Siddhartha Nudurupati, S., Hutton, E. W. H., Gasparini, N. M., Istanbulluoglu, E., & Tucker, G. E. (2017). Creative computing with Landlab: An open-source toolkit for building, coupling, and exploring two-dimensional numerical models of Earth-surface dynamics. *Earth Surface Dynamics*, *5*(1), 21–46. https://doi.org/10.5194/esurf-5-21-2017

Hoffimann, E., Barros, H., & Ribeiro, A. I. (2017). Socioeconomic inequalities in green space quality and Accessibility—Evidence from a Southern European city. *International Journal of Environmental Research and Public Health*, *14*(8). https://doi.org/10.3390/ijerph14080916

Homer, C.G., Dewitz, J.A., Yang, L., Jin, S., Danielson, P., Xian, G., Coulston, J., Herold, N.D., Wickham, J.D., and Megown, K. (2015). Completion of the 2011 National Land Cover Database for the conterminous United States-Representing a decade of land cover change information. *Photogrammetric Engineering and Remote Sensing*, v. 81, no. 5, p. 345-354

Horvát, E.-Á., Hanselmann, M., Hamprecht, F. A., & Zweig, K. A. (2012). One Plus One Makes Three (for Social Networks). *PLOS ONE*, *7*(4), 1–8. https://doi.org/10.1371/journal.pone.0034740

Huang, G., Zhou, W., & Cadenasso, M. L. (2011). Is everyone hot in the city? Spatial pattern of land surface temperatures, land cover and neighborhood socioeconomic characteristics in Baltimore, MD. *Journal of Environmental Management*, *92*(7), 1753–1759. https://doi.org/10.1016/j.jenvman.2011.02.006

Inkiläinen, E. N. M., McHale, M. R., Blank, G. B., James, A. L., & Nikinmaa, E. (2013). The role of the residential urban forest in regulating throughfall: A case study in Raleigh, North Carolina, USA. *Landscape and Urban Planning*, *119*, 91–103. https://doi.org/10.1016/J.LANDURBPLAN.2013.07.002

IPCC. (2007). *IPCC fourth assessment report*. *IPCC Fourth Assessment Report* (Vol. 1). https://doi.org/ISSN: 02767783

IPCC, Field, C. B., Barros, V. R., Stocker, T. F., Qin, D., Dokken, D. J., … Midgley, P. M. (2012). *Managing the Risks of Extreme Events and Disasters to Advance Climate Change Adaptation. A Special Report of Working Groups I and II of the Intergovernmental Panel on Climate Change*. Cambridge, U.K. . https://doi.org/10.1017/CBO9781139177245

James, P., Banay, R. F., Hart, J. E., & Laden, F. (2015). A Review of the Health Benefits of Greenness. *Current Epidemiology Reports*, *2*(2), 131–142. https://doi.org/10.1007/s40471-015-0043-7"

Jankowski, P., Czepkiewicz, M., Mlodkowski, M., & Zwolinski, Z. (2016). Geo-questionnaire: A Method and Tool for Public Preference Elicitation in Land Use Planning. *Transactions in GIS*. https://doi.org/10.1111/tgis.12191

Japec, L., Kreuter, F., Berg, M., Biemer, P., Decker, P., Lampe, C., … Usher, A. (2015). Big data in survey research: Aapor task force report. *Public Opinion Quarterly*, *79*(4), 839–880. https://doi.org/10.1093/poq/nfv039

Jefferson, A. J., Bhaskar, A. S., Hopkins, K. G., Fanelli, R., Avellaneda, P. M., & McMillan, S. K. (2017). Stormwater management network effectiveness and implications for urban watershed function: A critical review. *Hydrological Processes*, *31*(23), 4056–4080. https://doi.org/10.1002/hyp.11347

Johnson, D. P., Stanforth, A., Lulla, V., & Luber, G. (2012). Developing an applied extreme heat vulnerability index utilizing socioeconomic and environmental data. *Applied Geography*, *35*(1), 23–31. https://doi.org/10.1016/j.apgeog.2012.04.006

Jones, B., & Andrey, J. (2007). Vulnerability index construction: methodological choices and their influence on identifying vulnerable neighbourhoods. *International Journal of Emergency Management*, *4*(2), 269. https://doi.org/10.1504/IJEM.2007.013994

Kabisch, N., & Haase, D. (2014). Green justice or just green? Provision of urban green spaces in Berlin, Germany. *Landscape and Urban Planning*, *122*, 129–139. https://doi.org/10.1016/J.LANDURBPLAN.2013.11.016

Kappes, M. S., Papathoma-Köhle, M., & Keiler, M. (2012). Assessing physical vulnerability for multi-hazards using an indicator-based methodology. *Applied Geography*, *32*(2), 577–590. https://doi.org/10.1016/j.apgeog.2011.07.002

Karl, T. R., Meehl, G. A., Miller, C. D., Hassol, S. J., Waple, A. M., & Murray, W. L. (2008). *Weather and Climate Extremes in a Changing Climate Regions of Focus :* Retrieved from http://www.agci.org/dB/PDFs/Publications/07S1_USCCSP.pdf

Kenett, D. Y., & Portugali, J. (2012). Population movement under extreme events. *Proceedings of the National Academy of Sciences*, *109*(29), 11472–11473. https://doi.org/10.1073/pnas.1209306109

Khaleghi, M. R., Gholami, V., Ghodusi, J., & Hosseini, H. (2011). Efficiency of the geomorphologic instantaneous unit hydrograph method in flood hydrograph simulation. *Catena*, *87*(2), 163–171. https://doi.org/10.1016/j.catena.2011.04.005

Klinenberg, E. (1999). *Denaturalizing Disaster: A Social Autopsy of the 1995 Chicago Heat Wave*. *Violence in War and Peace: An Anthology*. https://doi.org/10.1023/A:1006995507723

Klosterman, R. E. (1997). Planning Support Systems: A New Perspective on Computer-Aided Planning. *Journal of Planning Education and Research*, *17*(1), 45–54. https://doi.org/10.1177/0739456X9701700105

Krause, P., Boyle, D. P., & Bäse, F. (2005). Advances in Geosciences Comparison of different efficiency criteria for hydrological model assessment. *Advances in Geosciences*, *5*(89), 89–97. https://doi.org/10.5194/adgeo-5-89-2005

Kuller, M., Bach, P. M., Ramirez-Lovering, D., & Deletic, A. (2017). Framing water sensitive urban design as part of the urban form: A critical review of tools for best planning practice. *Environmental Modelling and Software*, *96*, 265–282. https://doi.org/10.1016/j.envsoft.2017.07.003

Kunkel, K. E., Karl, T. R., Brooks, H., Kossin, J., Lawrimore, J. H., Arndt, D., … Wuebbles, D. (2013). Monitoring and understanding trends in extreme storms: State of knowledge. *Bulletin of the American Meteorological Society*, *94*(4), 499–514. Retrieved from http://www.scopus.com/inward/record.url?eid=2-s2.0-84876948034&partnerID=40&md5=77b8b10d5cac96728f48f8386b9e8eaf

La Rosa, D. (2014). Accessibility to greenspaces: GIS based indicators for sustainable planning in a dense urban context. *Ecological Indicators*, *42*, 122–134. https://doi.org/10.1016/j.ecolind.2013.11.011

Landry, S. M., & Chakraborty, J. (2009). Street trees and equity: Evaluating the spatial distribution of an urban amenity. *Environment and Planning A*, *41*(11), 2651–2670. https://doi.org/10.1068/a41236

Lee, A. C. K., & Maheswaran, R. (2011). The health benefits of urban green spaces: a review of the evidence. *Journal of Public Health*, *33*(2), 212–222. https://doi.org/10.1093/pubmed/fdq068

Lee, J. G., Selvakumar, A., Alvi, K., Riverson, J., Zhen, J. X., Shoemaker, L., & Lai, F. hsiung. (2012). A watershed-scale design optimization model for stormwater best management practices. *Environmental Modelling and Software*, *37*, 6–18. https://doi.org/10.1016/j.envsoft.2012.04.011

Lennon, M., Scott, M., & O'Neill, E. (2014). Urban Design and Adapting to Flood Risk: The Role of Green Infrastructure. *Journal of Urban Design*, *19*(5), 745–758. https://doi.org/10.1080/13574809.2014.944113

Li, X., & Gong, P. (2016). Urban growth models: progress and perspective. *Science Bulletin*, *61*(21), 1637–1650. https://doi.org/10.1007/s11434-016-1111-1

Lin, W., Yu, T., Chang, X., Wu, W., & Zhang, Y. (2015). Calculating cooling extents of green parks using remote sensing: Method and test. *Landscape and Urban Planning*, *134*, 66–75. https://doi.org/10.1016/j.landurbplan.2014.10.012

Liu, L., & Zhang, Y. (2011). Urban Heat Island Analysis Using the Landsat TM Data and ASTER Data: A Case Study in Hong Kong. *Remote Sensing*, *3*(7), 1535–1552. https://doi.org/10.3390/rs3071535

Liu, Y., Ahiablame, L. M., Bralts, V. F., & Engel, B. A. (2015). Enhancing a rainfall-runoff model to assess the impacts of BMPs and LID practices on storm runoff. *Journal of Environmental Management*, *147*, 12–23. https://doi.org/10.1016/j.jenvman.2014.09.005

Lloyd, C. (2006). *Local Models for Spatial Analysis*. https://doi.org/10.1201/9780203022825

Locke, D.H., M.Grove, J.W.T. Lu, A. Troy, J.P.M. O'Neil-Dunne, and B. Beck. (2010). Prioritizing preferable locations for increasing urban tree canopy in New York City. Cities and the Environment 3(1): article 4. http://escholarship.bc.edu/cate/vol3/iss1/4. 18 pp.

Locke, D., Grove, J. M., Galvin, M., O'Neil-Dunne, J. & Murphy, C. (2013). Applications of Urban Tree Canopy Assessment and Prioritization Tools: Supporting Collaborative Decision

Making to Achieve Urban Sustainability Goals, *Cities and the Environment (CATE): Vol. 6: Iss. 1*, Article 7. Available at: http://digitalcommons.lmu.edu/cate/vol6/iss1/7

Lovell, S. T., & Taylor, J. R. (2013). Supplying urban ecosystem services through multifunctional green infrastructure in the United States. *Landscape Ecology*, *28*(8), 1447–1463. https://doi.org/10.1007/s10980-013-9912-y

Maas, J., Verheij, R. A., Groenewegen, P. P., De Vries, S., & Spreeuwenberg, P. (2006). Green space, urbanity, and health: how strong is the relation? *Journal of epidemiology and community health, 60(7)*, 587-592.

Maidment, D. R. (2002). *Arc Hydro: GIS for water resources*. *Agriculture*. Redlands, California: ESRI Press.

Maidment, D. R. (1993). Developing a spatially distributed unit hydrograph by using GIS. *HydroGIS 93: Application of Geographic Information Systems in Hydrology and Water Resources*.

Maimaitiyiming, M., Ghulam, A., Tiyip, T., Pla, F., Latorre-Carmona, P., Halik, Ü., … Caetano, M. (2014). Effects of green space spatial pattern on land surface temperature: Implications for sustainable urban planning and climate change adaptation. *ISPRS Journal of Photogrammetry and Remote Sensing*, *89*, 59–66. https://doi.org/10.1016/J.ISPRSJPRS.2013.12.010

Malczewski, J., & Rinner, C. (2015). *Multicriteria Decision Analysis in Geographic Information Science*. *Analysis methods*. https://doi.org/10.1007/978-3-540-74757-4

Mallarach, J. M., & Marull, J. (2006). Impact assessment of ecological connectivity at the regional level: recent developments in the Barcelona Metropolitan Area. *Impact Assessment & Project Appraisal*, *24*(2), 127–137. Retrieved from http://search.ebscohost.com/login.aspx?direct=true&db=bth&AN=21583480&site=ehost-live

Malmqvist, P. A., Heinicke, G., Korrman, E., Stenstrom, T. A., & Svensson, G. (2006). *Strategic planning of sustainable urban water management*. Retrieved from https://www.iwapublishing.com/books/9781843391050/strategic-planning-sustainable-urban-water-management

Marney, Ronald A & W. (2012). Creation of a GIS Based Model for Determining the Suitability of Implementing Green Infrastructure: In The Town Of Berlin Maryland. Community and Regional Planning Program: Student Projects and Theses. Paper 14. http://digitalcommons.unl.edu/arch_crp_theses/14

Martin-Mikle, C. J., de Beurs, K. M., Julian, J. P., & Mayer, P. M. (2015). Identifying priority sites for low impact development (LID) in a mixed-use watershed. *Landscape and Urban Planning*, *140*, 29–41. https://doi.org/10.1016/J.LANDURBPLAN.2015.04.002

Matsuoka, R. H. (2010). Student performance and high school landscapes: Examining the links. *Landscape and Urban Planning*, *97*(4), 273–282. https://doi.org/10.1016/J.LANDURBPLAN.2010.06.011

Matthews, T. (2013). Institutional perspectives on operationalising climate adaptation through planning. *Planning Theory & Practice*, *14*(2), 198–210. https://doi.org/10.1080/14649357.2013.781208

Matthews, T., Lo, A. Y., & Byrne, J. A. (2015). Reconceptualizing green infrastructure for climate change adaptation: Barriers to adoption and drivers for uptake by spatial planners. *Landscape and Urban Planning*, *138*, 155–163. https://doi.org/10.1016/j.landurbplan.2015.02.010

Mazzorana, B., Simoni, S., Scherer, C., Gems, B., Fuchs, S., & Keiler, M. (2014). A physical approach on flood risk vulnerability of buildings. *Hydrology and Earth System Sciences*, *18*(9), 3817–3836. https://doi.org/10.5194/hess-18-3817-2014

McCarthy, J.J., Canziani, O.F., Leary, N.A., Dokken, D.J., White, K.S. (Eds.) (2001). Climate Change 2001: Impacts, Adaptation and Vulnerability. Cambridge University Press, Cambridge.

McCuen, R. H. (1979). Downstream effects of stormwater management basins. *Journal of the Hydraulics Division, ASCE*, *105*, 1343–1356.

Mccutcheon, S. C. (2003). Hydrologic Evaluation of the Curve Number Method for Forest Management in West Virginia Report Prepared for the West Virginia Division of Forestry, *30605*(706), 38.

McRae, B. H., Dickson, B. G., Keitt, T. H., & Shah, V. B. (2008). Using Circuit Theory to Model Connectivity in Ecology, Evolution, and Conservation. *Ecology*, *89*(10), 2712–2724. Retrieved from http://search.ebscohost.com/login.aspx?direct=true&db=a9h&AN=34964879&site=ehost-live

Meerow, S., & Newell, J. P. (2016a). Urban resilience for whom, what, when, where, and why? *Urban Geography*, *00*(00), 1–21. https://doi.org/10.1080/02723638.2016.1206395

Meerow, S., & Newell, J. P. (2017). Spatial planning for multifunctional green infrastructure: Growing resilience in Detroit. *Landscape and Urban Planning*, *159*, 62–75. https://doi.org/10.1016/j.landurbplan.2016.10.005

Meerow, S., Newell, J. P., & Stults, M. (2016b). Defining urban resilience: A review. *Landscape and Urban Planning*, *147*, 38–49. https://doi.org/10.1016/J.LANDURBPLAN.2015.11.011

Mees, H., & Driessen, P. P. J. (2011). Adaptation to climate change in urban areas: Climate-greening London, Rotterdam, and Toronto. *Climate Law*, *2*, 251–280.

Miles, B. C., (2014). Small-scale residential stormwater management in urbanized watersheds: A geoinformatics-driven ecohydrology modeling approach, Ph.D. Thesis, The University of North Carolina at Chapel Hill, https://cdr.lib.unc.edu/record/uuid:84f67003-6421-4b27-9a3a-39f367a1bc8c, 217 pp.

Miles, B., & Band, L. E. (2015). Green infrastructure stormwater management at the watershed scale: Urban variable source area and watershed capacitance. *Hydrological Processes*, *29*(9), 2268–2274. https://doi.org/10.1002/hyp.10448

Minsker, B., Baldwin, L., Crittenden, J., Kabbes, K., Karamouz, M., Lansey, K., … Williams, J. (2015). Progress and Recommendations for Advancing Performance-Based Sustainable and Resilient Infrastructure Design. *Journal of Water Resources Planning & Management*, *141*(12), 1–16. https://doi.org/10.1061/(ASCE)WR.1943-5452.0000521

Mirzaei, P. A. (2015). Recent challenges in modeling of urban heat island. *Sustainable Cities and Society*, *19*, 200–206. https://doi.org/10.1016/j.scs.2015.04.001

Mitchell, R. & Popham, F. (2008). Effect of exposure to natural environment on health inequalities: an observational population study. *Lancet 372*: 1655–60.

Montalto, F. A., Bartrand, T. A., Waldman, A. M., Travaline, K. A., Loomis, C. H., McAfee, C., … Boles, L. M. (2013). Decentralised green infrastructure: the importance of stakeholder behaviour in determining spatial and temporal outcomes. *Structure & Infrastructure Engineering: Maintenance, Management, Life-Cycle Design & Performance*, *9*(12), 1187–1205. https://doi.org/10.1080/15732479.2012.671834

Montalto, F., Behr, C., Alfredo, K., Wolf, M., Arye, M., & Walsh, M. (2007). Rapid assessment of the cost-effectiveness of low impact development for CSO control. *Landscape and Urban Planning*, *82*(3), 117–131. https://doi.org/http://dx.doi.org/10.1016/j.landurbplan.2007.02.004

Morris, N., (2003). OPENspace: The research center for inclusive access to outdoor environments.

Mueller, E. J., & Dooling, S. (2011). Sustainability and vulnerability: Integrating equity into plans for central city redevelopment. *Journal of Urbanism*, *4*(3), 201-222. doi:10.1080/17549175.2011.633346

Musa, S. I., Hashim, M., & Reba, M. N. M. (2017). A review of geospatial-based urban growth models and modelling initiatives. *Geocarto International*, *32*(8), 813–833. https://doi.org/10.1080/10106049.2016.1213891

Muzik, I. (1996a). Flood modelling with GIS-derived distributed unit hydrographs. *Hydrological Processes*, *10* (April), 1401–1409. https://doi.org/10.1002/(SICI)1099-1085(199610)10:10<1401::AID-HYP469>3.0.CO;2-3

Muzik, I. (1996b). GIS Derived Distributed Unit Hydrograph, a New Tool for Flood Modeling. *Water Resources*, *1*(235), 243–247. https://doi.org/10.4203/ccp.30.10.2

Myint, S. W., Wentz, E. A., Brazel, A. J., & Quattrochi, D. A. (2013). The impact of distinct anthropogenic and vegetation features on urban warming. *Landscape Ecology*, *28*(5), 959–978. https://doi.org/10.1007/s10980-013-9868-y

Mysiak, J., Giupponi, C., & Rosato, P. (2005). Towards the development of a decision support system for water resource management. *Environmental Modelling & Software*, *20*(2), 203–214. https://doi.org/10.1016/J.ENVSOFT.2003.12.019

Nagle, N. N., Buttenfield, B. P., Leyk, S., & Spielman, S. (2014). Dasymetric Modeling and Uncertainty. *Annals of the Association of American Geographers*, *104*(1), 80–95. https://doi.org/10.1080/00045608.2013.843439

National Land Cover Database 2011 (NLCD 2011). (2015, February 19). Product Data Downloads. Retrieved from: https://www.mrlc.gov/nlcd11_data.php

National Oceanic and Atmospheric Administration (NOAA) Digital Coast. (2018, March 22). Social Vulnerability Index 2010 (Census Tracts). Retrieved from: https://coast.noaa.gov/digitalcoast/data/sovi

Natural Resources Conservation Service (NRCS) - United States Department of Agriculture (USDA) Soil Conservation Service (SCS) (1986) Urban Hydrology for Small Watersheds. Technical Release No. 55 (TR-55). USDA-SCS, Washington DC.

Nicholls, S. (2001). Measuring the accessibility and equity of public parks: a case study using GIS. *Managing Leisure*, *6*(4), 201–219. https://doi.org/10.1080/13606710110084651

Nobre, A. D., Cuartas, L. A., Hodnett, M., Rennó, C. D., Rodrigues, G., Silveira, A., … Saleska, S. (2011). Height Above the Nearest Drainage – a hydrologically relevant new terrain model. *Journal of Hydrology*, *404*(1–2), 13–29. https://doi.org/10.1016/J.JHYDROL.2011.03.051

Nobre, A., Cuartas, L., Momo, M., Severo, D. L., Pinheiro, A., & Nobre, C. (2015). HAND contour: A new proxy predictor of inundation extent. *Hydrological Processes*, *30*.

Nordstrom, E. M., Ohman, K., & Eriksson, L. O. (2012). Approaches for aggregating preferences in participatory forest planning - an experimental study. *Open Forest Science Journal*, *5*, 23–32. https://doi.org/10.2174/1874398601205010023

Norton, B. A., Coutts, A. M., Livesley, S. J., Harris, R. J., Hunter, A. M., & Williams, N. S. G. (2015). Planning for cooler cities: A framework to prioritise green infrastructure to mitigate high temperatures in urban landscapes. *Landscape and Urban Planning*, *134*, 127–138. https://doi.org/10.1016/j.landurbplan.2014.10.018

National Research Council (NRC) (2008). Committee on Reducing Stormwater Discharge Contributions to Water Pollution, Water Science Technology Board 2008. *Urban Stormwater Management in the United States, National Academies Press*, 513p.

Openshaw, S., & Taylor, P. J. (1979). A million or so correlation coefficients: Three experiements on the modiable areal unit problem. *Statistical Methods in the Spatial Sciences*, 127–144. Retrieved from http://ci.nii.ac.jp/naid/10009667572/en/

Pakzad, P., Osmond, P., & Corkery, L. (2017). Developing Key Sustainability Indicators for Assessing Green Infrastructure Performance. *Procedia Engineering*, *180*, 146–156. https://doi.org/10.1016/j.proeng.2017.04.174

Park, J., Kim, J. H., Lee, D. K., Park, C. Y., & Jeong, S. G. (2017). The influence of small green space type and structure at the street level on urban heat island mitigation. *Urban Forestry and Urban Greening*, *21*, 203–212. https://doi.org/10.1016/j.ufug.2016.12.005

Pataki, D. E., Carreiro, M. M., Cherrier, J., Grulke, N. E., Jennings, V., Pincetl, S., Pouyat, R., Whitlow, T., & Zipperer, W. C. (2011). Coupling biogeochemical cycles in urban environments: ecosystem services, green solutions, and misconceptions. *Frontiers in Ecology and the Environment*, 9(1), 27-36.

Paudel, M., Nelson, E. J., & Scharffenberg, W. (2009). Comparison of Lumped and Quasi-Distributed Clark Runoff Models Using the SCS Curve Number Equation. *Journal of Hydrologic Engineering*, *14*(10), 1098–1106. https://doi.org/10.1061/(ASCE)HE.1943-5584.0000100

Pearsall, H., & Christman, Z. (2012). Tree-lined lanes or vacant lots? Evaluating non-stationarity between urban greenness and socio-economic conditions in Philadelphia, Pennsylvania, USA at multiple scales. *Applied Geography*, *35*(1–2), 257–264. https://doi.org/10.1016/j.apgeog.2012.07.006

Pennino, M. J., McDonald, R. I., & Jaffe, P. R. (2016). Watershed-scale impacts of stormwater green infrastructure on hydrology, nutrient fluxes, and combined sewer overflows in the mid-Atlantic region. *Science of the Total Environment*, 565, 1044–1053. https://doi.org/10.1016/j.scitotenv.2016.05.101

Perez-Pedini, C., Limbrunner, J. F., & Vogel, R. M. (2005). Optimal location of infiltration-based best management practices for storm water management. *Journal of Water Resources Planning & Management*, *131*(6), 441-448. doi:10.1061/(ASCE)0733-9496(2005)131:6(441)

Perkins, H. A., Heynen, N., & Wilson, J. (2004). Inequitable access to urban reforestation: The impact of urban political economy on housing tenure and urban forests. *Cities*, *21*(4), 291–299. https://doi.org/10.1016/j.cities.2004.04.002

Petrucci, G., Rioust, E., Deroubaix, J. F., & Tassin, B. (2013). Do stormwater source control policies deliver the right hydrologic outcomes? *Journal of Hydrology*, *485*, 188–200. https://doi.org/10.1016/j.jhydrol.2012.06.018

Pham, T.-T.-H., Apparicio, P., Séguin, A.-M., Landry, S., & Gagnon, M. (2012). Spatial distribution of vegetation in Montreal: An uneven distribution or environmental inequity? *Landscape and Urban Planning*, *107*(3), 214–224. https://doi.org/10.1016/J.LANDURBPLAN.2012.06.002

Philadelphia Water Department. (2009). *Green City Clean Waters. The Philadelphia Water Department.*

Philadelphia Water Department (PWD). (2018, March 22). Stormwater regulations. Retrieved from: https://www.pwdplanreview.org/manual/chapter-1/1.2-stormwater-regulations

Piemonti, A. D., Babbar-Sebens, M., & Jane Luzar, E. (2013). Optimizing conservation practices in watersheds: Do community preferences matter? *Water Resources Research*, *49*(10), 6425–6449. https://doi.org/10.1002/wrcr.20491

Pincetl, S. (2007). Accounting for environmental services in cities: the new frontier for sustainability. *Social and Environmental Accountability Journal*, 27(1), 3-8.

Pincetl, S., Chester, M., & Eisenman, D. (2016). Urban heat stress vulnerability in the U.S. Southwest: The role of sociotechnical systems. *Sustainability (Switzerland)*, *8*(9), 1–13. https://doi.org/10.3390/su8090842

Potts, A., Marengo, B., & Wible, D. (2015). The Real Cost of Green Infrastructure. *Weftec 2015*, *2015*(20), 4366–4378. https://doi.org/10.2175/193864715819555049

Price, R. K. (2000). Hydroinformatics and urban drainage: An agenda for the beginning of the 21st century. *Journal of Hydroinformatics*, *2*(2), 133.

Price, R., Vojinović, Z. (2011). *Urban Hydroinformatics: Data, Models and Decision Support for Integrated Urban Water Management*. London: IWA Publishing. https://doi.org/10.1016/j.envsoft.2011.03.010

Quinn, P., Beven, K., Chevallier, P., & Planchon, O. (1991). The prediction of hillslope flow paths for distributed hydrological modelling using digital terrain models. *Hydrological Processes*, *5*(1), 59–79. https://doi.org/10.1002/hyp.3360050106

Rai, A. (2018): Inferring Landscape Preferences from Social Media using Data Science Techniques (Doctoral dissertation).

Randhir, T. O., O'Connor, R., Penner, P. R., & Goodwin, D. W. (2001). A watershed-based land prioritization model for water supply protection. *Forest Ecology and Management, 143*(1-3), 47-56. doi:10.1016/S0378-1127(00)00504-1

Roy, A. H., Rhea, L. K., Mayer, A. L., Shuster, W. D., Beaulieu, J. J., Hopton, M. E., … St Amand, A. (2014). How much is enough? Minimal responses of water quality and stream biota to partial retrofit stormwater management in a suburban neighborhood. *PLoS ONE*, *9*(1), 1–14. https://doi.org/10.1371/journal.pone.0085011

Saha Ray, S. (2013). *Graph Theory with Algorithms and its Applications*. https://doi.org/10.1007/978-81-322-0750-4

Sample, D. J., Heaney, J. P., Wright, L. T., & Koustas, R. (2001). Geographic Information Systems, Decision Support Systems, and Urban Storm-Water Management. *Journal of Water Resources Planning and Management*, *127*(3), 155. https://doi.org/10.1061/(ASCE)0733-9496(2001)127:3(155)

Sampson, C. C., Bates, P. D., Neal, J. C., & Horritt, M. S. (2013). An automated routing methodology to enable direct rainfall in high resolution shallow water models. *Hydrological Processes*, *27*(3), 467–476. https://doi.org/10.1002/hyp.9515

Schmidtlein, M. C., Deutsch, R. C., Piegorsch, W. W., & Cutter, S. L. (2008). A sensitivity analysis of the social vulnerability index. *Risk Analysis*, *28*(4), 1099–1114. https://doi.org/10.1111/j.1539-6924.2008.01072.x

Schwarz, K., Fragkias, M., Boone, C. G., Zhou, W., McHale, M., Grove, J. M., … Cadenasso, M. L. (2015). Trees Grow on Money: Urban Tree Canopy Cover and Environmental Justice. *PLOS ONE*, *10*(4), 1–17. https://doi.org/10.1371/journal.pone.0122051

Sebti, A., Carvallo Aceves, M., Bennis, S., & Fuamba, M. (2016). Improving Nonlinear Optimization Algorithms for BMP Implementation in a Combined Sewer System. *Journal of Water Resources Planning and Management*, *142*(9), 04016030. https://doi.org/10.1061/(ASCE)WR.1943-5452.0000669

Sharma, A., Conry, P., Fernando, H. J. S., Hamlet, A. F., Hellmann, J. J., & Chen, F. (2016). Environmental Research Letters Green and cool roofs to mitigate urban heat island effects in the Chicago metropolitan area: evaluation with a regional climate model Green and cool roofs to mitigate urban heat island effects in the Chicago metropolitan are. *Environ. Res. Lett*, *11*(6), 1–16. https://doi.org/10.1088/1748-9326/11/6/064004

Shen, Z., Chen, L., & Xu, L. (2013). A Topography Analysis Incorporated Optimization Method for the Selection and Placement of Best Management Practices. *PLoS ONE*, *8*(1), 1–12. https://doi.org/10.1371/journal.pone.0054520

Shirk, A.J., and B.H. McRae. (2013). Gnarly Landscape Utilities: Core Mapper User Guide. The Nature Conservancy, Fort Collins, CO. Available at: http://www.circuitscape.org/gnarly-landscape-utilities.

Shoemaker, L., Riverson, J. J., Alvi, K., Zhen, J. X., Paul, S., & Rafi, T. (2009). *SUSTAIN - A Framework for Placement of Best Management Practices in Urban Watersheds to Protect Water Quality*. *Environmental Protection*. Retrieved from http://www.epa.gov/nrmrl/wswrd/wq/models/sustain/

Shuster, W., & Rhea, L. (2013). Catchment-scale hydrologic implications of parcel-level stormwater management (Ohio USA). *Journal of Hydrology*, *485*, 177–187. Retrieved from http://search.ebscohost.com/login.aspx?direct=true&db=a9h&AN=86396272&site=ehost-live

Singh, A., Minsker, B. S., & Valocchi, A. J. (2008). An interactive multi-objective optimization framework for groundwater inverse modeling. *Advances in Water Resources*, *31*(10), 1269–1283. https://doi.org/10.1016/J.ADVWATRES.2008.05.005

Sister, C., Wolch, J., Wilson, J., (2009). Got green? addressing environmental justice in park provision. *GeoJournal* 75 (3), 229–248.

Sivarajah, S., Smith, S. M., & Thomas, S. C. (2018). Tree cover and species composition effects on academic performance of primary school students. *PLoS ONE*, *13*(2), 1–11. https://doi.org/10.1371/journal.pone.0193254

Smith, B. K., Smith, J. A., Baeck, M. L., Villarini, G., & Wright, D. B. (2013). Spectrum of storm event hydrologic response in urban watersheds. *Water Resources Research*, *49*(5), 2649–2663. https://doi.org/10.1002/wrcr.20223

Smith, M. L. (2010). *Heterogeneity in the urban landscape: Impacts on hydrologic processes and nitrogen pollution*. Chapel Hill, NC: University of North Carolina. Retrieved from https://pqdtopen.proquest.com/doc/741140787.html?FMT=ABS

Strzepek, K., Yohe, G., Neumann, J., & Boehlert, B. (2010). Characterizing changes in drought risk for the United States from climate change. *Environmental Research Letters*, *5*(4). Retrieved from http://www.scopus.com/inward/record.url?eid=2-s2.0-78751558365&partnerID=40&md5=e2125e68a53c8d2e6e1af9543da49f3b

Su, M. D., Lin, M. C., Hsieh, H. I., Tsai, B. W., & Lin, C. H. (2010). Multi-layer multi-class dasymetric mapping to estimate population distribution. *Science of the Total Environment*, *408*(20), 4807–4816. https://doi.org/10.1016/j.scitotenv.2010.06.032

Susilo, K., Steets, B., Leisenring, M., & Strecker, E. (2006). *Structural BMP prioritization methodology: A guidance manual for strategic storm water quality project planning*. Los Angeles, California: GeoSyntec Consultants.

Sussams, L. W., Sheate, W. R., & Eales, R. P. (2015). Green infrastructure as a climate change adaptation policy intervention: Muddying the waters or clearing a path to a more secure future? *Journal of Environmental Management*, *147*, 184–193. https://doi.org/10.1016/j.jenvman.2014.09.003

Syrbe, R. U., & Walz, U. (2012). Spatial indicators for the assessment of ecosystem services: Providing, benefiting and connecting areas and landscape metrics. *Ecological Indicators*, *21*, 80–88. https://doi.org/10.1016/j.ecolind.2012.02.013

Takano, T., Nakamura, K., & Watanabe, M., (2002). Urban residential environments and senior citizens' longevity in megacity areas: The importance of walkable green spaces. *Journal of Epidemiology and Community Health*, *56(12)*, 913-918.

Tannier, C., Bourgeois, M., Houot, H., & Foltête, J.-C. (2016). Impact of urban developments on the functional connectivity of forested habitats: A joint contribution of advanced urban models and landscape graphs. *Land Use Policy*, *52*, 76–91.

Tannier, C., Foltête, J.-C., & Girardet, X. (2012). Assessing the capacity of different urban forms to preserve the connectivity of ecological habitats. *Landscape and Urban Planning*, *105*(1–2), 128–139. https://doi.org/10.1016/j.landurbplan.2011.12.008

Tate, E. (2012). Social vulnerability indices: A comparative assessment using uncertainty and sensitivity analysis. *Natural Hazards*, *63*(2), 325–347. https://doi.org/10.1007/s11069-012-0152-2

Tate, E. (2013). Uncertainty Analysis for a Social Vulnerability Index. *Annals of the Association of American Geographers*, *103*(3), 526–543. https://doi.org/10.1080/00045608.2012.700616

te Brömmelstroet, M., & Bertolini, L. (2008). Developing land use and transport PSS: Meaningful information through a dialogue between modelers and planners. *Transport Policy*, *15*(4), 251–259. https://doi.org/10.1016/j.tranpol.2008.06.001

Tetra Tech. (2017). Dead Run 5 Stormwater Management Model (SWMM). Received December 2017.

Thompson, C.W., Roe, J., Aspinall, P., Mitchell, R., Clow, A., & Miller, D., (2012). More green space is linked to less stress in deprived communities: Evidence from salivary cortisol patterns. *Landscape and Urban Planning 105*, 221-229.

Thywissen, K. (2006). Components of Risk. A Comparative Glossary. *SOURCE No. 2/2006*. UNU-EHS, Bonn.

Tippett, J. (2005). The value of combining a systems view of sustainability with a participatory protocol for ecologically informed design in river basins. *Environmental Modelling & Software*, *20*(2), 119–139. https://doi.org/10.1016/J.ENVSOFT.2003.12.016

Tobler, W. R. (1970). A Computer Movie Simulating Urban Growth in the Detroit Region. *Economic Geography*, *46*(sup1), 234. https://doi.org/10.2307/143141

Tran, L. T., O'Neill, R. V., & Smith, E. R. (2010). Spatial pattern of environmental vulnerability in the mid-Atlantic region, USA. *Applied Geography*, *30*(2), 191-202. doi:10.1016/j.apgeog.2009.05.003

Travis, Q. B., Asce, M., Mays, L. W., & Asce, F. (2008). Optimizing Retention Basin Networks. *Journal of Water Resources Planning and Management*, *134*(5), 432–439. https://doi.org/10.1061/ASCÊ0733-9496ˆ2008ˆ134:5ˆ432ˆ

Troxel, B., Piana, M., Ashton, M. S., & Murphy-Dunning, C. (2013). Relationships between bole and crown size for young urban trees in the northeastern USA. *Urban Forestry and Urban Greening*, *12*(2), 144–153. https://doi.org/10.1016/j.ufug.2013.02.006

Turner II, B. L., Kasperson, R. E., Matson, P. A., McCarthy, J. J., Corell, R. W., Christensen, L., . . . Schiller, A. (2003a). A framework for vulnerability analysis in sustainability science. *Proceedings of the National Academy of Sciences of the United States of America, 100*(14), 8074.

Turner II, B. L., Mastson, P. A., McCarthy, J. J., Corell, R. W., Christensen, L., Eckley, N., . . . Tyler, N. (2003b). Illustrating the coupled human—environment system for vulnerability analysis: Three case studies. *Proceedings of the National Academy of Sciences of the United States of America, 100*(14), 8080.

Tzoulas, K., Korpela, K., Venn, S., Yli-Pelkonen, V., Kazmierczak, A., Niemela, J., & James, P. (2007). Promoting ecosystem and human health in urban areas using Green Infrastructure: A literature review. *Landscape and Urban Planning*, *81*(3), 167–178. https://doi.org/10.1016/j.landurbplan.2007.02.001

United States Army Corps of Engineers. (2018, March 22). US Army Corps of Engineers Social Vulnerability Index-Explorer. Retrieved from: https://www.iwr.usace.army.mil/Missions/Social-Vulnerability-Index-Explorer/

United States Census Bureau (2009). *A Compass for Understanding and Using American Community Survey Data*. *Compass*.

United States Census Bureau; American Community Survey (ACS) (2012). American Community Survey 5-Year Estimates. Retrieved from https://www.census.gov/programs-surveys/acs/

United States Census Bureau; U.S. Census Summary File 1 (2012). *2010 U.S. Census Summary File 1: Census of Population and Housing*. Retrieved from https://www.census.gov/prod/cen2010/doc/sf1.pdf

United States Environmental Protection Agency (EPA). (2014). Addressing green infrastructure design challenges in the Pittsburgh region. Washington, DC.

United States Environmental Protection Agency (EPA). (2018, March 22). System for Urban Stormwater Treatment and Analysis IntegratioN (SUSTAIN). Retrieved from: https://www.epa.gov/water-research/system-urban-stormwater-treatment-and-analysis-integration-sustain

United States Environmental Protection Agency (EPA). (2018, March 22). Soil and Water Assessment Tool (SWAT) model. Retrieved from: https://swat.tamu.edu/

United States Environmental Protection Agency (EPA). (2018, March 22). EPA National Stormwater Calculator (SWC). Retrieved from: https://www.epa.gov/water-research/national-stormwater-calculator

United States Environmental Protection Agency (EPA). (2018, April 26). Green Infrastructure. Retrieved from http://www.epa.gov/green-infrastructure

Vaz Monteiro, M., Doick, K. J., Handley, P., & Peace, A. (2016). The impact of greenspace size on the extent of local nocturnal air temperature cooling in London. *Urban Forestry & Urban Greening*, *16*, 160–169. https://doi.org/10.1016/J.UFUG.2016.02.008

Viavattene, C., Scholes, L., Revitt, D. M., & Ellis, J. B. (2008). A GIS based decision support system for the implementation of Stormwater Best Management Practices. In *11th International Conference on Urban Drainage, Edinburgh, Scotland, UK* (pp. 1–9).

Vonk, G., Geertman, S., & Schot, P. (2005). Bottlenecks Blocking Widespread Usage of Planning Support Systems. *Environment and Planning A: Economy and Space*, *37*(5), 909–924. https://doi.org/10.1068/a3712

Walsh, C. J., Fletcher, T. D., & Ladson, A. R. (2005). Stream restoration in urban catchments through redesigning stormwater systems: looking to the catchment to save the stream. *Journal of the North American Benthological Society, 24(3),* 690-705.

Wang, G.-T., & Chen, S. (1996). A linear spatially distributed model for a surface rainfall-runoff system. *Journal of Hydrology*, *185*(1–4), 183–198. https://doi.org/10.1016/0022-1694(95)03001-8

Wang, Y., & Akbari, H. (2016). The effects of street tree planting on Urban Heat Island mitigation in Montreal. *Sustainable Cities and Society*, *27*, 122–128. https://doi.org/10.1016/j.scs.2016.04.013

Water Environment Research Foundation (WERF). (2017, August 8). Stormwater BMP Interactive Model. Retrieved from: https://www.werf.org/liveablecommunities/toolbox/model.htm

Weber, T., Sloan, A., & Wolf, J. (2006). Maryland's Green Infrastructure Assessment: Development of a comprehensive approach to land conservation. *Landscape and Urban Planning*, *77*(1–2), 94–110. https://doi.org/10.1016/j.landurbplan.2005.02.002

Wen, M., Zhang, X., Harris, C. D., Holt, J. B., & Croft, J. B. (2013). Spatial Disparities in the Distribution of Parks and Green Spaces in the USA. *Annals of Behavioral Medicine: A Publication of the Society of Behavioral Medicine*, 45(Suppl 1), 18–27. http://doi.org/10.1007/s12160-012-9426-x

Wendel, H. E. W., Downs, J. A., & Mihelcic, J. R. (2011). Assessing equitable access to urban green space: The role of engineered water infrastructure. *Environmental Science and Technology*, *45*(16), 6728–6734. https://doi.org/10.1021/es103949f

Williams, L. R. R., & Kapustka, L. A. (2000). Ecosystem vulnerability: A complex interface with technical components. *Environmental Toxicology and Chemistry*, *19*(4 II), 1055–1058. Retrieved from http://www.scopus.com/inward/record.url?eid=2-s2.0-0034063984&partnerID=40&md5=5e9f397c2163b67274647c084e35c8c2

Wolch, J. R., Byrne, J., & Newell, J. P. (2014). Urban green space, public health, and environmental justice: The challenge of making cities "just green enough." *Landscape and Urban Planning*, *125*, 234–244. https://doi.org/10.1016/j.landurbplan.2014.01.017

Wong, D. (2009). The SAGE Handbook of Spatial Analysis. London: SAGE Publications, Ltd. https://doi.org/10.4135/9780857020130

Washington State Department of Transportation (WSDOT). (2014). TR-55 Curve number tables: Appendix 4B; Washigton Department of Transport (WSDOT) Highway runoff manual (31-16.04).

Wu, C. Da, McNeely, E., Cedeño-Laurent, J. G., Pan, W. C., Adamkiewicz, G., Dominici, F., … Spengler, J. D. (2014). Linking student performance in Massachusetts elementary schools with the "greenness" of school surroundings using remote sensing. *PLoS ONE*, *9*(10), 1–9. https://doi.org/10.1371/journal.pone.0108548

Xiao, Q., & McPherson, E. G. (2002). Rainfall interception by Santa Monica ' s municipal. *Urban Ecosystems*, *6*, 291–302. https://doi.org/10.1023/B:UECO.0000004828.05143.67

Xu, D., & Guo, X. (2014). Compare NDVI extracted from Landsat 8 imagery with that from Landsat 7 imagery. *American Journal of Remote Sensing*, *2*(2), 10-14.

Yoon, D. K. (2012). Assessment of social vulnerability to natural disasters: A comparative study. *Natural Hazards*, *63*(2), 823–843. https://doi.org/10.1007/s11069-012-0189-2

Yu, D., Xun, B., Shi, P., Shao, H., & Liu, Y. (2012). Ecological restoration planning based on connectivity in an urban area. *Ecological Engineering*, *46*, 24–33. https://doi.org/10.1016/j.ecoleng.2012.04.033

Zardo, L., Geneletti, D., Pérez-Soba, M., & Van Eupen, M. (2017). Estimating the cooling capacity of green infrastructures to support urban planning. *Ecosystem Services*, *26*, 225–235. https://doi.org/10.1016/j.ecoser.2017.06.016

Zebardast, E. (2013). Constructing a social vulnerability index to earthquake hazards using a hybrid factor analysis and analytic network process (F'ANP) model. *Natural Hazards*, *65*(3), 1331–1359. https://doi.org/10.1007/s11069-012-0412-1

Zellner, M., Massey, D., Minor, E., & Gonzalez-Meler, M. (2016). Exploring the effects of green infrastructure placement on neighborhood-level flooding via spatially explicit simulations. *Computers, Environment and Urban Systems*, *59*, 116–128. https://doi.org/10.1016/j.compenvurbsys.2016.04.008

Zhang, X., Zhong, T., Feng, X., & Wang, K. (2009). Estimation of the relationship between vegetation patches and urban land surface temperature with remote sensing. *International Journal of Remote Sensing*, *30*(8), 2105–2118. https://doi.org/10.1080/01431160802549252

Zhang, Y., Murray, A. T., & Turner, B. L. (2017). Optimizing green space locations to reduce daytime and nighttime urban heat island effects in Phoenix, Arizona. *Landscape and Urban Planning*, *165*(May), 162–171. https://doi.org/10.1016/j.landurbplan.2017.04.009

Zhao, P., Xia, B., Hu, Y., & Yang, Y. (2013). A spatial multi-criteria planning scheme for evaluating riparian buffer restoration priorities. *Ecological Engineering*, *54*, 155–164. https://doi.org/10.1016/j.ecoleng.2013.01.037

Zheng, B., Myint, S. W., & Fan, C. (2014). Spatial configuration of anthropogenic land cover impacts on urban warming. *Landscape and Urban Planning*, *130*(1), 104–111. https://doi.org/10.1016/j.landurbplan.2014.07.001

Zogg, J., & Deitsch, K. (2013). *The flash flood potential index at WFO des Moines, Iowa*. National Weather Service. Retrieved from http://www.crh.noaa.gov/Image/dmx/hydro/FFPI/FFPI_WriteUp.pdf

APPENDIX A. SUPPLEMENTAL PSEUDOCODES AND METHODOLOGIES

A.1 Pseudocode of method used to calculate ecological indicators presented in Table B.2.

- Continuous patches of tree canopy

Step-1: Initiate an empty grid (G_{tc}) with the same raster resolution and spatial extent as input data.
Step-2: **for** t_c := 0% **to** 100% **step** Δ *tree canopy* **do**
    Create binary raster by identifying grid cells with tree canopy < t_c (i.e., grid cell with tree canopy < t_c = 1).
    Label all continuous connected grid cells (8-grid neighbors) as individual patches (p).
    Calculate area of each patch (A_p) and identify largest patch (A_{max}).
    Initiate an empty grid (g) with the same raster resolution and spatial extent as input data.
    for *each* A_p **do**
        Calculate ecologic susceptibility potential of patch p and add to g:
        $g = g + \left(1 + \frac{A_p}{A_{max}}\right) * \left(1 - \frac{t_c}{100}\right)$
    end
    Add to cumulative ecologic susceptibility potential: $G_{tc} = G_{tc}$ + g
Step-3: Scale G_{tc} to the interval [0,1].

- Continuous patches of impervious surfaces

Step-1: Initiate an empty grid (G_{is}) with the same raster resolution and spatial extent as input data.
Step-2: **for** i_s := 100% **to** 0% **step** Δ *impervious surfaces* **do**
    Create binary raster by identifying grid cells with impervious surfaces < i_s (i.e., grid cell with impervious surfaces < i_s = 1).
    Label all continuous connected grid cells (8-grid neighbors) as individual patches (p).
    Calculate area of each patch (A_p) and identify largest patch (A_{max}).
    Initiate an empty grid (g) with the same raster resolution and spatial extent as input data.
    for *each* A_p **do**
        Calculate ecologic susceptibility potential of patch p and add to g:
        $g = g + \left(1 + \frac{A_p}{A_{max}}\right) * \left(\frac{i_s}{100}\right)$
    end
    Add to cumulative ecologic susceptibility potential: $G_{is} = G_{is}$ + g
Step-3: Scale G_{is} to the interval [0,1].

- Identification of ecologic cores and landscape resistance to ecologic connectivity.

Step-1:	Define habitat integrity and landscape resistance values look-up table for input land cover/use data (Table B.2).
Step-2:	**for** *each input land cover/land use raster* **do** Create a habitat integrity value (H_v) and a landscape resistance raster (H_r) **end**
Step-3:	Calculate an average habitat value raster ($\overline{H_v}$) and an average landscape resistance raster ($\overline{H_r}$).
Step-4:	Apply a 2-D circular averaging filter (i.e., radius = 200 meters) to raster $\overline{H_v}$.
Step-5:	Create a binary raster that represent the location of ecologic cores (E_c) by identifying grid cells with $\overline{H_v} \geq 0.6$.
Step-6:	Label all continuous connected grid cells (8-grid neighbors) as individual ecologic cores. Calculate area of each ecologic core (A_{ec}) and identify largest core ($A_{ec_{max}}$). Eliminate ecologic cores with $A_{ec} < 0.1$ km^2
Step-7:	Computes the Euclidean distance transform (D_c) of the binary raster E_c (i.e., shortest Euclidean distance between a grid cell and a nonzero grid cell [ecologic cores])
Step-8:	Calculate landscape connectivity resistance (Lr) as: $D_c*(1+\overline{H_r})$
Step-9:	Scale Lr to the interval [0,1].

A.2 Cross-K function

The K-function is a widely used technique used to explore the global spatial clustering patterns of point data. Mathematically, it can be defined as:

$$K(r) = \frac{1}{\lambda}\frac{\sum_{i=1}^{n}\sum_{j=1}^{n} I(d_{i,j} \leq r)}{n}$$

where r is the search radius, $d_{i,j}$ is the Euclidean distance from between i and j, n is the total number of data points and λ is the average density of points. I takes the value of 1 if the $d_{i,j}$ is less than or equal to the search radius, otherwise it takes the value of 0. This function essentially measures the tendency of points to be close to each other as defined by the search radius distance. A version of this function is the cross-K function and it is used when two different sets of data points are considered. Finally, the cross-L function is the standardized cross-K function calculated as:

$$L(r) = \sqrt{\frac{K(r)}{\pi}} - r$$

Lastly, the application of the cross L-function often includes the performance of a Monte Carlo simulation to determine the statistical significance of the results and create a significance envelope.

A.3 Pseudocode of method used to calculate geo-preference scores (Section 4.2.3).

- Urban heat island (UHI) mitigation (g_1) and UHI mitigation in vulnerable areas (g_2).

Step-1: Initiate g_1 and g_2 as empty arrays with size N x 1.
Step-2: **for** *each* GSI_i **do**
    Calculate $Area_i$ (spatial arrangement of grid cells).
    Calculate eccentricity of $Area_i$ (E_i).
    Calculate mean land surface temperature (LST) of grid cells in $Area_i$ (T_i).
    Create a 90-meter buffer around $Area_i$.
    Calculate mean land surface temperature (LST) of grid cells only in buffer (TB_i).
    Difference between LST of $Area_i$ and buffer area: $UHI_i = T_i - TB_i$.
    if $UHI_i < 0$ **then** $UHI_i = 0$ **end**
    Calculate percentage of grid cells ($UHIVUL_i$) in buffered $Area_i$ (i.e., buffer & $Area_i$) with moderate to very high social susceptibility and UHI hazard exposure category.
end
Step-3: Scale arrays *Area*, *T*, [*E*+1] and [*UHI* +1] to the interval [0.01,1] (i.e., *sArea*, *sT*, *s*E and *sUHI*, respectively).
Step-4: Scale array *UHIVUL* to the interval [0,1] (*sUHIVUL*).
Step-5: **for** *each* $Area_i$ **do**
    $g_{i,1} = (sArea_i + sT_i + sE_i + sUHI_i) / 4$
    $g_{i,2} = g_{i,1} * sUHIVUL_i$
    Round $g_{i,1}$ and $g_{i,2}$ to nearest integer.
end

- Flash flooding mitigation in vulnerable areas (g_3)

Step-1: Initiate g_3 as empty array with size N x 1.
Step-2: Create an empty grid (F) with the same grid resolution and spatial extent as input data.
Step-3: Convert F to a binary grid in which grid cells with moderate to very high social susceptibility and flash flooding hazard exposure category are assigned a value of 1.

Step-4: **for** *each* GSI_i **do**
    Using the MDF method, identify grid cells down slope of GSI_i ($cells\_id_i$).
    Initialize GSI_i total potential runoff reduction in vulnerable areas: $Total\_BEN_i = 0$.
    for *each grid cell (c) in* $cells\_id_i$ **do**
        Calculate the Euclidean distance of grid cell c to nearest GSI_i grid cell ($dist_{i,c}$).
        if $dist_{i,c} <$ *distance threshold* and $F[c] = 1$ **then**
            Calculate the potential reduction in flow accumulation in c caused by GSI_i ($BEN_{i,c}$)
            $Total\_BEN_i = Total\_BEN_i + BEN_{i,c}$
        end
    end
    Calculate geo-preference score of GSI_i
    $g_{i,3} = Total\_BEN_i * \left[\frac{\mathbf{sum}(F[cells\_id_i])}{\mathbf{sum}(F)} + 1\right]$
end
Step-3: Round $g_{i,3}$ to nearest integers.

- Human health (g_4), ecological benefits (g_5) and policy and planning criteria (g_6)

Step-1: Initiate g_4, g_5 and g_6 as empty arrays with size N x 1.
Step-2: Calculate need for ecological restoration/protection (*ECO*) and social susceptibility (*SOSI*) using data and methods described in Chapters 2 & 3.
Step-3: Create a binary grid (*bSOSI*) in which grid cells with high to very high social susceptibility are assigned a value of 1.
Step-4: Create a binary grid (*ECOW*) that identifies (grid cell = 1) grid cells upslope of water bodies with moderate to very high susceptibility.
Step-5: Create a binary grid (*V*) that identifies vacant lots (grid cells = 1).
Step-6: Create an empty grid (*LUSE*) and assign grid cell values associated with the normalized preference given to different land uses and zoning regulations (see section 4.2.3.2).
Step-7: Create circular buffers around schools, hospitals, community spaces, parks, and green open spaces.
Initialize an empty grid (*HH*) with the same grid resolution and spatial extent as input data.
for *each location(L)* **do**
Create four different binary grids ($h_{L,r}$) use to represent buffers of radius (r): 0.25, 0.50, 0.75 and 1 mile.
$HH = HH + h_{L,r}**(1.25 - r)$
end
Step-8: Scale *HH* to the interval [0,1]
Step-9: **for** *each* GSI_i **do**
Create a 90-meter buffer (b) around $Area_i$ (spatial arrangement of grid cells).
$g_{i,4} = g_{i,4}$***sum(***$HH[b]$**)*** $\left[\frac{\mathbf{sum}(bSOSI[b])}{\mathbf{sum}(b)} + 1\right]$
$g_{i,5} =$ **mean(***$ECO[b]$**)** $+ ECOW[Area_i]$
$g_{i,6} =$ **sum(***$LUSE\ [b]$**)** $+ V[Area_i]$
end

Step-10: Scale arrays $g_{i,4}$, $g_{i,5}$, and $g_{i,6}$ to the interval [0.01,1]

A.4 Illustrative example of using a directed graph to represent the hydrologic connectivity of GSI.

Consider an example where there are three potential sites for GSI [A]. As presented in Section 4.3., the use of a directed graph to represent hydrologic connectivity of GSI assumes that each GSI site is a node in the graph and the edges between nodes represent the reduction in stormwater runoff volume to downslope GSI by implementing GSI upslope. For example, as illustrated in panel B, because GSI_2 is located downslope of GSI_1, implementation of GSI_1 reduces the total upslope drainage area of GSI_2 by a total equal to the upslope drainage area of GSI_1. In the directed graph network, the node of GSI_1 would be connected to the node of GSI_2 and the value of the edge between them would be equal to the upslope drainage area of GSI_1 [panel C]. Note,

however, that the opposite is not true, as implementation of GSI_2 would not reduce receiving runoff to GSI_1.

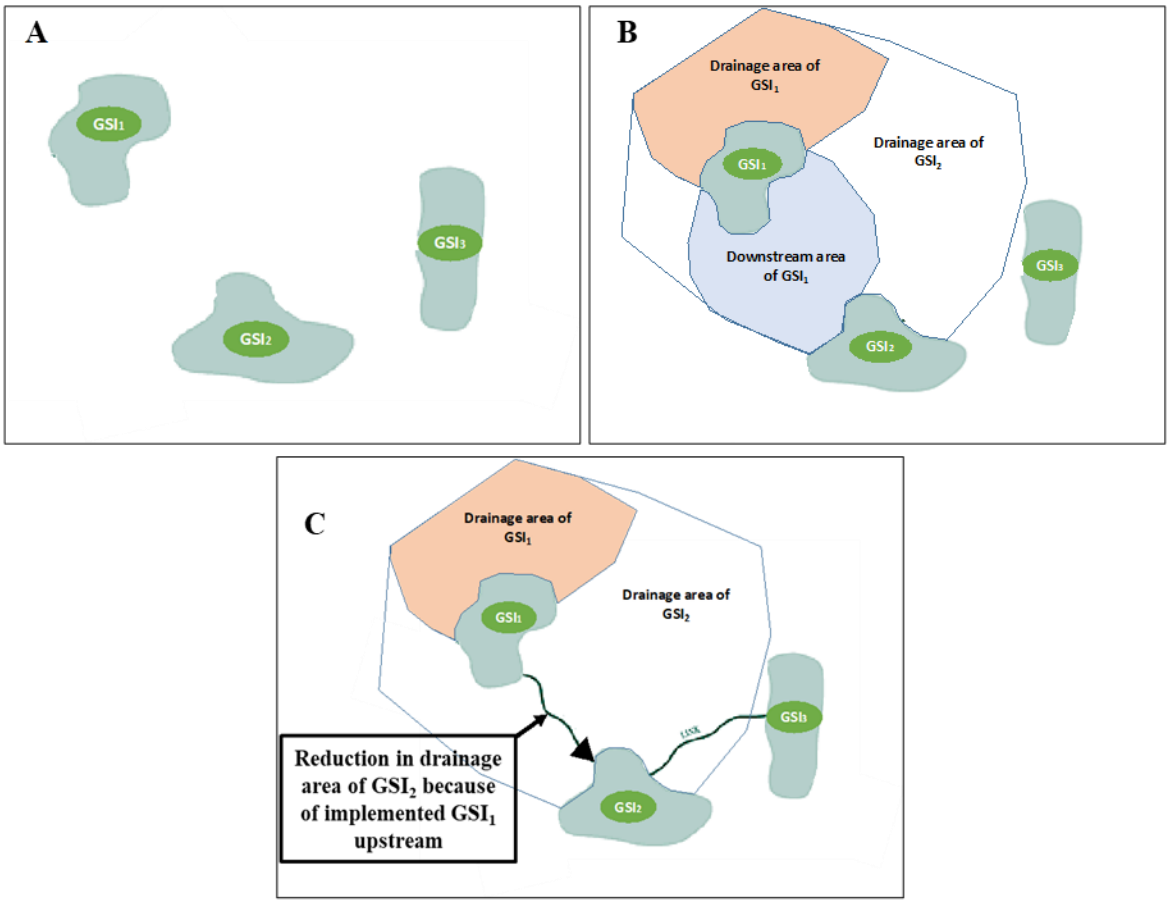

Figure A.1 Illustrative example of using a directed graph to represent the hydrologic connectivity of three potential GSI.

APPENDIX B. ADDITIONAL RESULTS AND SUPPLEMENTAL DATA

Table B.1 Collected data and sources for the quantification of socio-ecologic vulnerability.

Data layers	Data sources
Buildings footprints	OpenDataPhilly (https://www.opendataphilly.org/) Chicago Data Portal (https://data.cityofchicago.org/) Dallas OpenData (https://www.dallasopendata.com/) Baltimore Open Data (https://data.baltimorecity.gov/) USGS National Map Viewer (https://viewer.nationalmap.gov/advanced-viewer/) National Hydrography Dataset Plus (NHDPlus) (http://www.horizon-systems.com/nhdplus/NHDPlusV2_data.php) NRCS Soil Data (SSURGO) (https://websoilsurvey.sc.egov.usda.gov/App/HomePage.htm) EarthExplorer (https://earthexplorer.usgs.gov/) NOAA Atlas 14 (https://hdsc.nws.noaa.gov/hdsc/pfds/pfds_map_cont.html) LANDFIRE Program (https://www.landfire.gov/) FEMA Flood Map Service (https://msc.fema.gov/portal) US Census Bureau (https://www.census.gov/) EPA Impaired Waters and TMDLs (https://www.epa.gov/tmdl/impaired-waters-and-tmdls-resources-tools-and-databases)
Construction year of buildings	
Total buildings floors	
Buildings type	
Census boundaries (Tracts / Census Block Groups / Census Blocks)	
Community centers / Senior centers	
Hospitals	
Digital Elevation Model (DEM)	
Ecologic resistance / Habitat value	
Existing vegetation cover (EVC) Landfire	
Percent of immperviousness	
LANDSAT 8	
Land Use	
National Land Cover Database (NLCD)	
NOAA/FEMA flood maps	
Nursing Homes (0.5 mile)	
Parks (& open spaces)	
Schools	
NHDPlus Data	
Topographic slope	
Soils	
ASC / SF1 Data	
Street center lines	
Percent of tree canopy	
Vacant parcels	
Water & Streams	
Watersheds	
Zoning	
City Limits	

Table B.2 Habitat integrity and landscape resistance values used to identify ecological cores and calculate landscape connectivity. Refer to McRae et al., 2008 and Shirk & McRae, 2013 for more details about selected values and methods.

Class Description	Habitat Value	Resistance	Class ID	Source
Open Water	1	0	11	USGS NLCD, 2011
Developed, Open Space	0.48	0.52	21	
Developed, Low Intensity	0.36	0.64	22	
Developed, Medium Intensity	0.24	0.76	23	
Developed, High Intensity	0.15	0.85	24	
Barren Land	0.76	0.24	31	
Deciduous Forest	0.93	0.07	41	
Evergreen Forest	0.93	0.07	42	
Mixed Forest	0.93	0.07	43	
Shrub/Scrub	0.95	0.05	52	
Herbaceuous	0.83	0.17	71	
Hay/Pasture	0.44	0.56	81	
Cultivated Crops	0.32	0.68	82	
Woody Wetlands	0.89	0.11	90	
Emergent Herbaceuous Wetlands	0.89	0.11	95	
Roads	0	1	1	
Open Water	1	0	11	USGS LANDFIRE EVC, 2010
Developed-Upland Deciduous Forest	0.48	0.52	13	
Developed-Upland Evergreen Forest	0.48	0.52	14	
Developed-Upland Mixed Forest	0.48	0.52	15	
Developed-Upland Herbaceous	0.48	0.52	16	
Developed-Upland Shrubland	0.48	0.52	17	
Developed - Low Intensity	0.36	0.64	22	
Developed - Medium Intensity	0.24	0.76	23	
Developed - High Intensity	0.15	0.85	24	
Developed-Roads	0	1	25	
Barren	0.76	0.24	31	
Tree Cover >= 20 and < 30%	0.93	0.07	102	
Tree Cover >= 30 and < 40%	0.93	0.07	103	
Tree Cover >= 40 and < 50%	0.93	0.07	104	
Tree Cover >= 50 and < 60%	0.93	0.07	105	
Tree Cover >= 60 and < 70%	0.93	0.07	106	
Tree Cover >= 70 and < 80%	0.93	0.07	107	
Tree Cover >= 80 and < 90%	0.93	0.07	108	
Tree Cover >= 90 and <= 100%	0.93	0.07	109	
Shrub Cover >= 20 and < 30%	0.95	0.05	112	
Shrub Cover >= 30 and < 40%	0.95	0.05	113	
Shrub Cover >= 40 and < 50%	0.95	0.05	114	
Shrub Cover >= 50 and < 60%	0.95	0.05	115	
Shrub Cover >= 60 and < 70%	0.95	0.05	116	
Shrub Cover >= 70 and < 80%	0.95	0.05	117	
Shrub Cover >= 80 and < 90%	0.95	0.05	118	
Shrub Cover >= 90 and < 100%	0.95	0.05	119	
Herb Cover >= 80 and < 90%	0.83	0.17	128	
Herb Cover >= 90 and <= 100%	0.83	0.17	129	

Table B.3 Curve numbers (CN) assigned to different land cover classifications in the NLCD 2011 data. CN values gathered from the most common values in the literature (NRCS TR-55, 1986; WSDOT, 2014) and are adjusted based in the percent of imperviousness of the grid cells [Equation 4.1].

NLCD 2011		
Land cover description	**Class value**	**Curve number**
Open water	11	1
Developed, Open Space	21	0.4
Developed, Low Intensity	22	0.55
Developed, Medium Intensity	23	0.65
Developed High Intensity	24	0.83
Barren Land (Rock/Sand/Clay)	31	0.65
Deciduous Forest	41	0.52
Evergreen Forest	42	0.48
Mixed Forest	43	0.48
Shrub/Scrub	52	0.3
Grassland/Herbaceous	71	0.22
Pasture/Hay	81	0.35
Cultivated Crops	82	0.4
Woody Wetlands	90	1
Emergent Herbaceous Wetlands	95	1

Figure B.1 Spatial cluster of autocorrelation as identified by LISA for Baltimore, MD (bottom) and Philadelphia, PA (top). The four scenarios presented include: A-absolute counts/Census Block Groups, B-population density/Census Block Groups, C-absolute counts/Census Blocks, and D-population density/ Census Blocks

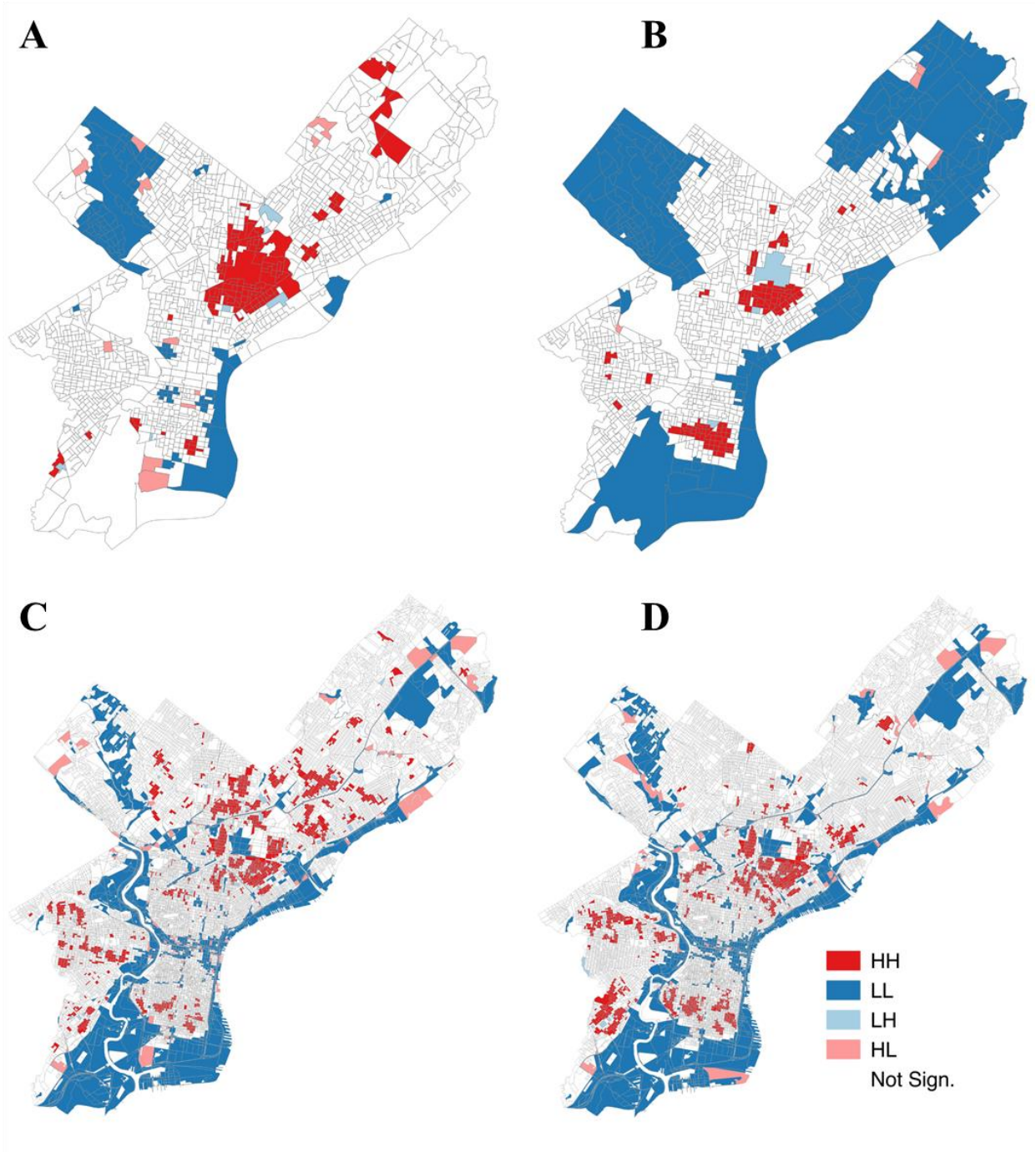

Figure B.1(cont.)

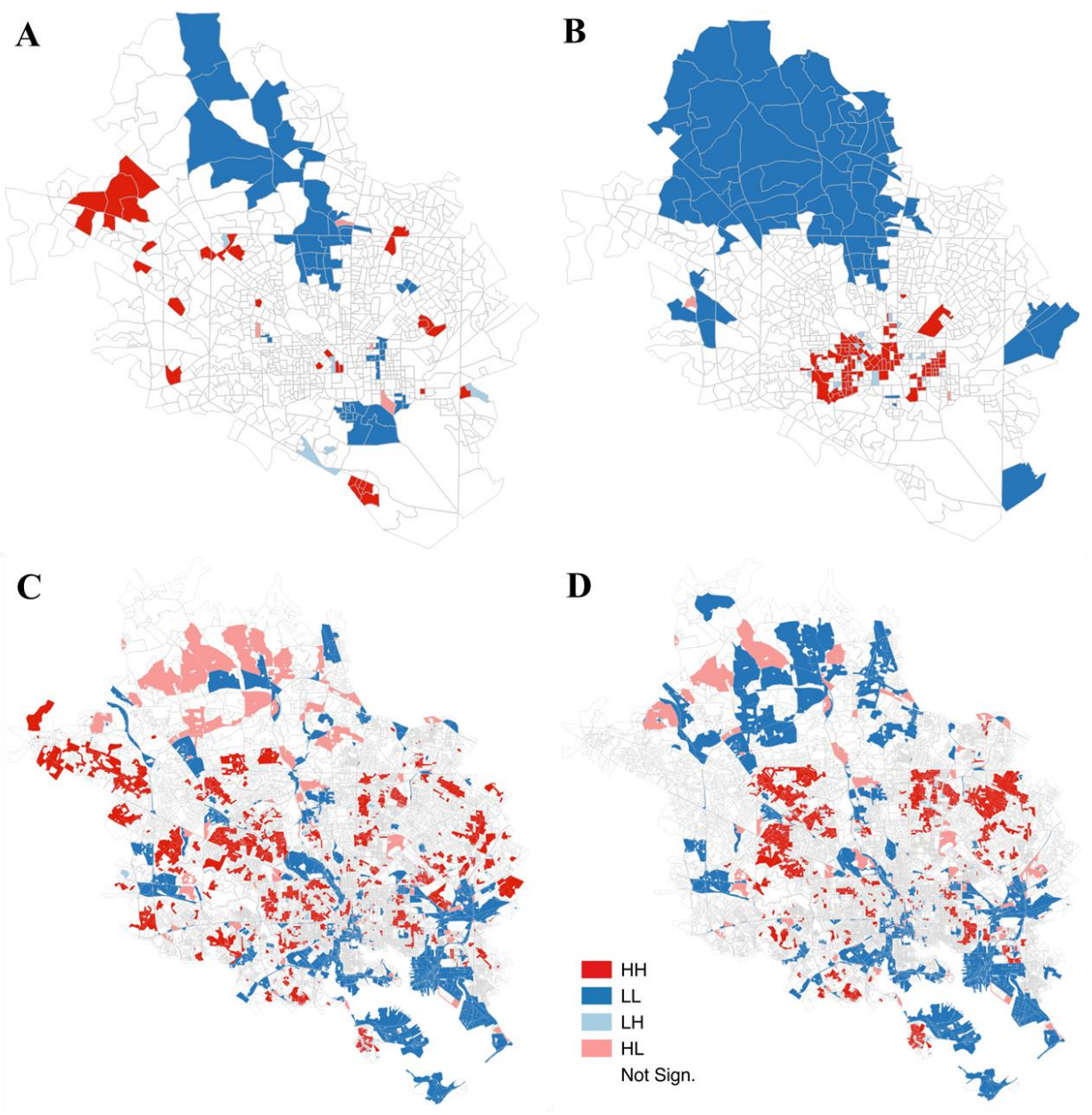

Figure B.2 Distribution of the range of land surface temperatures for different circular buffer sizes. The legend presents the radius of the circular buffers in raster cells (i.e., 10 meter raster). It was noted that for a circular buffer of 9 pixels (i.e., 90 meters) 90% of the total area had a land surface temperature range within the buffers less than or equal to 5 °F.

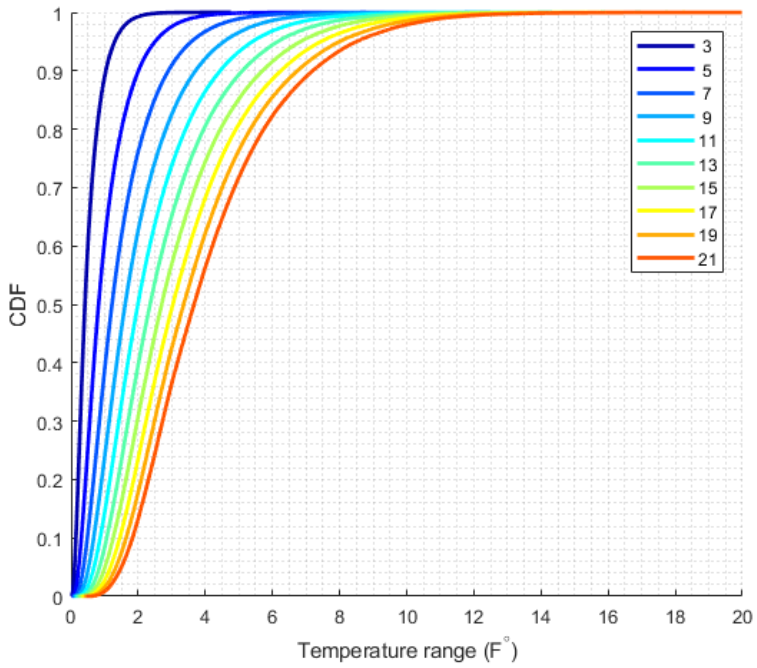

Figure B.3 Changes in distribution of hazard exposure severity and social susceptibility as a function of distance from the GSI calculated using Census Block Group. For each disk buffer, the plotted bars represent the different categories of social susceptibility [i.e., Left: Very Low, Right: Very High]. Top graph (A) presents the change in distribution relative to the area of the disk buffer. Bottom graph (B) presents the change in distribution relative to the total area associated with each of the potential combinations of vulnerability (i.e., stacked percentages). Lastly, the color of the bar correspond to the hazard exposure severity of urban heat island [i.e., legend].

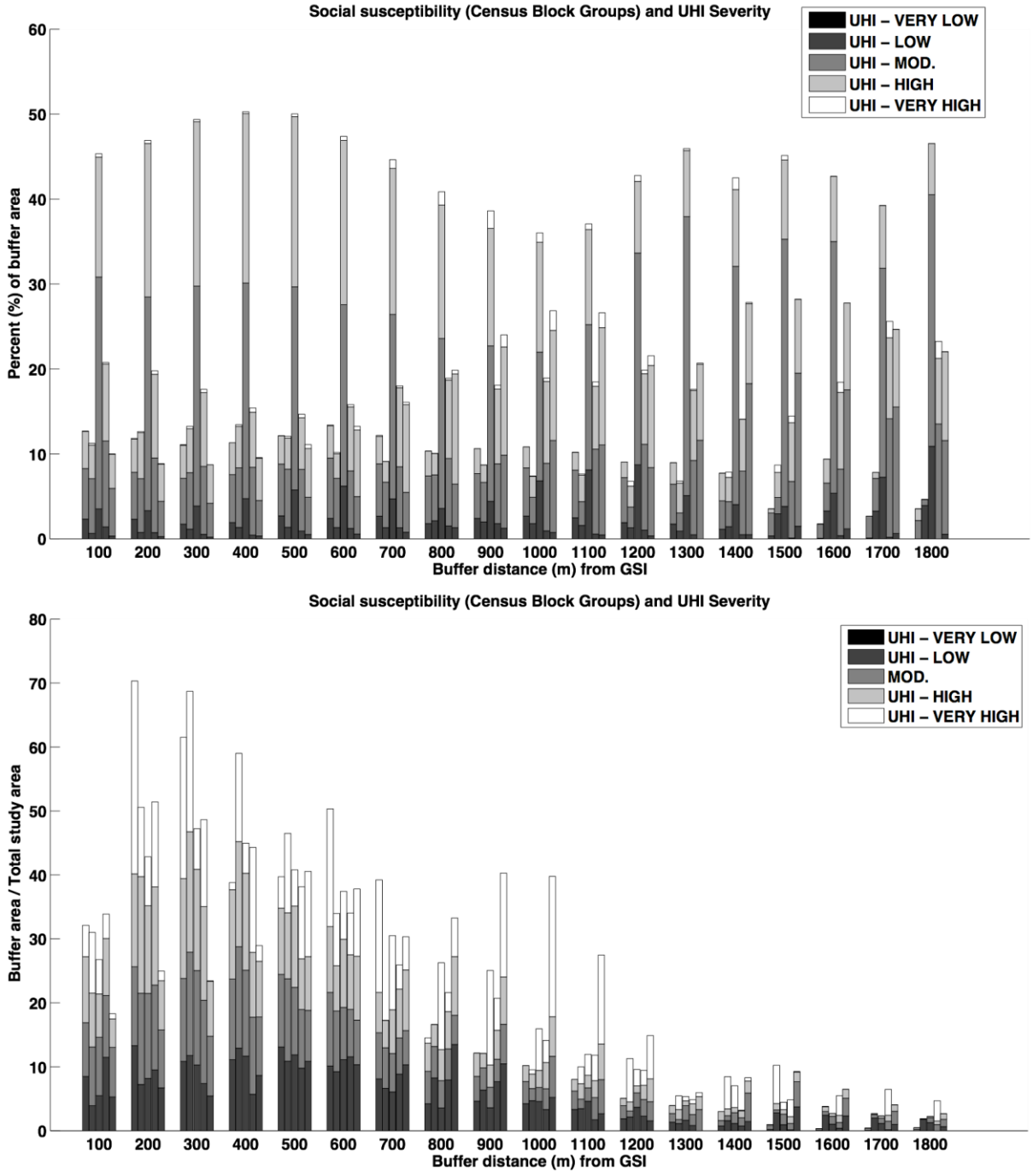

Figure B.4 Distribution of land surface temperature between areas with imperviousness greater than 50% and no trees were compared to areas that had a higher tree canopy. Results showed that areas without trees could have up to a 0.3 to 0.4 lower probability of having the same land surface temperature as areas with trees.

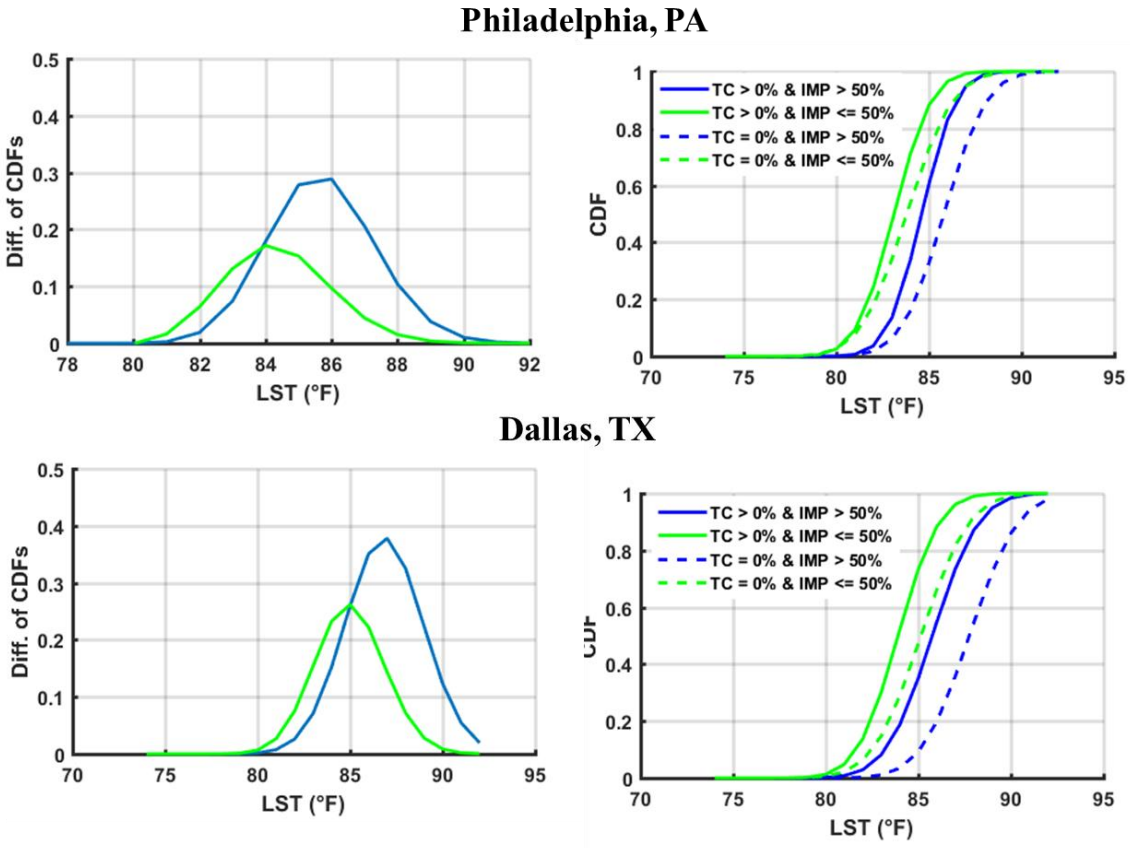

Figure B.5 Geographic location of Dead Run 5 (DR5) case study watershed (Section 4.3).

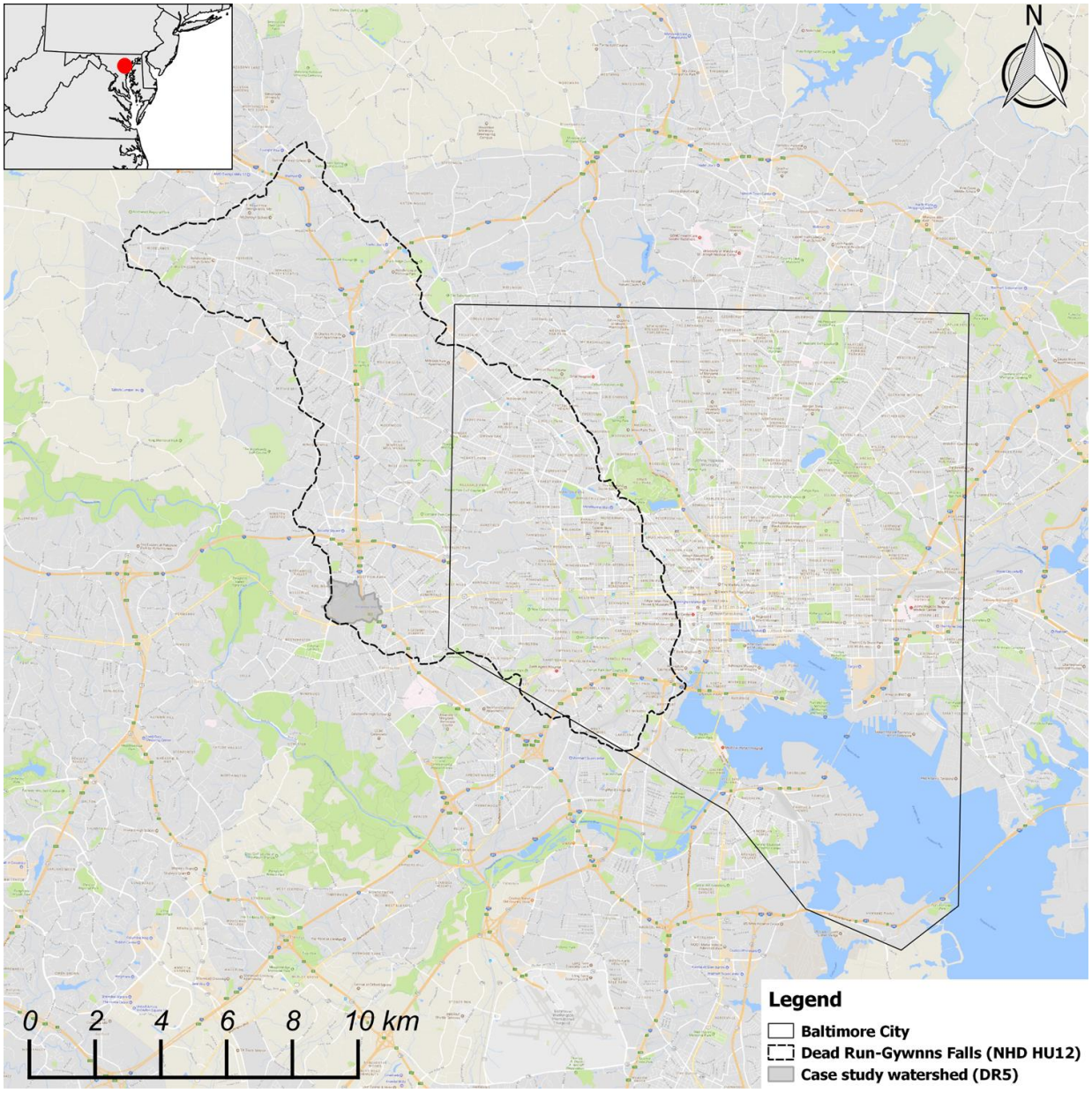

Figure B.6 Geographic location of Philadelphia's case study watershed (Section 4.3).

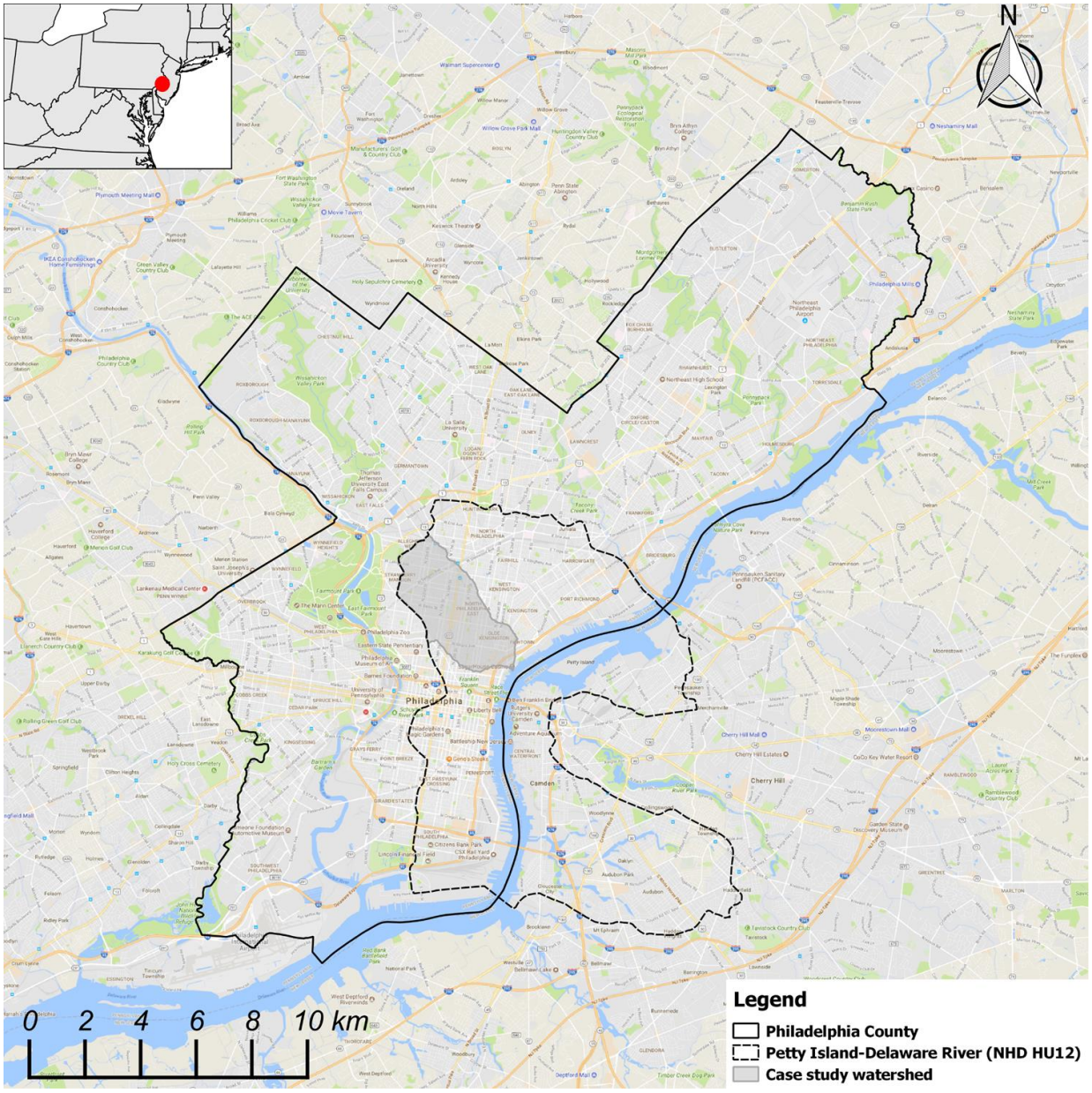

Figure B.7 Geographic location of Dallas' case study watershed (Section 4.3).